NASA CONTRACTOR REPORT

NASA CR-544

GENERAL PURPOSE AIRBORNE SIMULATOR - CONCEPTUAL DESIGN REPORT

by Daniel C. Clark and John Kroll

Prepared by
CORNELL AERONAUTICAL LABORATORY, INC.
Buffalo, N. Y.
for Flight Research Center

NATIONAL AERONAUTICS AND SPACE ADMINISTRATION • WASHINGTON, D. C. • AUGUST 1966

GENERAL PURPOSE AIRBORNE SIMULATOR - CONCEPTUAL DESIGN REPORT

By Daniel C. Clark and John Kroll

Prepared under Contract No. NAS 4-607 by
CORNELL AERONAUTICAL LABORATORY, INC.
Buffalo, N.Y.

for Flight Research Center

NATIONAL AERONAUTICS AND SPACE ADMINISTRATION

For sale by the Clearinghouse for Federal Scientific and Technical Information
Springfield, Virginia 22151 – Price $3.75

ABSTRACT AND SUMMARY

The Flight Research Department of Cornell Aeronautical Laboratory is engaged in the design and construction for the NASA Flight Research Center of a general purpose airborne simulator (GPAS) capable of both model controlled and response feedback types of variable stability operation. The simulator airplane is a Lockheed JetStar.

This report is concerned with the functional design of the GPAS system. Methods are developed for calculating theoretical control loop gains for the model controlled system as a function of dynamic pressure and aircraft weight. The magnitudes of these theoretical loop gains are based on satisfying dynamic performance criteria in the NASA design specifications. The results of analog computer simulations supplement the theoretical studies of the closed-loop behavior of the model controlled systems. A comparison is made of the system performance using theoretical control loop gains and the gain values estimated to be achievable in actual flight. The appendices deal with aircraft data, equations of motion, transfer functions and also with special problems associated with acceleration feedback loops.

It is concluded that the GPAS system, as designed and presented in this report, will provide satisfactory variable stability operation using either the model controlled system (MCS) or the response feedback system (RFS). The methods and techniques presented in this report are shown to be satisfactory for establishing the proper levels of control system gains to achieve the specified model controlled performance. However, the model controlled system is expected to be limited, essentially, to simulating aircraft with slower dynamic response than the JetStar because effects due to such phenomena as structural flexibility, turbulence, and noise will preclude the actual use of the gain levels required for simulation of faster responding airplanes. Such simulations will probably only be realizeable with the response feedback system.

ACKNOWLEDGEMENTS

The authors wish to acknowledge the contributions of Robert F. Gavin and Joseph J. Beale who performed the total force equations analog computer simulations, and John M. Schuler, Francis E. Pritchard, Donald W. Rhoads, and Joseph L. Francis for their many valuable technical inputs during this study. They also would like to thank the Lockheed Georgia Company for use of the JetStar derivative, mass, and inertial characteristics which were essential for the design of the general purpose airborne simulator.

TABLE OF CONTENTS

LIST OF TABLES

LIST OF ILLUSTRATIONS

LIST OF SYMBOLS

I. Aircraft Geometry, Mass, and Inertia

m	aircraft mass, slugs
W	aircraft weight, lb
g	gravitational constant, 32.17 ft/sec^2
S	reference area, ft^2
I_{xx}	moment of inertia about x-body axis, slug-ft^2
I_{yy}	moment of inertia about y-body axis, slug-ft^2
I_{zz}	moment of inertia about z-body axis, slug-ft^2
I_{xz}	product of inertia, body axes, slug-ft^2
$\bar{c}$	mean aerodynamic chord, ft
b	reference span, ft
z_T	thrust moment arm, ft, (positive along + z axis)
$\bar{x}$	c.g. location ahead of position for which basic data applies, ft ($\bar{x} = 0$ for all studies)
ℓ	distance from c.g. to cockpit, ft
ψ	distance from c.g. to arbitrary point along x body axis, ft

II. Aircraft Motion Variables

V	total velocity of c.g., ft/sec
α	angle of attack, rad or deg
γ	flight path angle, rad or deg
h	altitude, ft
M	Mach number

II. Aircraft Motion Variables, continued

a	speed of sound, ft/sec
$\bar{q}$	dynamic pressure, lb/ft^2, $\frac{1}{2}\rho V^2$
β	sideslip angle, rad or deg
p	roll rate, component of angular velocity about x -body axis, rad/sec or deg/sec
q	pitch rate, component of angular velocity about y -body axis, rad/sec or deg/sec
r	yaw rate, component of angular velocity about z -body axis, rad/sec or deg/sec
ψ, θ, ϕ	Euler angles defining orientation of body axes, rad or deg
ρ	density of air, slug/ft^3
$\rho_0, \rho_h, \rho_{h^2}$	coefficients in polynomial expression for density as a function of altitude, $\rho = \rho_0 + \rho_h h + \rho_{h^2} h^2$
α_I	angle of attack in still air, rad or deg
β_I	sideslip angle in still air, rad or deg
α_G	incremental angle of attack due to gusts, rad or deg
β_G	incremental sideslip angle due to gusts, rad or deg
n_x	longitudinal acceleration, g's, positive along + x -wind axis
n_y	lateral acceleration, g s, positive along + y -body axis
n_z	normal acceleration, g s, positive along + z -body axis

III. Aircraft Dynamic Mode Properties

ω_{θ_s}	short period natural frequency, rad/sec
ζ_{θ_s}	short period damping ratio

III. Aircraft Dynamic Mode Properties, Continued

ω_{θ_p}	phugoid natural frequency, rad/sec
ζ_{θ_p}	phugoid damping ratio
ω_ψ	Dutch roll natural frequency, rad/sec
ζ_ψ	Dutch roll damping ratio
τ_s	spiral time constant, sec
τ_r, τ_R	roll time constant, sec
ω_ϕ	roll numerator frequency, rad/sec
ζ_ϕ	roll numerator damping ratio
$\lvert\phi/\beta\rvert$	magnitude of roll to sideslip ratio

IV. Forces and Moments

T	thrust, lb
L	lift, lb or rolling moment about x-body axis, ft-lb
D	drag, lb
M	pitching moment about y-body axis, ft-lb
N	yawing moment about z-body axis, ft-lb
Y	side force along y-body axis, lb
Z	component of aerodynamic forces along z-body axis, lb
C_L	lift coefficient, $C_L = L/\bar{q}S$
C_D	drag coefficient, $C_D = D/\bar{q}S$
C_Y	side force coefficient, $C_Y = Y/\bar{q}S$
C_ℓ	rolling moment coefficient, $C_\ell = L/\bar{q}Sb$
C_m	pitching moment coefficient, $C_m = M/\bar{q}S\bar{c}$
C_n	yawing moment coefficient, $C_n = N/\bar{q}Sb$

IV. Forces and Moments, Continued

$C_{m_{(A)}}$ aerodynamic pitching moment coefficient at trim angle of attack; approx. equal to $-z_T/\bar{c}\ C_D$

C_{L_0} lift coefficient at zero angle of attack

C_{m_0} moment coefficient at zero angle of attack

C_{D_0} drag coefficient at zero angle of attack

$A_{C_D}, B_{C_D}, C_{C_D}$ coefficients in polynomial expression for drag coefficient, JetStar only, $C_D = A_{C_D} + B_{C_D}\alpha + C_{C_D}\alpha^2$

K_D constant in polynomial expression for drag coefficient, model (SST) only, $C_D = C_{D_0} + K_D\alpha^2$

V. Control System Variables

δ_e elevator deflection, positive T.E. down, rad or deg

δ_a aileron deflection, positive left aileron T.E. down, rad or deg

δ_r rudder deflection, positive T.E. left, rad or deg

δ_h JetStar stabilizer deflection, positive L.E. up, rad or deg

i_c Model (SST) canard deflection, positive T.E. down, rad or deg

δ_T nondimensional throttle deflection,

ΔT change in thrust, lb

τ_V velocity channel filter time constant, sec

Z'_V equivalent drag due to velocity including Mach number effects, sec^{-1} (Section 2.2)

Z'_{δ_e} equivalent elevator lift coefficient, sec^{-1} (Section 2.2)

D'_{δ_e} equivalent elevator drag coefficient, $\frac{ft/sec^2}{rad}$ (Section 2.2)

e error, comm and variable minus JetStar variable

V. Control System Variables, Continued

e_α	$\Delta\alpha_c - \Delta\alpha$, angle of attack error, deg
$e_{\dot\alpha}$	$\dot\alpha_c - \dot\alpha$, angle of attack rate error, deg/sec
e_V	$\Delta V_c - \Delta V$, velocity error, ft/sec
$e_{\dot V}$	$\dot V_c - \dot V$, acceleration error, ft/sec^2
e_h	$\Delta h_c - \Delta h$, altitude error, ft
$e_{\dot h}$	$\dot h_c - \dot h$, rate of climb error, ft/sec
e_{n_z}	$\Delta n_{z_c} - \Delta n_z$, normal acceleration error, g's
e_{n_Y}	$\Delta n_{Y_c} - \Delta n_Y$, lateral acceleration error, g's
e_β	$\beta_c - \beta$, sideslip error, deg
$e_{\dot\beta}$	$\dot\beta_c - \dot\beta$, sideslip rate error, deg/sec
e_p	$p_c - p$, roll rate error, deg/sec
e_ϕ	$\Delta\phi_c - \Delta\phi$, roll angle error, deg
δ_e/e_α	MCS angle of attack error to elevator gain, deg/deg
$\delta_e/e_{\dot\alpha}, (\delta_e/e_{\dot\alpha})_\alpha$	MCS angle of attack rate error to elevator gain, sec
δ_e/e_V	MCS velocity error to elevator gain, deg-sec/ft
$\delta_e/e_{\dot V}$	MCS acceleration error to elevator gain, deg-sec^2/ft
δ_e/e_h	MCS altitude error to elevator gain, deg/ft
$\delta_e/e_{\dot h}$	MCS altitude rate error to elevator gain, deg-sec/ft
δ_e/e_{n_z}	MCS normal acceleration error to elevator gain, deg/g
$\Delta T/e_V$	MCS velocity error to the throttle gain, lb sec/ft
$\Delta T/e_{\dot V}$	MCS acceleration error to the throttle gain, lb sec^2/ft
$\Delta T/e_h$	MCS altitude error to the throttle gain, lb/ft
$\Delta T/e_{\dot h}$	MCS altitude rate error to the throttle gain, lb sec/ft
δ_r/e_β	MCS sideslip angle error to the rudder gain, deg/deg

V. Control System Variables, Continued

$\delta_r/e_{\dot{\beta}}$	MCS sideslip angle rate error to the rudder gain, sec
δ_r/e_{n_y}	MCS lateral acceleration error to the rudder gain, deg/g
δ_a/e_p	MCS roll rate error to the ailerons gain, sec
δ_a/e_ϕ	MCS bank angle error to the ailerons gain, deg/deg
δ_e/α	RFS angle of attack to the elevator gain
$\delta_e/\dot{\alpha}$	RFS angle of attack rate to the elevator gain, sec
δ_e/q	RFS pitch rate to the elevator gain, sec
$\delta_e/\dot{q}$	RFS pitch acceleration to the elevator gain, sec^2
δ_e/V	RFS perturbation velocity to the elevator gain, deg-sec/ft
$\delta_e/\dot{V}$	RFS acceleration to the elevator gain, deg-sec^2/ft
δ_e/δ_{e_p}	RFS elevator stick position to the elevator gain, deg/in.
δ_e/F_e	RFS elevator stick force to the elevator gain, deg/lb
δ_r/β	RFS angle of sideslip to the rudder gain, deg/deg
$\delta_r/\dot{\beta}$	RFS angle of sideslip rate to the rudder gain, sec
δ_r/r	RFS yaw rate to the rudder gain, sec
$\delta_r/\dot{r}$	RFS yaw acceleration to the rudder gain, sec^2
δ_r/p	RFS roll rate to the rudder gain, sec
$\delta_r/\dot{p}$	RFS roll acceleration to the rudder gain, sec^2
δ_r/δ_{a_p}	RFS aileron wheel position to the rudder gain, deg/deg
δ_r/δ_{r_p}	RFS rudder pedal position to the rudder gain, deg/in.
δ_r/F_r	RFS rudder pedal force to the rudder gain, deg/lb
δ_a/p	RFS roll rate to the ailerons gain, sec
$\delta_a/\dot{p}$	RFS roll acceleration to the ailerons gain, sec^2
δ_a/ϕ	RFS bank angle to the ailerons gain, deg/deg

V. Control System Variables, Continued

δ_a/β	RFS sideslip angle to the ailerons gain, deg/deg
$\delta_a/\dot{\beta}$	RFS sideslip angle rate to the ailerons gain, sec
δ_a/r	RFS yaw rate to the ailerons gain, sec
$\delta_a/\dot{r}$	RFS yaw acceleration to the ailerons gain, sec^2
δ_a/δ_{r_p}	RFS rudder pedal position to the ailerons gain, deg/in.
δ_a/δ_{a_p}	RFS aileron wheel position to the ailerons gain, deg/deg
δ_a/F_a	RFS aileron wheel force to the ailerons gain, deg/lb
$\delta_r'/e_{\dot{\beta}}$	The gain $\delta_r/e_{\dot{\beta}}$ associated with n_Y feedback, sec
$(\delta_e/e_{\dot{\alpha}})_{n_z}$	The gain $\delta_e/e_{\dot{\alpha}}$ associated with Δn_z feedback, sec
$(\delta_e/e_{\dot{\alpha}})_{MOD}$	Modified $(\delta_e/e_{\dot{\alpha}})_{n_z}$ (appendix D), sec

VI. Stability Derivatives, Nondimensional. (Dimensional Derivatives are presented in Appendix A)

C_{L_α}	$\partial C_L/\partial\alpha$, rad^{-1} or deg^{-1}
$C_{L_{\delta_e}}$	$\partial C_L/\partial\delta_e$, rad^{-1} or deg^{-1}
C_{D_α}	$\partial C_D/\partial\alpha$, rad^{-1} or deg^{-1}
C_{m_α}	$\partial C_m/\partial\alpha$, rad^{-1} or deg^{-1}
$C_{m_{\dot{\alpha}}}$	$\partial C_m/\partial\left(\frac{\dot{\alpha}\bar{c}}{2V}\right)$, rad^{-1}
C_{m_q}	$\partial C_m/\partial\left(\frac{q\bar{c}}{2V}\right)$, rad^{-1} or deg^{-1}
$C_{m_{\delta_e}}$	$\partial C_m/\partial\delta_e$, rad^{-1} or deg^{-1}
C_{Y_β}	$\partial C_Y/\partial\beta$, rad^{-1} or deg^{-1}
$C_{Y_{\delta_r}}$	$\partial C_Y/\partial\delta_r$, rad^{-1} or deg^{-1}
C_{ℓ_p}	$\partial C_\ell/\partial\left(\frac{pb}{2V}\right)$, rad^{-1} or deg^{-1}
C_{ℓ_r}	$\partial C_\ell/\partial\left(\frac{rb}{2V}\right)$, rad^{-1} or deg^{-1}

VI. Stability Derivatives, Nondimensional, Continued

C_{l_β}	$\partial C_l / \partial \beta$	, rad^{-1} or deg^{-1}
$C_{l_{\delta_r}}$	$\partial C_l / \partial \delta_r$	, rad^{-1} or deg^{-1}
$C_{l_{\delta_a}}$	$\partial C_l / \partial \delta_a$	, rad^{-1} or deg^{-1}
C_{n_p}	$\partial C_n / \partial \left(\frac{pb}{2V}\right)$	, rad^{-1} or deg^{-1}
C_{n_r}	$\partial C_n / \partial \left(\frac{rb}{2V}\right)$	, rad^{-1} or deg^{-1}
C_{n_β}	$\partial C_n / \partial \beta$	, rad^{-1} or deg^{-1}
$C_{n_{\delta_r}}$	$\partial C_n / \partial \delta_r$	, rad^{-1} or deg^{-1}
$C_{n_{\delta_a}}$	$\partial C_n / \partial \delta_a$	, rad^{-1} or deg^{-1}
$C_{L_{i_c}}$	$\partial C_L / \partial i_c$	, rad^{-1} or deg^{-1}
$C_{m_{i_c}}$	$\partial C_m / \partial i_c$	, rad^{-1} or deg^{-1}
$C_{L_{\delta_k}}$	$\partial C_L / \partial \delta_k$	, rad^{-1} or deg^{-1}
$C_{m_{\delta_k}}$	$\partial C_m / \partial \delta_k$	, rad^{-1} or deg^{-1}
$C_{l_{\beta_\alpha}}$	$\partial C_{l_\beta} / \partial \alpha$	, rad^{-2} or deg^{-2}
$C_{l_{\delta_{r_\alpha}}}$	$\partial C_{l_{\delta_r}} / \partial \alpha$	, rad^{-2} or deg^{-2}
$C_{l_{r_\alpha}}$	$\partial C_{l_r} / \partial \alpha$	, rad^{-2} or deg^{-2}
$C_{n_{\beta_\alpha}}$	$\partial C_{n_\beta} / \partial \alpha$	, rad^{-2} or deg^{-2}
$C_{n_{r_\alpha}}$	$\partial C_{n_r} / \partial \alpha$	, rad^{-2} or deg^{-2}
$C_{n_{p_\alpha}}$	$\partial C_{n_p} / \partial \alpha$	, rad^{-2} or deg^{-2}

VII. Additional Symbols and Subscripts

s	Laplace Transform variable, rad/sec
Δ	incremental change from a reference condition
$s_{1...76}$	roots of transfer function numerators (See Appendix B)
$K_{1...24}$	gains of transfer function (See Appendix B)

VII. Additional Symbols and Subscripts, Continued

A, B, C, D, E	coefficients of s in characteristic equation and transfer function numerators (Section 3, appendix B)
$u(t)$	the unit step-function
$\bar{\alpha}/\delta_e$	short-period steady-state angle of attack per unit elevator deflection
k	ratio of $\Delta V/\Delta\delta_e)_{ss}$ to $\dot{\gamma}/\Delta T)_{ss}$
t	real time, sec
$(\dot{})$	dot over symbol indicates differentiation with respect to time
sub e	elevator or elevon
sub a	aileron
sub r	rudder
sub JS	JetStar
sub ss	steady state
sub m, M	refers to model (SST)
sub t, T	indicates trim conditions
sub p	refers to pilot or cockpit location
sub c	command
sub 0	open-loop
sub x	along + x axis
MCS	model-controlled system
RFS	response feedback system
GPAS	general purpose airborne simulator
SST	supersonic transport
CAL	Cornell Aeronautical Laboratory

SECTION 1

INTRODUCTION

The Cornell Aeronautical Laboratory, Inc., under a NASA sponsored contract, is currently installing a model controlled variable stability system in a Lockheed JetStar. In essence, a model controlled system uses high gain control loops to make the airplane duplicate the response, in certain variables, of a model of a simulated aircraft whose equations of motion are programmed on an airborne analog computer. The control motions of the evaluation pilot are the inputs to the analog computer model and the resulting response of this model are the responses desired for the JetStar. Response variables of the model are compared with those of the JetStar and the resulting error signals actuate the proper control surfaces to minimize the errors. If sufficiently high control loop gains can be achieved, the errors will be small and the model dynamics will be reproduced with a high degree of fidelity. The JetStar with its variable stability equipment is referred to as the General Purpose Airborne Simulator (GPAS).

Another type of variable stability system has been used extensively in the past and is still being used today. This system, called the response feedback system, operates in a different manner from the n odel-following type of system. In a response feedback system the airplane motion variables are measured and signals proportional to these variables actuate the various control surfaces. The force and moment changes due to the control deflections effectively change the stability derivatives to correspond to those of a simulated airplane. One of the difficult problems associated with the use of a response feedback system is calibration, that is, the determination of the combination of control system gains that gives the desired set of dynamic characteristics. These gains are usually first estimated by analytical methods. To check these estimates the closed-loop airplane response is measured in flight and the records are reduced to verify that the proper dynamics have been achieved. If desired dynamic characteristics have not been obtained, the procedure must be repeated. For certain sets of dynamic characteristics this iteration process can be time consuming and sensitive

to the base airplane characteristics. Furthermore, the identification of the simulated airplane characteristics from flight test data can, in itself, be a difficult and time consuming process.

The model controlled variable stability system promises to alleviate this calibration problem. Once the flight test data establishes that the airplane is actually following the model responses, then the remaining "calibrations", which would normally be performed on the ground, are concerned with setting the proper characteristics on the airborne analog computer. The important factor is that many characteristics of the simulation, such as natural frequencies and damping ratios, are known to the precision with which analog potentiometers can be set. This is far more accurate than any flight-test data.

There are areas of difficulty for a model controlled system. Simulating high frequency and fast responding airplanes is difficult because the gains required are much higher than for the corresponding response feedback system. Also, the model controlled system can introduce spurious responses if an inappropriate model is used or if the wrong variables are followed. In particular, it is not possible to obtain the proper response to turbulence without actually measuring the gust velocity and feeding it to the model. Also, except for the most limited simulations, extensive analog equipment is required for the model because the model following loops essentially eliminate all airplane-like characteristics from the motion variables that are being used for following (e.g. there is no effect on normal acceleration from the gravitational force when an acceleration following loop is used) and all the characteristics that are pertinent to the simulation must be incorporated in the equations of motion for the model. Conversely, in the use of response feedback systems full advantage can be taken of many normal airplane characteristics to simplify and minimize the amount of equipment required for the simulation. However, for simulation of low-frequency airplanes, the model controlled approach is particularly appropriate because it makes the calibration problem so much easier. One fact should be emphasized and clearly understood. No matter what type of

control system is used and no matter what system components are involved, for a given simulation the airplane's control motion (elevator, ailerons, rudder and throttle) are the same.

This report deals with the conceptual design of the GPAS variable stability system which is basically the model-following type. The system design is based on performance criteria established by NASA and the following control loops are provided: angle of attack, angle of sideslip, normal acceleration, lateral acceleration, bank angle, roll rate, altitude and velocity. In addition, response feedback loops are provided. These loops can either augment the model-following loops or be used independently thereby providing a backup system.

In the analysis and design of the GPAS variable stability system reported herein, the ability of the system to simulate the responses of a specific vehicle was evaluated. Characteristics representative of a supersonic transport were used, although the dynamics were not those of any specific proposed SST design.

SECTION 2

DESIGN OF LONGITUDINAL MCS CONTROL LOOPS

In order to obtain satisfactory static and dynamic model following in an MCS control loop, two requirements must be met simultaneously. They are: 1) a closed-loop bandwidth of at least 1.5, and preferably 3 or more, times the highest significant frequencies of the model, and 2) a loop gain large enough to insure small steady-state errors (Reference 1). In a regulator control loop, these two requirements are not necessarily compatible; loop gain affects both bandwidth and steady-state response simultaneously. If it is desired to limit the closed-loop bandwidth the the minimum value consistent with good dynamic model following, it is possible that static errors may be excessive. If, on the other hand, the static errors are limited to an acceptable value, then the bandwidth may be too large and the system disturbance response unacceptable. One way to avoid these problems is to use integration in the forward loop (i.e., a type 1 system) in which case for a stable system the static error is zero for any finite loop gain, and the loop gain can still be adjusted to vary closed-loop bandwidth. Such a loop is invariably more difficult to stabilize than a regulator loop, however, because of the added phase lag at all frequencies contributed by the integrator.

In designing the GPAS control loops, loop gains and compensation were selected in all cases to provide desirable closed-loop bandwidth and damping rather than proper statics. These gains, in general, result in excessive static errors in any given loop (considered alone) but considerably smaller errors when model-following of all significant motion variables is attempted simultaneously. This reduction of static errors when several variables are followed simultaneously is due to cross-coupling between control loops, which in all cases studied was beneficial. (See Reference 2).

For the phugoid control loops, the values of gain required to achieve the desired closed-loop frequencies and damping ratios are always lower than the values required to achieve static errors of less than 10 percent. For

this reason, to null static errors, forward loop integration was used in the ΔV and $\dot{\alpha}$ control loops as explained in Section 2.2. However, forward loop integration cannot be used in the short-period control loops for the following reasons. The angle of attack response of the model to elevator command inputs has two steady-state values; one is the short-period steady state which occurs within a few seconds after application of the control input, and the other is the final value that exists after all short-period and phugoid transients decay, assuming a stable phugoid response and no further action of the controls. These two steady-state values are not equal, and it is the short-period value that is important from a handling qualities standpoint. Thus, an integrating loop does not insure zero error in the short-period steady state. Further, model angle of attack cannot be considered as a desirable variable to be followed after decay of the short-period transients if flight path matching is desired. In the phugoid mode, the phugoid control loops cause JetStar angle of attack to be whatever value is required to minimize errors in flight path model following (i.e., minimize errors in ΔV and $\dot{\alpha}$). Angle of attack, as controlled by the elevator, is used to adjust C_L to the values necessary for proper flight path matching, with little consideration given to JetStar attitude. The throttle loop adjusts thrust to account for changes in C_D and longitudinal axis gravity components. It is apparent then that zero error in the final steady-state value of angle of attack, as would result through use of an integrating angle of attack loop, can be achieved only at the expense of flight path matching. The JetStar elevator must be "time-shared", controlling short-period angle of attack and long-period flight path. Similar arguments show that forward loop integration should not be used with a normal acceleration control loop.

In Sections 2.1 and 2.2 below, equations are developed which predict closed-loop bandwidth and damping in all longitudinal MCS loops based on non-integrating, or regulator, loops. Low gain forward loop integrations were later added to the ΔV and $\dot{\alpha}$ loops to insure adequate steady-state accuracy. Even without the integrations, for several flight conditions the short term accuracy is excellent in all MCS loops with relatively low loop gains, primarily due to the benefits of inter-loop coupling and following of

several variables simultaneously. However, even small static errors in $\dot{h}$, for example, can result in divergence or drift between the altitudes of the model and JetStar after a long period of time. This is unacceptable for long-term flight-path model following.

Reynolds points out in Reference 1 that if it is desired to model-follow a given variable, then that same variable should be used directly in an MCS feedback control loop. Because the GPAS work statement requires model following of $\Delta\alpha$ or Δn_{z_p} as well as ΔV and $\dot{h}$, MCS control loops are provided for all of these variables, as shown in Figure 2.1.* In addition, time derivatives of $\Delta\alpha$ and ΔV are provided to insure adequate short-period and phugoid damping and effect some input lead compensation to reduce phase lags in model following. The altitude loop controls altitude errors by insuring that steady-state errors in $\dot{h}$ are zero. The forward loop compensation network in the ΔV loop insures zero steady-state error in velocity and, for large values of τ_V, does not significantly influence phugoid dynamics.

2.1 ANALYSIS OF SHORT-PERIOD CONTROL LOOPS

Referring to Figure 2.1 it is evident that the elevator actuator command signal is related to the model inputs and JetStar motion variables by equation 2.1.

$$\Delta\delta_{e_c} = \left(\frac{\delta_e}{e_\alpha}\right)(\Delta\alpha_c - \Delta\alpha) + \left(\frac{\delta_e}{e_{\dot{\alpha}}}\right)(\dot{\alpha}_c - \dot{\alpha}) \left(\frac{\delta_e}{e_{n_z}}\right)(\Delta n_{z_c} - \Delta n_{z_x}) + \left(\frac{\delta_e}{e_V}\right)(\Delta V_c - \Delta V) + \left(\frac{\delta_e}{e_{\dot{V}}}\right)(\dot{V}_c - \dot{V}) \quad (2.1)$$

The variable Δn_{z_x} is the perturbation normal acceleration of the JetStar measured x feet ahead of the c.g. and is given by equation 2.2. When $x = 0$, Δn_{z_x} is the acceleration at the c.g. When $x = \ell$, $\Delta n_{z_x} = \Delta n_{z_p}$,

---

*The phugoid control loop configuration shown in Figure 2.1 is inadequate because of poor transient response to model thrust commands. A more suitable arrangement is shown in Figure 2.3 and explained in Section 2.2.1.

the cockpit normal acceleration.

$$\Delta n_{z_x} = \Delta n_z - \frac{x}{g}\dot{q} = \frac{V}{g}\left\{Z_\alpha \Delta\alpha + Z_{\delta_e}\Delta\delta_e + \frac{Z_V}{V_t}\Delta V\right\} - \frac{x}{g}\dot{q} \qquad (2.2)$$

In analyzing closed-loop short-period dynamics, the JetStar velocity is assumed to be constant and the perturbation velocity terms of equations 2.1 and 2.2 can be neglected. Further, as described in Section 1.5.1 of Reference 3, the quantitative requirements on closed-loop performance of the short-period control loops are expressed in terms of augmented short-period undamped natural frequency and damping ratio rather than static accuracy. Accordingly, the model inputs can be set to zero in equation 2.1, resulting in equation 2.3.

$$\Delta\delta_{e_c} = -\left(\frac{\delta_e}{e_\alpha}\right)\Delta\alpha - \left(\frac{\delta_e}{e_{\dot{\alpha}}}\right)\dot{\alpha} - \left(\frac{\delta_e}{e_{n_z}}\right)\Delta n_{z_x} \qquad (2.3)$$

In normal MCS control loop operation, either δ_e/e_α or δ_e/e_{n_z} is zero; that is, either a $\Delta\alpha$ loop or a Δn_z loop is used. If a $\Delta\alpha$ loop is used, the elevator command signal is represented by equation 2.4a. If a Δn_z loop is used, substitution of equation 2.2 into equation 2.3 results in equation 2.4b.

$\Delta\alpha$ loop:
$$\Delta\delta_{e_c} = -\left(\frac{\delta_e}{e_\alpha}\right)\Delta\alpha - \left(\frac{\delta_e}{e_{\dot{\alpha}}}\right)\Delta\dot{\alpha} \qquad (2.4a)$$

Δn_{z_x} loop:
$$\Delta\delta_{e_c} = -\left(\frac{\delta_e}{e_{\dot{\alpha}}}\right)\dot{\alpha} - \left(\frac{\delta_e}{e_{n_z}}\right)\left[\frac{V_t}{g}\left(Z_\alpha\Delta\alpha + Z_{\delta_e}\Delta\delta_e\right) - \frac{x}{g}\dot{q}\right] \qquad (2.4b)$$

For the moment, let us assume the luxury of an elevator actuator with no dynamic lags; that is, $\Delta\delta_{e_c} = \Delta\delta_e$. Then equation 2.4b can be rearranged into equation 2.5.

$$\Delta\delta_e = \Delta\delta_{e_c} = \frac{-\frac{V_t}{g}Z_\alpha\left(\frac{\delta_e}{e_{n_z}}\right)}{1+\frac{V_t}{g}Z_{\delta_e}\left(\frac{\delta_e}{e_{n_z}}\right)}\Delta\alpha + \frac{-\left(\frac{\delta_e}{e_{\dot{\alpha}}}\right)}{1+\frac{V_t}{g}Z_{\delta_e}\left(\frac{\delta_e}{e_{n_z}}\right)}\dot{\alpha} + \frac{\frac{x}{g}\left(\frac{\delta_e}{e_{n_z}}\right)}{1+\frac{V_t}{g}Z_{\delta_e}\left(\frac{\delta_e}{e_{n_z}}\right)}\dot{q} \qquad (2.5)$$

Now equations 2.4a and 2.5 are of the same form. In other words,

$$\Delta\delta_e = P_\alpha \Delta\alpha + P_{\dot\alpha}\dot\alpha + P_{\dot q}\dot q \tag{2.6}$$

where, when a $\Delta\alpha$ loop is used,

$$\left.\begin{aligned} P_\alpha &= -\frac{\delta_e}{e_\alpha} \\ P_{\dot\alpha} &= -\frac{\delta_e}{e_{\dot\alpha}} \\ P_{\dot q} &= 0 \end{aligned}\right\} \tag{2.7}$$

and, when a Δn_{z_χ} loop is used,

$$\left.\begin{aligned} P_\alpha &= \frac{-\frac{V_t}{g} Z_\alpha \left(\frac{\delta_e}{e_{n_z}}\right)}{1+\frac{V_t}{g} Z_{\delta_e}\left(\frac{\delta_e}{e_{n_z}}\right)} \\ P_{\dot\alpha} &= \frac{-\left(\frac{\delta_e}{e_{\dot\alpha}}\right)}{1+\frac{V_t}{g} Z_{\delta_e}\left(\frac{\delta_e}{e_{n_z}}\right)} \\ P_{\dot q} &= \frac{\frac{\chi}{g}\left(\frac{\delta_e}{e_{n_z}}\right)}{1+\frac{V_t}{g} Z_{\delta_e}\left(\frac{\delta_e}{e_{n_z}}\right)} \end{aligned}\right\} \tag{2.8}$$

equation 2.6 can be used in conjunction with either equation 2.7 or 2.8 to establish proper loop gain levels provided that short-period natural frequency and damping ratio can be expressed in terms of P_α, $P_{\dot\alpha}$, and $P_{\dot q}$.

Assuming constant velocity, the short-period behavior of an airplane is predicted quite accurately by solving the lift and pitching moment equations simultaneously for $\Delta\alpha$ and q. These equations are given below, where Z_θ has been neglected (Reference 1).

$$\left.\begin{aligned} \dot\alpha - q - Z_\alpha \Delta\alpha &= Z_{\delta_e}\Delta\delta_e \\ \dot q - M_q q - M_{\dot\alpha}\dot\alpha - M_\alpha \Delta\alpha &= M_{\delta_e}\Delta\delta_e \end{aligned}\right\} \tag{2.9}$$

If equation 2.6 is substituted in equations 2.9 the resulting homogeneous equations constitute a second-order system with natural frequency and damping expressed by equations 2.10 and 2.11.

$$\omega_{\theta_s}^2 = \frac{-M_\alpha + M_q Z_\alpha - (M_{\delta_e} - M_q Z_{\delta_e}) P_\alpha}{1 - Z_{\delta_e} P_{\dot\alpha} - (M_{\delta_e} + M_{\dot\alpha} Z_{\delta_e}) P_{\dot q}} \tag{2.10}$$

$$2\zeta_{\theta_s}\omega_{\theta_s} = \frac{-M_\alpha - M_q - Z_\alpha - Z_{\delta_e} P_\alpha - (M_{\delta_e} - M_q Z_{\delta_e}) P_{\dot\alpha} + (M_{\delta_e} - M_\alpha Z_{\delta_e}) P_{\dot q}}{1 - Z_{\delta_e} P_{\dot\alpha} - (M_{\delta_e} + M_{\dot\alpha} Z_{\delta_e}) P_{\dot q}} \tag{2.11}$$

In order to insure that a desired value of natural frequency and damping ratio results in a unique set of feedback gains when normal acceleration feedback is used, P_α and $P_{\dot q}$ must be related. When angle of attack feedback is used, $P_{\dot q} = 0$ and P_α and $P_{\dot\alpha}$ are uniquely determined by a specified set, ω_{θ_s} and ζ_{θ_s}. For the Δn_{z_x} feedback cases the gain (δ_e / e_{n_z}) can be eliminated between the expressions for P_α and $P_{\dot q}$ in equation 2.8, resulting in

$$P_{\dot q} = -\left(\frac{x}{V_t Z_\alpha}\right) P_\alpha \tag{2.12}$$

We now make the following definitions:

$$\lambda \triangleq -\frac{x}{V_t Z_\alpha} \tag{2.13}$$

$$\Delta\omega_{\theta_s}^2 \triangleq \omega_{\theta_s}^2 - (M_q Z_\alpha - M_\alpha) \tag{2.14}$$

$$\Delta(2\zeta_{\theta_s}\omega_{\theta_s}) \triangleq 2\zeta_{\theta_s}\omega_{\theta_s} - (-M_{\dot\alpha} - M_q - Z_\alpha) \tag{2.15}$$

The parameter λ is directly proportional to the distance of the feedback accelerometer from the c.g. The term $\Delta\omega_{\theta_s}^2$ is the difference between the closed-loop natural frequency squared and the open-loop natural frequency squared. The increase in damping from open- to closed-loop is given by $\Delta(2\zeta_{\theta_s}\omega_{\theta_s})$. In equations 2.10 and 2.11 the term Z_{δ_e} can be neglected for values of augmented natural frequency and damping ratio up to and including those specified by the design requirements. If this is done, equations 2.10 through 2.15 can be combined and solved for the values of P_α and $P_{\dot\alpha}$ required to achieve a specified closed-loop ω_{θ_s} and ζ_{θ_s}. The required values of P_α and $P_{\dot\alpha}$ are given by equations 2.16 and 2.17.

$$P_{\alpha} = \frac{\Delta \omega_{\theta_s}^2}{-M_{\delta_e}\left(1-\lambda \omega_{\theta_s}^2\right)} \tag{2.16}$$

$$P_{\dot{\alpha}} = \frac{\Delta\left(2\zeta_{\theta_s}\omega_{\theta_s}\right)\left(1-\lambda\omega_{\theta_s}^2\right)+\lambda\left(Z_{\alpha}+2\zeta_{\theta_s}\omega_{\theta_s}\right)\Delta\omega_{\theta_s}^2}{-M_{\delta_e}\left(1-\lambda\omega_{\theta_s}^2\right)} \tag{2.17}$$

Solving equations 2.7 and 2.8 for the feedback gains in the short-period control loops, we get for $\Delta\alpha$ and $\dot{\alpha}$ feedback:

$$\frac{\delta_e}{e_{\alpha}} = -P_{\alpha} \qquad \text{and} \qquad \frac{\delta_e}{e_{\dot{\alpha}}} = -P_{\dot{\alpha}} \tag{2.18}$$

and for Δn_{z_α} and $\dot{\alpha}$ feedback:

$$\frac{\delta_e}{e_{n_z}} = -\frac{g}{V_t}\cdot\frac{P_{\alpha}}{Z_{\alpha}+Z_{\delta_e}P_{\alpha}} \tag{2.19}$$

$$\frac{\delta_e}{e_{\dot{\alpha}}} = -\frac{Z_{\alpha}P_{\dot{\alpha}}}{Z_{\alpha}+Z_{\delta_e}P_{\alpha}}$$

In both cases, P_{α} and $P_{\dot{\alpha}}$ are determined by equations 2.16 and 2.17.

Some interpretations of equations 2.16 through 2.19 are in order. First, when angle of attack feedback is used, the parameter λ is identically zero. Since M_{δ_e} is always negative, the gains P_{α} and $P_{\dot{\alpha}}$ are always positive and always increase with increasing frequency and damping ratio. This is also true for c.g. acceleration feedback. Hence, according to equations 2.18 and 2.19, the δ_e/e_{α} and $\delta_e/e_{\dot{\alpha}}$ pair are both always negative, and the δ_e/e_{n_z} and $\delta_e/e_{\dot{\alpha}}$ pair are positive and negative respectively. Note that the value of $\delta_e/e_{\dot{\alpha}}$ associated with the $\Delta\alpha$ loop is always a larger negative number than that associated with the Δn_z (c.g.) loop. Secondly, note that infinite values of P_{α} and $P_{\dot{\alpha}}$ result with acceleration feedback when $\lambda\omega_{\theta_s}^2 = 1$. Because negative values of P_{α} and $P_{\dot{\alpha}}$ are always destabilizing to the short-period mode*, it can be concluded that $\lambda\omega_{\theta_s}^2 < 1$ is

*See appendix C

required for the desired frequency and damping ratio to be achieved with finite positive values of P_α and $P_{\dot\alpha}$. Consequently, for a given desired closed-loop bandwidth the accelerometer must be located aft of the value of x given below.

$$x < -\frac{V_t Z_\alpha}{\omega_{\theta_s}^2} \tag{2.20}$$

Considering eighteen combinations of JetStar velocity, altitude, and weight, if the accelerometer is located more than two feet ahead of the c.g., for some flight conditions an augmented short-period natural frequency of 9 rad/sec cannot be achieved. Perhaps more important is the definite indication that closed-loop bandwidth is sensitive to c.g. shifts for those flight conditions where $\bar{q} S C_{L_\alpha}/m$ is small.* This problem of limited bandwidth with forward mounted accelerometer is considered further in appendix C.

2.2 ANALYSIS OF PHUGOID CONTROL LOOPS

Reynolds (Reference 1) has noted that an accurate approximation of phugoid dynamics can be obtained by assuming that angle of attack is instantaneously proportional to elevator deflection, and phugoid dynamics derive primarily from the lift and drag equations. If we let $(\bar{\alpha}/\delta_e)$ be the short-period steady-state angle of attack per unit elevator deflection, given by equation 2.21 and replace $\Delta\theta$ and its derivatives by equation 2.22, we get Reynolds' phugoid equations from Reference 1. These equations are repeated below as equations 2.23 and 2.24 for convenience.

$$\frac{\bar{\alpha}}{\delta_e} = \frac{M_{\delta_e} - M_q Z_{\delta_e}}{-M_\alpha + M_q Z_\alpha} \tag{2.21}$$

$$\dot{h} = V_t(\Delta\theta - \Delta\alpha) \tag{2.22}$$

$$\dot{V} + D_V \Delta V + \frac{g}{V_t}\dot{h} = -V_t\left(D_\alpha + \frac{g}{V_t}\right)\left(\frac{\bar{\alpha}}{\delta_e}\right)\Delta\delta_e + \frac{\Delta T}{m} \tag{2.23}$$

* $-V_t Z_\alpha \approx \bar{q} S C_{L_\alpha}/m$

$$\frac{\alpha_t}{V_t}\dot{V} - \frac{Z_V}{V_t}\Delta V - \frac{1}{V_t}\dot{h} - \frac{Z_\theta}{V_t}\dot{h} = \left[(Z_\alpha + Z_\theta)\left(\frac{\bar{\alpha}}{\delta_e}\right) + Z_{\delta_e} \right] \Delta\delta_e \quad (2.24)$$

We now define new effective elevator drag and lift control derivatives as follows:

$$D'_{\delta_e} = V_t\left(D_\alpha + \frac{g}{V_t}\right)\left(\frac{\bar{\alpha}}{\delta_e}\right) \quad (2.25)$$

$$Z'_{\delta_e} = (Z_\alpha + Z_\theta)\left(\frac{\bar{\alpha}}{\delta_e}\right) + Z_{\delta_e} \quad (2.26)$$

It is apparent from equation 2.26 that in controlling phugoid dynamics, the elevator is used to effectively provide direct lift control through changes in lift due to changes in angle of attack that result from elevator inputs. The whole aircraft is used as a lift "amplifier" for elevator inputs, since $|Z'_{\delta_e}| >> |Z_{\delta_e}|$. It should be apparent, as discussed in the introduction to this section, that after the short-period transients decay when the elevator and throttle are used to control ΔV and $\dot{h}$, $\Delta\alpha$ cannot be expected to follow model input commands. This again points out the "time-sharing" of the elevator in causing short-period $\Delta\alpha$ to follow $\Delta\alpha_m$ and long-period $\Delta\alpha$ to help in following ΔV_m and $\dot{h}_m$.

Consider the consequences of feeding ΔV and $\dot{V}$ to the elevator and $\dot{h}$ to the throttle as suggested in Reference 1. Let us assume for now that the short-period control loop gains δ_e/e_α or δ_e/e_{n_z} and $\delta_e/e_{\dot{\alpha}}$ are zero and account for their influence. The altitude loop and the forward loop integration on e_V are considered later, so $\Delta T/e_{\dot{h}} = 0$ and $\tau_V = \infty$ in Figure 2.1. The elevator and throttle command signals are given by equations 2.27 and 2.28.

$$\Delta\delta_e = \left(\frac{\delta_e}{e_V}\right)(\Delta V_c - \Delta V) + \left(\frac{\delta_e}{e_{\dot{V}}}\right)(\dot{V}_c - \dot{V}) \quad (2.27)$$

$$\Delta T = \frac{\Delta T}{e_{\dot{h}}}(\dot{h}_m - \dot{h}) \quad (2.28)$$

Equations 2.25 through 2.28 can be substituted into equations 2.23 and 2.24 and the resulting equations constitute a second-order system with undamped natural frequency and damping given by equations 2.29 and 2.30.

$$\omega_{\theta_p}^2 = \frac{Z_\theta\left[D_V - D'_{\delta_e}\left(\frac{\delta_e}{e_V}\right)\right] + V_t\left[\frac{g}{V_t} + \frac{1}{m}\left(\frac{\Delta T}{e_{\dot{k}}}\right)\right]\left[-\frac{Z_V}{V_t} + Z'_{\delta_e}\left(\frac{\delta_e}{e_V}\right)\right]}{1 - D'_{\delta_e}\left(\frac{\delta_e}{e_{\dot{V}}}\right)} \tag{2.29}$$

$$2\zeta_{\theta_p}\omega_{\theta_p} = \frac{Z_\theta\left[1 - D'_{\delta_e}\left(\frac{\delta_e}{e_{\dot{V}}}\right)\right] + D_V - D'_{\delta_e}\left(\frac{\delta_e}{e_V}\right) + V_t\left[\frac{g}{V_t} + \frac{1}{m}\left(\frac{\Delta T}{e_{\dot{k}}}\right)\right]\left[\frac{\alpha_t}{V_t} + Z'_{\delta_e}\left(\frac{\delta_e}{e_{\dot{V}}}\right)\right]}{1 - D'_{\delta_e}\left(\frac{\delta_e}{e_{\dot{V}}}\right)} \tag{2.30}$$

These equations can be simplified with little loss of accuracy by assuming that

$$\left.\begin{aligned} Z_\theta &\approx 0 \\ D'_{\delta_e}\left(\frac{\delta_e}{e_{\dot{V}}}\right) &\ll 1 \end{aligned}\right\} \tag{2.31}$$

Making these approximations, we note that when the feedback loops are open (i.e., $\delta_e/e_V = \delta_e/e_{\dot{V}} = \Delta T/e_{\dot{k}} = 0$), the unaugmented phugoid frequency is given by

$$\omega_{\theta_{p_0}}^2 = -\frac{g}{V_t} Z_V$$

This is an acceptable approximation for subsonic flight in most airplanes but loses considerable accuracy in transonic flight where the influence of M_V becomes large. A more accurate representation of phugoid frequency can be obtained by dividing the constant term of the exact fourth-order longitudinal characteristic equation by the square of the approximate short-period natural frequency, resulting in

$$\omega_{\theta_p}^2 = \frac{g\left[\frac{Z_V}{V_t} M_\alpha - M_V Z_\alpha\right]}{-M_\alpha + M_q Z_\alpha} \tag{2.32}$$

Now, since $M_q Z_\alpha \ll -M_\alpha$ for the JetStar, then

$$\frac{1}{-M_\alpha + M_q Z_\alpha} \approx -\frac{1}{M_\alpha}\left(1 + \frac{M_q Z_\alpha}{M_\alpha}\right)$$

Substituting this in equation 2.32, we get

$$\omega_{\theta_{p_0}}^2 = -\frac{g}{V_t}\left(Z_V - V_t M_V \frac{Z_\alpha}{M_\alpha}\right)\left(1 + \frac{M_q Z_\alpha}{M_\alpha}\right) \tag{2.33}$$

Equation 2.33 incorporates the effect of M_V on the phugoid frequency. We can conveniently compensate for Mach number effects on open-loop phugoid frequency by defining a new Z_V, as in equation 2.34.

$$Z'_V = \left(Z_V - V_t \frac{Z_\alpha}{M_\alpha} M_V\right)\left(1 + \frac{M_q}{M_\alpha} Z_\alpha\right) \tag{2.34}$$

The use of equation 2.34 predicts the phugoid divergence that exists when the JetStar is operated above Mach 0.75 without the Mach trim compensator. Incorporating Z'_V into the equations for the phugoid control loops insures proper representation of the phugoid dynamics throughout the GPAS flight envelope with the JetStar Mach trim compensator disabled. Substituting equations 2.31 and 2.34 into 2.29 and 2.30, we get:

$$\omega_{\theta_p}^2 = \left[g + \frac{V_t}{m}\left(\frac{\Delta T}{e_{\dot{k}}}\right)\right]\left[-\frac{Z'_V}{V_t} + Z'_{\delta_e}\left(\frac{\delta_e}{e_V}\right)\right] \tag{2.35}$$

$$2\zeta_{\theta_p}\omega_{\theta_p} = D_V - D'_{\delta_e}\left(\frac{\delta_e}{e_V}\right) + \left[g + \frac{V_t}{m}\left(\frac{\Delta T}{e_{\dot{k}}}\right)\right]\left[Z'_{\delta_e}\left(\frac{\delta_e}{e_{\dot{V}}}\right) + \frac{\alpha_t}{V_t}\right] \tag{2.36}$$

Equations 2.35 and 2.36 are the basic equations from which phugoid dynamics can be predicted.* All calculations in this report relating to the configuration of Figure 2.1 are based on equations 2.36 as shown herein. The gains $\Delta T/e_{\dot{k}}$ and δ_e/e_V both primarily influence phugoid frequency, and $\delta_e/e_{\dot{V}}$ primarily influences phugoid damping. Because three gains are required to specify the two quantities ω_{θ_p} and ζ_{θ_p}, two of the gains must be related so that when ω_{θ_p} and ζ_{θ_p} are specified, a unique set

---

*Strictly speaking, if Z_θ of equation 2.30 is neglected, then the α_t term should also be discarded. However, when actuator and sensor dynamics are neglected, somewhat more accurate results are obtained if α_t is retained. Discarding α_t, however, always results in gains $\delta_e/e_{\dot{V}}$ that are too large (ζ_{θ_p} too high) which is conservative when actuator and sensor dynamics are considered.

of feedback gains can be computed from equations 2.35 and 2.36. The two frequency adjusting gains can be related by equating static loop gains in the elevator and throttle loops. This is equivalent to an equal weighting of static errors in each of the two phugoid control loops, or assigning equal importance to model following of ΔV and $\dot{h}$. Expressed in equation form:

$$\frac{\delta_e}{e_V} \cdot \lim_{s \to 0} \left\{ \frac{\Delta V}{\Delta \delta_e}(s) \right\} = V_t \frac{\Delta T}{e_{\dot{h}}} \cdot \lim_{s \to 0} \left\{ \frac{\Delta \theta}{\Delta T}(s) - \frac{\Delta \alpha}{\Delta T}(s) \right\} \tag{2.37}$$

These steady-state transfer functions are tabulated for 18 flight conditions in appendix B where:

$$K_1 = \lim_{s \to 0} \left\{ \frac{\Delta V}{\Delta \delta_e}(s) \right\} \approx -V_t \frac{Z'_{\delta_e}}{Z'_V}$$

$$K_6 = \lim_{s \to 0} \left\{ \frac{\Delta \alpha}{\Delta T}(s) \right\} \approx 0$$

$$K_7 = \lim_{s \to 0} \left\{ \frac{\Delta \theta}{\Delta T}(s) \right\} \approx \frac{1}{mg}$$

If we define

$$k = \frac{K_1}{V_t (K_7 - K_6)} \tag{2.38}$$

then, from equation 2.37,

$$\frac{\Delta T}{e_{\dot{h}}} = k \frac{\delta_e}{e_V} \tag{2.39}$$

When equation 2.39 is substituted in equations 2.35 and 2.36 and they are solved simultaneously for δ_e/e_V and $\delta_e/e_{\dot{V}}$, we get:

$$\frac{\delta_e}{e_V} = -\frac{B}{2A} + \sqrt{\left(\frac{B}{2A}\right)^2 + \frac{C}{A}} \tag{2.40}$$

where:

$$A = \frac{V_t Z'_{\delta_e} k}{m}$$

$$B = g Z'_{\delta_e} - \frac{k}{m} Z'_V \qquad (2.41)$$

$$C = \omega_{sp}^2 + \frac{g}{V_t} Z'_V$$

$$\frac{\delta_e}{e_{\dot{V}}} = \frac{1}{Z'_{\delta_e}} \left\{ \frac{2\zeta_{sp}\omega_{sp} - D_V + D'_{\delta_e}\left(\frac{\delta_e}{e_V}\right)}{g + \frac{V_t}{m}\left(\frac{\Delta T}{e_{\dot{h}}}\right)} - \frac{\alpha_t}{V_t} \right\} \qquad (2.42)$$

Gains determined from equations 2.39, 2.40 and 2.42 produce, within acceptable tolerance, the desired phugoid frequency and damping as specified in Section 2.3.

In order to limit steady-state altitude and velocity errors to acceptable values for all GPAS flight conditions, forward loop integrations were added to the $\dot{h}$ and ΔV loops, as shown in Figure 2.1. The $\dot{h}$ integration was implemented by using a Δh control loop in the throttle channel. The integration was implemented by a low gain forward loop integrator. In both loops, the ratio of rate to position gain was determined by trial-and-error on the analog computer, and a value of 20 seconds* was used satisfactorily in the analog studies. These integrating loops tend to reduce the phugoid damping ratio below the nominal value, but do not degrade the model following. The Δh loop insures zero steady-state drift between model and Jet-Star altitudes.

*i.e., in Figure 2.1, $\frac{\Delta T/e_{\dot{h}}}{\Delta T/e_h} = 20$ sec, $\tau_v = 20$ sec

2.2.1 Modified Phugoid Control Loops

Phugoid MCS control loops where ΔV and $\dot{V}$ are fed to the elevator and $\dot{h}$ and $\ddot{h}$ are fed to the throttle do not perform satisfactorily in response to thrust commands to the model. The model-following responses of the JetStar to step changes of model thrust bear little resemblance to the model responses during the first seconds of the transient. The problem is primarily due to the high-frequency content of the model velocity and acceleration signals caused by sudden thrust changes and the fact that these signals ($\dot{V}_m$ and ΔV_m) are fed to the elevator channel of the JetStar. The sudden change in elevator position that occurs for a step change of model thrust creates a pitching moment disturbance which excites the JetStar short-period motions. This is illustrated by Figure 2.2, where the normal acceleration and angle of attack traces of the model and JetStar differ significantly for about forty-five seconds after application of the thrust command signal. The analog computer results indicate that this effect is not particularly large but is definitely noticeable to the pilot as a sudden change in normal acceleration.

The input in Figure 2.2 is a sudden reduction of model thrust by about 25%. In order to match the sudden change in $\dot{V}_m$ that results when the model thrust is rapidly reduced, if the JetStar elevator is used to effect changes in $\dot{V}$ of the JetStar, a sudden increase in JetStar angle of attack is required in order to decrease speed. This increase in angle of attack is apparent in Figure 2.2 and is not, of course, a feature of the $\Delta\alpha_m$ response. It also results in an initial error in $\ddot{h}$ due to the lift associated with the angle of attack change. In other words, when ΔV_m and $\dot{V}_m$ are fed to the JetStar elevator, it is not possible to follow model outputs that result from changes in model thrust without incurring significant errors for a sizable period of time after the input is applied to the model.

The only apparent "cure" to this problem is to rearrange the elevator and throttle MCS phugoid control loops, feeding ΔV and $\dot{V}$ to the throttle and $\ddot{h}$ to the elevator. In this manner, a change in throttle setting of the model results directly (through e_V) in a corresponding change in the

JetStar throttle position, which is the desired result. This is in contrast to the devious chain of events leading to a reduction of JetStar thrust when the control loops of Figure 2.1 are used.

Because we are interested in fixed-control phugoid dynamics to establish phugoid MCS control loop bandwidth, we study the closed-loop system that results from the following feedback equations, using the configuration of Figure 2.3.*

$$\Delta T = -\left(\frac{\Delta T}{e_V}\right)\Delta V - \left(\frac{\Delta T}{e_{\dot V}}\right)\dot V \tag{2.43}$$

$$\Delta\delta_e = -\left(\frac{\delta_e}{e_{\dot h}}\right)\dot h \tag{2.44}$$

Substituting equations 2.43 and 2.44 into equations 2.23 and 2.24, and also introducing the relation given by equations 2.25, 2.26, and 2.34, there results a second-order characteristic equation with the following natural frequency and damping:

$$\omega_{\theta_p}^2 = \frac{1}{m+\left(\frac{\Delta T}{e_{\dot V}}\right)}\left\{\left[mD_V+\left(\frac{\Delta T}{e_{\dot V}}\right)\right]\left[Z_\theta - V_t Z'_{\delta_e}\left(\frac{\delta_e}{e_{\dot h}}\right)\right] - mZ_V\left[\frac{g}{V_t} - D'_{\delta_e}\left(\frac{\delta_e}{e_{\dot h}}\right)\right]\right\} \tag{2.45}$$

$$2\zeta_{\theta_p}\omega_{\theta_p} = \frac{1}{m+\left(\frac{\Delta T}{e_{\dot V}}\right)}\left\{Z_\theta\left(\frac{\Delta T}{e_{\dot V}}\right) + mD_V + \left(\frac{\Delta T}{e_V}\right) - \left[\left(m+\frac{\Delta T}{e_{\dot V}}\right)V_t Z'_{\delta_e} + m\alpha_t D'_{\delta_e}\right]\left(\frac{\delta_e}{e_{\dot h}}\right)\right\} \tag{2.46}$$

Equations 2.45 and 2.46 contain three control loop gains which must be used to control two parameters, ω_{θ_p} and ζ_{θ_p}. There is no clear requirement for the gain $\Delta T/e_{\dot V}$ at this point, since it is $\dot h$ and ΔV that must be controlled. Hence, we assume a value of zero for $\Delta T/e_{\dot V}$ (at least until

*The gain $\delta_e/e_{\dot h}$ and the time constant τ_V are, as before, sufficient to insure satisfactory long-term flight-path matching without significantly influencing phugoid dynamics. The values used satisfactorily in the analog studies were $\frac{\delta_e}{\dot h}\Big/\frac{\delta_e}{h}$ = 20 sec and τ_V = 20 sec.

a requirement is established). Further, α_t and Z_θ are known to have little influence on phugoid dynamics from the previous phugoid loop studies, and they are neglected hereafter. After implementing these changes, equations 2.45 and 2.46 reduce to

$$\omega_{\theta_p}^2 = -\frac{g}{V_t} Z'_V + \left\{ Z'_V D'_{\delta_e} - V_t Z'_{\delta_e} \left[D_V + \frac{1}{m} \left(\frac{\Delta T}{e_V} \right) \right] \right\} \frac{\delta_e}{e_i} \tag{2.47}$$

$$2\zeta_{\theta_p} \omega_{\theta_p} = -V_t Z'_{\delta_e} \left(\frac{\delta_e}{e_i} \right) + D_V + \frac{1}{m} \left(\frac{\Delta T}{e_V} \right) \tag{2.48}$$

If we substitute equation 2.48 into equation 2.47, a quadratic equation in δ_e/e_i results, with the following solution.

$$\frac{\delta_e}{e_i} = -\frac{B}{2A} \pm \sqrt{\left(\frac{B}{2A} \right)^2 - \frac{C}{A}} \tag{2.49}$$

where $A = (V_t Z'_{\delta_e})^2 > 0$

$$B = 2\zeta_{\theta_p} \omega_{\theta_p} V_t Z'_{\delta_e} - Z_V D'_{\delta_e} \approx 2\zeta_{\theta_p} \omega_{\theta_p} V_t Z'_{\delta_e}$$

$$C = \omega_{\theta_p}^2 + g/V_t Z_V \approx \Delta \omega_{\theta_p}^2 > 0$$

and $\Delta\omega_{\theta_p}^2 = \omega_{\theta_p}^2 - \omega_{\theta_{p_o}}^2$

where $\omega_{\theta_{p_o}}$ is the open-loop JetStar value for the phugoid natural frequency. If equation 2.49 is used to solve for δ_e/e_i for arbitrary values of ζ_{θ_p} and ω_{θ_p}, one soon discovers that complex values of gain result if values of ζ_{θ_p} less than approximately one (critical damping) are assumed. This is because both $\Delta T/e_V$ and $\Delta T/e_i$ increase both phugoid frequency and damping simultaneously as is evident from equations 2.47 and 2.48 by inspection.* Using these two feedback gains it is not possible to reduce ζ_{θ_p} to 0.50, the design value as specified in Section 2.3. If, however, one accepts heavy damping ($\zeta > 1$) of the phugoid

---

* $\frac{\delta_e}{e_i} < 0$ and $\frac{\Delta T}{e_V} > 0$ increases $2\zeta_{\theta_p}\omega_{\theta_p}$ and ω_{θ_p}.

mode as satisfactory, the gain values necessary to achieve a desired value of closed-loop phugoid frequency can be easily determined. The procedure is to require a negative real solution of equation 2.49 for the gain $\delta_e/e_{\dot{h}}$, with the radical set equal to zero to obtain a minimum value for ζ_{θ_p}. The value of ζ_{θ_p} may be obtained from the equation

$$B^2 - 4AC = 0 \tag{2.50}$$

which is actually the discriminant of the quadratic equation for $\delta_e/e_{\dot{h}}$. Now $\delta_e/e_{\dot{h}}$ may be obtained from equation 2.49 and then $\Delta T/e_V$ from equation 2.48. Making use of the definitions from equation 2.49, and noting that $2\zeta_{\theta_p}\omega_{\theta_p} V_t Z'_{\delta_e} \gg Z'_V D'_{\delta_e}$ when $\zeta_{\theta_p} \approx 1$ the actual closed-loop phugoid damping ratio is given by equation 2.51.

$$\zeta_{\theta_p} = \sqrt{1 - \left(\frac{\omega_{\theta_{p_o}}}{\omega_{\theta_p}}\right)^2} = \frac{\sqrt{\Delta\omega_{\theta_p}^2}}{\omega_{\theta_p}} \tag{2.51}$$

Clearly, the greater the augmented phugoid frequency, the closer the phugoid damping ratio approaches unity. Since $B^2 - 4AC = 0$, equation 2.49 is easily solved for the value of $\delta_e/e_{\dot{h}}$ that results in the minimum closed-loop value of ζ_{θ_p} as given by equation 2.51. Thus,

$$\frac{\delta_e}{e_{\dot{h}}} = -\frac{B}{2A} = -\frac{\sqrt{\Delta\omega_{\theta_p}^2}}{VZ'_{\delta_e}} \quad \text{rad-sec/ft} \tag{2.52}$$

Substituting equations 2.51 and 2.52 into equation 2.48 yields the value of the remaining phugoid gain, $\Delta T/e_V$, given by equation 2.53.

$$\frac{\Delta T}{e_V} = m\left\{\sqrt{\Delta\omega_{\theta_p}^2} - D_V\right\} \quad \text{lb-sec/ft} \tag{2.53}$$

Equations 2.52 and 2.53 are the basic modified phugoid forward loop gain equations. Analog computer results indicate good accuracy in predicting phugoid dynamics using these equations as well as excellent phugoid and flight-path model following for both elevator and throttle commands to the model.

Gain values determined from these equations are listed in Table 2.1, along with the expected closed-loop JetStar phugoid damping ratio. A closed-loop phugoid frequency of $\omega_{\theta_p} = 0.3$ rad/sec is selected to provide adequate model following for the highest required phugoid frequency of the model. The JetStar data used in these calculations are listed in appendix A.

The modified phugoid loops perform satisfactorily without the use of a $\dot{V}$ control loop. However, this loop is incorporated in the GPAS system (electronics) in order to provide flexibility in the choice of phugoid control systems. The configuration of Figure 2.3 is shown in Section 4.1 to be superior (and less complex) than that of Figure 2.1. Accordingly, the system is designed according to Figure 2.3. However, it would be possible to convert it (by re-wiring) to the configuration of Figure 2.1.

2.2.2 Influence of Angle of Attack Feedback on Phugoid Loop Gains

In calculating short-period loop gains, valid approximations are that velocity is constant and that the phugoid loop gains do not influence the short-period loops. The converse is not true. When the short-period loops are closed, the angle of attack per unit commanded elevator deflection is significantly reduced by the greatly increased longitudinal stability provided by the angle of attack feedback. In order to maintain a constant loop gain for the phugoid elevator loops, the elevator command signal from the phugoid feedback terms must be made proportional to the $\Delta\alpha$ loop gain. This will insure that the actual incremental control surface deflections that result from the phugoid feedback signals will be the same regardless of the value of the $\Delta\alpha$ loop gain.

When angle of attack feedback is used, the steady-state closed-loop angle of attack per unit commanded control deflection is given by

$$\frac{\bar{\alpha}}{\delta_{e_c}} = \frac{1}{1 + \left(\frac{\delta_e}{e_\alpha}\right)\left(\frac{\bar{\alpha}}{\delta_e}\right)} \left(\frac{\bar{\alpha}}{\delta_e}\right) \qquad (2.54)$$

$\frac{\bar{\alpha}}{\delta_{e_c}}$ — closed loop

$\left(\frac{\bar{\alpha}}{\delta_e}\right)$ — open loop (eq. 2.21)

Referring to Figure 2.1, equation 2.54 is used to replace $\bar{\alpha}/\delta_e$ in equations 2.25 and 2.26, and if equation 2.27 is considered to represent the commanded value of incremental elevator deflection, then the phugoid loop gains determined by solving equations 2.40 and 2.42 can be compensated for angle of attack feedback by multiplying by the factor $1 + \left(\delta_e/e_\alpha\right)\left(\bar{\alpha}/\delta_e\right)$, that is:

$$\left.\frac{\delta_e}{e_v}\right)_{\substack{\Delta\alpha \text{ LOOP} \\ \text{CLOSED}}} = \left.\frac{\delta_e}{e_v}\right)_{\substack{\Delta\alpha \text{ LOOP} \\ \text{OPEN}}} \cdot \left[1 + \left(\frac{\delta_e}{e_\alpha}\right)\left(\frac{\bar{\alpha}}{\delta_e}\right)\right] \tag{2.55}$$

$$\left.\frac{\delta_e}{e_{\dot{v}}}\right)_{\substack{\Delta\alpha \text{ LOOP} \\ \text{CLOSED}}} = \left.\frac{\delta_e}{e_{\dot{v}}}\right)_{\substack{\Delta\alpha \text{ LOOP} \\ \text{OPEN}}} \cdot \left[1 + \left(\frac{\delta_e}{e_\alpha}\right)\left(\frac{\bar{\alpha}}{\delta_e}\right)\right] \tag{2.56}$$

The throttle channel has no short-period feedback loops, and the gain $\Delta T/e_{\dot{h}}$ is used directly as determined from equations 2.39 and 2.40.

In like manner, the phugoid gain $\delta_e/e_{\dot{h}}$ of Figure 2.3 is compensated for angle of attack feedback by using equation 2.57. Numerical values for the JetStar are listed in Table 2.1.

$$\left.\frac{\delta_e}{e_{\dot{h}}}\right)_{\substack{\Delta\alpha \text{ LOOP} \\ \text{CLOSED}}} = \left[1 + \left(\frac{\bar{\alpha}}{\delta_e}\right)\frac{\delta_e}{e_\alpha}\right] \cdot \left.\frac{\delta_e}{e_{\dot{h}}}\right)_{\substack{\Delta\alpha \text{ LOOP} \\ \text{OPEN}}} \tag{2.57}$$

The throttle gain $\Delta T/e_v$ is not influenced by elevator control loops.

2.2.3 Influence of Normal Acceleration Feedback On Phugoid Loop Gains

A similar situation exists for the case of combined Δn_{z_α} short-period and phugoid loops. As shown in equation 2.2, the normal accelerometer senses incremental angle of attack, elevator displacement, velocity, and perhaps pitch acceleration. If we neglect elevator actuator dynamics* and assume that $\dot{\alpha}$ and $\dot{q}$ feedback signals do not influence the phugoid mode, then the elevator feedback signal is composed of the terms in

*considered in appendix C.

equation 2.58.

$$\Delta\delta_e = -\left(\frac{\delta_e}{e_{n_z}}\right)\Delta n_{z_\alpha} - \left(\frac{\delta_e}{e_V}\right)\Delta V - \left(\frac{\delta_e}{e_{\dot{V}}}\right)\dot{V} \qquad (2.58)$$

Substituting equation 2.2 for Δn_{z_α} (without the $\dot{q}$ term) and rearranging, we get

$$\left[1 + \frac{V_t}{g} Z_{\delta_e} \frac{\delta_e}{e_{n_z}}\right]\Delta\delta_e = -\frac{V_t}{g} Z_\alpha \left(\frac{\delta_e}{e_{n_z}}\right)\Delta\alpha - \left[\frac{Z_V}{g}\left(\frac{\delta_e}{e_{n_z}}\right) + \frac{\delta_e}{e_V}\right]\Delta V - \left(\frac{\delta_e}{e_{\dot{V}}}\right)\dot{V} \qquad (2.59)$$

Assuming incremental angle of attack instantly proportional to elevator control deflection, the term $\Delta\alpha$ can be replaced by $\left(\bar{\alpha}/\delta_e\right)\Delta\delta_e$. Making this substitution and solving for $\Delta\delta_e$, we get:

$$\left[1 + \frac{V_t}{g}\left(\frac{\delta_e}{e_{n_z}}\right)\left(Z_{\delta_e} + \frac{\bar{\alpha}}{\delta_e} Z_\alpha\right)\right]\Delta\delta_e = -\left[\frac{Z_V}{g}\left(\frac{\delta_e}{e_{n_z}}\right) + \left(\frac{\delta_e}{e_V}\right)\right]\Delta V - \left(\frac{\delta_e}{e_{\dot{V}}}\right)\dot{V} \qquad (2.60)$$

Two significant effects of Δn_{z_α} feedback on the elevator phugoid control loops are evident. They are: 1) a portion of the ΔV feedback signal is derived from the accelerometer, and 2) the phugoid loop gains δ_e/e_V and $\delta_e/e_{\dot{V}}$ must be increased as a function of δ_e/e_{n_z} in order to maintain constant elevator phugoid loop gain. Considering equation 2.60 first without Δn_{z_α} feedback, and second with this feedback, it is easily shown that

$$\left(\frac{\delta_e}{e_V}\right)_{\substack{\Delta n_z \text{ LOOP} \\ \text{CLOSED}}} = \left(\frac{\delta_e}{e_V}\right)_{\substack{\Delta n_z \text{ LOOP} \\ \text{OPEN}}} \cdot \left[1 + \frac{V_t}{g}\left(\frac{\delta_e}{e_{n_z}}\right)\left(Z_{\delta_e} + \frac{\bar{\alpha}}{\delta_e} Z_\alpha\right)\right] - \frac{Z_V}{g}\left(\frac{\delta_e}{e_{n_z}}\right) \qquad (2.61)$$

$$\left(\frac{\delta_e}{e_{\dot{V}}}\right)_{\substack{\Delta n_z \text{ LOOP} \\ \text{CLOSED}}} = \left(\frac{\delta_e}{e_{\dot{V}}}\right)_{\substack{\Delta n_z \text{ LOOP} \\ \text{OPEN}}} \cdot \left[1 + \frac{V_t}{g}\left(\frac{\delta_e}{e_{n_z}}\right)\left(Z_{\delta_e} + \frac{\bar{\alpha}}{\delta_e} Z_\alpha\right)\right] \qquad (2.62)$$

The open-loop values of δ_e/e_V and $\delta_e/e_{\dot{V}}$ are, of course, computed from equations 2.40 and 2.42.

Since Z_V is always negative, the normal acceleration contribution to the ΔV feedback in equation 2.61 is a positive quantity and always requires an increase in the value of δ_e/e_V to restore loop gain to its proper value. The factor $1 + \frac{V_t}{g}\left(\frac{\delta_e}{e_{n_z}}\right)\left(Z_{\delta_e} + \frac{\bar{\alpha}}{\delta_e} Z_\alpha\right)$ represents the increase in

longitudinal stability provided by the Δn_{z_x} feedback that must be overcome by increasing the gains δ_e / e_V and $\delta_e / e_{\dot{V}}$.

In a similar manner, it can be shown that the influence of Δn_{z_x} feedback on the modified elevator phugoid loop gain $\delta_e / e_{\dot{h}}$ is accounted for by using equation 2.63.

$$\left.\frac{\delta_e}{e_{\dot{h}}}\right)_{\substack{\Delta n_z \text{ LOOP} \\ \text{CLOSED}}} = \left[1 + \frac{V_t}{g}\left(Z_{\delta_e} + \frac{\bar{\alpha}}{\delta_e} Z_\alpha\right) \frac{\delta_e}{e_{n_z}}\right] \cdot \left.\frac{\delta_e}{e_{\dot{h}}}\right)_{\substack{\Delta n_z \text{ LOOP} \\ \text{OPEN}}} \qquad (2.63)$$

The influence of the ΔV portion of the accelerometer signal on the closed-loop JetStar phugoid dynamic using the modified phugoid loops is negligible. Table 2.1 lists values of $\delta_e / e_{\dot{h}}$ with the Δn_z loop closed. Equation 2.61 through 2.63 hold for any accelerometer location.

2.3 CLOSED-LOOP DYNAMICS

In order to satisfy the requirements of the GPAS work statement insofar as longitudinal model following is concerned, the following approximate closed-loop natural frequencies and damping ratios should be provided:

1.	Short-period dynamics	ω_{θ_s}	= 9 rad/sec
		ζ_{θ_s}	= 0.5
2.	Phugoid dynamics	ω_{θ_p}	= 0.3 rad/sec
		ζ_{θ_p}	= 0.5

Based on these values, techniques described in Sections 2.1 and 2.2, and data from appendix A, the closed-loop gains listed in Table 2.1 and 2.2 were computed. The influence of the short-period loops on the phugoid calculations were based on a c.g. - mounted accelerometer. Other accelerometer locations are considered in appendix C and Section 4.1.

Using the loop gains for the longitudinal GPAS control loops of Figure 2.1 as listed in Table 2.2 ($\Delta\alpha$, ΔV, and $\dot{h}$, feedback loops with $\dot{\alpha}$ and $\dot{V}$ compensation) and actuator dynamics (ω_η = 44 rad/sec, ζ = 0.7 for the elevator; ω_η = 4 rad/sec, ζ = 0.5 for the throttle), the exact

closed-loop transfer functions were calculated (by digital computer) for five flight conditions. The resulting closed-loop augmented short-period and phugoid natural frequencies and damping ratios are plotted in Figure 2.4 along with the desired values of each. The results show that the methods for calculating the gain as developed in this report are adequate when $\Delta\alpha$ feedback is used. It is evident from Figure 2.4 that the errors introduced by neglecting certain terms in the approximate equations or by omitting actuator dynamics, are not serious and primarily result in a loss of damping ratio relative to the desired value of 0.5 for both short-period and phugoid modes. However, when an n_{z_α} control loop is used, the effect of actuator dynamics is large on the closed-loop short-period damping and further consideration (Appendix D) must be given to the calculation of the $\delta_e/e_{\dot{\alpha}}$ gain.

A typical closed-loop JetStar response to a unit step in the elevator command signal is presented in Figure 2.5. It is evident that the closed-loop longitudinal dynamics are almost exactly the desired values for both short-period and phugoid modes. Figure 2.5 was obtained from solving linear perturbation equations. Similar results were obtained for the five flight conditions of Figure 2.4 when using total force equations in the JetStar simulation (Section 4.1).

2.4 LONGITUDINAL CONTROL LOOP CONFIGURATION

The functional requirements for the MCS and RFS control loops are set forth in Reference 3, paragraph 2.1. Functional block diagrams of the control loops for the four JetStar controls (elevator, throttle, aileron, and rudder), designed to comply with the requirements, are presented in Figures 2.6, 2.7, 3.2, and 3.3. A brief description of the longitudinal control loops is given below. The lateral-directional control loops are discussed in Section 3.3.

2.4.1 Elevator Channel Functional Block Diagram (Figure 2.6)

The elevator is used primarily to effect model-following of short-period variables (angle of attack or normal acceleration) and one phugoid variable

(rate of climb). When using the RFS, the elevator is the only longitudinal control.

The primary elevator MCS control loops are h , $\dot{h}$, and $\Delta\alpha$ or Δn_{z_c}. In addition, the results of the preliminary design show the clear need for an $\dot{\alpha}$ feedback loop to damp the closed-loop short-period and for an $\dot{\alpha}_m$ model input to reduce phase lags in the following of short-period variables. In the normal acceleration loop, provision is made for using either c. g. or cockpit normal acceleration as the feedback quantity. Pitch acceleration compensation is provided in the acceleration loop. The q and $\Delta\theta$ loops are provided for only in the context of future system expansion as directed by Reference 3, paragraph 2.1.5. The altitude loop is provided to prevent long term deviation between model and JetStar altitudes and to limit altitude errors to reasonable values after long approach or climb-out simulations.

The RFS control loops shown in Figure 2-6 are those called out in Reference 3, paragraph 2.1.6.1. The RFS gains are shown as shaded blocks in all three control surface loops. Switching is provided to select the MCS loops, or the RFS loops, or both as required by Reference 3, paragraph 2.1.9.

In general, each MCS control loop consists of an input gain control, a summing amplifier, an electrical filter, a function generator, and a forward-loop gain control. The input gain control is nominally set to unity for one-to-one model following and something other than unity for scaled model following (a range from zero to two is provided in all cases). The input summing amplifier compares the scaled desired value (model) with the actual value (JetStar) of the variable and forms the error in the control loop. Provisions are made to pass the error signal through an electrical filter, as the need for such filters develops in the future for bending mode or other forward-loop compensation, and into the function generator. The function generator is used to automatically adjust the level of forward-loop gain as a function of certain aircraft properties in order to maintain closed-loop frequencies, damping ratios, and static gain at appropriate levels throughout the JetStar

flight envelope. The function generators implement the gain programs discussed in Section 2.5 below. The output of the function generator passes through a level control that establishes the loop gain for some reference flight condition (all gain changes in the function generator are referred to this value).

The output signals from all MCS and RFS control loops are summed to form the command signal to the elevator simulation servo system (SSS). Also included in this command signal are elevator wheel position and force command signals for use with the RFS. The horizontal stabilizer position is fed into the elevator command signal so that the automatic trim balance system (Reference 4) can operate without changing the pitching moment balance on the JetStar. The automatic trim is needed to prevent dangerous transients when the variable stability system is disengaged. Without the pitching moment balance feature, the trim system would introduce spurious pitching motion which could disturb the test pilot during certain simulations. Also provided is a balance servo to insure that the elevator SSS engages smoothly. A limiter is provided to limit the elevator control surface authority as required by Reference 3, paragraph 3.2.2. The output of the limiter ($\bar{\delta}_{e_c}$) is the command signal to the elevator control surface servo.

2.4.2 Throttle Channel Functional Block Diagram (Figure 2.7)

The throttle channel, in combination with the elevator channel, controls the longitudinal phugoid mode and flight path behavior of the JetStar. The throttle is primarily responsible for controlling speed through the ΔV control loop. The $\dot{V}$ loop is provided because the original phugoid control system required it. The current design does not use this loop, but its presence in the system is desirable to provide flexibility (see Section 2.2.1). No RFS loops or control authority limits are used with the throttle control system. The thrust command signal, ΔT_c , is fed to a set of throttle servos which directly control net thrust. This direct command or control of thrust is obtained by converting thrust to engine pressure ratio (using an altitude function generator) and then positioning the throttles to obtain the commanded

engine pressure ratio by means of an integrating throttle control loop employing measured engine pressure ratio as the feedback (Reference 9).

2.5 LONGITUDINAL CONTROL LOOP GAIN SCHEDULING

In Reference 5, plots of MCS control loop gains necessary to achieve certain specific control loop bandwidths are presented. These plots resulted from calculation procedures described in Sections 2 and 3. The philosophy behind the calculations leading to these gain programs was to determine gain levels necessary for the desired closed-loop bandwidth, with all loops closed simultaneously, and without regard to the realizability of these gains in flight. The calculated MCS gains are primarily functions of dynamic pressure, or aircraft weight, or both. It was hoped that the maximum gain levels computed in this fashion would be less than or equal to gain levels in similar loops actually achieved in practice with CAL variable stability aircraft. This was not the case, and further work was necessary to estimate maximum gain levels that can be achieved in practice, and the effect of gain reductions on the model-following performance of the JetStar. Accordingly, a study was performed to estimate maximum gain levels attainable for both MCS and RFS operations. The results of this study are presented in Section 5.1.

If we assume that the gain levels listed in Table 5.1 are representative limit values that can be achieved in the JetStar, it is possible to modify the gain programs of Reference 5 by simply limiting the gains to these values when the program calls for larger values, and supplying the desired levels when the program values are less than the limit values. It is emphasized that these gain limits are estimated so that gain programming capability is provided in all channels where the original work required it, even if the gain programs call for levels exceeding the maximum estimated gains throughout most or all of the flight envelope. If the estimated limits should prove to be pessimistic, the system as constructed will be capable of operating with higher gains and proper scheduling.

The longitudinal gain schedules for δ_e/e_α, $\delta_e/e_{\dot\alpha}$, $\delta_e/e_{\dot\gamma}$, $\Delta T/e_V$, and δ_e/e_{n_z} are presented in Figures 2.8 to 2.12. Since the original gain schedules were presented in Reference 5, it was decided to modify the phugoid control loops in accordance with Figure 2.3 and to delete the model-following loop for dynamic pressure. Accordingly, the gains δ_e/e_V, $\delta_e/e_{\dot V}$, $\delta_e/e_{\bar q}$, and $\Delta T/e_{\dot\gamma}$ are not plotted in this report. If they should ever be required, they are listed correctly in Table 2.2. The gains associated with the modified phugoid loops are $\delta_e/e_{\dot\gamma}$, δ_e/e_h, and $\Delta T/e_V$. The altitude error gain δ_e/e_h is always .05 $\delta_e/e_{\dot\gamma}$ as noted in Section 2.2.1.

In the gain scheduling plots for δ_e/e_α and $\delta_e/e_{\dot\alpha}$ (Figures 2.8 and 2.9), the unlimited as well as the limited control system gains are shown. This provides information on both the desired level of gain and the estimated limit gain in a single plot for each channel. The unlimited values are from Tables 2.1 and 2.2. The gain limits are from Table 5.1.

The gain schedule for $\delta_e/e_{\dot\gamma}$ depends on the level of the gains δ_e/e_α or δ_e/e_{n_z}, depending on whether a $\Delta\alpha$ or a Δn_z loop is used for matching short-period dynamics. Figure 2.10(a) shows the gain schedule of $\delta_e/e_{\dot\gamma}$ with the $\Delta\alpha$ or Δn_z loop open. This gain schedule is needed in order to compute the proper gain schedule, using equations 2.56 or 2.63, with the $\Delta\alpha$ or Δn_z loop closed. Figure 2.10(b) shows the gain schedule of $\delta_e/e_{\dot\gamma}$ computed from equation 2.56 using (1) the unlimited values of the gain δ_e/e_α and (2) the estimated limit value of δ_e/e_α = 10. Similarly, Figure 2.10(c) shows the gain schedule of $\delta_e/e_{\dot\gamma}$ computed from equation 2.63 using (1) the unlimited δ_e/e_{n_z} and (2) the limit value of δ_e/e_{n_z} = 10 deg/g. If these estimated limit values should prove to be correct, as determined from flight test, then the $\delta_e/e_{\dot\gamma}$ gain schedules given in Figures 2.10(b) and 2.10(c) should be used as plotted (i.e., combination of unlimited plus limit values).

The level of normal acceleration gain δ_e/e_{n_z} was computed in three ways. The values in Table 2.2, based on unlimited gain, are very large and certainly not realizable for the medium and low dynamic pressure flight conditions. The second method was to compute δ_e/e_{n_z} based on values of $P_\alpha = -\delta_e/e_\alpha$

limited to 10, using equation 2.19. The resulting acceleration gains, while somewhat less than the unlimited values, are still considerably larger than the estimated gain limit of 10 deg/g. Consequently, the estimated acceleration loop gain schedule is given by the 10 deg/g limit line in Figure 2.12. The short-period damping gain schedule for $\delta_e/e_{\dot{\alpha}}$ as given in Figure 2.9 should be used with the δ_e/e_{n_z} loop as well as the δ_e/e_{α} loop. The rationale for using the same gain schedule of $\delta_e/e_{\dot{\alpha}}$ for both $\Delta\alpha$ and Δn_z loops is developed in Appendix D, but in summary, it evolves from the need for additional damping when the effect of actuator lags is taken into account when using a Δn_z loop.

SECTION 3

DESIGN OF LATERAL-DIRECTIONAL MCS CONTROL LOOPS

The techniques and calculations used to compute gains for the aileron and rudder MCS control loops are discussed in this section. As in the case of the longitudinal MCS control loops, the desired results are expressed in terms of closed-loop bandwidth and damping rather than steady-state gain. The influence of control system dynamics is neglected in order to develop design equations but is incorporated in the analog computer simulation work described in Section 4 and in Appendix C. The control loop configurations are illustrated in Figure 3.1.

3.1 ANALYSIS OF RUDDER CONTROL LOOPS

The rudder MCS control loops use β or n_{y_x} feedback to increase the Dutch roll frequency of the JetStar and $\dot{\beta}$ feedback to damp this mode. An analysis similar to that of Section 2.1 is presented below in order to allow the gains δ_r/e_β or δ_r/e_{n_y} and $\delta_r/e_{\dot{\beta}}$ to be computed given the open-loop characteristics of the JetStar and a desired Dutch roll natural frequency and damping ratio. According to Reference 3, paragraph 1.5.1.2, the JetStar must be capable of following a model with ω_{ψ_m} = 5 rad/sec and ζ_{ψ_m} = 0.1. Applying a 1.5 bandwidth factor and a reasonable damping criteria results in closed-loop JetStar Dutch roll requirements of ω_ψ = 7.5 rad/sec and ζ_ψ = 0.5.

3.1.1 Dutch Roll Natural Frequency, ω_ψ

There are several approximations relating the Dutch roll natural frequency to stability derivatives (Appendix B, Equation B.2-2).

Approximation 1 $\omega_\psi^2 = C$

C is the exact coefficient of s^2 in the fourth-order lateral-directional characteristic equation.

Approximation 2 $\omega_\psi^2 = C'$

C' is the approximate value of C:

$$C' = N_\beta + Y_\beta (N_r + L_p) + L_p N_r - N_p L_r$$

Approximation 3 $\omega_\psi^2 = N_\beta$

To determine which approximation was best for closed-loop gain calculations, each of the three equations given above were applied to the open-loop JetStar and the results compared with the actual value of natural frequency determined by digital computation. Approximation 1 was best for 5, Approximation 2 was best for 7, and Approximation 3 was best for 6 of the 18 flight conditions. Based on these results, it was decided to use Approximation 3 since it is the simplest equation:

$$\omega_\psi^2 = N_\beta \tag{3.1}$$

In equation 3.1, N_β is the closed-loop value of directional stability. The closed-loop value of this derivative can be written in terms of the open-loop or basic airframe directional stability plus the increment due to directional control:

$$N_\beta = N_{\beta_o} - N_{\delta_r} \frac{\delta_r}{e_\beta} \tag{3.2}$$

where N_{β_o} = open-loop directional stability, sec^{-2}

N_{δ_r} = directional control derivative, sec^{-2}

δ_r / e_β = control system gain.

Solving for δ_r / e_β, we get

$$\frac{\delta_r}{e_\beta} = \frac{\omega_\psi^2 - N_{\beta_o}}{-N_{\delta_r}} \tag{3.3}$$

Table 3. 1 shows the computed gains using equation 3. 3 and data from Appendix A for flight conditions throughout the JetStar flight envelope. Direct calculation of Dutch roll frequency using these gains and the exact equations on a digital computer show the actual Dutch roll frequency to be in the range from 7. 29 to 7. 55 rad/sec.

When a lateral acceleration loop is used instead of a sideslip angle loop, the rudder will respond to the error signal in lateral acceleration. The gain δ_r / e_{n_Y} can be related to the already calculated values of δ_r / e_β as described below. When sideslip angle feedback is used, the fixed-control equation describing rudder motions is

$$\delta_r = -\frac{\delta_r}{e_\beta}\beta - \frac{\delta_r}{e_{\dot\beta}}\dot\beta \tag{3.4}$$

The lateral accelerometer* reads

$$n_Y = \frac{V_t}{g}\left[Y_{\beta_0}\beta + Y_{\delta_r}\delta_r\right] \tag{3.5}$$

Using lateral acceleration feedback to control Dutch roll frequency and sideslip rate feedback to control Dutch roll damping, the fixed control rudder motions are given by equation 3. 6

$$\delta_r = -\frac{\delta_r}{e_{n_Y}} n_Y - \frac{\delta_r'}{e_{\dot\beta}}\dot\beta \tag{3.6}$$

In this equation, the prime indicates that the Dutch roll damping gain associated with the lateral acceleration loop differs from that associated with the sideslip angle loop. Combining equations 3. 5 and 3. 6 results in

*Accelerometer locations other than the c. g. are considered in Appendix C.

$$\delta_r = -\left\{ \frac{\frac{V_t}{g} Y_{\beta_o} \left(\frac{\delta_r}{e_{n_Y}} \right)}{1 + \frac{V_t}{g} Y_{\delta_r} \left(\frac{\delta_r}{e_{n_Y}} \right)} \right\} \beta - \left\{ \frac{\frac{\delta'_r}{e_{\dot{\beta}}}}{1 + \frac{V_t}{g} Y_{\delta_r} \left(\frac{\delta_r}{e_{n_Y}} \right)} \right\} \dot{\beta} \quad (3.7)$$

Equating coefficients in equations 3.4 and 3.7 and solving for $\delta'_r/e_{\dot{\beta}}$ and δ_r/e_{n_Y} in terms of $\delta_r/e_{\dot{\beta}}$ and δ_r/e_{β}, we get

$$\frac{\delta'_r}{e_{\dot{\beta}}} = \frac{Y_{\beta_o} \left(\frac{\delta_r}{e_{\dot{\beta}}} \right)}{Y_{\beta_o} - Y_{\delta_r} \left(\frac{\delta_r}{e_{\beta}} \right)} \quad (3.8)$$

$$\frac{\delta_r}{e_{n_Y}} = \frac{V_t}{g} \cdot \frac{\left(\frac{\delta_r}{e_{\beta}} \right)}{Y_{\beta_o} - Y_{\delta_r} \left(\frac{\delta_r}{e_{\beta}} \right)} \quad (3.9)$$

Thus, once values of δ_r/e_{β} and $\delta_r/e_{\dot{\beta}}$ are calculated for the β loops, the n_Y loop gains follow immediately from equations 3.8 and 3.9. The gains δ_r/e_{n_Y} and $\delta'_r/e_{\dot{\beta}}$ listed in Table 3.1 are calculated in this manner.

3.1.2 Dutch Roll Damping Ratio - ζ_ψ

If one assumes rudder motions given by $\delta_r = -\delta_r/e_{\dot{\beta}} \dot{\beta}$ and substitutes for δ_r in the lateral-directional equations in Section A.1.2 of Appendix A, the resulting characteristic equation is fourth-order in the Laplace transform variable s. Neglecting α_t and I_{xz}, the coefficients of the fourth and

third power terms are

$$s^4 \rightarrow A = 1 + Y_{\delta_r}\left(\frac{\delta_r}{e_{\dot{\beta}}}\right) \tag{3.10}$$

$$s^3 \rightarrow B = -Y_\beta - N_r - L_p - \left[N_{\delta_r} + Y_{\delta_r}(N_r + L_p)\right]\frac{\delta_r}{e_{\dot{\beta}}} \tag{3.11}$$

The characteristic equation factors into the Dutch roll, spiral, and roll subsidence modes as shown in equation 3.12.

$$\left(s + \frac{1}{\tau_R}\right)\left(s + \frac{1}{\tau_S}\right)\left(s^2 + 2\zeta_\psi \omega_\psi s + \omega_\psi^2\right) = 0 \tag{3.12}$$

From equation 3.12,

$$\frac{B}{A} = 2\zeta_\psi \omega_\psi + \frac{1}{\tau_S} + \frac{1}{\tau_R} \tag{3.13}$$

By assuming that $1/\tau_S$ is negligible and that $1/\tau_R = -L_p$, we can combine equations 3.10, 3.11, and 3.13 to get

$$\frac{\delta_r}{e_{\dot{\beta}}} = -\frac{2\zeta_\psi \omega_\psi + N_r + Y_\beta}{N_{\delta_r} + Y_{\delta_r}(N_r + 2\zeta_\psi \omega_\psi)} \tag{3.14}$$

The value of Y_β in equation 3.14 is sensitive to the gain δ_r/e_β because Y_{δ_r} is not zero. Taking this fact into account, the design equation for the Dutch roll damping gain is

$$\frac{\delta_r}{e_{\dot{\beta}}} = -\frac{2\zeta_\psi \omega_\psi + N_r + Y_{\beta_o} - Y_{\delta_r}\left(\delta_r/e_\beta\right)}{N_{\delta_r} + Y_{\delta_r}(N_r + 2\zeta_\psi \omega_\psi)} \tag{3.15}$$

For reasonably large values of ζ_ψ and ω_ψ, the N_r term in the denominator of equation 3.15 can be neglected. The values of $\delta_r/e_{\dot{\beta}}$ and $\delta_r'/e_{\dot{\beta}}$ listed in Table 3.1 were computed based on $2\zeta_\psi \omega_\psi \gg N_r$. If yaw rate feedback (through δ_r/r) is used to augment Dutch roll damping, the derivative N_r in equation 3.15 is the augmented value.

It should be noted that the equation for Dutch roll damping gain on page 4 of Reference 6 is incorrect and should be replaced by equation 3.15. The Dutch roll damping gain schedules in Reference 6 are also incorrect. Correct plots are presented in Figure 3.5 and 3.8 of this report.

3.2 ANALYSIS OF AILERON CONTROL LOOPS

The aileron control loops use p and ϕ feedback to the aileron to achieve desirable values of the roll subsidence and spiral mode time constants τ_R and τ_S. Because Reference 3, paragraph 1.5.1.2 requires that the JetStar be capable of following a model with $\tau_{R_m} = 0.10$ sec, the 1.5 bandwidth factor requires that $\tau_R = 0.067$ sec for the closed-loop JetStar. In addition, because long term model following is desired, the spiral mode must be stable.

3.2.1 Roll Mode Time Constant, τ_R

A good approximation to the roll mode time constant can be obtained from the equation $\frac{1}{\tau_R} \cong -L_p$

By substituting $L_p = L_{p_o} - L_{\delta_a} \delta_a/e_p$ and solving for δ_a/e_p, we get

$$\frac{\delta_a}{e_p} = \frac{1/\tau_R + L_{p_o}}{L_{\delta_a}} \tag{3.16}$$

To indicate the accuracy of the equation $1/\tau_R \cong -L_p$, Table 3.2 shows the actual values of $1/\tau_R$ and L_p for the open-loop airplane. The approximation is quite good. Table 3.1 shows the values of δ_a/e_p estimated to give a value of $\tau_R = .067$ sec.

3.2.2 Spiral Mode Time Constant, τ_S

There is no simple expression which relates the spiral mode to a given control system gain. The equation

$$\frac{1}{\tau_S} = \frac{E}{D}$$

is a good approximation if exact values of the coefficients E and D (Appendix B, Equation B.2-2) from the characteristic equation are used. All of the control gains contribute to changes in E and D and therefore the spiral root. The coefficient E is usually small and can be either positive or negative, thereby influencing the stability of the spiral mode. The coefficient D is usually much larger than E and rarely changes sign; it contributes only to the magnitude of the spiral time constant.

Numerical calculations indicate that changes in E are primarily influenced by a term containing the product of the gains δ_a/e_ϕ and δ_r/e_β. The gain δ_r/e_β acting by itself will destabilize the spiral mode, but the two gains acting together have a strong stabilizing effect.

Table 3.3 compares the exact change in E with that given by the expression:

$$\Delta E \cong \frac{\delta_a}{e_\phi} \cdot \frac{\delta_r}{e_\beta} L_{\delta_a} \left[-N_{\delta_r} (1+\alpha_t^2) + Y_{\delta_r} (\alpha_t N_p - N_r) \right] \geq 0 \quad (3.17)$$

The change in E is defined as $\Delta E = E_{\substack{\text{CLOSED} \\ \text{LOOP}}} - E_{\substack{\text{OPEN} \\ \text{LOOP}}}$

The coefficient D is also primarily influenced by two control gains, namely δ_a/e_p and δ_r/e_β. These two gains occur in a term which accounts for approximately 90% of the change in the magnitude of D between the open- and closed-loop values. Since these gains make D more positive, they tend to reduce the magnitude of the spiral root and move it closer to the origin. The approximate change in D due to δ_a/e_p and δ_r/e_β is given by equation 3.18.

$$\Delta D \cong \left[N_{\beta_o} L_{\delta_a} \frac{\delta_a}{e_p} + L_{p_o} N_{\delta_r} \frac{\delta_r}{e_\beta} - L_{\delta_a} N_{\delta_r} \frac{\delta_a}{e_p} \cdot \frac{\delta_r}{e_\beta} \right] \quad (3.18)$$

To insure a reasonable level of spiral stability and acceptable bank angle following, the gain δ_a/e_ϕ was taken as one-tenth of the gain δ_a/e_p as suggested in preliminary analysis of Reference 1. Presence of the gain δ_a/e_ϕ insures spiral stability. Table 3.4 lists the spiral roots ($-1/\tau_s$) for the closed-loop JetStar using $\delta_a/e_\phi = 1/10\ \delta_a/e_p$ and the values of δ_r/e_β

listed in Table 3.1. In forming Table 3.4 the gain δ_a/e_ρ was selected to give τ_R = 0.10 sec, and these numbers were not recalculated when τ_R was reduced to 0.067 sec.

3.3 LATERAL-DIRECTIONAL CONTROL LOOP CONFIGURATION

The functional requirements for the lateral-directional control loops are established in Reference 3, paragraph 2.1. In order to comply with these requirements, functional block diagrams of the over-all system were prepared, with outputs from each channel commanding an appropriate force or moment producing device of the JetStar. The lateral-directional channels are discussed below. The longitudinal channels are discussed in Section 2.4.

3.3.1 Rudder Channel Functional Block Diagram (Figure 3.2)

The rudder channel contains the MCS and RFS control loops required by paragraphs 2.1.1 and 2.1.6.2 of Reference 3. The rudder MCS loops are used to control β or n_{Y_ρ}, with the $\dot{\beta}$ loop used for Dutch roll damping in either case. In addition, a yaw rate loop is shown for future expansion. A choice of c. g. or cockpit acceleration is provided in the lateral acceleration loop, and yaw acceleration compensation is included in this loop. Rudder pedal position and force signals are provided for use with the RFS. The aileron cross-coupling term used with the RFS provides a ready means for changing the basic airplane roll-to-yaw control coupling. A balance servo and authority limiter is provided for the command signal to the SSS.

3.3.2 Aileron Channel Functional Block Diagram (Figure 3.3)

The aileron channel contains the MCS and RFS loops required by paragraph 2.1.1 and 2.1.6.3 of Reference 3. The aileron MCS loops are used to control ρ and ϕ, with no future expansion loops required. Aileron wheel position and force signals are provided for use with the RFS mode of operation. The rudder cross-coupling term used with the RFS provides a ready means for changing the basic airplane yaw-to-roll control coupling. A

balance servo and authority limiter is provided for the command signal to the aileron SSS.

3.4 LATERAL-DIRECTIONAL CONTROL LOOP GAIN SCHEDULING

The introductory comments of the first two paragraphs of Section 2.5 are valid for lateral-directional as well as longitudinal MCS control loops. These comments should be read before proceeding to examine the lateral-directional gain schedules presented below.

The data for the unlimited gains plotted in Figures 3.4 through 3.8 are listed in Table 3.1 and were computed using the equations of Sections 3.1 and 3.2. In Figures 3.4, 3.5 and 3.7, it is estimated that the desired gain levels cannot be achieved anywhere within the JetStar flight envelope. These gain restrictions, if the estimates are correct, will seriously reduce the capability of following the lateral responses of fast models. The degradations associated with these gain reductions when following a supersonic transport model are discussed in Section 4. There should be no problem in achieving values of gain δ_a/e_ϕ that are ten percent of the unlimited values of δ_a/e_p, and this gain schedule is recommended even though δ_a/e_p will apparently be limited according to Figure 3.6. The gain schedule for δ_r'/e_β is apparently realizable throughout the JetStar flight envelope, although the considerations of Appendix D indicate that levels somewhat higher than plotted in Figure 3.8 will actually be required. Apparently a constant value of δ_r'/e_β will suffice, however.

SECTION 4

ANALOG COMPUTER SIMULATION

In order to validate the techniques used to determine MCS control loop gain requirements, extensive analog computer simulations were performed. Two separate and independent analog computer programs were written to evaluate the longitudinal control loops, while the lateral-directional loops were studied with a single program on one computer. In the longitudinal analysis, one computer simulated both the model and the JetStar using two three-degree-of-freedom linear perturbation equation programs. Analog computer records obtained from this machine are sub-titled "perturbation equations". A much more complete simulation of both longitudinal and lateral-directional GPAS behavior was performed with the other computer using six-degree-of-freedom equations for both the model and JetStar. These equations were the nonlinear equations used to predict both static and dynamic behavior of an aircraft and have been termed "total force equations". Analog records for longitudinal responses obtained from this simulation are sub-titled "total force equations" and compare favorably with the perturbation equation solutions. All lateral-directional responses were obtained using total force equations, so notes to that effect are not included with lateral-directional analog computer results. The equations used are given in Appendix A.

In the longitudinal simulations, records are presented that show the responses of the model and JetStar to both elevator and throttle inputs to the model with the two phugoid loop configurations considered earlier and both unlimited and limited MCS forward loop gains. The lateral-directional responses for aileron and rudder commands to the model with both limited and unlimited gains are also presented. The longitudinal loops were closed with unlimited gains while studying the lateral responses, although a direct check for the worst (lowest $\bar{q}$) flight condition, .5H40, shows the lateral responses to be insensitive to longitudinal control loop gains. The longitudinal responses are independent of the lateral control loop gains as well.

4.1 MODEL-FOLLOWING WITH ELEVATOR AND THROTTLE INPUTS

In this section, some representative analog computer records are presented that show the results obtained when model-following an SST model using the control loops analyzed in Sections 2.1 and 2.2. All analog computer records were obtained using the elevator and throttle actuator dynamics shown on Figure 2.4. Some of the records were obtained using perturbation equations and others using total force equations, as noted on the figures.

Figure 4.1 shows model-following using a $\Delta\alpha$ short-period control loop and the configuration of Figure 2.1 for a flight condition in the center of the GPAS flight envelope. Two time scales are shown for the same input so that both phugoid and short-period model following can be evaluated. The input was a one-degree step command to the model elevator. The short-period angle of attack response shows little error until about fifteen seconds have elapsed, after which time angle of attack is used to help reduce errors in the phugoid mode. A constant error of about ten percent is noted in following ΔV, implying a need to boost the ΔV_M signal by ten percent and reduce this error. The approach taken in the MCS loop design, however, is to leave all input weighting gains at unity when one-to-one following is attempted. Instead, the steady-state error in the flight path variables $\dot{h}$ and ΔV was removed by using low-gain integrating loops on these variables. With the perturbation equations, $\dot{h} = V\gamma$, so accuracy of following $\dot{h}$ can be determined by viewing the γ_M and γ traces of Figure 4.1. Errors are almost indistinguishable. The lack of phase lags between model input and JetStar response variables is largely due to following $\dot{\alpha}_M$ and $\dot{V}_M$ as well as the primary variables. The JetStar elevator and throttle excursions necessary to effect the model following are not unreasonable for a fairly severe maneuver. Note that no excessive thrust transients are called for, in common with results obtained for all flight conditions with a variety of control loop configurations.

Figure 4.2 is similar to Figure 4.1 except that slightly different forward loop gains were used, the analog computer solved complete nonlinear total

force equations, and some different variables are shown. The gains of Figure 4.2 are taken directly from the gain programs described and presented in Section 2.5. The numerical values were taken from the faired curves for this flight condition and not the actual data points. Note the similarity of results, indicating that linear perturbation equations are satisfactory in studying the longitudinal MCS control loops. The steady-state errors in both $\dot{h}$ and ΔV are clearly zero in Figure 4.2, a result of having the low-gain forward loop integration in the ΔV loop and of following h_M as well as $\dot{h}_M$.

Figures 4.3 and 4.4 illustrate the conclusion that if it is desired to model follow a given single variable somewhat better results are obtained if all control loop variables are followed as well as the single variable of interest. In these figures, the error in normal acceleration is always larger when only Δn_z is followed than when Δn_z, ΔV, $\dot{V}$, and $\dot{h}$ are followed simultaneously.

Figures 4.5, 4.6, and 4.7 illustrate the effect of feeding back and recording various combinations of c.g. and cockpit normal acceleration. The first thing to note is that regardless of the location of the accelerometer, model-following of the phugoid mode occurs with equally high fidelity in all three records, thus leading to the conclusion that the accelerometer location influences only short-period model following. When normal acceleration feedback is used, a host of problems are introduced into the short-period model following. For example, location of the accelerometer at the c.g. results in significantly lower short-period damping ratios than are obtained with a $\Delta\alpha$ loop because of the positive elevator servo position feedback introduced by the accelerometer. This is due to $C_{L_{\delta_e}}$ and is explained in Appendix D. In Figure 4.6, this problem is compensated for by modifying the feedback accelerometer output according to equation D.4 to eliminate the elevator position feedback and readjusting loop gains for the desired ω_{θ_s} and ζ_{θ_s}. The unmodified Δn_z signal was recorded, rather than the modified signal that was used for short-period feedback, because the unmodified Δn_z represents the true normal acceleration

experienced by an observer located at the c.g. An alternate way to alleviate this problem is to increase the short-period damping gain, $\delta_e/e_{\dot{\alpha}}$ This technique was used in Figures 4.5 and 4.7 and the rationale behind the choice of the numerical value used is explained in Appendix D.

If the feedback accelerometer is located in the cockpit (the best location for cockpit acceleration model-following), the desired closed-loop bandwidth (i.e., ω_{θ_s}) cannot be achieved as noted in Section 2.1 and studied further in Appendix C.

The short-period following of model cockpit normal acceleration using a c.g. feedback accelerometer and cockpit recording accelerometer is shown in Figure 4.5. The sudden change in $\Delta n_{z_{p_M}}$ at the start of the transient, due to $\dot{q}_M$, is extremely high in frequency (limited only by the dynamics of the model elevator actuator) and cannot reasonably be expected to reproduce in the JetStar response. After one second has elapsed, however, the JetStar has recovered from this sudden input and follows satisfactorily. Figure 4.6 is essentially the same as Figure 4.5 insofar as the influence of the feedback loops on short-period dynamics is concerned. The primary difference is that c.g. acceleration is both fed back and recorded in Figure 4.6. The Δn_z response is more well damped in Figure 4.6, primarily because the pitch acceleration component that is present in a cockpit-mounted accelerometer is absent at the c.g. In Figure 4.7, a cockpit-mounted accelerometer is used for both feedback and recording purposes. This Δn_{z_p} response is better than that of Figure 4.5, but it is not clear whether this is due to using a cockpit acceleration control loop or because the closed-loop short-period damping ratio is considerably higher in Figure 4.7 than in Figure 4.5* or both.

*Because the closed-loop bandwidth is approximately 3 rad/sec for a cockpit feedback accelerometer and 9 rad/sec with a c.g. accelerometer, all other things being equal, the damping ratio is higher using a cockpit accelerometer. The damping remains essentially constant.

Because the longitudinal MCS control loop gains called for by the calculation techniques described in this report are somewhat higher than can be achieved in practice, it was necessary to investigate the influence of limiting MCS gains to realistic values on the model-following performance. This is best done by analog computer simulation. The worst flight condition from the standpoint of high gain requirements is that associated with the lowest dynamic pressure, namely .5H40. Accordingly, model-following performance was investigated for both elevator and throttle commands with unlimited and limited MCS control loop gains at this flight condition. In addition, the modified phugoid loops of Figure 2.3 had not yet been checked by analog computation, and runs were performed to investigate the long-period behavior with these new loops. The results of this study, using an SST model, are depicted in Figures 4.8 through 4.13. Figures 4.8 through 4.10 show little difference in the GPAS behavior for elevator commands to the model using unlimited or limited control loop gains with either the original or modified phugoid loops. Thus we conclude that the SST model does not tax the GPAS system for elevator commands at the most severe flight condition, and therefore that the SST model longitudinal responses can be matched throughout the JetStar flight envelope. It is also evident that the modified phugoid loops perform satisfactorily for elevator inputs to the model.

The model-following behavior of the GPAS system in response to thrust command signals is shown in Figures 4.11 through 4.13. The problems associated with the original phugoid control loops are clearly evident in Figure 4.11 and, to a lesser extent in Figure 4.12. Note the disturbance in Δn_{z_p} and $\dot{h}$ in both of these traces. The use of limited gains tends to alleviate the problems somewhat in Figure 4.12, but the responses are still unsatisfactory. With limited gains, the long-term phugoid following is poor until the forward loop integrations on $\dot{h}$ (i.e. the Δh loop) and ΔV finally restore proper model-following. The closed-loop phugoid damping of the JetStar is inadequate in Figure 4.12. The limited gains work well with the modified phugoid loops. The Δn_{z_p} and $\dot{h}$ responses closely approximate those of the model, and the phugoid following is excellent after

the first half cycle has elapsed. Because the modified phugoid loops work well with both elevator and throttle commands, they were chosen for installation in the JetStar.

4.2 MODEL-FOLLOWING WITH AILERON AND RUDDER INPUTS

This section presents the results of analog computer studies of GPAS lateral-directional model-following performance. The primary objectives of this study were to determine if the control system gains as calculated by the methods of Section 3 would give acceptable model-following behavior within the GPAS flight envelope, and to determine the influence of limiting rudder and aileron control loop gains to estimated realizable values. The unlimited gains (Table 3.1) establish levels of frequency, damping ratio, and time constants that remain approximately constant throughout the JetStar flight envelope. It is estimated that some of these gain levels cannot be achieved in actual flight. A survey of gain levels used during the past in many CAL flight tests indicates that for some flight conditions the gains estimated for GPAS are substantially higher than those which have actually been used in flight with other airplanes (Section 5). If the GPAS control loop gains are restricted to lower levels, then the desired lateral-directional frequency, damping ratio and time constants cannot be achieved throughout the GPAS flight envelope.

GPAS model-following performance was recorded for five flight conditions representing the extremes of the JetStar flight envelope. Both the JetStar and the model, or SST, were nominally at the same speed and altitude. Studies were not made for the case of different reference flight conditions. The five flight conditions are tabulated and spotted on the GPAS flight envelope shown in Figure 4.14.

All five flight conditions were investigated on the analog computer using the unlimited loop gains. Then the lowest dynamic pressure flight condition was selected and analyzed with limited control loop gains in order to establish the degradation of performance associated with limiting the gains to

realistic levels.

Although the longitudinal equations and control loops were operative, none of the longitudinal variables were recorded. The GPAS longitudinal configuration was that of Figure 2.1 with $\Delta\alpha$ rather than Δn_z feedback and the gains used are listed in Table 2.2. Detailed numerical values associated with this simulation can be found in Reference 7.

4.2.1 Angle Of Sideslip Feedback (β -Loop)

A survey of the β, ϕ, and φ analog records for each flight condition with unlimited gains gives an immediate impression of the over-all β-loop model-following performance. The time histories of JetStar variables are practically identical with the time histories of the corresponding model variables. This inspection leads to the qualitative judgment that β-loop model-following performance is generally satisfactory if loop gain requirements can be met. There are no gross discrepancies.

Each lateral-directional analog computer response is considered individually below.

4.2.1.1 .55H20 δ_a Input

Figure 4.15 shows the airframe response for both the SST and JetStar for a 0.1 degree step aileron input to the SST. The SST begins its initial positive roll rate accompanied by an initial negative sideslip response. This negative sideslip is due to a negative value of yawing moment due to rolling, N_φ. As the roll angle builds up, the SST begins slipping to the right and β becomes positive. This positive sideslip induces a negative rolling moment which tends to reduce the roll rate. Figure 4.15 indicates little difference between the SST and JetStar airframe responses. There is computer noise in the model roll rate signal which the closed-loop JetStar follows nicely.

The sideslip error begins to build up slightly as the run progresses. The JetStar's rudder becomes more positive which is in a direction to reduce this error. At the end of the run the JetStar's rudder angle is about + 0.1 degree. With a control gain of δ_r/e_β =33.8, the value of e_β should be about 0.003 degrees. The analog trace indicates a value of about 0.004 degrees.

The roll rate error remains practically zero throughout the run except for a small bump during the initial response. The roll angle error remains at a constant positive value. The JetStar's aileron is following primarily with the bank angle error and is remaining at an angle between .05 and .1 degree. With a control gain of δ_a/e_ϕ =.315 the corresponding roll angle error should be between 0.16 and 0.32 degrees. The analog record shows that e_ϕ stays between .15 and 0.25 degrees.

4.2.1.2 .55H20 δ_r Input

Figure 4.16 shows the response of the SST and JetStar for a 0.2 degree step rudder input to the SST. The initial sideslip response is positive and the accompanying dihedral moment begins rolling the SST to the left. As the bank angle becomes more negative the sideslip increases to the left and the dihedral moments begin rolling the airplane to the right. The difference between the SST and JetStar response is almost imperceptible.

The largest sideslip error occurs during the initial oscillation and then approaches zero. The JetStar's rudder also approaches zero toward the end of the run.

The initial bank angle error is negative but then becomes positive while the roll rate error remains negative. There is considerable noise in the roll rate error which is reflected in the JetStar's aileron response. The peak aileron deflection of about -0.1 degree occurs at the beginning of the run. With a control gain of δ_a/e_p =3.15 seconds, this is equivalent to a

roll rate error of e_p = -.032 deg/sec. The analog record indicates about -.025 deg/sec.

4.2.1.3 .23H0 δ_a Input

Figure 4.17 shows the response of the JetStar and SST to a 0.1 degree step aileron input to the SST. The response is characterized by initial positive rolling, the buildup of positive sideslip, and the resulting roll reversal due to dihedral moments.

The sideslip traces for the two airplanes appear identical, but there is an obvious dip in the roll angle of the JetStar about three-quarters of the way through the run. A closer look also shows a secondary dip in the roll angle about half-way through the run. A look at the roll rate traces indicate that the same effect occurs there also. The reason for this occurrence is unknown. Figure 4.17 shows that the sideslip error is always positive, and after the initial oscillation it tends to build up slightly. The rudder does not seem to be responding properly to the sideslip error at the beginning of the run. The value of e_β at the first peak is almost the same as that near the end of the run. The JetStar's rudder, however, shows a gradual buildup. Near the end of the run the rudder deflection of about 1 degree corresponds with the value of $e_\beta \cong .01$ degree.

The roll rate error starts out positive and then becomes negative. The bank angle becomes increasingly positive. The aileron deflection remains essentially constant after the initial peak. This is due to the magnitude and sign of the roll rate and bank angle errors. The aileron deflection is given by

$$\delta_a = \frac{\delta_a}{e_p} \left\{ e_p + \frac{1}{10} e_\phi \right\}$$

The term in brackets is essentially constant throughout the run.

4.2.1.4 .23H0 δ_r Input

Figure 4.18 shows the airframe response to a 0.5 degree step rudder input to the SST. The initial positive sideslip response creates dihedral moments which roll the airplane to the left. The ensuing negative sideslip creates dihedral moments tending to reverse the roll. The sideslip angle traces in Figure 4.18 appear identical for both airplanes. The roll rate and bank angle traces, though not as good as the sideslip response, are acceptable.

The corresponding error responses in Figure 4.18 show that maximum e_β occurs during the first peak of the oscillation and then rapidly approaches zero.

Again the rudder does not seem to be responding properly to sideslip errors at the beginning of the run. The rudder deflection at the peak value of e_β should be about 1.5 degree.

The aileron deflection remains essentially constant during the middle of the run because of the magnitude and sign relation between e_p and e_ϕ, as previously discussed.

4.2.1.5 .75H20 δ_a Input

Figure 4.19 shows the SST and JetStar response for a 0.5 degree step aileron input to the SST. The response is one of almost pure rolling. The sideslip traces appear identical for both airplanes. The roll rate and bank angle traces have the same shape for each airplane, but a close look shows that the initial roll acceleration and steady-state roll rate of the JetStar are less than those of the SST. The difference in roll rates is reflected in the bank angle traces which show the JetStar lagging the SST. This effect stands out in the roll rate error and bank angle error responses. The aileron deflection remains essentially constant after the initial peak. The

roll rate error and the bank angle error are such that when multiplied by their respective control gains, they yield a constant aileron deflection.

4.2.1.6 .75H20 δ_r Input

Figure 4.20 shows the response of the JetStar and SST to a 0.5 degree step rudder input to the SST. At first glance the sideslip responses of both airplanes appear identical, but a closer look reveals that the magnitude of the JetStar's sideslip angle is less than that of the SST. The same is true for the roll rate responses.

The error responses in Figure 4.20 show that a steady-state sideslip error exists while the roll rate error approaches zero. The bank angle error increases with time. The JetStar's ailerons respond properly to roll rate error and bank angle error, but the rudder does not seem to respond properly to its input error signals. At the first peak of the e_β trace, $e_{\dot{\beta}}$ equals zero. At this time, the rudder deflection should respond to e_β only. Using a sideslip error gain of $\delta_r/e_\beta = 18.7$, a sideslip angle error of 0.08 degrees should result in a rudder deflection of 1.5 degree. The actual rudder deflection is less than half this value. Toward the end of the run, the rudder behaves normally. The measured rudder deflection is 0.46 degrees and its computed value is 0.56 degrees.

4.2.1.7 .525H4 δ_a Input

Figure 4.21 shows the SST and JetStar airframe response for a 0.5 degree step aileron input to the SST. Initial sideslip oscillations are small and β builds up as the bank angle increases. The roll rates increase and level off to the steady state similar to a first-order system, indicating an almost pure rolling response. The sideslip angle traces match quite well, but the roll rate traces show that the JetStar lags the SST during the initial roll acceleration and also levels out to a lower value of steady-state roll rate early in the run. As the run progresses, the two

roll rates become more nearly equal. The lower roll rate of the JetStar is reflected in the lower bank angle as shown in the bottom trace of Figure 4.21.

The error response traces show the slight buildup of sideslip angle error. The roll rate error indicates an initial peak value followed by a decay to near zero error at the end. The roll angle error builds up to almost 3 degrees out of an actual bank angle of about 25 degrees. The aileron angle remains almost constant after its initial peak.

4.2.1.8 .525H4 δ_r Input

Figure 4.22 shows the airframe response for a 0.5 degree step rudder input to the SST. The sideslip and roll rates exhibit an initial oscillation followed by a decay to a steady-state value while the bank angle continually builds up. The rolling of the SST is due primarily to dihedral effects. Toward the end of the run where steady-state conditions prevail, the dihedral moment of the SST is balanced by the roll damping moment.

The error responses in Figure 4.22 show that the largest errors occur during the initial oscillation. The peak sideslip error is about 0.07 degrees out of a peak sideslip angle of about 0.5 degrees. The peak roll rate error is about -.15 deg/sec and occurs when the roll rates are about -0.75 deg/sec. The roll rate error decays to zero while the sideslip error acquires a steady-state value.

4.2.1.9 .50H40 δ_a Input

Figure 4.23 shows the airframe response for both the SST and JetStar for a 0.5 degree step aileron input to the SST. The SST begins its initial roll to the right. The accompanying buildup in positive sideslip angle creates dihedral moments that eventually overcome the control moment and begin rolling the airplane to the left. Both roll rate and sideslip angle

follow the model satisfactorily with the extreme control loop gains used here. This is the most severe flight condition from the standpoint of gain requirements.

Figure 4.24 shows the model-following performance with loop gains reduced to the estimated maximum levels that can be realized in flight. The most obvious result of limiting the gains, for aileron inputs, is a loss of fidelity in following roll rate. Except for the first second or two, however, the roll rate response shows little change from Figure 4.23. The bank angle following remains satisfactory. The sideslip angle following is degraded somewhat, but is probably still acceptable.

4.2.1.10 .50H40 δ_r Input

Figure 4.25 shows the JetStar and SST airframe response to a 0.5 degree step rudder input to the SST. The response shows the initial build-up of positive sideslip angle and the corresponding negative roll caused by dihedral moments. As the roll angle becomes more negative, the sideslip angle begins to reduce and eventually becomes negative. The model-following for rudder inputs is satisfactory for β, p, and ϕ, with the best results in the sideslip channel. Static errors in bank angle and roll rate are evident after a considerable period of time.

In Figure 4.26, the results of reducing control loop gains to acceptable levels is primarily a loss of fidelity in following sideslip angle. The roll rate response follows the model acceptably in magnitude, but a noticeable time delay is introduced. The bank angle model-following is improved, primarily because δ_a / e_ϕ was not reduced so bank angle is weighted more heavily relative to the other variables.

4.2.1.11 Summary Of β -Loop Performance

The analog computer records show in general that satisfactory roll rate, bank angle, and sideslip angle performance are achieved with the unlimited control system gains. This judgment is based on visual inspection of the SST and JetStar airframe response analog records in the absence of quantitative acceptance criteria. The assumed rudder and aileron control system dynamics(ω_n = 44 rad/sec, ζ = 0.7) were adequate for achieving desired closed-loop dynamics without instability due to control phase lags. The feedback gains were almost always larger than current estimates of levels than can be achieved in practice. A study of system performance with limited control loop gains indicates that marginal lateral-directional performance can be achieved for an SST model with the JetStar operating at a low dynamic pressure flight condition. The system performance improves with a given level of control loop gain as the JetStar dynamic pressure increases. It is not likely that acceptable model-following of a faster model will be possible at low dynamic pressures.

Lateral-directional model-following is superior with the longitudinal control loops closed, primarily because JetStar dynamic pressure and altitude are then controlled in response to disturbances caused by lateral-directional maneuvers. The two systems (i.e. model and JetStar) are not allowed to "drift" apart.

4.2.2 Lateral Acceleration Feedback (n_{Y} -Loop)

In comparison with the fidelityof airframe responses shown earlier for β -loop operation, similar responses for n_{Y_φ} -loop operation indicate that accurate n_{Y_φ} matching does not occur. The roll modes for the two airplanes do indicate reasonable roll rate and bank angle matching, however. This is because the individual modes of the lateral-directional dynamics are essentially independent. Acceleration loop performance was studied for only two flight conditions, namely .55H20 and .75H20. For the .55H20

flight condition, a comparison is made of the performance with and without actuator dynamics.

Descriptions of some problems associated with the use of acceleration feedback are presented in Appendices C and D. All computer results contained herein were for cockpit acceleration feedback. As the accelerometer is moved forward from the c.g., the bandwidth ω_ψ is reduced and the damping ratio ζ_ψ is increased, all other things being equal.

4.2.2.1 .55H20 δ_r Input

Figure 4.27 shows the airframe responses of the SST and JetStar for a 0.5° step rudder input to the SST and unlimited control loop gains. The cockpit acceleration traces show some semblance of acceleration following, but the fidelity is poor. The initial peak in acceleration for both airplanes is due primarily to the instantaneous yaw acceleration that results from deflection of the rudder. The positive step function of rudder input to the SST creates a positive side force and a negative yaw acceleration. Since β equals zero initially, the lateral acceleration at the pilot's location is given by

$$n_{Y_p}(0+) = \left[\frac{V_t}{g} Y_{\delta_r} + \frac{\ell}{g} N_{\delta_r} \right] \delta_r$$

The term $\ell/g \; N_{\delta_r}$ is negative while $V_t/g \; Y_{\delta_r}$ is positive. Because the magnitude of $\ell/g \; N_{\delta_r}$ is greater than that of $V_t/g \; Y_{\delta_r}$ the sum of the two terms is negative. Therefore, for a positive rudder deflection the initial value of N_{Y_p} is negative.

Figure 4.27 also clearly shows that attempts at matching n_{Y_p} can yield a JetStar sideslip angle response that is completely different from that of the model.

Comparison of the roll rate and bank angle responses of both airplanes indicates reasonable model-following performance of the roll mode. There

is an unexplained flattening of the JetStar's roll rate response during the first oscillation, but there seems to be no subsequent adverse effects.

The magnitude of e_β is of the same order as β itself. The initial spike in acceleration error is due to the δ_r step input to the SST while the immediate drop off is due to the JetStar rudder response. The roll rate error shows an oscillatory build-up followed by a decay to essentially zero.

The initial deflection of the JetStar rudder to the acceleration error is immediate and large. It is limited in response only by rudder servo dynamics. The steady-state lateral acceleration error of -.001 g. The initial response of the JetStar Aileron is in a direction to reduce the roll rate produced by the JetStar rudder. Figure 4.27 shows that the JetStar has an initial positive roll rate produced by its rudder.

4.2.2.2 .55H20 δ_a Input

Figure 4.28 shows the airframe response of the JetStar and SST for a 0.5° step aileron input to the SST. The SST sideslip builds up with bank angle but the sideslip angle remains small. The response is almost pure rolling. The initial step in SST pilot acceleration is due to the yawing acceleration created by the step aileron input. The pilot acceleration remains less than .01 g throughout this maneuver for both the JetStar and SST. Comparison of roll rate and bank angle traces indicate good model-following in this mode.

In Figure 4.28, the acceleration error is small. The sideslip angle error is the same order of magnitude as the sideslip angles. The largest roll rate error occurs initially then decays to zero in a damped oscillatory manner. The bank angle error increases but levels off in time. At the end of the run the bank angle error is about 1 degree out of a total bank angle of 25 degrees.

4.2.2.3 .75H20 δ_r Input

Figure 4.29 shows the airframe response of both the SST and JetStar for a 0.5 degree step rudder input to the SST. The initial peak in the SST pilot acceleration is due to the yaw acceleration $N_{\delta_r} \delta_r$. The general nature of the JetStar's n_{γ_p} response is the same as that of the SST, but the magnitudes of the two responses do not compare favorably. The flattening of the first crest of the JetStar's n_{γ_p} response appears to result from the JetStar's initial rapid β response, but no calculations have been made to verify this.

The JetStar has an initial tendency to roll right due to positive L_{δ_r} . Roll rate model-following during the first oscillation is erratic, but the steady-state roll rates agree very well. The bank angle traces for both airplanes are almost identical. The JetStar is about 1 degree less than the SST at the end of the record.

The error responses in Figure 4.29 clearly show the initial acceleration error $e_{n_{\gamma_p}}$ due to the step rudder input to the SST. There is an immediate drop in the acceleration error as the JetStar's rudder responds to the error signal.

4.2.2.4 .55H20 δ_r Input - No Actuator Dynamics

Figure 4.30 shows the airframe response of the JetStar and SST for a 0.5° step rudder input to the SST. In this figure, actuator dynamics (7 cps, 70% damped) for the JetStar rudder and aileron were not present in comparison with Figure 4.27 where they were present. The major differences between Figure 4.30 and 4.27 is in the magnitude of the β response. The peak values of the JetStar β without actuator dynamics are roughly one-half those with actuator dynamics. Without actuator dynamics, the roll response of the aircraft is almost identical with the model.

The β error response in Figure 4.30 indicates a peak error of about 0.6 degrees while that in Figure 4.27 gives a peak error of about 0.9 degrees. Thus, although the JetStar β response is of lower magnitude, it is phased different with respect to β_M so that the magnitude of the β errors is about the same.

The initial character of the roll rate error is different with the error magnitude being less when actuator lags are absent.

4.2.2.5 .55H20 δ_a Input - No Actuator Dynamics

Figure 4.31 shows the airframe response at .55H20 for a 0.5 degree step aileron input to the SST. Comparing Figure 4.31 with Figure 4.28, the most obvious difference is in the sideslip angle traces. In Figure 4.31 the magnitude of the JetStar's sideslip angle is roughly one-half that of Figure 4.28 during the initial oscillations. The acceleration traces in Figure 4.31 are noisy but appear generally to be the same as those in Figure 4.28. The same is true for the roll rate and bank angle responses.

The major difference in the error responses of these figures is in the magnitude of the sideslip angle error. The β errors in Figure 4.31 are approximately one-half those of Figure 4.28. Although there is no attempt to match β it is interesting to note that control systems dynamics have a greater effect on the β response than on the lateral acceleration or roll responses.

4.2.2.6 Summary Of n_{Y_p} -Loop Performance

The analog records show in general that satisfactory acceleration (n_{Y_p}) following is not achieved. Roll rate and bank angle following, however, are satisfactory. Actuator dynamics degrade acceleration following, but the most obvious effect is on the sideslip (β) response of

the JetStar.

Because model-following is generally unsatisfactory with unlimited acceleration gains, no attempt was made to study the influence of gain limiting on n_{Y_p} performance.

SECTION 5

ESTIMATED RFS GAIN AND PERFORMANCE LIMITS

Previous to the preliminary GPAS design review in November 1964, a set of RFS gains necessary to meet or exceed the requirements of the GPAS Work Statement (Reference 3), Tables I and II, was established. Various approximate equations as well as root-locus plots and analog computer studies were used to determine the required gain levels. In many cases, these gains exceed the highest values of similar gains ever used on existing CAL variable stability aircraft by a large margin, thus indicating a potential serious problem area in the RFS system. Accordingly, a study was made of gain limitations on the CAL B-26 and T-33 variable stability aircraft, and the reasons for these limitations, for all channels for which the information is available. In many cases, no limit values of gain have been established in these aircraft because the particular channels have never been used in a program or sufficient gain was available for the purpose of the experiment before any limit occurred.

A table of maximum channel gains for all RFS feedback loops was prepared, along with reasons for limiting the gain to the values shown. This table is presented herein as Table 5.1 and was the basis for a study of estimated RFS performance limits. The performance limits were established either by calculating the gains necessary to achieve the desired performance and comparing the resulting gains with the limit values, or by computing the performance associated with the estimated maximum gains and comparing the performance with that which is desired. In either case, it is possible to establish satisfactory operating points for the JetStar in terms of the parameters $\bar{q}$ (dynamic pressure) and h (altitude).

In the paragraphs that follow, each RFS performance requirement set forth in the GPAS Work Statement, Tables I and II, is considered. Approximate equations used to calculate the RFS gains are given and the estimated

performance limits are derived. In all cases, eighteen JetStar flight conditions encompassing the extremes of the flight envelope are considered for both light and heavy configurations.

5.1 SHORT-PERIOD AND PHUGOID PROPERTIES - ω_{θ_s} AND ζ_{θ_s}, ω_{θ_p} ζ_{θ_p}

The levels of longitudinal RFS feedback gains necessary to meet the requirements of the work statement are listed in Tables 5.2 and 5.3. In these tables, the gains δ_e/V and $\delta_e/\dot{V}$ are computed with δ_e/α set to the values shown in the first gain column, since the remaining gains all are sensitive to δ_e/α. The following equations were used:

$$\frac{\delta_e}{\alpha} = \frac{\omega_{\theta_s}^2 + M_\alpha - M_q Z_\alpha}{-M_{\delta_e}} \tag{5.1}$$

$$\frac{\delta_e}{\dot{\alpha}} = \frac{2\zeta_{\theta_s}\omega_{\theta_s} + M_{\dot{\alpha}} + M_q + Z_\alpha}{-M_{\delta_e}} \tag{5.2}$$

$$\frac{\delta_e}{V} = \frac{\omega_{\theta_p}^2 + \frac{g}{V_t} Z'_V}{-Z'_{\delta_e}} \left[1 - \left(\frac{\bar{\alpha}}{\delta_e}\right)\frac{\delta_e}{\alpha}\right] \quad \text{(rad-sec/ft)} \tag{5.3}$$

$$\frac{\delta_e}{\dot{V}} = \frac{1 - \left(\frac{\bar{\alpha}}{\delta_e}\right)\frac{\delta_e}{\alpha}}{-Z'_{\delta_e}} \left[\frac{2\zeta_{\theta_p}\omega_{\theta_p} - D_V - D'_{\delta_e}\left(\frac{\delta_e}{V_t}\right)}{g} - \frac{\alpha_t}{V_t}\right] \quad \text{(rad-sec}^2\text{/ft)} \tag{5.4}$$

where

$$Z'_V = \left(Z_V - V\frac{Z_\alpha}{M_\alpha} M_V\right)\left(1 + \frac{Z_\alpha}{M_\alpha} M_q\right)$$

$$Z'_{\delta_e} = (Z_\alpha + Z_{\dot{\alpha}})\left(\frac{\bar{\alpha}}{\delta_e}\right) + Z_{\delta_e}$$

$$\left(\frac{\bar{\alpha}}{\delta_e}\right) = \frac{M_{\delta_e} - M_q Z_{\delta_e}}{-M_\alpha + M_q Z_\alpha}$$

For those situations in Tables 5.1 and 5.2 where the gain $\delta_e/\dot{\alpha}$ is sufficient to provide the proper short-period damping ratio, the gain δ_e/q can be used to augment $\delta_e/\dot{\alpha}$. Because δ_e/q influences longitudinal static sensitivities as well as pitch damping, it should not be used except as necessary to augment $\delta_e/\dot{\alpha}$.

The following conclusions can be derived from Tables 5.2 and 5.3, using Figure 5.1 as an aid in visualizing the flight regimes associated with a line of constant dynamic pressure, $\bar{q}$:

5.1.1 The desired short-period frequency ω_{θ_s} =6.32 rad/sec can be achieved for JetStar flight conditions when $\bar{q}$ > 100 lb/ft^2.

5.1.2 When ω_{θ_s} = 6.32 rad/sec

a. ω_{θ_p} = 0.15 rad/sec can be achieved for a light JetStar throughout the flight envelope with the possible exception of low-speed, high-altitude operating points.

b. ω_{θ_p} = 0.15 rad/sec can be achieved for a heavy JetStar below $h \approx$ 30,000 feet.

c. ζ_{θ_p} = 0.15 is possible for all flight conditions except .23HO.

d. ζ_{θ_p} = 0.5 is possible for a heavy JetStar when $\bar{q}$ > 200 lb/ft^2 and for a light JetStar when $\bar{q}$ > 200 lb/ft^2.

e. ζ_{θ_s} = 1.5 is possible only when $\bar{q}$ > 350 lb/ft^2 in the lightweight configuration.*

f. ζ_{θ_s} = 0.5 is possible when $\bar{q}$ > 100 lb/ft^2, light and $\bar{q}$ > 150 lb/ft^2, heavy.

g. ζ_{θ_s} = 0 is always possible.

---

* Elevator actuator dynamics will probably prevent this high damping ratio from being realized.

5.1.3 The short-period frequency ω_{θ_s} = 3 rad/sec can be achieved for all flight conditions.

5.1.4 When ω_{θ_s} =3 rad/sec

a. ω_{θ_p} = 0.15 rad/sec is always possible.

b. ω_{θ_p} = 0.15 is always possible.

c. ζ_{θ_p} = 0.5 is possible when $\bar{q}$ > 70 lb/ft^2, light and when $\bar{q}$ > 100 lb/ft^2, heavy.

d. ζ_{θ_p} = 1.5 is possible when $\bar{q}$ > 150 lb/ft^2, light and when $\bar{q}$ > 200 lb/ft^2, heavy.*

e. ζ_{θ_s} = 0.5 is always possible.

f. ζ_{θ_s} = 0 is always possible.

5.2 LATERAL-DIRECTIONAL PROPERTIES

The lateral-directional properties that must be controlled in the RFS mode are:

1. Dutch roll natural frequency and damping ratio - ω_ψ, ζ_ψ
2. Magnitude of roll to sideslip ratio - $|\phi/\beta|$
3. Ratio of roll numerator frequency to Duch roll frequency - ω_ϕ/ω_ψ
4. Roll mode time constant - τ_R
5. Spiral mode time contant - τ_S

These properties, or the RFS gains necessary to achieve them, can be determined with accuracy sufficient for design purposes from the following equations:

$$\frac{\delta_r}{\beta} = \frac{\omega_\psi^2 - N_{\beta_0}}{N_{\delta_r}} \qquad (5.5)$$

* Elevator actuator dynamics will probably prevent this high damping ratio from being realized.

$$\frac{\delta_r}{\dot{\beta}} = \frac{2\zeta_\psi \omega_\psi + Y_{\beta_0} + N_r + Y_{\delta_r}\left(\frac{\delta_r}{\beta}\right)}{N_{\delta_r} + 2\zeta_\psi \omega_\psi Y_{\delta_r}} \tag{5.6}$$

$$\left|\frac{\phi}{\beta}\right| = \left|\frac{L_\beta}{N_\beta}\right| \sqrt{\frac{1 + \frac{N_\beta L_r^2}{L_\beta^2}}{1 + \frac{L_p^2}{N_\beta}}} \tag{5.7}$$

$$\frac{\omega_\phi}{\omega_\psi} = \sqrt{1 - \frac{N_{\delta_{a_c}} L_\beta}{L_{\delta_{a_c}} N_\beta}} \tag{5.8}$$

$$\tau_R = \frac{-1}{L_p + L_{\delta_a}\frac{\delta_a}{p}} \tag{5.9}$$

$$\tau_s = \frac{V_t}{g\tau_\beta} \cdot \frac{1}{\frac{L_\beta}{N_\beta} N_r - L_r} \tag{5.10}$$

5.2.1 Dutch Roll Frequency and Damping Ratio - ω_ψ, ζ_ψ

Table 5.4 summarizes the values of RFS gains δ_r/β and $\delta_r/\dot{\beta}$ necessary to achieve combined values of ω_ψ = 5 rad/sec, ζ_ψ = 0.5; ω_ψ = 2.5 rad/sec, ζ_ψ = 1.0; and ω_ψ = 2.5 rad/sec, ζ_ψ = 0.5. Some results that are clearly evident from Table 5.4 and Figure 5.1 are:

1. The desired Dutch roll natural frequency ω_ψ = 5 can be achieved when $\bar{q}$ > 200 lb/ft^2 for a light JetStar and when $\bar{q}$ > 300 lb/ft^2 for a heavy JetStar.
2. The desired Dutch roll damping ratio ζ_ψ = 1.0 probably cannot be achieved at any flight condition.
3. When ω_ψ = 5 rad/sec, ζ_ψ = 0.5 is possible for the lightweight JetStar only when $\bar{q}$ > 300 lb/ft^2.
4. When ω_ψ = 5 rad/sec, ζ_ψ = 0.5 is not possible for a heavy JetStar at any flight condition.

5. When ω_ψ = 2.5 rad/sec, ζ_ψ = 0.5 is possible when $\bar{q}$ > 200 lb/ft^2 for a light JetStar and when $\bar{q}$ > 300 lb/ft^2 for a heavy JetStar.

As in the case of the longitudinal parameters, the portions of the JetStar flight envelope where the particular Dutch roll properties set forth in Tables 5.4 are possible are clearly evident from Figure 5.1 by noting which flight conditions are included within the RFS capabilities. The envelope of these flight conditions (a line of constant $\bar{q}$) establishes minimum values of dynamic pressure for which the prescribed operation of the RFS is possible.

5.2.2 Magnitude of Roll to Sideslip Ratio - $|\phi/\beta|$

Equation 5.7, obtained from Reference 8, indicates that $|\phi/\beta|$ is primarily influenced by the dihedral derivative, L_β . It is also influenced materially by N_β , and to a lesser extent by L_p and L_r . Since N_β is usually reserved to control Dutch roll frequency, the gain δ_a/β is used to vary L_β , and hence $|\phi/\beta|$. Table 5.5 shows the values of δ_a/β necessary to cause L_β and $|\phi/\beta|$ to be zero. Also shown are the values of $|\phi/\beta|$ associated with δ_a/β = - 10, the maximum negative gain value from Table 5.1. It is concluded that the values of $|\phi/\beta|$ required by the work statement should be obtainable throughout the JetStar flight envelope provided that L_p and N_β are not augmented. When small values of τ_e and/or large values of ω_ψ are desired (i.e., large values of L_p and/or N_β), the maximum value of $|\phi/\beta|$ will be less than shown in Table 5.5.

5.2.3 Ratio of Roll Numerator Frequency to Dutch Roll Frequency - $\frac{\omega_\phi}{\omega_\psi}$

According to equation 5.8, from Reference 8, the frequency ratio ω_ϕ/ω_ψ is influenced by L_β and N_β and the control derivatives $L_{\delta_{a_c}}$ and $N_{\delta_{a_c}}$. These control derivatives can be effectively changed, for terms in the numerator of the JetStar transfer functions, by changing the gearing between the aileron wheel and the aileron and rudder. The effective lues of $L_{\delta_{a_c}}$ and $N_{\delta_{a_c}}$ are given by equations 5.11 and 5.12.

$$L_{\delta_{a_c}} = L_{\delta_a}\left(\frac{\delta_a}{\delta_{a_p}}\right) + L_{\delta_r}\left(\frac{\delta_r}{\delta_{a_p}}\right) \tag{5.11}$$

$$N_{\delta_{a_c}} = N_{\delta_a}\left(\frac{\delta_a}{\delta_{a_p}}\right) + N_{\delta_r}\left(\frac{\delta_r}{\delta_{a_p}}\right) \tag{5.12}$$

Substituting 5.11 and 5.12 into 5.8, we can solve for the ratio of the aileron and rudder to aileron wheel control gearing sensitivities, given by 5.13.

$$\frac{\left(\frac{\delta_r}{\delta_{a_p}}\right)}{\left(\frac{\delta_a}{\delta_{a_p}}\right)} = -\frac{\left[1-\left(\frac{\omega_\phi}{\omega_\psi}\right)^2\right]\frac{N_\beta}{L_\beta}L_{\delta_a} - N_{\delta_a}}{\left[1-\left(\frac{\omega_\phi}{\omega_\psi}\right)^2\right]\frac{N_\beta}{L_\beta}L_{\delta_r} - N_{\delta_r}} \tag{5.13}$$

In equation 5.13, N_β and L_β are the augmented values if δ_r/β and/or δ_a/β are not zero; otherwise they are the JetStar values. The control derivatives L_{δ_a}, N_{δ_a}, L_{δ_r}, and N_{δ_r} are always the JetStar values.

Using equation 5.13 with JetStar stability and control derivatives, the gain ratios shown in Table 5.6 were computed. It is anticipated that these ratios can be achieved for all flight conditions when δ_a/δ_{a_p} is small. These gains do not influence the closed-loop characteristic equation or structural stability.

5.2.4 Roll Mode Time Constant - τ_R

Small values of τ_R are difficult to obtain. It is easily shown that arbitrarily large values of τ_R are possible for $\delta_a/p < 1$ sec. Table 5.7 shows the values of τ_R that result when $\delta_a/p = -2$, the estimated maximum negative value from Table 5.1. From Table 5.7 and Figure 5.1, the minimum required value of $\tau_R = 0.1$ sec can be obtained when $\bar{q} > 100$ lb/ft^2 for a light JetStar and $\bar{q} > 300$ lb/ft^2 for a heavy JetStar.

The large difference is primarily due to a substantial change in roll inertia with weight for the JetStar.

5.2.5 Spiral Model Time Constant - τ_s

Equation 5.10, from Reference 8, was used to compute the spiral mode time constant. With $\delta_a / r = \pm 4$, the extreme values from Table 5.1, the spiral mode time constant exceeds the requirements of the GPAS work statement for all flight conditions. This is apparent from the entries in Table 5.7, which were calculated using normal JetStar values of τ_R. When τ_R is made smaller by δ_a / p feedback, the available range of τ_s is reduced.

SECTION 6

CONTROL SYSTEM CONSIDERATIONS

In this section, a brief analysis of the effect of simulation servo system nonlinearities on MCS and RFS variable stability operation is presented. The "elevator-throttle coupling problem" is discussed. It is shown that the so-called "excessive thrust transients" do not exist, and that the analog computer records in Reference 1 illustrating this problem are incorrect. The basic elevator-throttle coupling problem has, to a great extent, been solved by redesign of the phugoid control loops, revising the previous δ_e/e_v and $\delta_e/e_{\dot{z}}$ loops to the final $\delta_e/e_{\dot{z}}$ and δ_e/e_v loops.

6.1 CONTROL SYSTEM NONLINEARITIES

In the MCS and RFS control system design, linear control surface actuators and jet engine dynamics were used. The only control system limitations were expressed in terms of limited bandwidth as characterized by (second-order) control surface servos with 7 cps undamped natural frequencies and 70% critical damping and engines with 0.7 cps natural frequencies and 50% critical damping. Based on analog computer time histories obtained with a variety of aircraft operating points, control loop configurations, and input magnitudes, it does not appear that control system rate limiting will degrade the fidelity of simulation. This conclusion is based on the assumption that the simulation servo systems are capable of providing control surface rates of at least 60 deg/sec, as required in Reference 3, paragraph 3.2.1, for any control surface loading up to the hinge moment limits and that the jet engine thrust rate limit is approximately 500 lb/sec per engine. For any reasonable model configuration and control excursions, these rate limits are not approached in normal GPAS operation.

The JetStar has adequate control surface control power to simulate any reasonable model configuration with properties inside the limits of Reference 3, paragraph 1.5.1.2, except for the low dynamic pressure

operating points along the left-hand boundary of Figure 5.1. However, the thrust available from the JetStar is insufficient to allow a matched (one-to-one) simulation of an SST model during climb-out flight. These are obvious limitations, however, that cannot be corrected by conventional design.

Analog computer records indicate that for proper control of the phugoid mode, hysteresis and deadband in the elevator control system should not exceed about 0.05 deg and in the thrust control system about 50 pounds. The aileron and rudder servos should also be capable of resolving 0.05 degree inputs.

Zero-memory control surface nonlinearities due to kinematic relations between linear actuator displacements and rotary surface motions (i.e., nonlinear gearing) appear as forward loop nonlinearities and will be automatically compensated for by command and feedback of the aircraft motion variables in the MCS control loops. This type of nonlinearity is more likely to cause trouble with the RFS loops, where direct control surface responses to motion variable feedbacks are involved.

6.2 ELEVATOR - THROTTLE COUPLING

During the performance of the preliminary design study reported in Reference 1, large thrust transients were discovered in the analog computer results with elevator command inputs to the model for low-speed, low-altitude flight.* The model used then was identical to the model used in the current preliminary system design studies. The GPAS control loops in both cases were adjusted to provide a near one-to-one match between the model and JetStar responses, using Δn_z or $\Delta\alpha$, $\dot{\alpha}$, ΔV, and $\dot{V}$ feedback control loops to the JetStar elevator and an $\dot{V}$ feedback control loop to the throttle.

---

* See Reference 1, Figures 5.4a and 5.4b, pp. 61 and 62, and Figure 6.1a p. 78.

The GPAS time history simulations were performed on two separate analog computers, one solving linear perturbation equations in three degrees of freedom and the other solving total force equations in six degrees of freedom with all significant nonlinearities incorporated. At no time during all the work done on the two independent computers, for both model elevator and thrust commands, was there any evidence of excessive thrust transients. Even when the aircraft and control loop configuration of Reference 1 was duplicated, no excessive thrust transients were noted.

Figure 4.1 shows a typical JetStar thrust transient response obtained when following an SST model excited by a step of elevator command signal. Note the absence of any large-amplitude high-frequency thrust transients and that the peak thrust excursions occur at the model phugoid frequency. Almost identical results were obtained using angle of attack or normal acceleration short-period feedback loops. Neither the normal acceleration loop high-pass filter nor the aircraft velocity coupling to the throttle used in Reference 1 were found to be beneficial to the system in any way. They did not, however, cause the excess thrust transients. They were discarded in the present design.

The "basic interaction problem between the elevator and throttle control loops"* is primarily one of designing control loops so that throttle inputs do not excite spurious angle of attack and normal acceleration transients. A comparison of Figures 4.11 and 4.12 shows that the redesign of the phugoid loops minimizes these transients, and that the normal acceleration response follows the model quite closely for large step changes in model thrust.

* Reference 3, paragraph 2.2.5, page 8

SECTION 7

CONCLUSIONS AND RECOMMENDATIONS

Based on the methods and results described in this report, the following conclusions and recommendations are presented:

1. The methods of this report are satisfactory in establishing proper levels of MCS and RFS control loop gain for all flight conditions.

2. Phugoid loop gains in the elevator channel are sensitive to the magnitude of the short-period gains δ_e/e_α or δ_e/e_{n_z}. The converse is not true.

3. Whenever possible, motion variables and their time derivatives should be model-followed simultaneously (e.g., ΔV_m and $\dot{V}_m$, $\Delta\alpha_m$ and $\dot{\alpha}_m$).

4. Low-gain forward-loop integrations in the $\dot{h}$ and ΔV control loops are necessary to eliminate the steady-state errors in flight-path matching.

5. Inherent cross-coupling between MCS control loops is usually beneficial in improving the simultaneous model following of several model motion variables. Exceptions may occur with gross differences in model and JetStar lift characteristics.

6. Long-term model following of model angle of attack is not important or even desirable if accurate flight-path matching is required. It is only necessary that the short-period "steady-state" and transient response be accurately reproduced. After decay of short-period transients, the JetStar angle of attack must assume whatever values are required to effect accurate flight-path matching. Thus, the elevator is "time-shared" between the short-period and phugoid modes.

7. Input gain modifications used to minimize steady-state errors in model following almost always degrade the fidelity of dynamic model following. Moreover, the proper settings for these input gains depend on the magnitude of the input signals, since the JetStar behavior is nonlinear for large maneuvers. Forward loop integrations are the only satisfactory way to eliminate this problem.

8. No large thrust transients caused by elevator-throttle loop coupling are evident for any combination of flight condition or input to the model that was studied.

9. When JetStar flight path motions are controlled using loops that feed ΔV and $\dot{V}$ to the elevator and $\dot{\gamma}$ to the throttle, it is not possible to satisfactorily follow model inputs resulting from a change in model thrust. These loops do perform satisfactorily for elevator commands fed to the model, however. Control loops where $\dot{\gamma}$ is fed to the elevator and ΔV is fed to the throttle are satisfactory for either type of model input, and have been incorporated in the hardware design.

10. Normal acceleration feedback is apparently subject to severe limitations. When the feedback accelerometer is located in the cockpit, the desired closed-loop short-period bandwidth cannot be realized. When the accelerometer is located at the c.g., considerable difficulty is encountered in achieving satisfactory short-period damping, and cockpit accelerations are in error because of contributions from JetStar pitch acceleration. Similar comments hold for lateral acceleration feedback.

11. Control surface servo resolution of 0.05 degrees and thrust resolution of 50 pounds are necessary for proper MCS and RFS operation.

12. The MCS and RFS gain levels necessary to meet the requirements of Reference 3, paragraph 1.5, cannot generally be achieved in the JetStar. However, the simulation of SST-class aircraft is possible up to the performance limits of the JetStar.

13. It is recommended that the "future expansion loops" provided for in the initial design be incorporated. The yaw and pitch rate loops will be helpful in augmenting Dutch roll and short-period damping, which is marginal with the estimated gain limits on $\dot{\beta}$ and $\dot{\alpha}$. The pitch attitude loop should yield excellent phugoid model following.

REFERENCES

1. Reynolds, P. A., Pritchard, F. E., and Schelhorn, A. E. : Preliminary Design Study for a General Purpose Airborne Simulator. CAL Report No. TE-1795-F-1, August 1963.

2. Clark, D. C.: Design of Longitudinal Control Loops for a General Purpose Airborne Simulator GPAS Memo 37, November, 1964.

3. Statement of Work for the Design and Development of a General Purpose Airborne Simulator. NASA PR 1768, April 17, 1964

4. Bock, D.: JetStar Automatic Trim Circuit. GPAS Memo No. 26, September 1964.

5. Bock, D. and Clark, D. C.: General Purpose Airborne Simulator - Conceptual Design Study GPAS Memo 53, November 1964.

6. Kroll, J. : Design of Lateral-Directional Control Loops for a General Purpose Airborne Simulator. GPAS Memo No. 38, November 1964.

7. Kroll, J.: GPAS Lateral-Directional Model Following Performance - Analog Computer Studies GPAS Memo 91 February, 1965.

8. Newell, F. D.: Criteria for Acceptable Representation of Airplane Dynamic Responses in Simulators Used for Pilot Training. CAL Report No. BM-1642-F-1, 1 September 1962. (NAVTRADEVCEN 1146-1).

9. Schelhorn, A.: Throttle Servo Design. GPAS Memo No. 116, 14 April 1965.

---

* May be obtained from the Cornell Aeronautical Laboratory, Inc.
**May be obtained from the NASA Flight Research Center.

TABLE 2.1 PHUGOID LOOP GAINS FOR ω_{θ_p} = 0.3 RAD/SEC USING PHUGOID CONTROL LOOPS OF FIGURE 2.3

Code*	$\bar{q}$ lb/ft²	Phugoid Loop Gains With Open Short-Period Loops eq. 2.52, 2.53		ζ_{θ_p}	(see Table 2.2 for $\Delta\alpha$ and Δn_z loop gains)	
		$\delta_e/e_{\dot{\theta}}$ deg-sec/ft	$\Delta T/e_v$ lb-sec/ft		$\delta_e/e_{\dot{\theta}}$ deg-sec/ft	
					$\Delta\alpha$ loop closed eq. 2.57	Δn_z loop closed eq. 2.63
.23L0	78.4	-.0486	155	.752	-1.29	-0.423
.4L0	238	-.0201	201	.955	-0.176	-0.110
.53L0	408	-.0118	199	.960	-0.0583	-0.0446
.35L20	83.6	-.0485	196	.917	-1.33	-0.465
.55L20	206	-.0206	205	.956	-0.222	-0.131
.75L20	383	-.0119	214	1.010	-0.0596	-0.0459
.5L40	68.7	-.0550	205	.951	-1.98	-0.605
.65L40	116	-.0340	210	.966	-0.670	-0.296
.8L40	176.5	-.0247	235	1.085	-0.272	-0.159
↑Light	Heavy→					
.23H0	78.4	-.0773	260	.823	-2.27	-0.728
.4H0	238	-.0288	326	.951	-0.300	-0.179
.53H0	408	-.0172	325	.957	-0.100	-0.0740
.35H20	83.6	-.0728	313	.825	-2.23	-0.742
.55H20	206	-.0312	331	.959	-0.380	-0.217
.75H20	383	-.0174	342	.995	-0.100	-0.0750
.5H40	68.7	-.0827	326	.946	-3.30	-0.960
.65H40	116	-.0539	336	.966	-1.18	-0.498
.8H40	176.5	-.0335	373	1.070	-0.455	-0.248

* .23L0 corresponds to Mach 0.23, lightweight (23,900 lb) on the deck; .55H20 is Mach 0.55, heavyweight (38,200 lb) at 20,000 ft, etc.

TABLE 2.2 CLOSED-LOOP GAINS REQUIRED FOR NOMINAL SHORT-PERIOD AND PHUGOID CHARACTERISTICS OF ω_{θ_s} = 9 RAD/SEC, ω_{θ_p} = .3 RAD/SEC, $\zeta_{\theta_s} = \zeta_{\theta_p}$ = 0.5 USING THE CONFIGURATION OF FIGURE 2.1

	$\Delta\alpha$ LOOP				$\Delta\alpha$ & Δn_z LOOPS	Δn_z LOOP					PHUGOID LOOP GAINS WITH OPEN SHORT-PERIOD LOOPS	
FLIGHT CODE	δ_e/e_α	$\delta_e/e_{\dot\alpha}$ SEC	δ_e/e_v DEG-SEC / FT	$\delta_e/e_{\dot v}$ DEG-SEC^2 / FT	$\Delta T/e_{\dot\alpha}$ LB-SEC / FT	δ_e/e_{n_z} DEG / g	$\delta_e/e_{\dot\alpha}$ SEC	δ_e/e_v DEG-SEC / FT	$\delta_e/e_{\dot v}$ DEG-SEC^2 / FT	$\left(\frac{\delta_e}{e_{\dot\alpha}}\right)_{MOD.}$ SEC	δ_e/e_v DEG-SEC / FT	$\delta_e/e_{\dot v}$ DEG-SEC^2 / FT
.23L0	-26.1	-2.35	1.29	6.29	65.8	54.4	-0.772	0.931	2.07	-1.331	0.0487	0.237
.40L0	-7.81	-0.599	0.164	0.671	128	10.1	-0.373	0.168	0.417	-0.467	0.0187	0.0764
.525L0	-4.10	-0.275	0.0689	0.283	106	3.67	-0.209	0.0752	0.215	-0.240	0.0139	0.0570
.35L20	-24.5	-2.35	1.20	5.28	100	49.4	-0.819	0.737	1.843	-1.327	0.0435	0.192
.55L20	-9.13	-0.814	0.259	1.10	102	12.5	-0.479	0.215	0.648	-0.599	0.0239	0.102
.75L20	-4.18	-0.339	0.0594	0.156	223	3.59	-0.260	0.0634	0.120	-0.291	0.0119	0.0311
.5L40	-29.7	-3.04	2.02	7.69	109	63.4	-0.931	0.919	2.36	-1.587	0.0562	0.214
.65L40	-16.8	-1.68	0.781	3.09	109	29.4	-0.742	0.465	1.37	-1.040	0.0396	0.157
.8L40	-10.1	-0.982	0.823	1.50	79.4	13.4	-0.577	0.562	0.878	-0.710	0.0746	0.136
.23H0	-28.22	-2.70	1.70	8.60	111	87.9	-0.864	1.32	2.76	-1.475	0.0579	0.293
.40H0	-8.58	-0.746	0.279	1.12	193	17.0	-0.449	0.267	0.672	-0.558	0.0271	0.108
.525H0	-4.59	-0.375	0.114	0.476	174	6.39	-0.277	0.118	0.352	-0.315	0.0196	0.0816
.35H20	-26.5	-2.66	2.01	8.34	155	80.8	-0.885	1.17	2.78	-1.447	0.0655	0.272
.55H20	-9.96	-0.957	0.432	1.76	169	20.9	-0.544	0.339	1.00	-0.681	0.0353	0.144
.75H20	-4.65	-0.428	0.0662	0.221	437	6.22	-0.321	0.0749	0.165	-0.358	0.0115	0.0383
.5H40	-32.1	-3.37	3.48	12.8	162	104	-0.982	1.46	3.72	-1.710	0.0876	0.321
.65H40	-18.1	-1.88	1.33	4.86	174	48.5	-0.799	0.746	2.06	-1.131	0.0609	0.223
.8H40	-11.1	-1.12	1.26	2.26	138	22.6	-0.635	0.783	1.28	-0.789	0.0921	0.166

Appendix D

TABLE 3.1 LATERAL-DIRECTIONAL MCS CONTROL LOOP GAINS FOR NOMINAL CHARACTERISTICS OF ω_ψ = 7.5 RAD/SEC, ζ_ψ = 0.5, τ_e = .067 SEC

		β Loop			n_Y Loop	
Code	$\bar{q}$ lb/ft^2	δ_r/e_β	$\delta_r/e_{\dot\beta}$ sec	δ_a/e_p sec	δ_r/e_{n_Y} deg/g	$\delta_{r'}/e_{\dot\beta}$ sec
.23L0	78.4	60.3	7.76	4.49	-171	.488
.4L0	238	18.2	2.42	1.26	-49.1	.440
.53L0	408	9.91	1.38	0.629	-24.9	.399
.35L20	83.6	56.2	7.42	4.31	-159	.498
.55L20	206	21.5	2.92	1.53	-58.6	.466
.75L20	383	11.6	1.67	0.684	-28.8	.465
.5L40	68.7	69.1	9.25	5.30	-196	.512
.65L40	116	40.9	5.54	2.78	-114	.511
.8 L40	176.5	28.8	3.98	1.76	-78.2	.567
↑Light	Heavy↓					
.23H0	78.4	94.4	12.3	14.1	-279	.505
.4H0	238	28.8	3.84	4.28	-84.1	.474
.53H0	408	16.0	2.20	2.33	-44.6	.444
.35H20	83.6	87.9	11.65	13.2	-261	.513
.55H20	206	33.8	4.58	4.88	-99.4	.492
.75H20	383	18.7	2.62	2.33	-51.6	.507
.5H40	68.7	108	14.4	15.8	-320	.521
.65H40	116	64.0	8.64	8.36	-189	.526
.8H40	176.5	45.4	6.21	5.39	-132	.592

TABLE 3.2

ACCURACY OF THE APPROXIMATE EQUATION $\tau_R \cong -\frac{1}{L_p}$ FOR THE OPEN-LOOP JETSTAR

CODE	τ_R*	$-1/L_p$
.23L0	.4801	.4866
.40L0	.2680	.2707
.525L0	.1996	.2020
.35L20	.6146	.6274
.55L20	.3811	.3864
.75L20	.2672	.2689
.50L40	.9497	.9805
.65L40	.7189	.7335
.75L20	.5609	.5702
.23H0	1.20	1.3464
.40H0	.7645	.7586
.525H0	.580	.5670
.35H20	1.535	1.7406
.55H20	1.086	1.0818
.75H20	.7704	.7578
.50H40	2.379	2.7247
.65H40	1.987	2.0479
.80H40	1.608	1.5957

* τ_R is obtained from the fourth-order characteristic equation by digital computation.

TABLE 3.3

COMPARISON OF THE EXACT CHANGE IN THE COEFFICIENT E OF THE CHARACTERISTIC EQUATION WITH THAT GIVEN BY THE APPROXIMATION $\Delta E \cong \frac{\delta_a}{e_\phi} \frac{\delta_r}{e_\beta} L_{\delta_a} \left[-N_{\delta_r} (1+\alpha_t^2) + Y_{\delta_r} (\alpha_t N_p - N_r) \right]$

CODE	ΔE EXACT	ΔE APPROX
.23L0	46.94	44.4
.40L0	37.26	32.8
.525L0	30.04	24.4
.35L20	50.11	46.5
.55L20	43.53	38.9
.75L20	36.95	30.3
.50L40	54.53	51.2
.65L40	51.14	46.8
.80L40	48.24	43.3
.23H0	58.34	53.2
.40H0	53.21	48.2
.525H0	48.27	42.0
.35H20	58.7	53.2
.55H20	53.74	48.8
.75H20	50.46	44.4
.50H40	61.84	55.2
.65H40	57.77	52.6
.80H40	55.57	50.5

TABLE 3.4

SPIRAL ROOTS OF CLOSED-LOOP JETSTAR

CODE	$-1/\tau_s$ ~ sec	δ_a/e_ρ ~ sec
.23L0	-.07566	2.76
.40L0	-.06379	.701
.525L0	-.05250	.316
.35L20	-.08222	2.70
.55L20	-.07467	.912
.75L20	-.06436	.381
.50L40	-.08890	3.40
.65L40	-.08637	1.76
.80L40	-.08319	1.10
.23H0	-.09025	9.14
.40H0	-.08746	2.72
.525H0	-.08325	1.45
.35H20	-.09349	8.59
.55H20	-.09114	3.15
.75H20	-.08741	1.48
.50H40	-.09633	10.4
.65H40	-.09548	5.48
.80H40	-.09451	3.51

calculated for $\begin{cases} \delta_a/e_\rho \text{ to give } \tau_R = +.10 \text{ sec from equation 3.16} \\ \delta_a/e_\phi = \frac{1}{10}\,\delta_a/e_\rho \\ \delta_r/e_\beta \text{ given by Table 3.1} \end{cases}$

using equation 3.17

TABLE 5.1 DESIGN VALUES OF GPAS RFS GAINS

Gain	Derivative Changed	Range	Units	Primary Function	Estimated Max. Established by*
δ_e/α	M_α	±10	-	short-period frequency	(1) and (2)
$\delta_e/\dot{\alpha}$	$M_{\dot{\alpha}}$	±1	sec	short-period damping	(2)
δ_e/q	M_q	±3	sec	short-period damping	(3)
$\delta_e/\dot{q}$	–	±.1	sec^2	elevator servo compensation	(2)
δ_e/V	M_V	±.5	deg-sec/ft	phugoid frequency	(2)
$\delta_e/\dot{V}$	$M_{\dot{V}}$	±1	$deg\text{-}sec^2/ft$	phugoid damping	(2)
δ_r/β	N_β	±10	-	Dutch-roll frequency; directional stability	(1) and (2)
$\delta_r/\dot{\beta}$	$N_{\dot{\beta}}$	±1	sec	Dutch-roll damping	(2)
δ_r/r	N_r	±4	sec	Dutch-roll damping	(3)
$\delta_r/\dot{r}$	–	±.1	sec^2	rudder servo compensation	(2)
δ_r/p	N_p	±4	sec	roll to yaw coupling	(3)
$\delta_r/\dot{p}$	–	±.1	sec^2	rudder servo compensation	(2)
δ_a/ϕ	L_ϕ	±5	-	roll attitude stabilization	(3)
δ_a/p	L_p	±2	sec	roll mode time constant	(1) and (2)
$\delta_a/\dot{p}$	–	±.1	sec^2	aileron servo compensation	(2)
δ_a/r	L_r	±4	sec	spiral mode time constant	(3)
$\delta_a/\dot{r}$	–	±.1	sec^2	aileron servo compensation	(1) and (2)
δ_a/β	L_β	±10		roll to yaw ratio; ω_ϕ/ω_ψ	(2)
$\delta_a/\dot{\beta}$	–	±1	sec	phase compensation	(2)
δ_e/δ_{e_p}	$M_{\delta_{e_c}}$	0 to 10	deg/in.	elevator control gearing	(3)
δ_a/δ_{a_p}	$L_{\delta_{a_c}}$	0 to 1	deg/deg	aileron control gearing	(3)
δ_r/δ_{r_p}	$N_{\delta_{r_c}}$	0 to 30	deg/in.	rudder control gearing	(3)
δ_e/F_e	–	0 to 1	deg/lb	elevator force command sensitivity	(3)
δ_a/F_a	–	0 to .2	deg/lb	aileron force command sensitivity	(3)
δ_r/F_r	–	0 to .5	deg/lb	rudder force command sensitivity	(3)
δ_a/δ_{r_p}	$L_{\delta_{r_c}}$	±5	deg/in.	roll due to yaw command	(3)
δ_r/δ_{a_p}	$N_{\delta_{a_c}}$	±1	deg/deg	yaw due to roll command	(3)
δ_{a_c}/δ'_r	L_{δ_r}	±2	deg/deg	roll due to yaw control derivative	(3)
δ_{r_c}/δ'_a	N_{δ_a}	±2	deg/deg	yaw due to roll control derivative	(3)

* 1) structural instability; 2) noise, 3) sufficient for the task
Reference: Figures 1-1 through 1-3, GPAS Memo No. 53

TABLE 5.2 RFS GAINS NECESSARY TO ACHIEVE LONGITUDINAL DYNAMICS SHOWN BELOW – ω_{θ_S} = 6.32 RAD/SEC

			Gains with ω_{θ_S} = 6.32					
	$\bar{q}$	δ_e/α ω_{θ_S} =	$\delta_e/\dot{\alpha}$ sec			δ_e/V deg-sec/ft	$\delta_e/\dot{V}$ deg-sec²/ft	
Code	lb/ft²	6.32	ζ_{θ_S} = 0	0.5	1.5	ω_{θ_p} = 0.15	ζ_{θ_p} = 0.15	.50
.23L0	78.4	12.3*	-.662	1.45*	5.69*	.0431	-.306	-2.67*
,4L0	238	3.33	-.381	.307	1.69*	-.0635	-.0907	-.530
.53L0	408	1.49	-.297	.105	.908	-.0291	-.0431	-.234
.35L20	83.6	11.6*	-.479	1.51*	5.48*	-.233	-.432	-3.26*
.55L20	206	4.03	-.306	.481	2.05*	-.101	-.185	-.895
.75L20	383	1.52	-.242	..166	.982	-.0555	-.0617	-.303
.5L40	68.7	14.2*	-.361	2.03*	6.80*	-.710*	-.434	-5.83*
.65L40	116	7.80	-.284	1.09	3.85*	-.367	-.495	-2.83*
.8L40	176.5	4.46	-.251	.615	2.35*	-.378	-.170	-1.21*
↕ Light Heavy								
.23H0	78.4	13.4*	-.550	1.73*	6.29*	.215	-1.11*	-4.92*
.4H0	238	3.76	-.311	.431	1.92*	-.101	-.0968	-.844
.53H0	408	1.78	-.242	.191	1.06*	-.0498	-.0840	-.411
.35H20	83.6	12.6*	-.391	1.75*	6.03*	-.359	-.427	-5.17*
.55H20	206	4.46	-.249	.598	2.29*	-.177	-.257	-1.47*
.75H20	383	1.80	-.198	.242	1.12*	-.0840	-.109	-.519
.5H40	68.7	15.4*	-.295	2.28*	7.42*	-1.11*	-.438	-9.44*
.65H40	116	8.50	-.233	1.25*	4.22*	-.622*	-.334	-4.29*
.8H40	176.5	5.01	-.204	.729	2.59*	-.597*	-.0961	-1.86*

* Exceeds maximum estimated value from Table 5.1

TABLE 5.3 RFS GAINS NECESSARY TO ACHIEVE LONGITUDINAL DYNAMICS SHOWN BELOW – ω_{θ_s} = 3 RAD/SEC

			Gains With ω_{θ_s} = 3					
	$\bar{q}$	δ_e/α	$\delta_e/\dot{\alpha}$ sec			δ_e/V deg-sec/ft	$\delta_e/\dot{V}$ deg-sec^2/ft	
Code	lb/ft^2	ω_{θ_s} = 3	ζ_{θ_s} = 0	0.5	1.5	ω_{sp} = 0.15	ζ_{sp} = .15	0.50
.23L0	78.4	1.97	-.662	.342	2.35*	.00966	-.0687	-.598
.4L0	238	-.0406	-.381	-.0544	.599	-.0141	-.0201	-.118
.53L0	408	-.482	-.297	-.107	.275	-.00638	-.00944	-.0513
.35L20	83.6	1.89	-.479	.463	2.35*	-.0523	-.0970	-.733
.55L20	206	.178	-.306	.0676	.814	-.0227	-.0414	-.200
.75L20	383	-.474	-.242	-.0487	.339	-.0123	-.0137	-.0671
.5L40	68.7	2.54	-.361	.772	3.04*	-.160	-.0976	-1.31*
.65L40	116	1.06	-.284	.369	1.68*	-.0825	-.111	-.636
.8L40	176.5	.222	-.251	.160	.982	-.0850	-.0382	-.272
Light ↑ / Heavy ↓								
.23H0	78.4	2.24	-.550	.533	2.70*	.0483	-.250	-1.11*
.4H0	238	.125	-.311	.0411	.746	-.0225	-.0216	-.189
.53H0	408	-.344	-.242	-.0365	.375	-.0111	-.0187	-.0913
.35H20	83.6	2.15	-.391	.624	2.66*	-.0807	-.0961	-1.16*
.55H20	206	3.15	-.249	.153	.957	-.0397	-.0576	-.330
.75H20	383	-.357	-.198	.0110	.428	-.0188	-.0245	-.116
.5H40	68.7	2.83	-.295	.926	3.37*	-.250	-.0986	-2.13*
.65H40	116	1.24	-.233	.472	1.88*	-.140	-.0751	-.965
.8H40	176.5	.449	-.204	.239	1.12*	-.134	-.0216	-.419

* Exceeds maximum estimated value from Table 5.1

TABLE 5.4 RFS GAINS REQUIRED FOR SPECIFIED DUTCH ROLL PROPERTIES

		ω_ψ = 5 rad/sec, ζ_ψ = 0.5		ω_ψ = 2.5 rad/sec, ζ_ψ = 1.0		ω_ψ = 2.5 rad/sec, ζ_ψ = 0.5	
Code	$\bar{q}$ lb/ft^2	δ_r/β	$\delta_r/\dot{\beta}$ sec	δ_r/β	$\delta_r/\dot{\beta}$ sec	δ_r/β	$\delta_r/\dot{\beta}$ sec
.23L0	78.4	-25.7*	-5.07*	-4.97	-6.22*	-4.97	-2.36*
.4L0	238	-7.10	-1.55*	-.448	-1.73*	-.448	-.677
.53L0	408	-3.45	-.869	.462	-.948	.426	-.360
.35L20	83.6	-23.9*	-4.87*	-4.51	-5.57*	-4.51	-2.31*
.55L20	206	-8.53	-1.90*	-.771	-2.06*	-.771	-.871
.75L20	383	-4.03	-1.07	.484	-1.14*	.484	-.471
.5L40	68.7	-29.6*	-6.10*	-5.89	-6.73*	-5.89	-2.96*
.65L40	116	-17.1*	-3.65*	-2.81	-3.93*	-2.81	-1.75*
.8L40	176.5	-11.6*	-2.61*	-1.27	-2.77*	-1.27	-1.24*
Light ↑							
Heavy ↓							
.23H0	78.4	-40.8*	-8.09*	-8.68	-9.81*	-8.68	-3.56*
.4H0	238	-11.8*	-2.50*	-1.56	-2.77*	-1.56	-1.15*
.53H0	408	-6.11	-1.42*	-.191	-1.53*	-.191	-.634
.35H20	83.6	-37.9*	-7.68*	-7.96	-8.73*	-7.96	-3.71*
.55H20	206	-14.0*	-3.00*	-2.09	-3.24*	-2.09	-1.42*
.75H20	383	-7.17	-1.71*	-.226	-1.81*	-.266	-.790
.5H40	68.7	-46.8*	-9.56*	-10.1	-10.5*	-10.1	-4.68*
.65H40	116	-27.3*	-5.71*	-5.25	-6.12*	-5.25	-2.78*
.8H40	176.5	-18,9*	-4.10*	-3.03	-4.33*	-3.03	-1.98*

*Exceeds maximum estimated values from Table 5.1

TABLE 5.5 ROLL TO SIDESLIP RATIO PROPERTIES

		$\left\lvert \frac{\phi}{\beta} \right\rvert = 0$	$\frac{\delta_a}{\beta} = -10$
Code	$\bar{q}$, lb/ft^2	δ_a/β	$\lvert\phi/\beta\rvert$
.23L0	78.4	2.46	11.1
.4L0	238	1.45	10.7
.53L0	408	1.53	11.1
.35L20	83.6	2.24	13.2
.55L20	206	1.32	13.2
.75L20	383	0.69	13.1
.5L40	68.7	2.29	15.9
.65L40	116	1.62	17.0
.8L40	176.5	0.78	15.4
Light ↑ / Heavy ↓			
.23H0	78.4	3.38	9.41
.4H0	238	1.70	8.98
.53H0	408	1.28	9.13
.35H20	83.6	2.99	10.0
.55H20	206	1.57	9.94
.75H20	383	0.86	10.1
.5H40	68.7	3.00	10.5
.65H40	116	1.71	10.7
.8H40	176.5	0.92	10.1

TABLE 5.6 RANGE OF CONTROL GAIN RATIO $\frac{\delta_r}{\delta_{a_p}} \Big/ \frac{\delta_a}{\delta_{a_p}}$ NECESSARY TO MEET THE VALUES OF ω_ϕ/ω_ψ REQUIRED BY THE GPAS WORK STATEMENT

		$\frac{\delta_r}{\delta_{a_p}} \Big/ \frac{\delta_a}{\delta_{a_p}}$	
Code	$\bar{q}$, lb/ft^2	$\omega_\phi/\omega_\psi = 0.5$	$\omega_\phi/\omega_\psi = 1.5$
.23L0	78.4	1.05	-.555
.4L0	238	1.88	-.809
.53L0	408	1.56	-.791
.35L20	83.6	1.17	-.731
.55L20	206	2.31	-.883
.75L20	383	16.9	-1.39
.5L40	68.7	1.19	-.570
.65L40	116	5.59	-.829
.8L40	176.5	17.7	-1.39
Light ↑ / Heavy ↓			
.23H0	78.4	.840	-.396
.4H0	238	1.61	-.752
.53H0	408	2.38	-.892
.35H20	83.6	.924	-.472
.55H20	206	1.85	-.803
.75H20	383	7.98	-1.28
.5H40	68.7	.987	-.472
.65H40	116	1.82	-.814
.8H40	176.5	13.5	-1.23

TABLE 5.7 ROLL AND SPIRAL MODE TIME CONSTANTS

		Roll Mode Time Constant	Spiral Mode Time Constant $\delta_a/p = 0$	
	$\bar{q}$	$\frac{\delta_a}{p} = -2$ sec	$\frac{\delta_a}{r} = 4$	$\frac{\delta_a}{r} = -4$
Code	lb/ft^2	τ_R sec	τ_s sec	τ_s sec
.23L0	78.4	.128	-2.43	2.08
.4L0	238	.046	-1.66	1.60
.53L0	408	.027	-1.61	1.55
.35L20	83.6	.128	-1.96	1.83
.55L20	206	.053	-1.58	1.54
.75L20	383	.027	-1.42	1.41
.5L40	68.7	.159	-1.84	1.76
.65L40	116	.090	-1.54	1.50
.8L40	176.5	.060	-1.49	1.48
Light ↑ / Heavy ↓				
.23H0	78.4	.373	-3.70	2.89
.4H0	238	.130	-1.68	1.61
.53H0	408	.076	-1.52	1.48
.35H20	83.6	.361	-2.53	2.29
.55H20	206	.149	-1.58	1.54
.75H20	383	.077	-1.40	1.38
.5H40	68.7	.450	-2.28	2.12
.65H40	116	.252	-1.58	1.54
.8H40	176.5	.168	-1.47	1.46

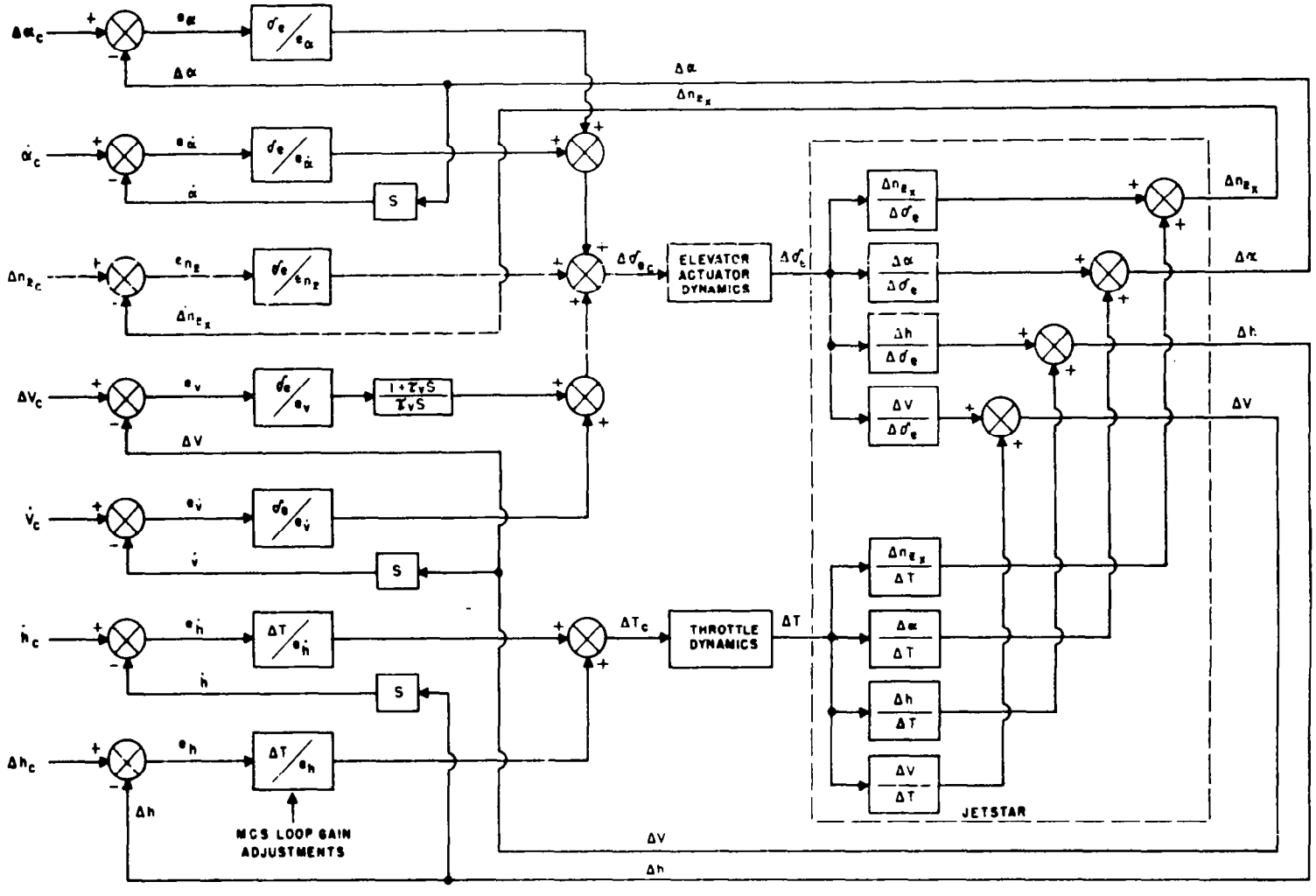

FIGURE 2.1 BLOCK DIAGRAM OF THE ORIGINAL LONGITUDINAL MCS CONTROL LOOPS

Configuration of Figure 2.1

$$\frac{\delta_e}{e_{n_z}} = 6.22 \text{ deg/g} \qquad \frac{\delta_e}{e_v} = 0.0749 \frac{\text{deg-sec}}{\text{ft}}$$

$$\frac{\delta_e}{e_{\dot{\alpha}}} = -0.321 \text{ sec} \qquad \frac{\delta_e}{e_{\dot{v}}} = 0.165 \frac{\text{deg-sec}^2}{\text{ft}}$$

$$\tau_v = 20 \text{ sec} \qquad \frac{\Delta T}{e_{\dot{h}}} = 437 \frac{\text{lb-sec}}{\text{ft}}$$

$$\frac{\Delta T}{e_h} = 21.8 \text{ lb/ft}$$

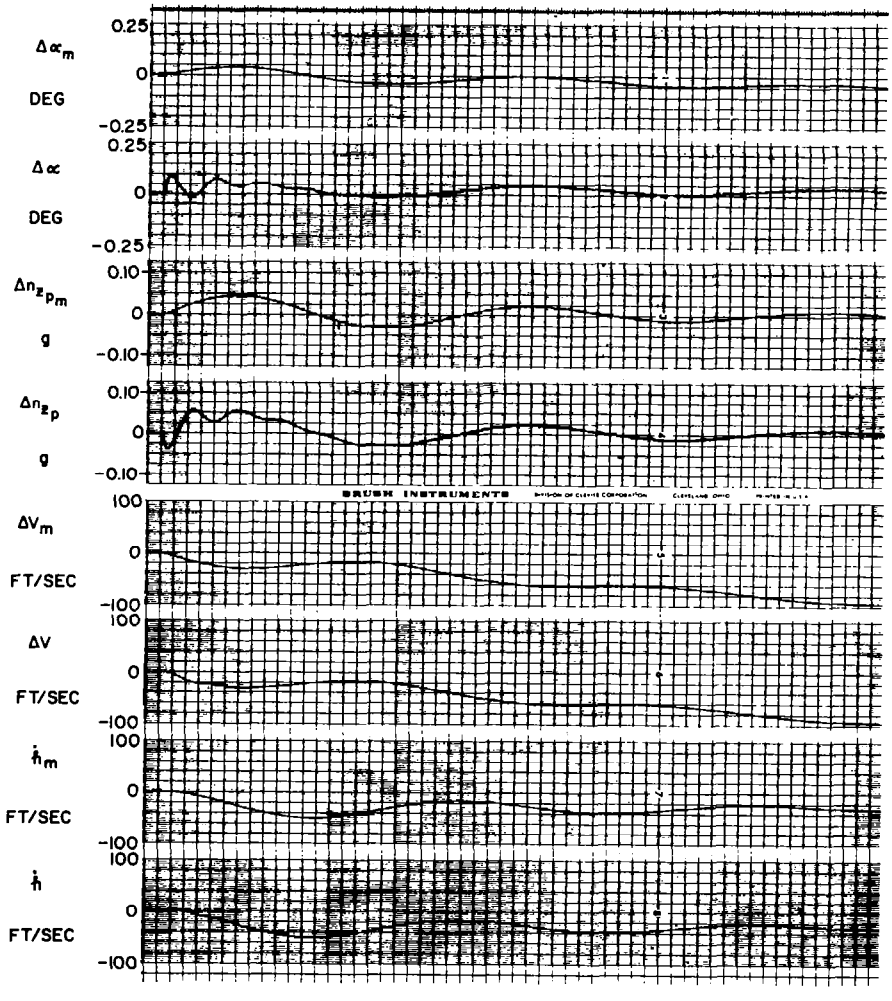

FIGURE 2.2 GPAS RESPONSE TO MODEL THRUST COMMAND
.75H20 MODEL AND JETSTAR

$\Delta T_m = -12,500\ u(t)$ LB

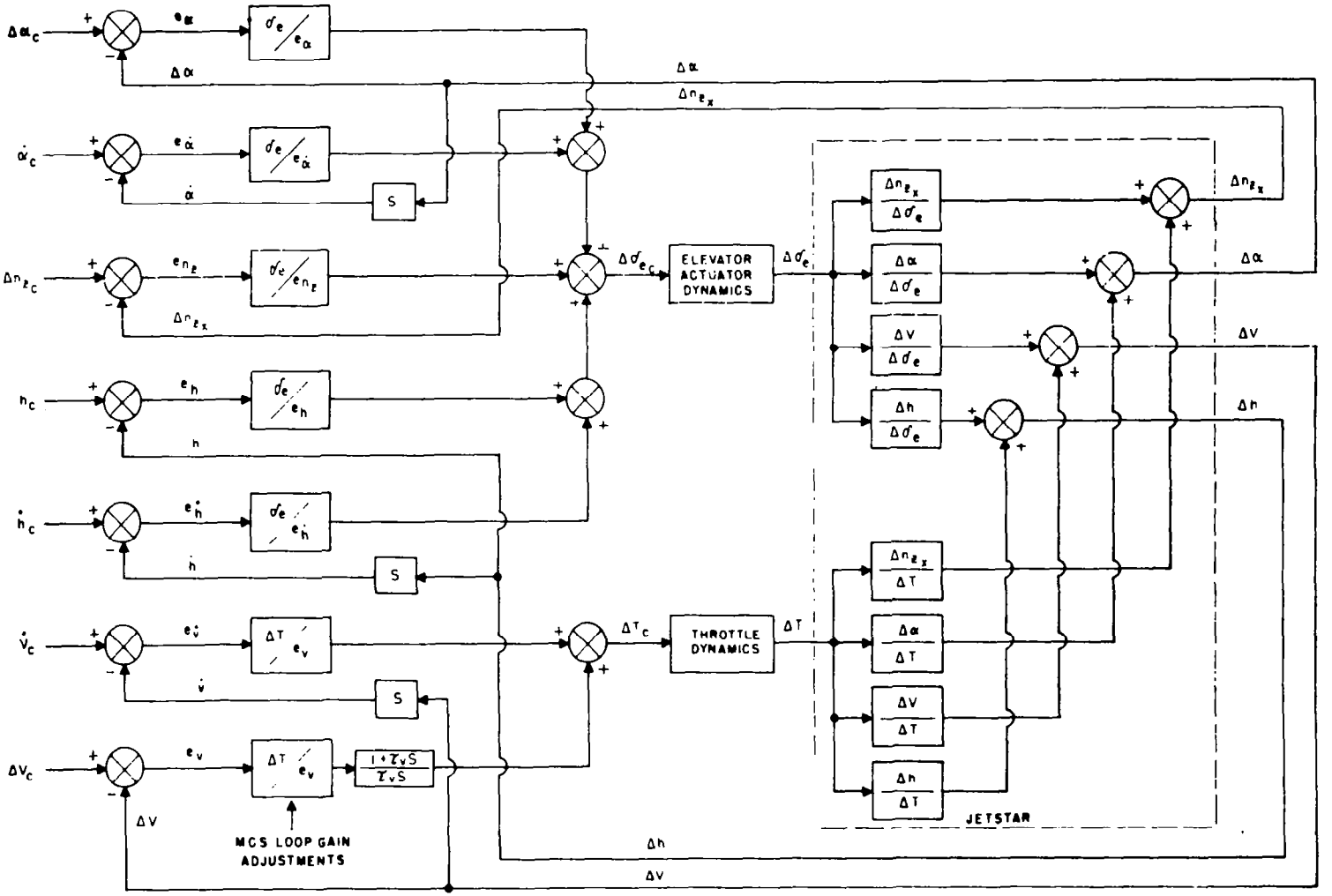

FIGURE 2.3 BLOCK DIAGRAM OF THE MODIFIED LONGITUDINAL MCS CONTROL LOOPS

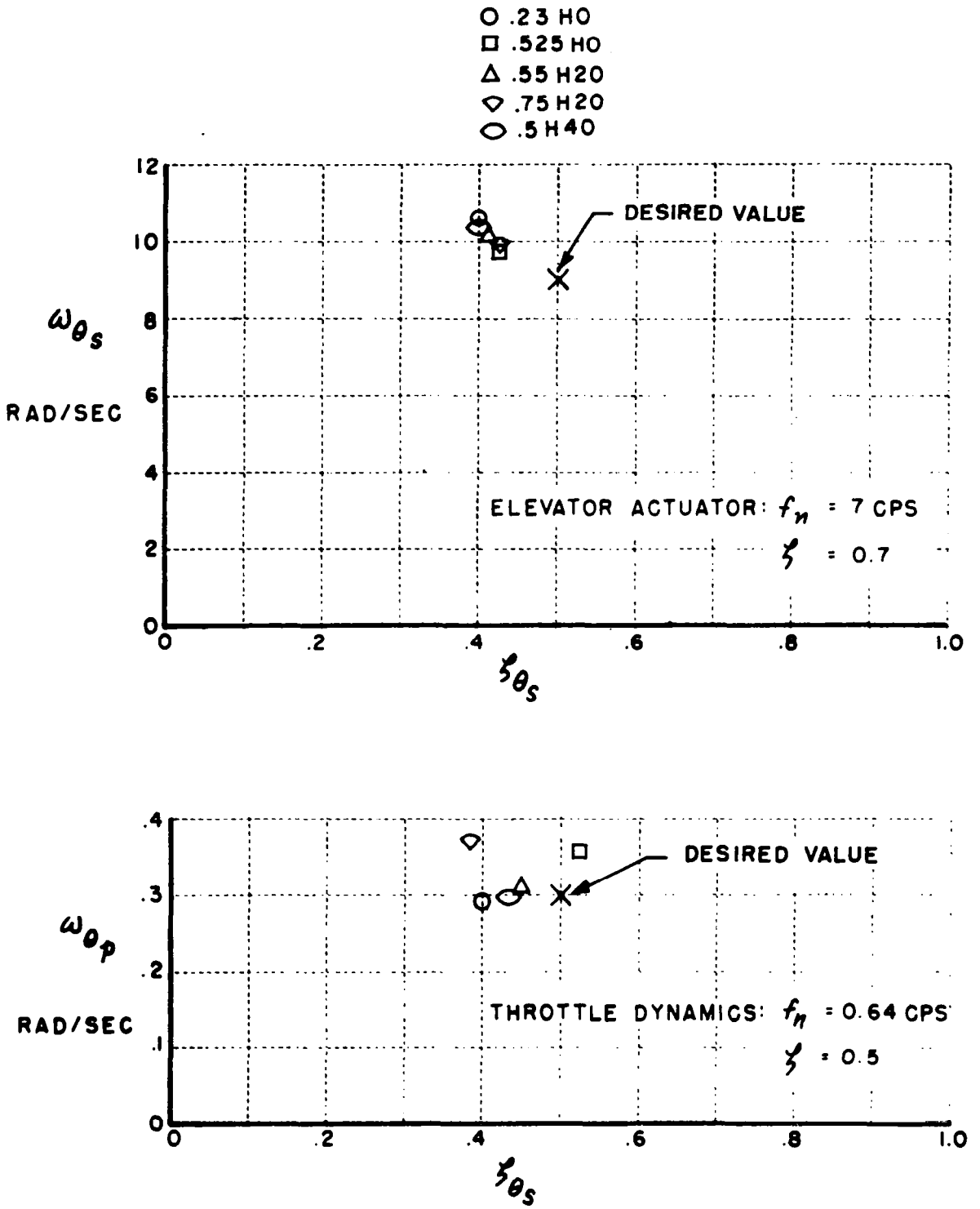

FIGURE 2.4 CLOSED-LOOP JETSTAR SHORT-PERIOD AND PHUGOID ROOTS. USING $\Delta\alpha$, $\dot{\alpha}$, ΔV, $\dot{V}$, AND $\dot{h}$ CONTROL LOOPS IN THE CONFIGURATION OF FIGURE 2.1.

$$\frac{\Delta T}{e_{\dot{t}}} = 213 \frac{\text{lb-sec}}{\text{ft}} \qquad \frac{\delta_e}{e_{n_z}} = 0$$

$$\frac{\delta_e}{e_v} = 0.365 \frac{\text{deg-sec}}{\text{ft}} \qquad \frac{\delta_e}{e_\alpha} = -9.49$$

$$\frac{\delta_e}{e_{\dot{v}}} = 1.42 \frac{\text{deg-sec}^2}{\text{ft}} \qquad \frac{\delta_e}{e_{\dot{\alpha}}} = -0.846 \text{ sec}$$

$$\frac{\Delta T}{e_h} = 0 \qquad \tau_v = \infty$$

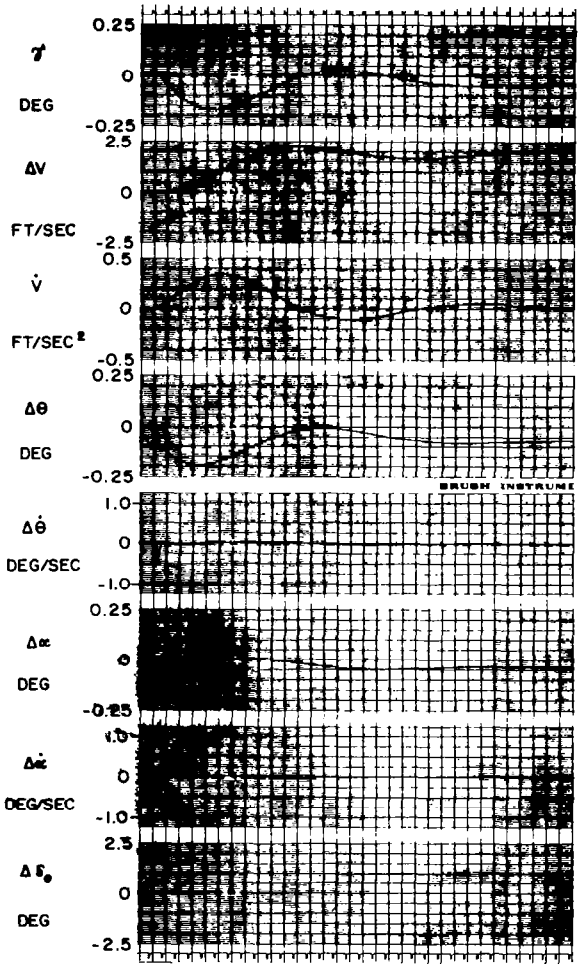

FIGURE 2.5 CLOSED-LOOP JETSTAR RESPONSE TO A UNIT STEP FUNCTION ELEVATOR COMMAND SIGNAL-.55H20

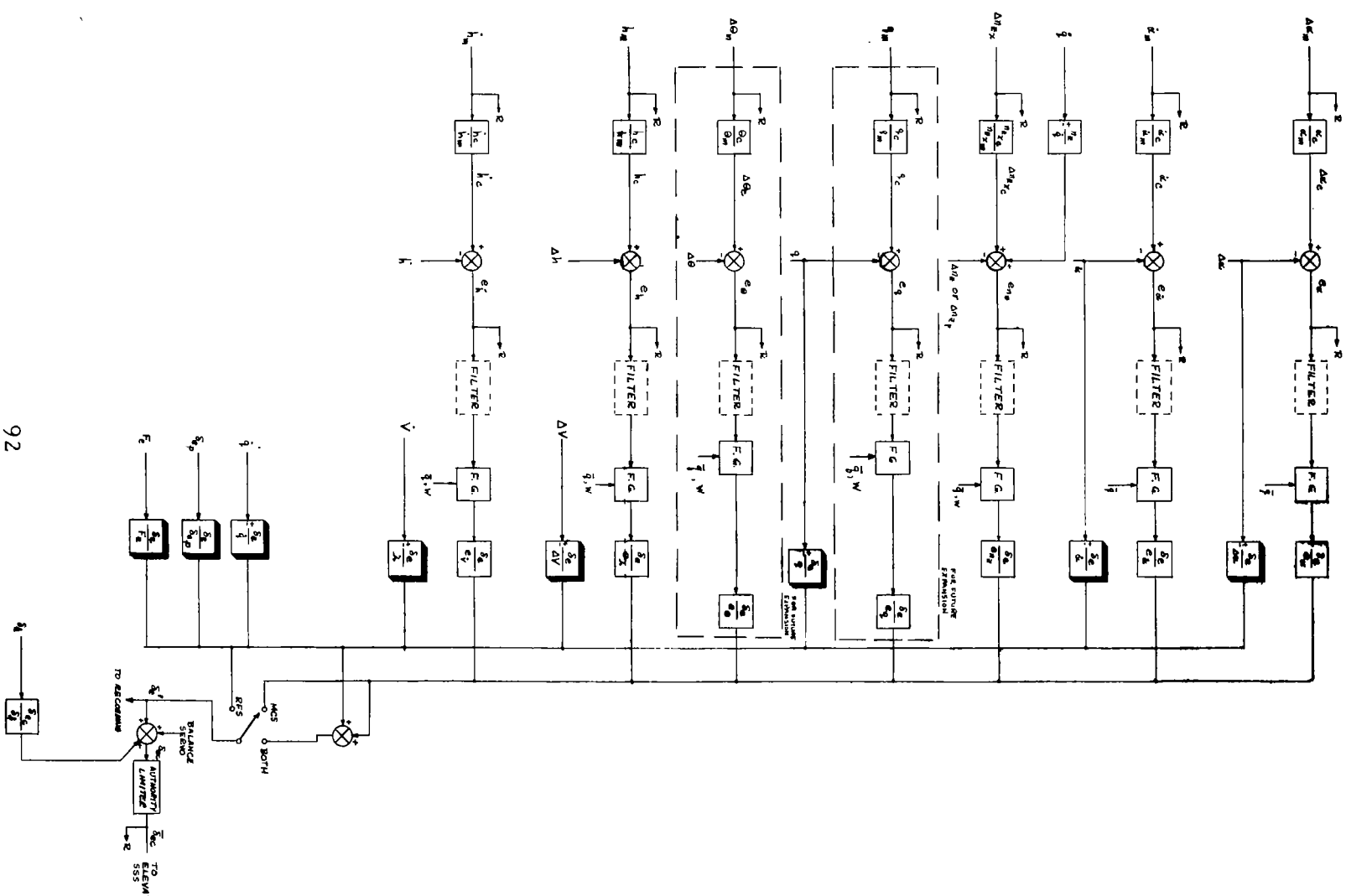

FIGURE 2.6 ELEVATOR CHANNEL – FUNCTIONAL BLOCK DIAGRAM

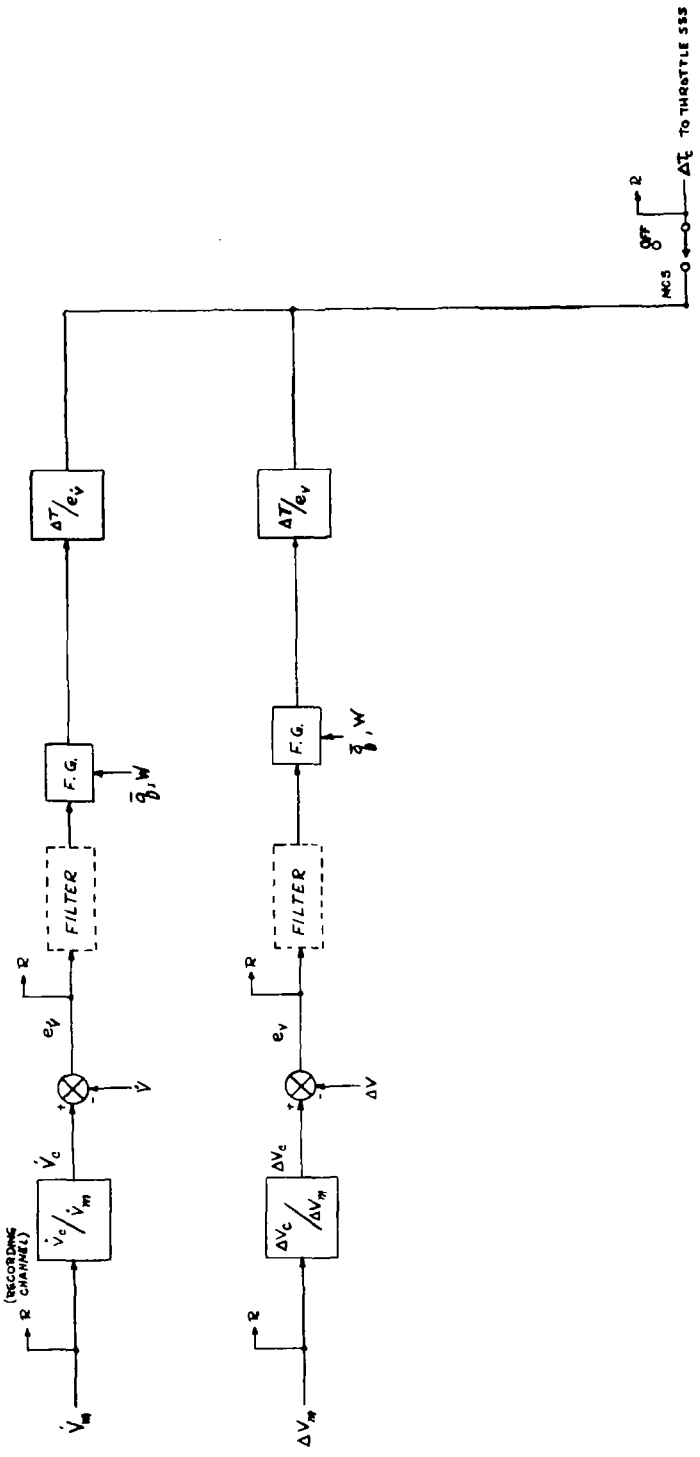

FIGURE 2.7 THROTTLE CHANNEL - FUNCTIONAL BLOCK DIAGRAM

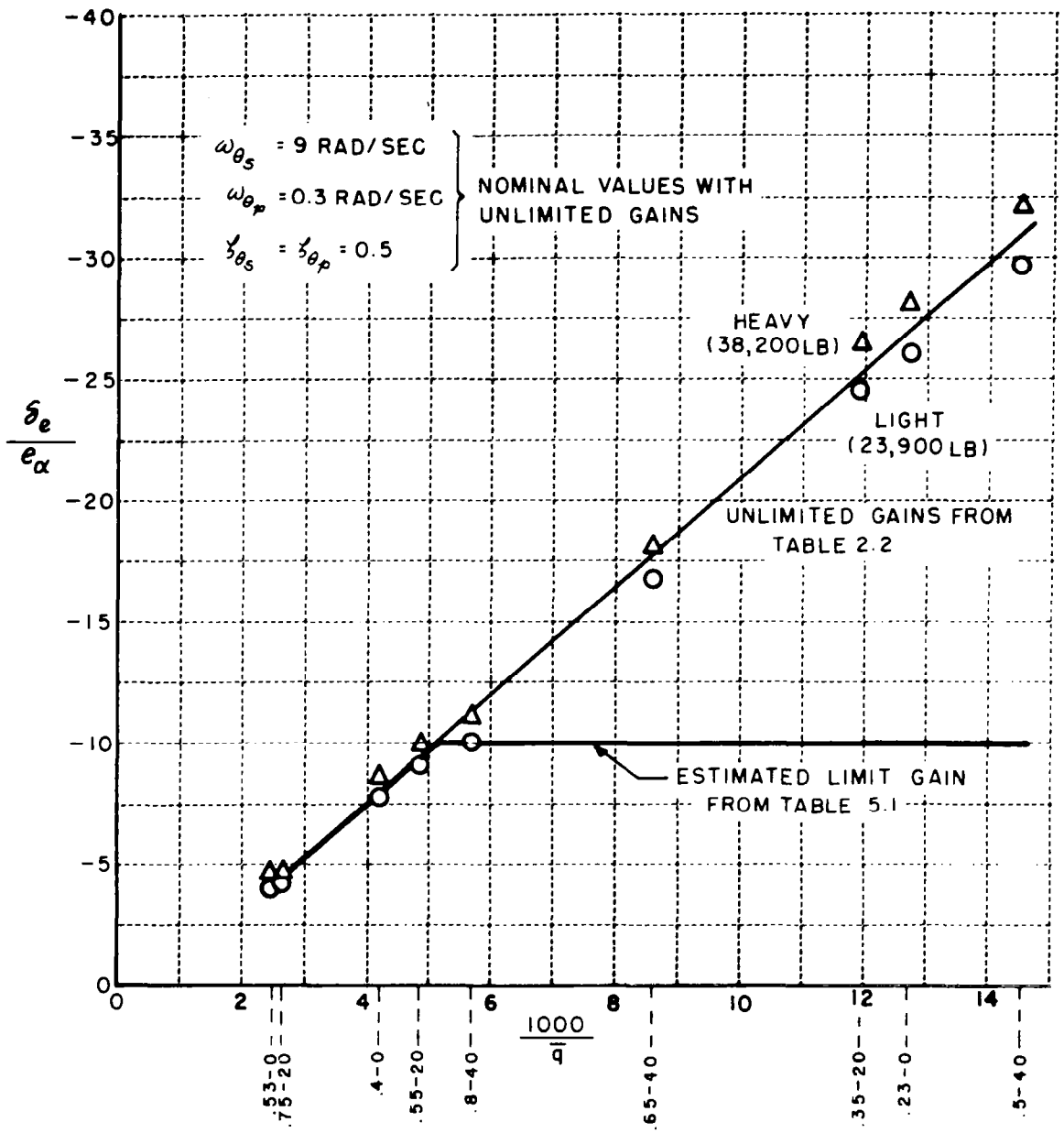

FIGURE 2.8 LONGITUDINAL ANGLE OF ATTACK GAIN VS. INVERSE DYNAMIC PRESSURE

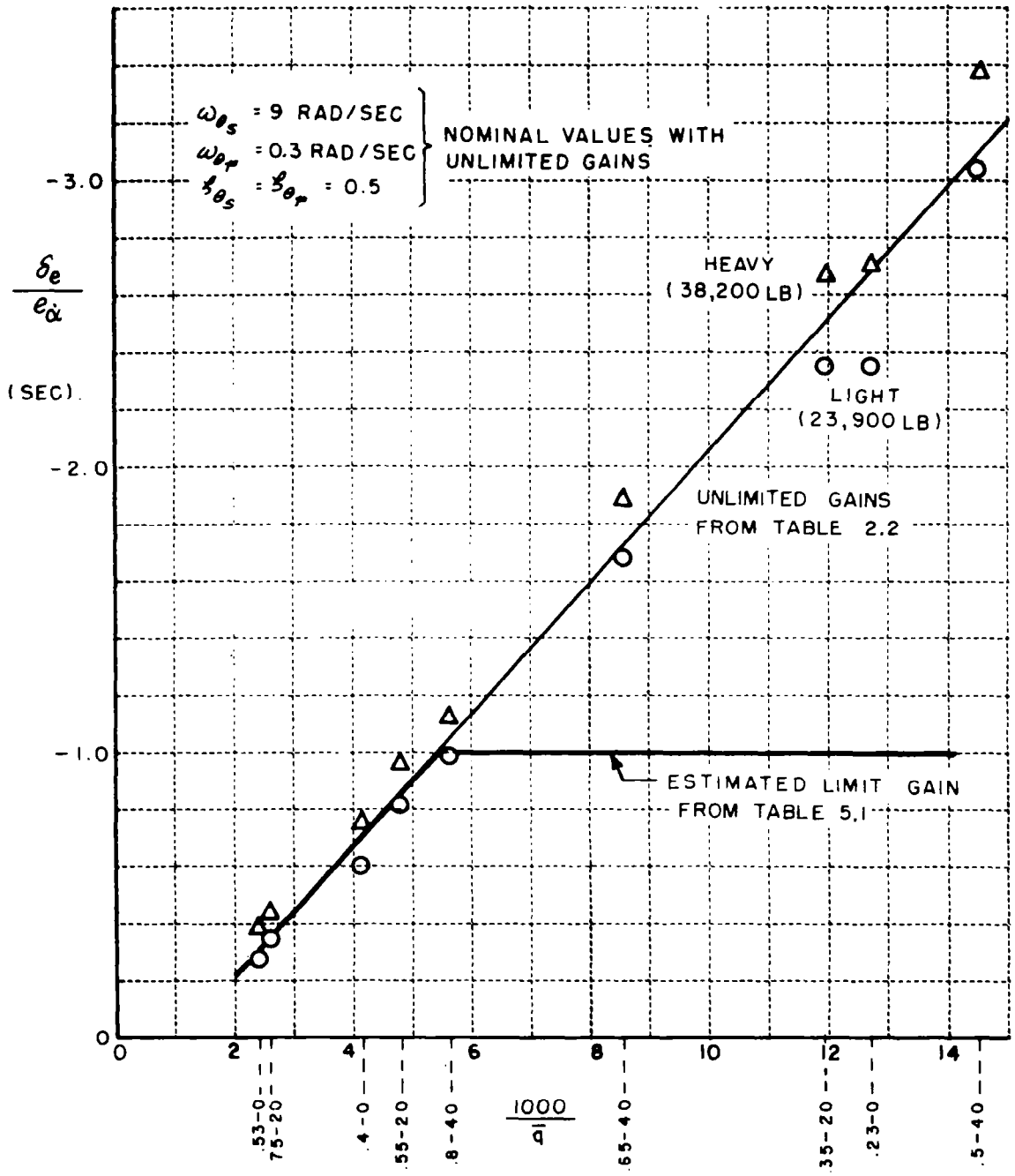

FIGURE 2.9 LONGITUDINAL SHORT-PERIOD DAMPING GAIN VS. INVERSE DYNAMIC PRESSURE

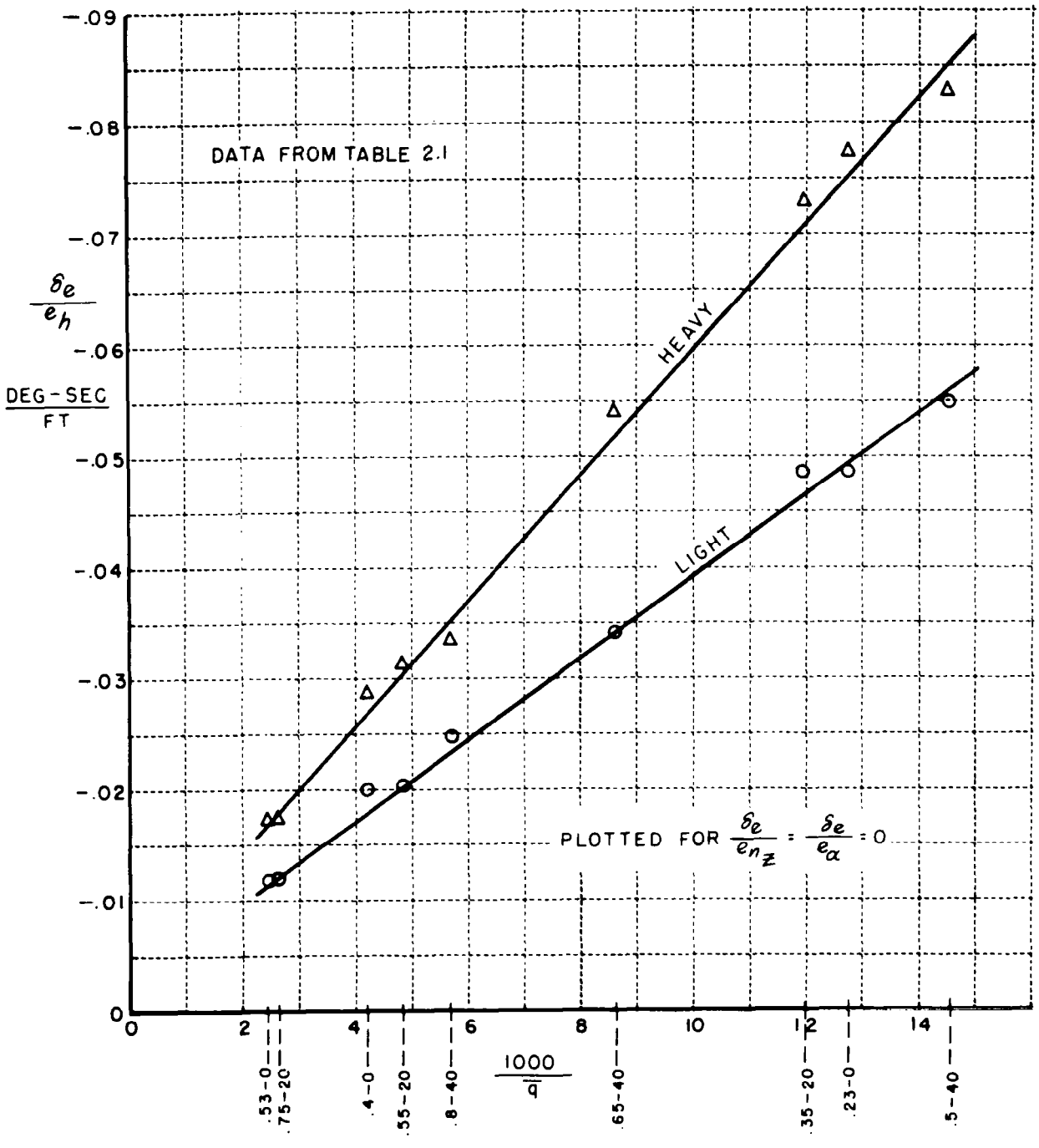

FIGURE 2.10(a) LONGITUDINAL ELEVATOR PHUGOID CONTROL LOOP GAIN VS. INVERSE DYNAMIC PRESSURE

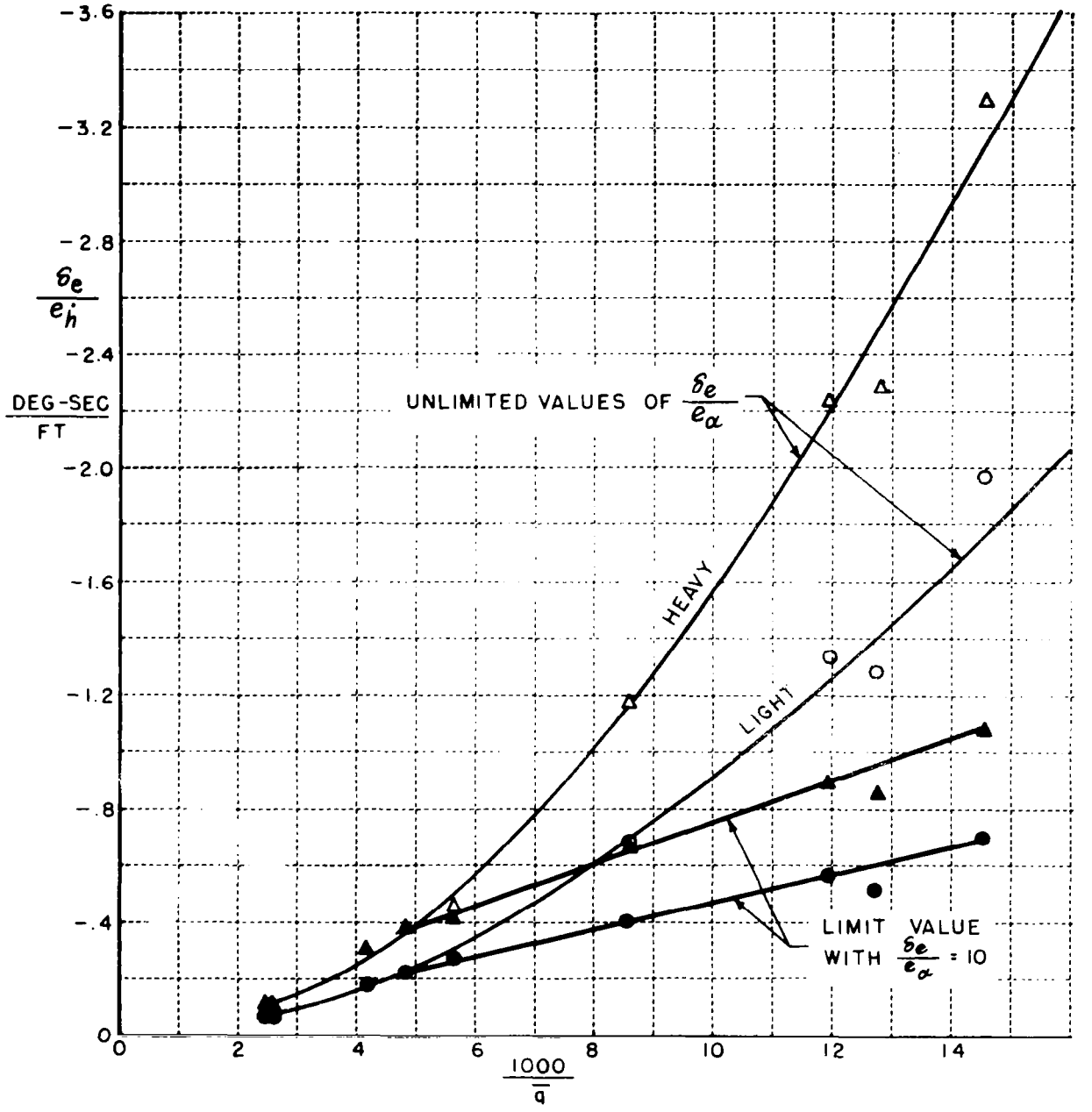

FIGURE 2.10(b) LONGITUDINAL ELEVATOR PHUGOID CONTROL LOOP GAIN VS. INVERSE DYNAMIC PRESSURE ($\Delta\alpha$ LOOP)

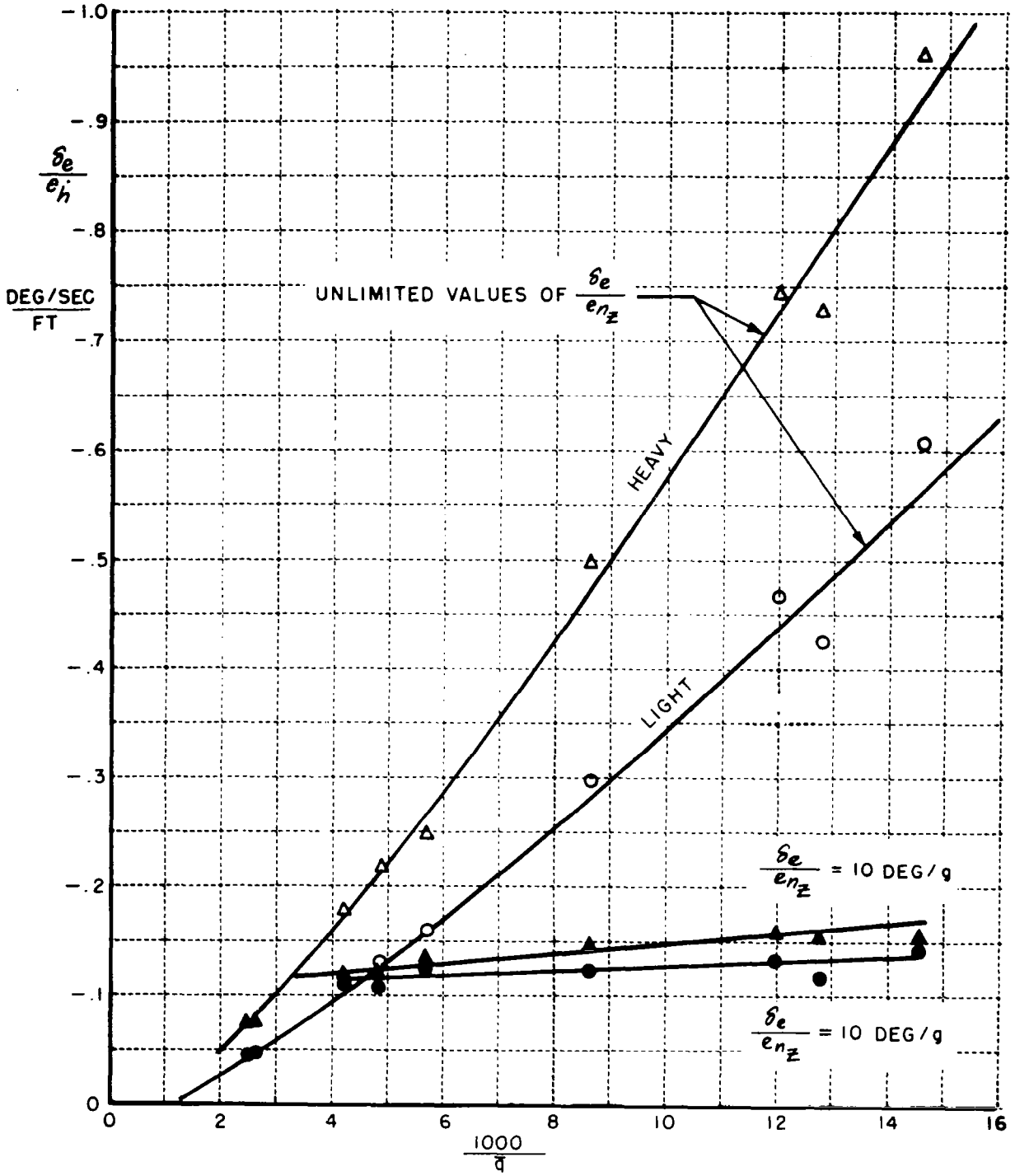

FIGURE 2.10(c) LONGITUDINAL ELEVATOR PHUGOID CONTROL LOOP GAIN VS. INVERSE DYNAMIC PRESSURE (Δn_Y LOOP)

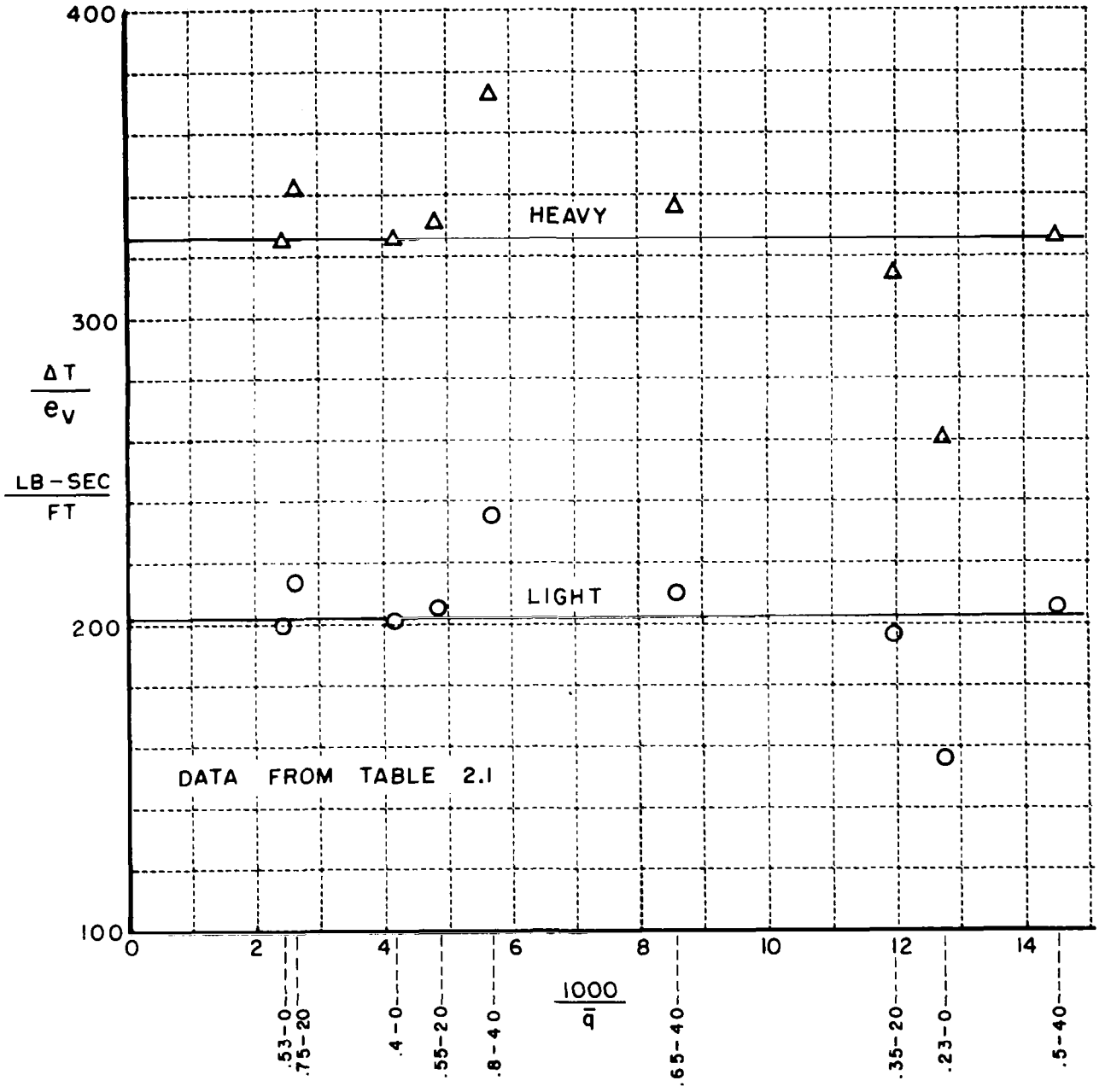

FIGURE 2.11 LONGITUDINAL THROTTLE PHUGOID CONTROL LOOP GAIN VS. INVERSE DYNAMIC PRESSURE

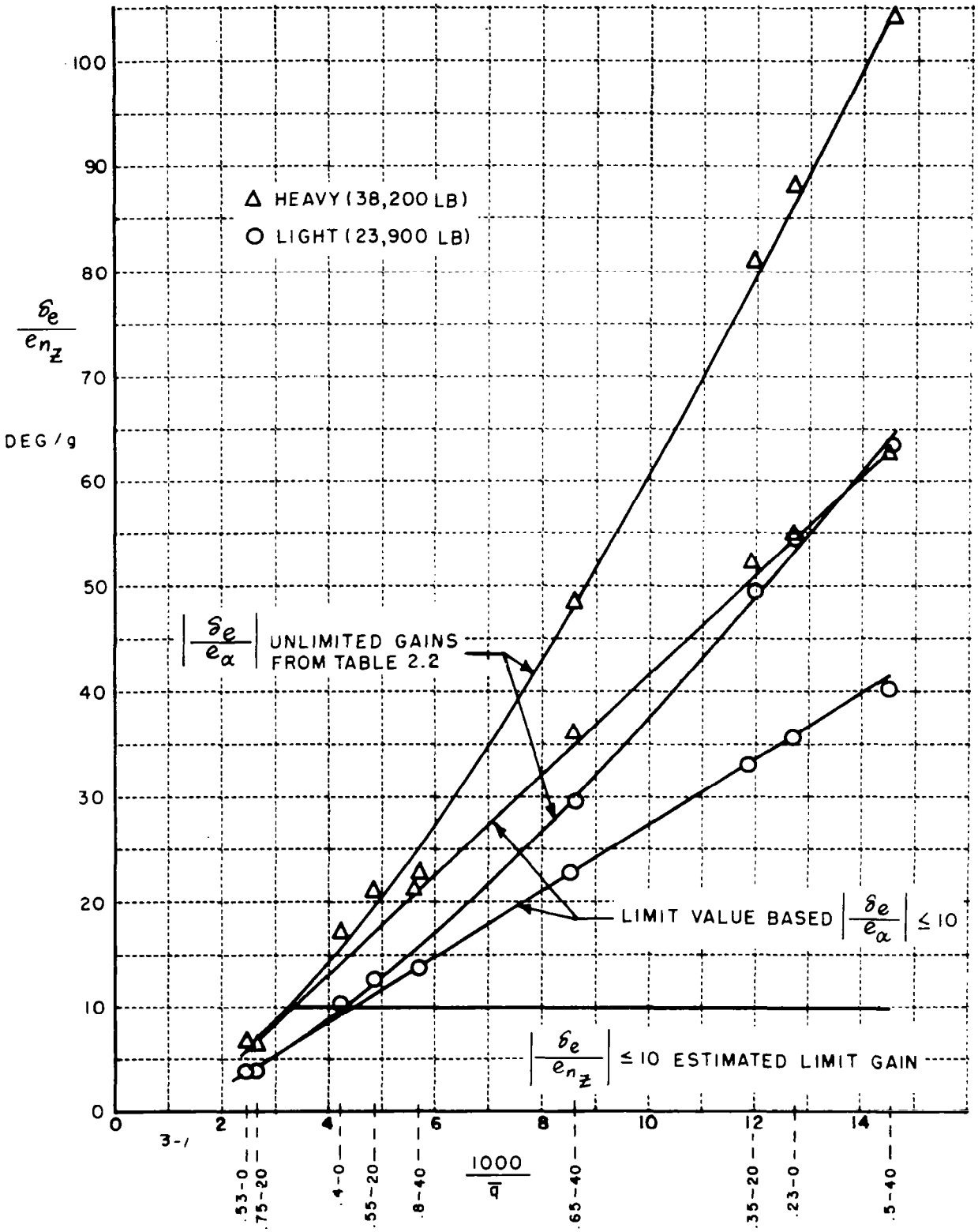

FIGURE 2.12 LONGITUDINAL NORMAL ACCELERATION GAIN VS. INVERSE DYNAMIC PRESSURE

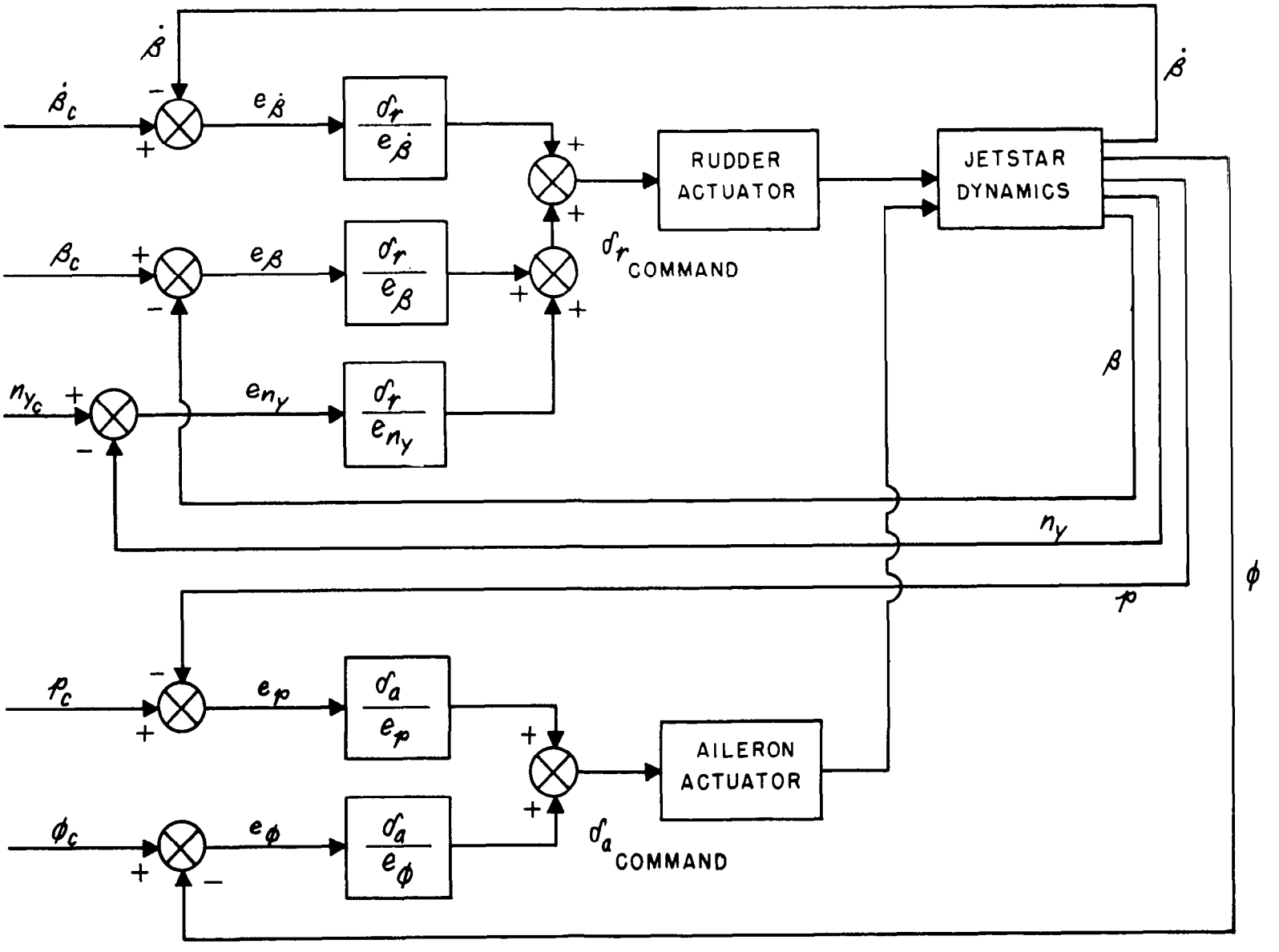

FIGURE 3.1 GPAS LATERAL-DIRECTIONAL CONTROL SYSTEM BLOCK DIAGRAM

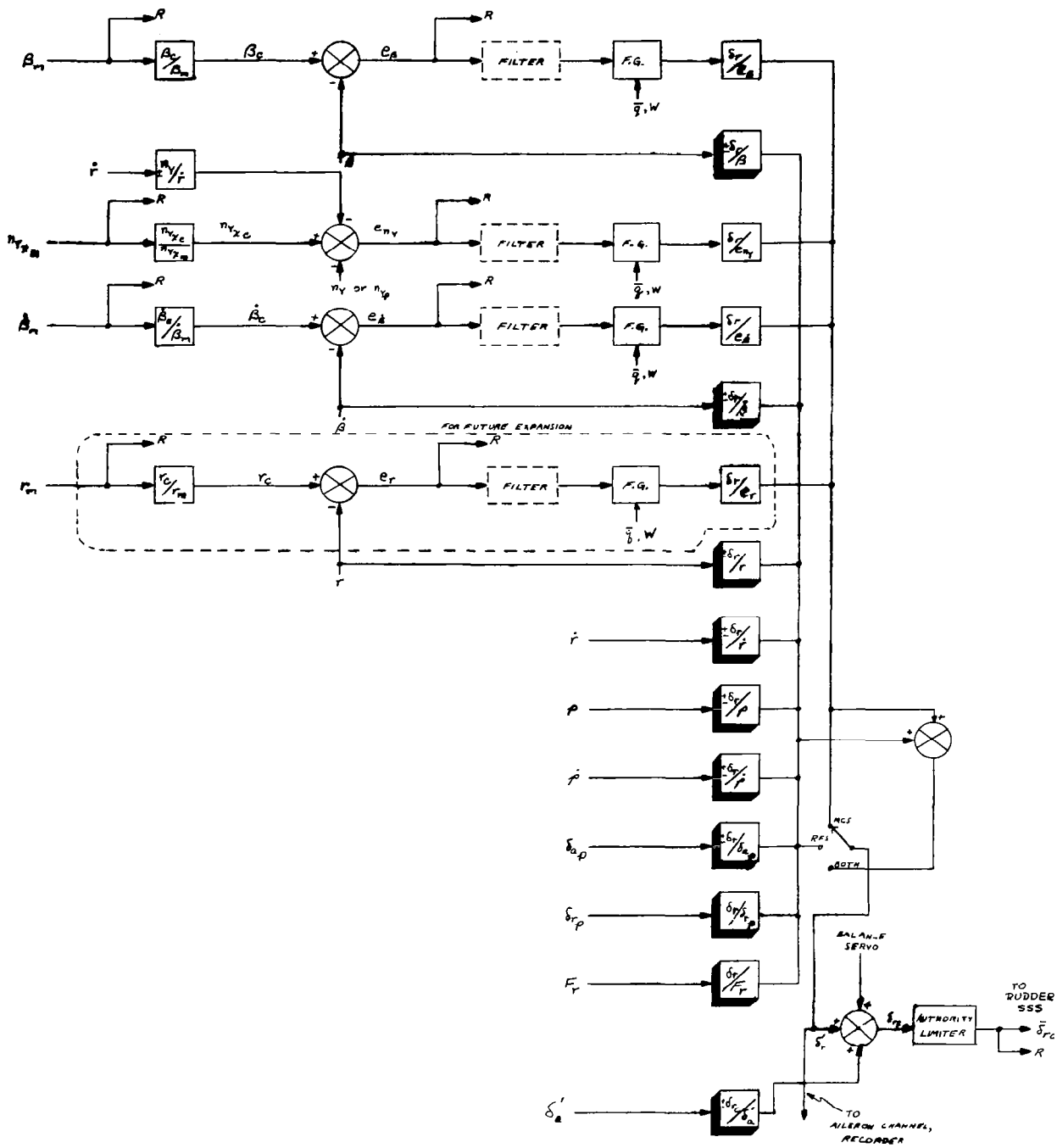

FIGURE 3.2 RUDDER CHANNEL – FUNCTIONAL BLOCK DIAGRAM

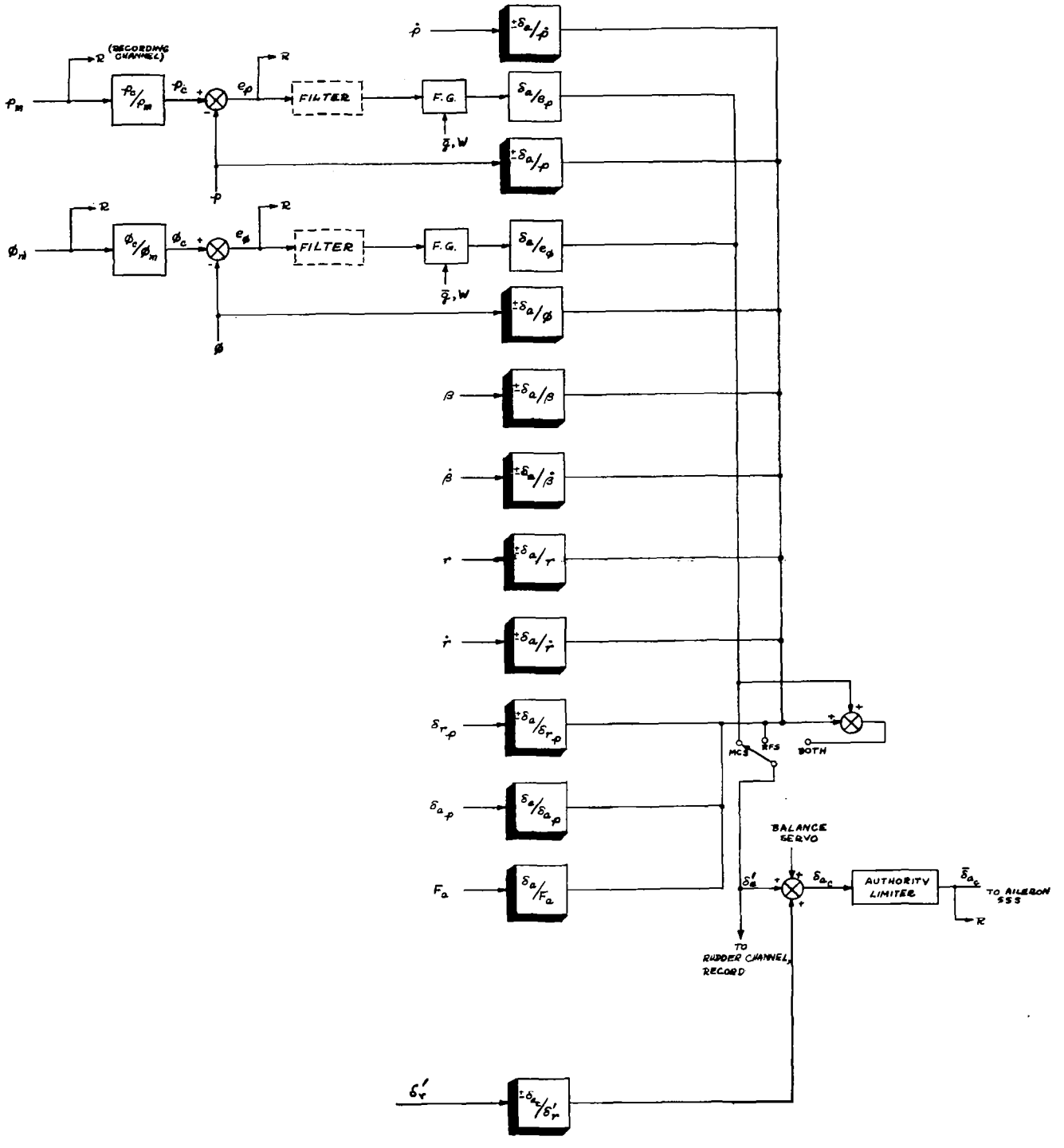

FIGURE 3.3 AILERON CHANNEL – FUNCTIONAL BLOCK DIAGRAM

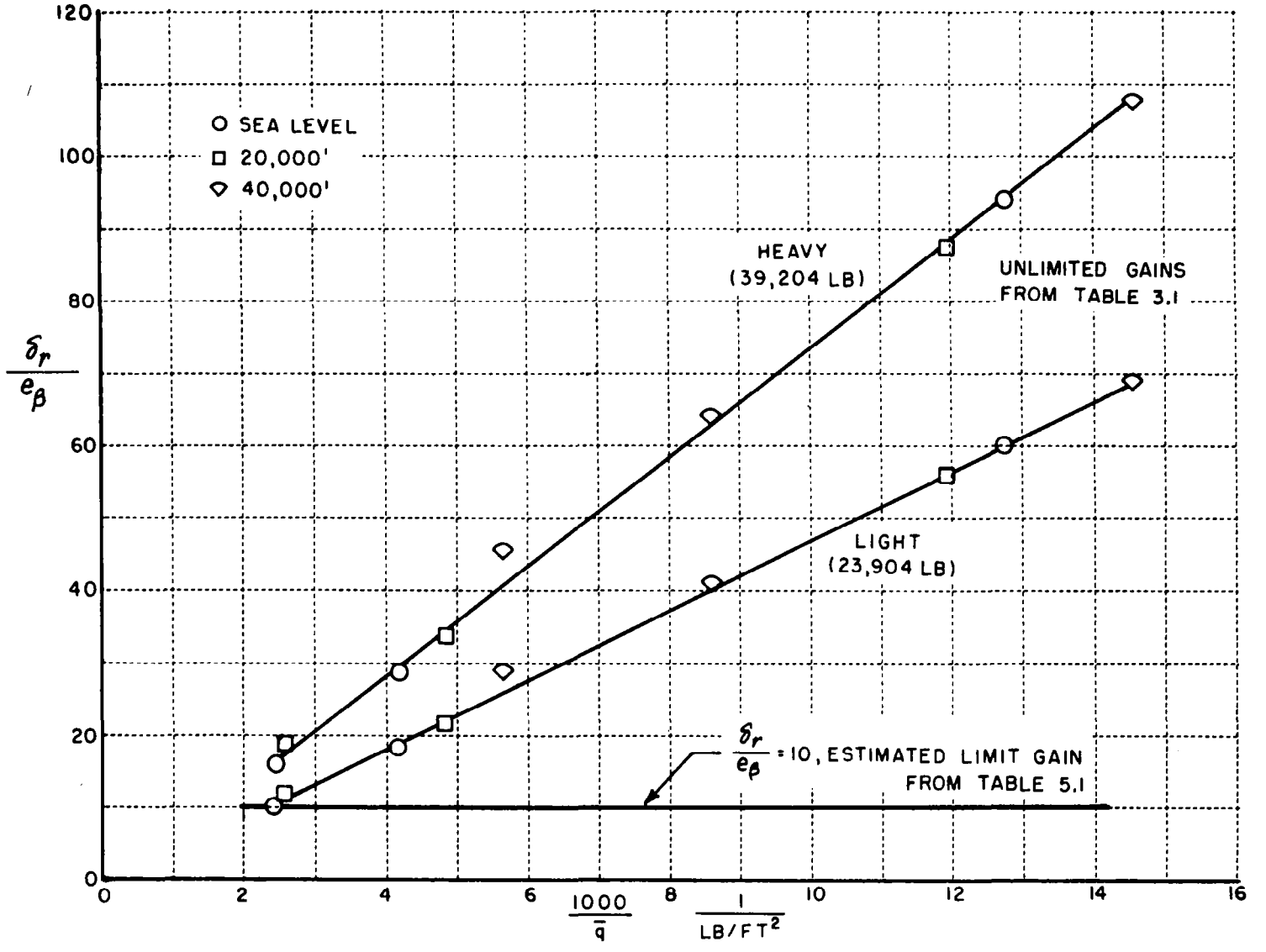

FIGURE 3.4 LATERAL-DIRECTIONAL ANGLE OF SIDESLIP GAIN VS. INVERSE DYNAMIC PRESSURE

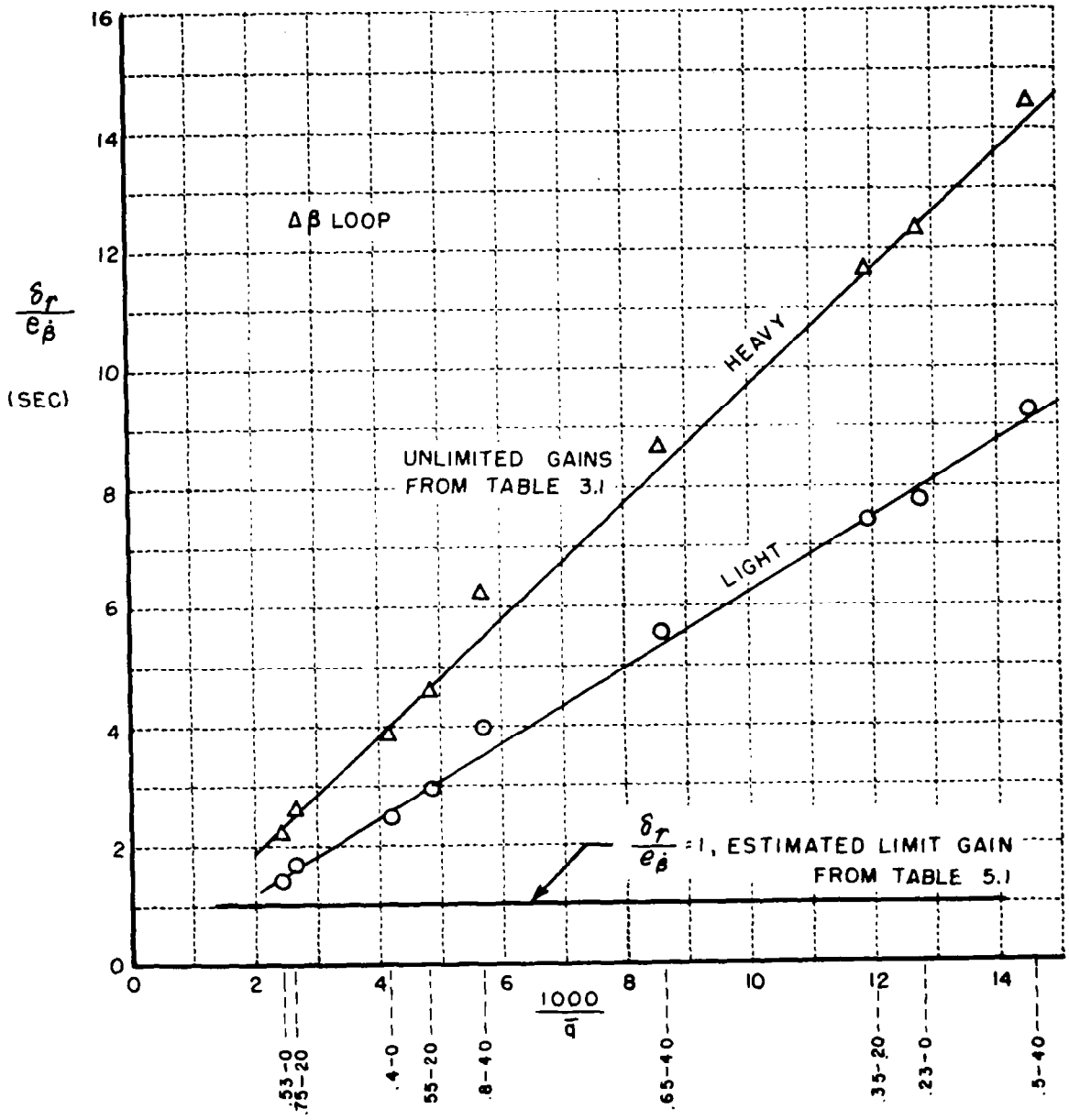

FIGURE 3.5 LATERAL-DIRECTIONAL DUTCH-ROLL DAMPING GAIN VS. INVERSE DYNAMIC PRESSURE - β LOOP

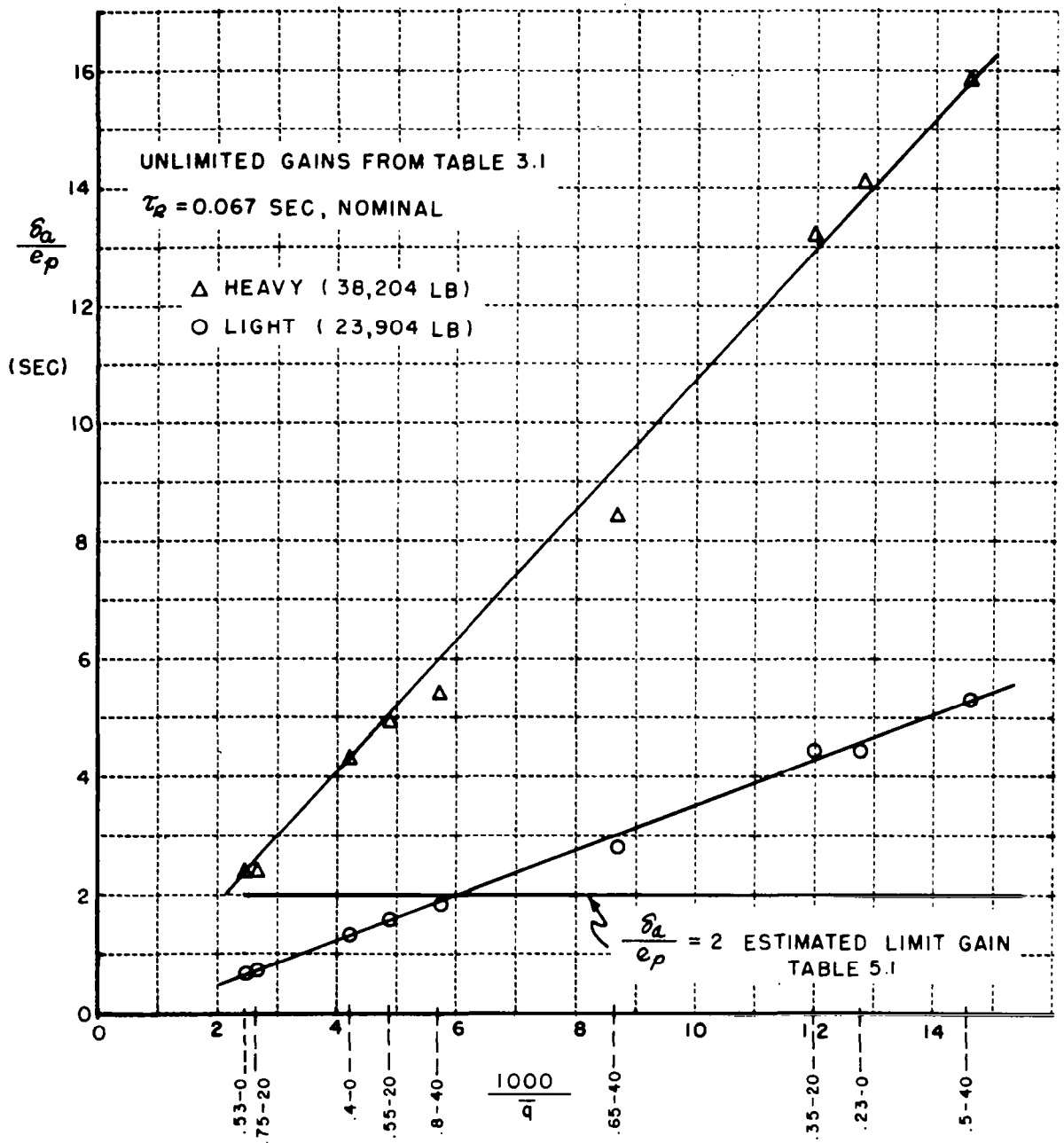

FIGURE 3.6 LATERAL-DIRECTIONAL ROLL RATE GAIN VS. INVERSE DYNAMIC PRESSURE

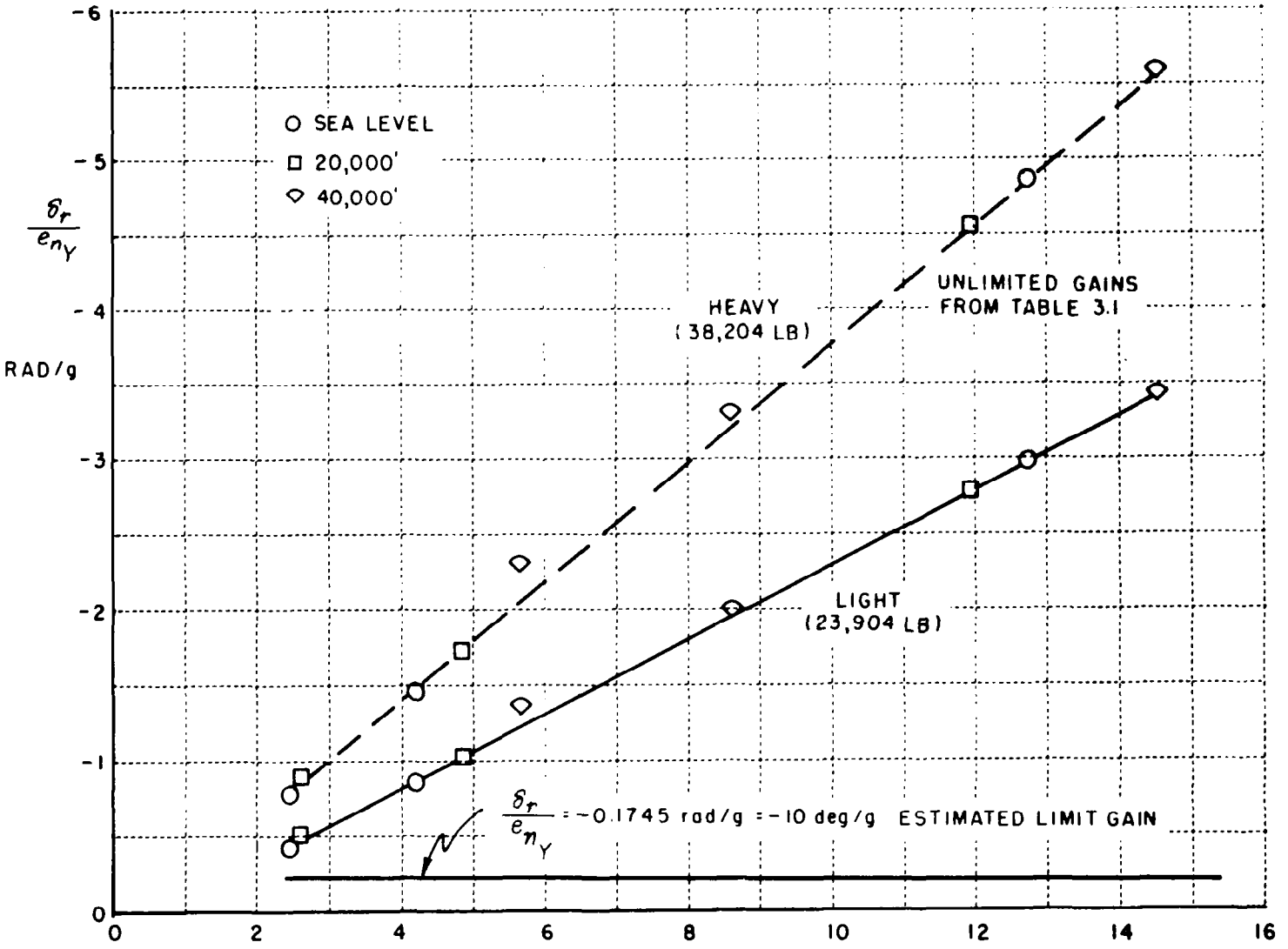

FIGURE 3.7 LATERAL-DIRECTIONAL LATERAL ACCELERATION GAIN VS. INVERSE DYNAMIC PRESSURE

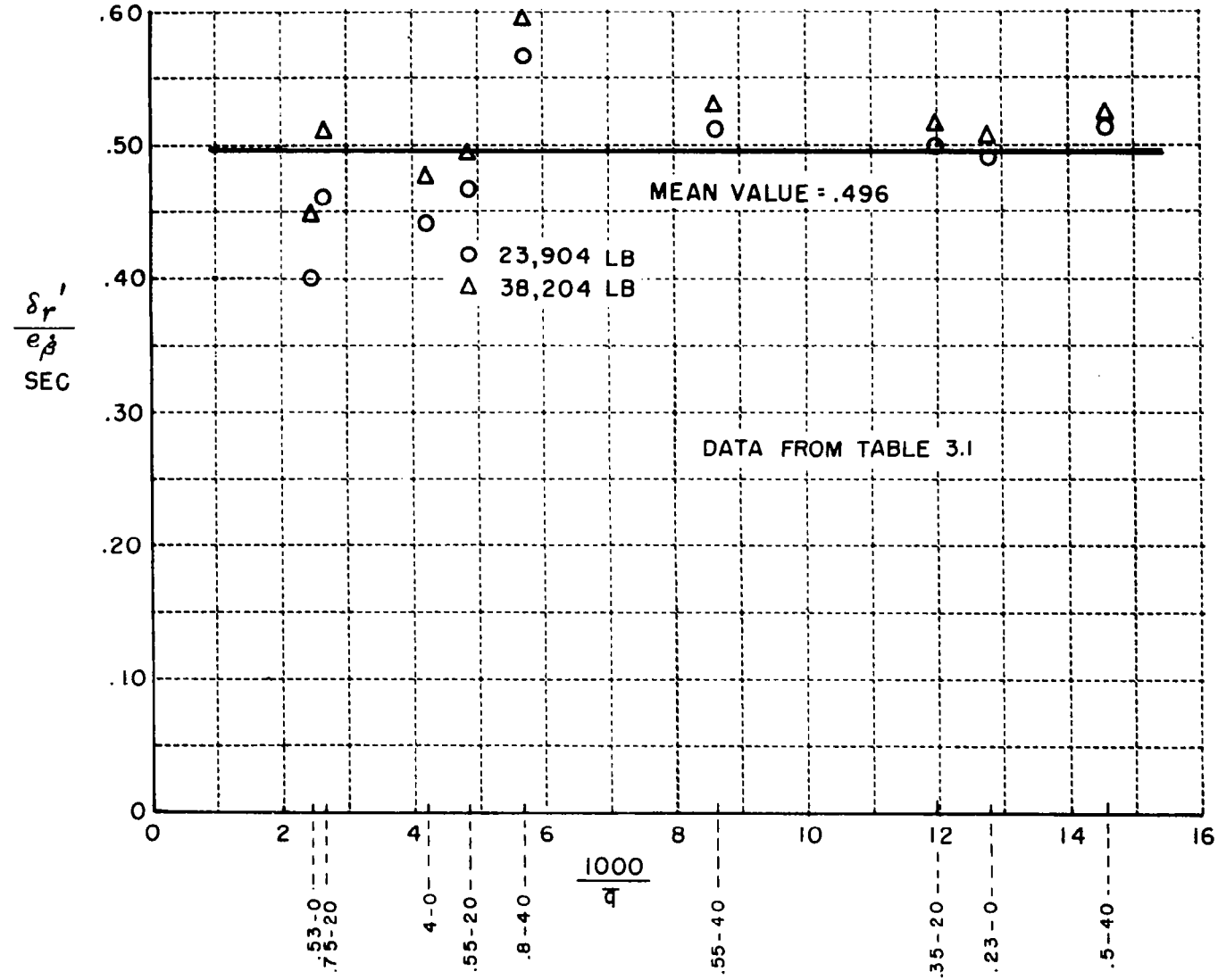

FIGURE 3.8 LATERAL-DIRECTIONAL DUTCH ROLL DAMPING GAIN VS. INVERSE DYNAMIC PRESSURE - Δn_Y LOOP

Forward Loop Gains

$$K_{\dot{h}} \equiv \frac{\Delta T}{e_{\dot{h}}} = 213 \frac{\text{lb-sec}}{\text{ft}} \qquad \frac{\delta_e}{e_\alpha} = -9.49 \qquad \frac{\delta_e}{e_{n_z}} = 0$$

$$\frac{\delta_e}{e_V} = 0.365 \frac{\text{deg-sec}}{\text{ft}} \qquad \frac{\delta_e}{e_{\dot{\alpha}}} = -0.846 \text{ sec}$$

$$\frac{\delta_e}{e_{\dot{V}}} = 1.42 \frac{\text{deg-sec}^2}{\text{ft}} \qquad \frac{\Delta T}{e_h} = 0$$

$$\tau_V = \infty$$

Input Gains

$$\frac{\alpha_c}{\alpha_m} = \frac{\dot{\alpha}_c}{\dot{\alpha}_m} = \frac{V_c}{V_m} = \frac{\dot{V}_c}{\dot{V}_m} = \frac{\dot{h}_c}{\dot{h}_m} = 1.0$$

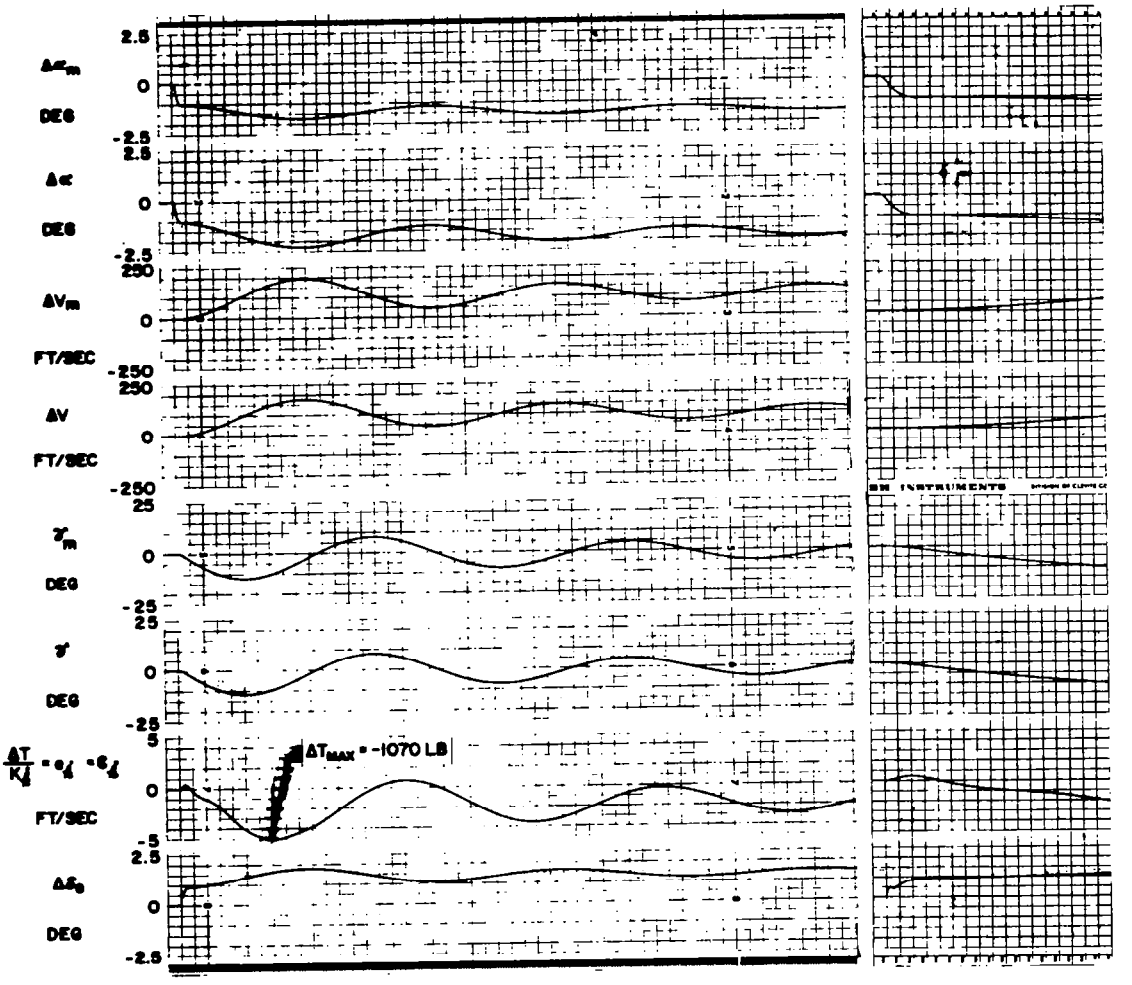

FIGURE 4.1 MODEL FOLLOWING A .55L20 SST WITH A .55H20 GPAS: $\Delta\delta_{e_m} = 1.0$ u(t) DEG (PERTURBATION EQUATIONS)

Forward Loop Gains

$$\left\{\begin{array}{lll} \frac{\Delta T}{e_{\dot{h}}} = 168\ \frac{\text{lb-sec}}{\text{ft}} & \frac{\delta_e}{e_\alpha} = -9.5 & \frac{\delta_e}{e_{n_z}} = 0 \\ \frac{\delta_e}{e_V} = 0.45\ \frac{\text{lb-sec}}{\text{ft}} & \frac{\delta_e}{e_{\dot{\alpha}}} = -0.86\ \text{sec} & \\ \frac{\delta_e}{e_{\dot{V}}} = 1.75\ \frac{\text{deg-sec}^2}{\text{ft}} & \frac{\Delta T}{e_h} = 8.4\ \text{lb/ft} & \end{array}\right.$$

$$\tau_V = 20\ \text{sec}$$

Input Gains

$$\left\{\frac{\alpha_c}{\alpha_m} = \frac{\dot{\alpha}_c}{\dot{\alpha}_m} = \frac{V_c}{V_m} = \frac{\dot{V}_c}{\dot{V}_m} = \frac{\dot{h}_c}{\dot{h}_m} = \frac{h_c}{h_m} = 1.0\right.$$

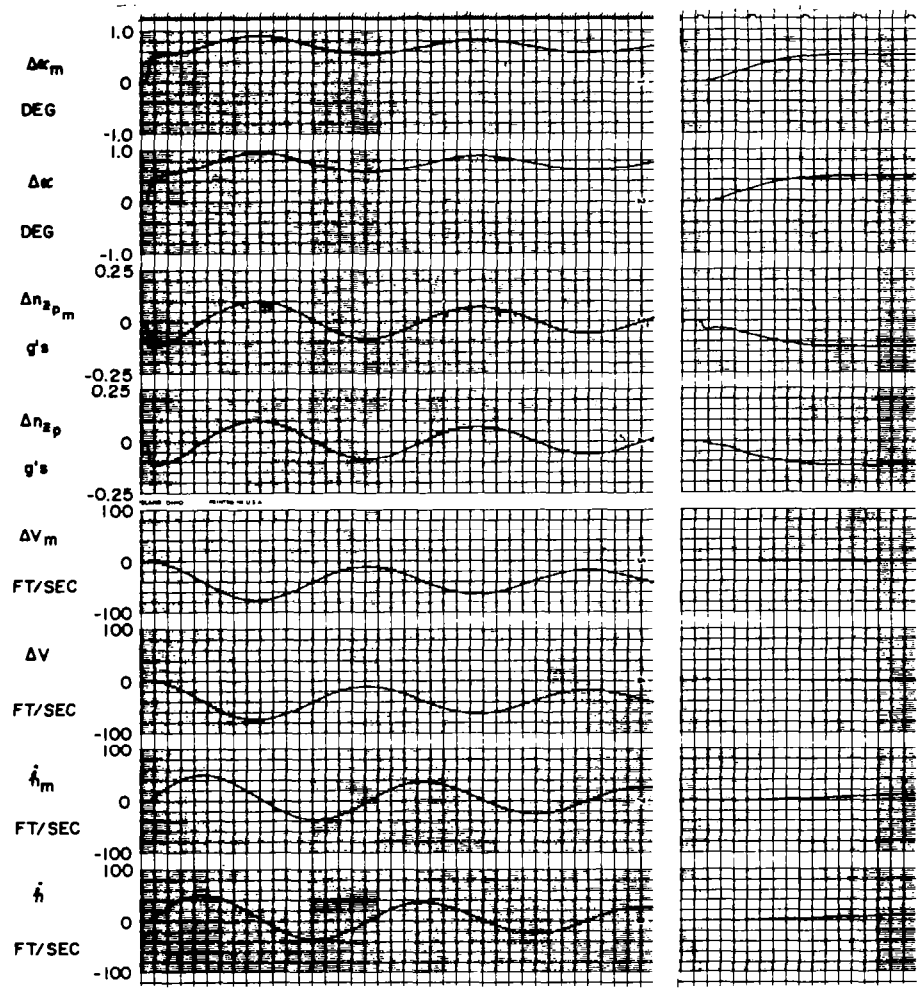

FIGURE 4.2 MODEL FOLLOWING A .55H40 SST WITH A .55H20 GPAS; $\Delta\delta_{e_m} = -0.5\ u(t)$ DEG (TOTAL FORCE EQUATIONS)

Forward Loop Gains

$$\frac{\delta_e}{e_V} = 0.156 \frac{\text{deg-sec}}{\text{ft}} \qquad \frac{\delta_e}{e_{n_z}} = 20.9 \text{ deg/g}$$

$$\frac{\delta_e}{e_{\dot{V}}} = 1.11 \frac{\text{deg-sec}^2}{\text{ft}} \qquad \frac{\delta_e}{e_{\dot{\alpha}}} = -0.543 \text{ sec}$$

$$\tau_V = \infty \qquad \frac{\delta_e}{e_{\alpha}} = 0$$

$$\frac{\Delta T}{e_{\dot{h}}} = 164 \frac{\text{lb-sec}}{\text{ft}} \qquad \frac{\Delta T}{e_h} = 0$$

ıput Gains

$$\frac{\Delta n_{z_c}}{\Delta n_{z_m}} = \frac{V_c}{V_m} = \frac{\dot{V}_c}{\dot{V}_m} = \frac{\dot{h}_c}{\dot{h}_m} = 1.0; \quad \frac{\dot{\alpha}_a}{\dot{\alpha}_m} = 0$$

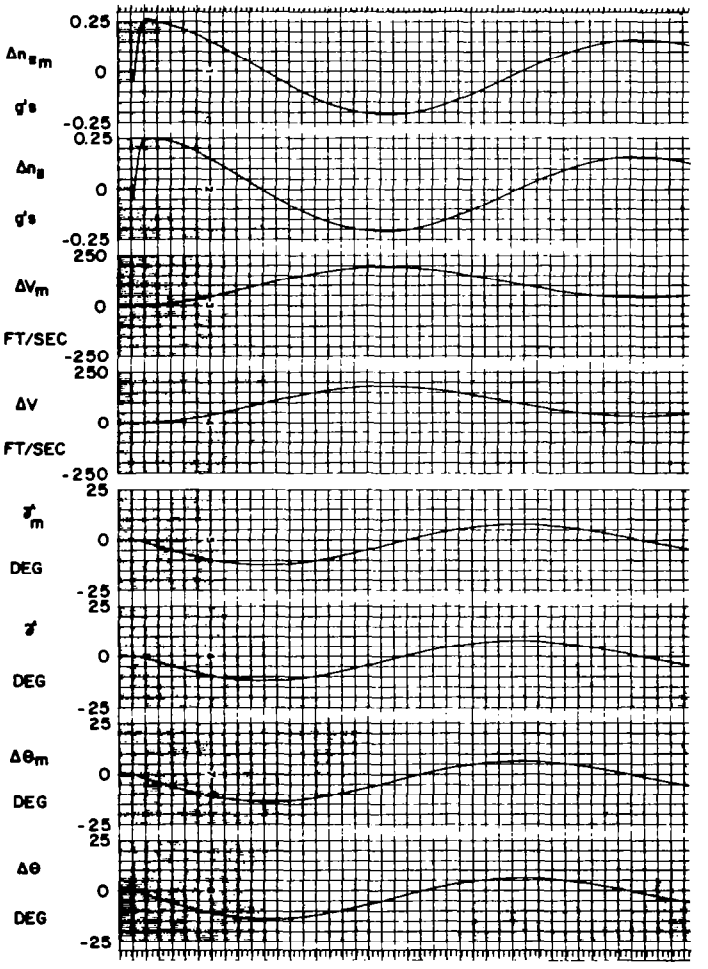

FIGURE 4.3 MODEL FOLLOWING A .55L20 SST WITH A .55H20 GPAS; $\Delta\delta_{e_m} = 1.0$ u(t) DEG (PERTURBATION EQUATIONS)

Forward Loop Gains

$$\frac{\delta_e}{e_v} = 0 \qquad \frac{\delta_e}{e_{n_z}} = 20.9 \text{ deg/g}$$

$$\frac{\delta_e}{e_{\dot{v}}} = 0 \qquad \frac{\delta_e}{e_{\dot{\alpha}}} = -0.543$$

$$\tau_v = \infty \qquad \frac{\delta_e}{e_{\alpha}} = 0$$

$$\frac{\Delta T}{e_{\dot{h}}} = 0 \qquad \frac{\Delta T}{e_h} = 0$$

Input Gains

$$\frac{\Delta n_{z_c}}{\Delta n_{z_m}} = 1.0 \qquad \frac{\dot{\alpha}_c}{\dot{\alpha}_m} = 0$$

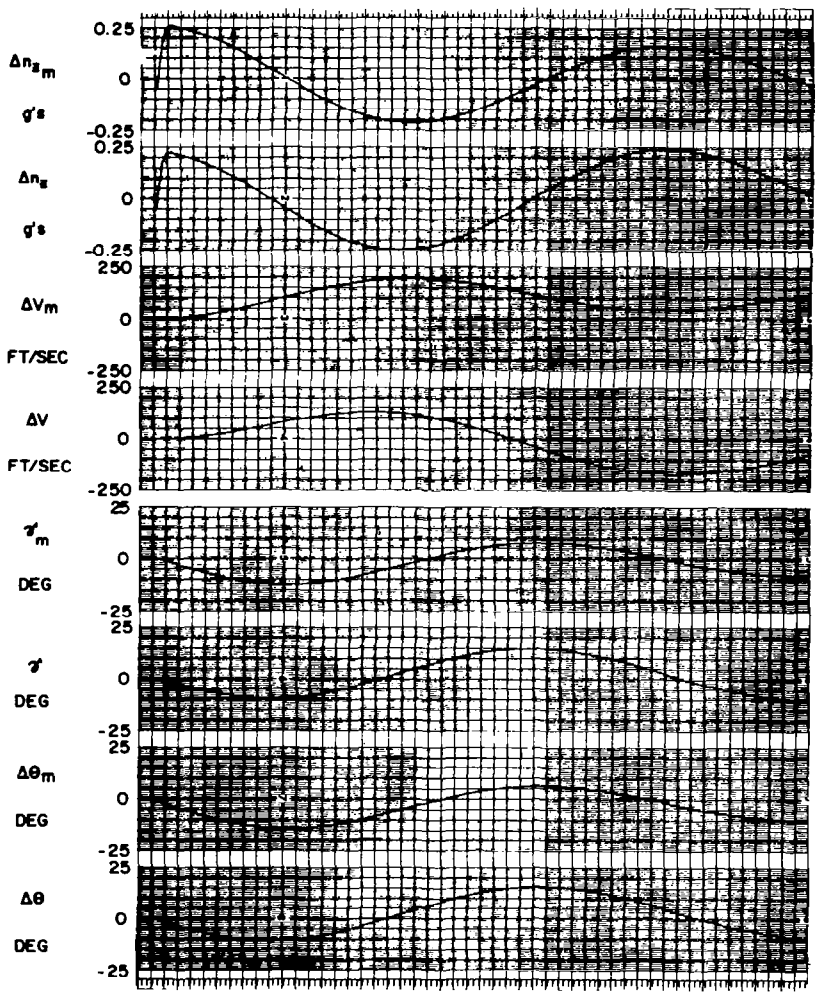

FIGURE 4.4 MODEL FOLLOWING NORMAL ACCELERATION OF A .55L20 SST WITH A .55H20 GPAS; $\Delta\delta_{e_m}$ = 1.0 u(t) DEG (PERTURBATION EQUATIONS)

Forward Loop Gains

$$\frac{\delta_e}{e_V} = 0.34 \frac{\text{deg-sec}}{\text{ft}} \qquad \frac{\delta_e}{e_{n_z}} = 19.5 \text{ deg/g}$$

$$\frac{\delta_e}{e_{\dot{V}}} = 0.96 \frac{\text{deg-sec}^2}{\text{ft}} \qquad \frac{\delta_e}{e_\alpha} = 0$$

$$\tau_V = 20 \text{ sec} \qquad \frac{\delta_e}{e_{\dot{\alpha}}} = -0.75$$

$$\frac{\Delta T}{e_h} = 8.4 \text{ lb/ft} \qquad \frac{\Delta T}{e_{\dot{h}}} = 168 \frac{\text{lb-sec}}{\text{ft}}$$

Input Gains

$$\frac{\Delta n_{z_c}}{\Delta n_{z_m}} = \frac{\dot{\alpha}_c}{\dot{\alpha}_m} = \frac{V_c}{V_m} = \frac{\dot{V}_c}{\dot{V}_m} = \frac{h_c}{h_m} = \frac{\dot{h}_c}{\dot{h}_m} = 1.0$$

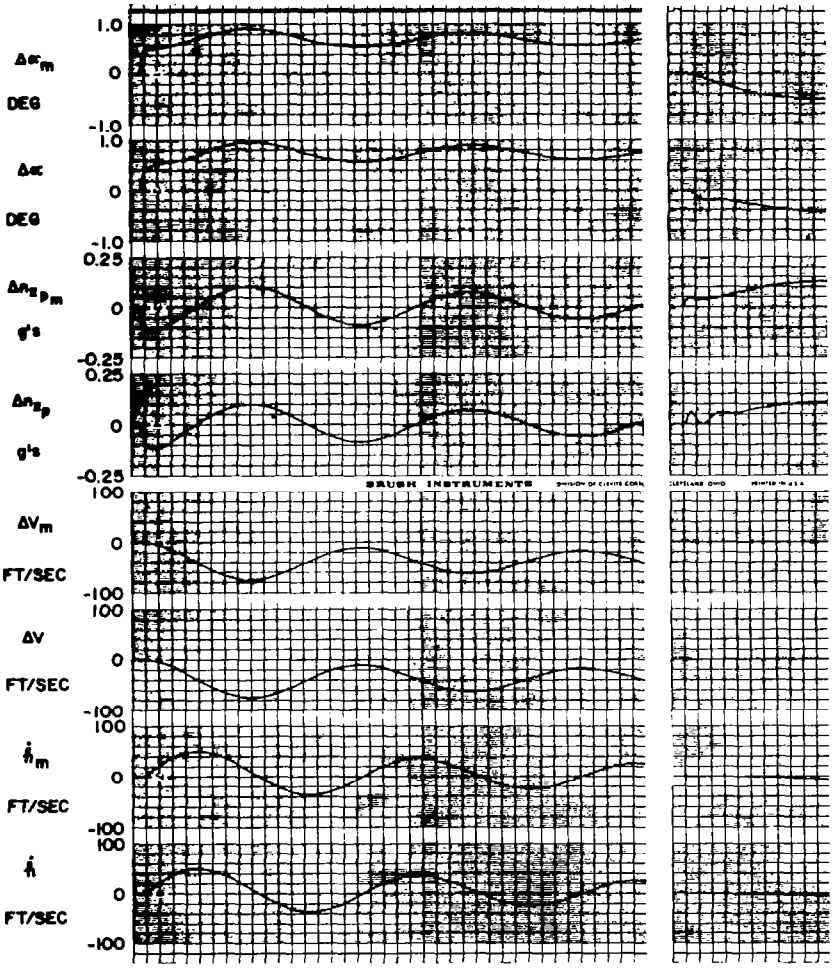

Input: $\Delta\delta_{e_m} = -0.5$ u(t) deg $\qquad \Delta\delta_{e_m} = +0.5$ u(t) deg

FIGURE 4.5 MODEL-FOLLOWING RESPONSE – .55H20 SST AND GPAS Δn_z FEEDBACK, Δn_{z_p} RECORD (TOTAL FORCE EQUATIONS)

Forward Loop Gains

$$\frac{\delta_e}{e_v} = 0.596 \frac{\text{deg-sec}}{\text{ft}} \qquad \frac{\delta_e}{e_{n_z}} = 36.8 \text{ deg/g}$$

$$\frac{\delta_e}{e_{\dot{v}}} = 1.76 \frac{\text{deg-sec}^2}{\text{ft}} \qquad \frac{\delta_e}{e_\alpha} = 0$$

$$\tau_v = 20 \text{ sec} \qquad \frac{\delta_e}{e_{\dot{\alpha}}} = -0.957$$

$$\frac{\Delta T}{e_h} = 8.45 \text{ lb/ft} \qquad \frac{\Delta T}{e_{\dot{h}}} = 169 \frac{\text{lb-sec}}{\text{ft}}$$

Input Gains

$$\frac{\Delta n_{z_c}}{\Delta n_{z_{pm}}} = \frac{\dot{\alpha}_c}{\dot{\alpha}_m} = \frac{V_c}{V_m} = \frac{\dot{V}_c}{\dot{V}_m} = \frac{h_c}{h_m} = \frac{\dot{h}_c}{\dot{h}_m} = 1.0$$

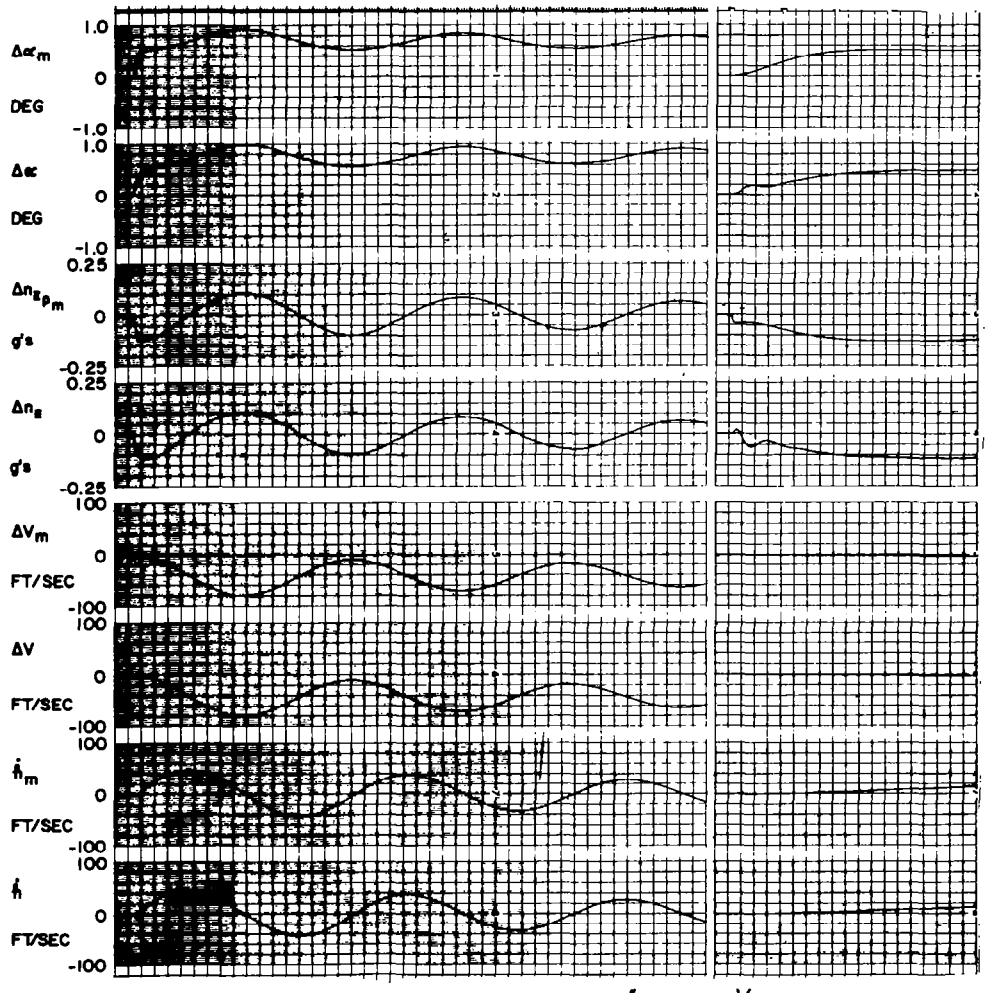

Modified Δn_z Feedback: $\Delta n_z' = \Delta n_z - \frac{V}{g} Z_{\delta_e} \Delta\delta_e$ (see Appendix D)

FIGURE 4.6 MODEL-FOLLOWING RESPONSE - .55H20 SST AND GPAS $\Delta n_z'$ FEEDBACK, Δn_z RECORD INPUT; $\Delta\delta_{e_m}$ = -0.5 u(t) DEG (TOTAL FORCE EQUATIONS)

Forward Loop Gains

$$\frac{\delta_e}{e_V} = 0.34 \frac{\text{deg-sec}}{\text{ft}} \qquad \frac{\delta_e}{e_{n_{z_p}}} = 19.5 \text{ deg/g}$$

$$\frac{\delta_e}{e_{\dot{V}}} = 0.96 \frac{\text{deg-sec}^2}{\text{ft}} \qquad \frac{\delta_e}{e_\alpha} = 0$$

$$\tau_V = 20 \text{ sec} \qquad \frac{\delta_e}{e_{\dot{\alpha}}} = -0.75 \text{ sec}$$

$$\frac{\Delta T}{e_h} = 8.4 \text{ lb/ft} \qquad \frac{\Delta T}{e_{\dot{h}}} = 168 \frac{\text{lb-sec}}{\text{ft}}$$

Input Gains

$$\frac{\Delta n_{z_c}}{\Delta n_{z_{p_m}}} = \frac{\dot{\alpha}_c}{\dot{\alpha}_m} = \frac{V_c}{V_m} = \frac{\dot{V}_c}{\dot{V}_m} = \frac{h_c}{h_m} = \frac{\dot{h}_c}{\dot{h}_m} = 1.0$$

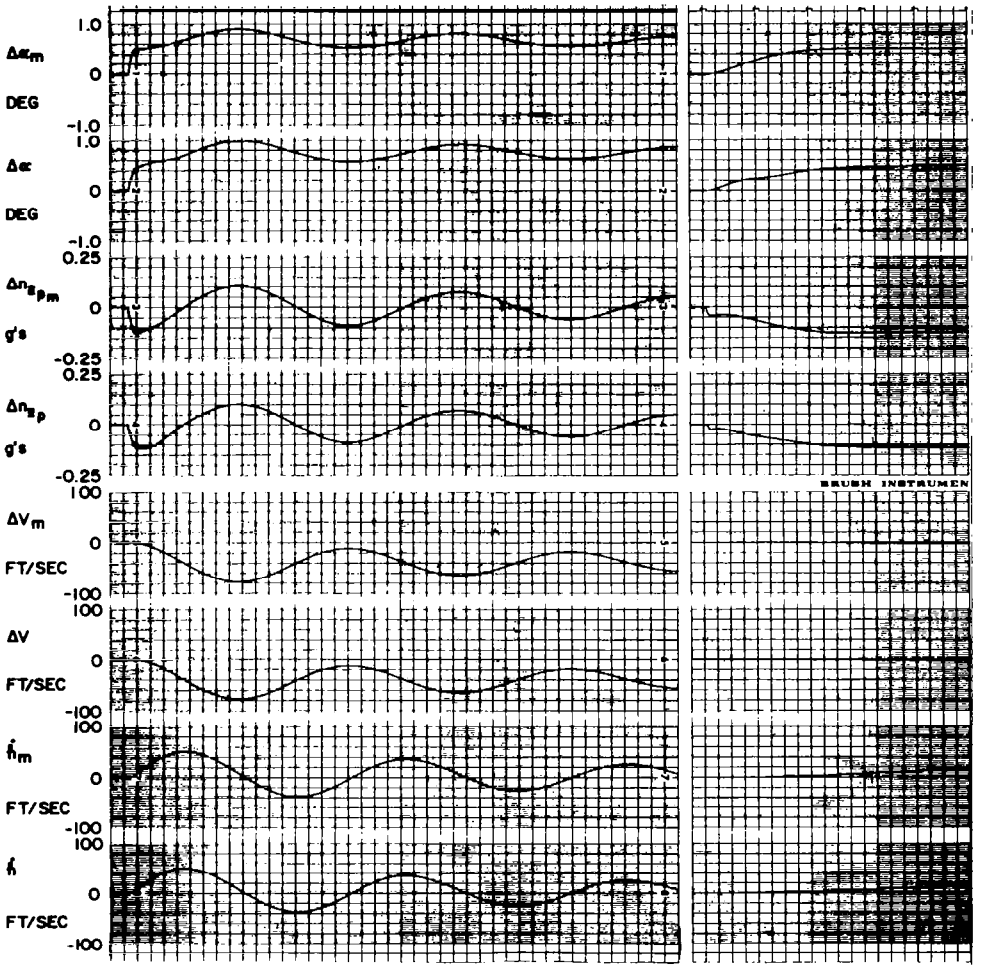

FIGURE 4.7 MODEL-FOLLOWING RESPONSE – .55H20 SST AND GPAS Δn_{z_p} FEEDBACK AND RECORD; INPUT: $\Delta \delta_{e_m} = -0.5$ u(t) DEG (TOTAL FORCE EQUATIONS)

Input Gains = 1.0

$\frac{\delta_e}{e_\alpha} = -31.0$ $\quad \frac{\delta_e}{e_V} = 3.26 \frac{\text{deg-sec}}{\text{ft}}$ $\quad \frac{\Delta T}{e_h} = 8.4 \text{ lb/ft}$ $\quad \tau_V = 20 \text{ sec}$

$\frac{\delta_e}{e_{\dot\alpha}} = -3.08 \text{ sec}$ $\quad \frac{\delta_e}{e_{\dot V}} = 12.5 \frac{\text{deg-sec}^2}{\text{ft}}$ $\quad \frac{\Delta T}{e_{\dot h}} = 168 \frac{\text{lb-sec}}{\text{ft}}$

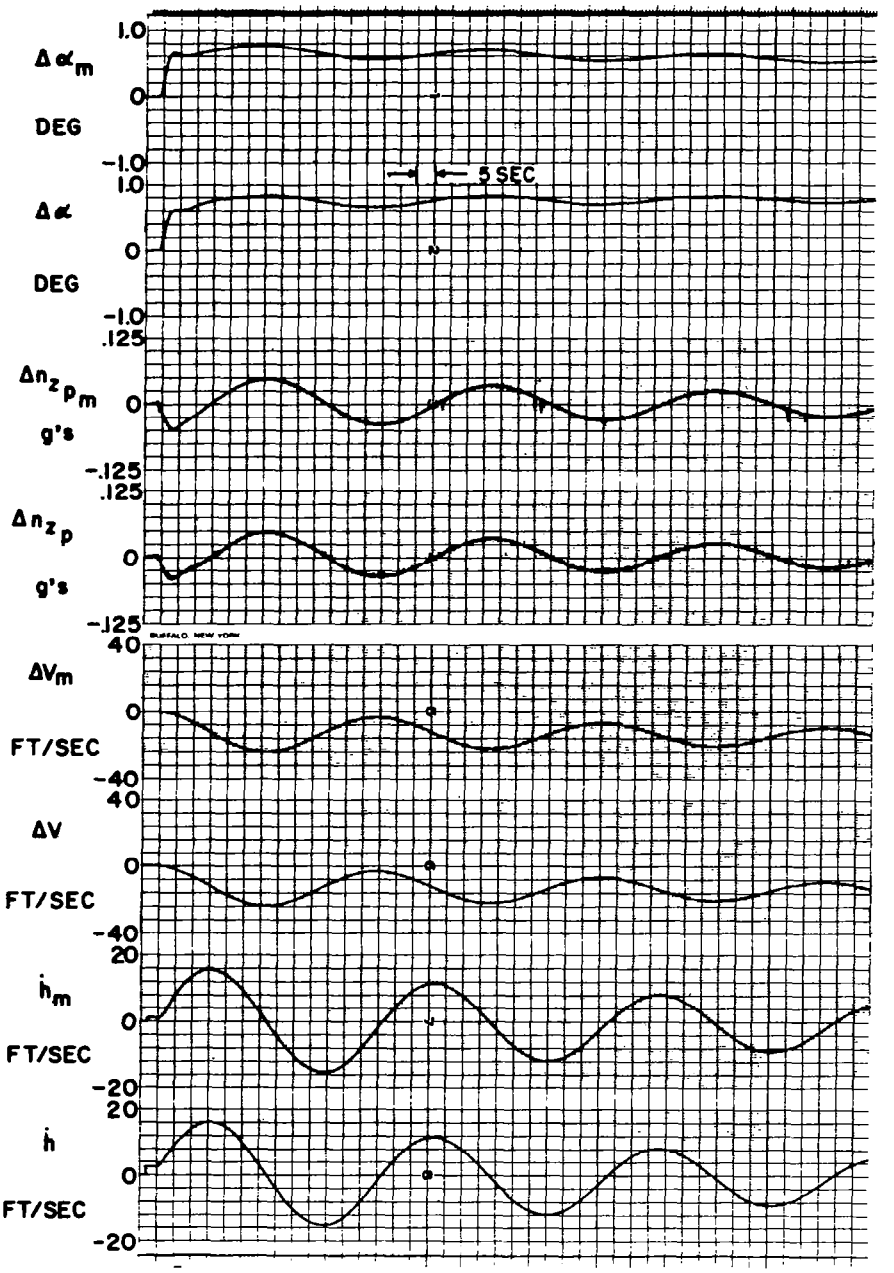

FIGURE 4.8 LONGITUDINAL MODEL-FOLLOWING RESPONSE WITH ORIGINAL PHUGOID LOOPS AND UNLIMITED GAINS - .5H40 $\Delta\delta_{e_m} = -0.5\ u(t)$ DEG (TOTAL FORCE EQUATIONS)

Input Gains = 1.0

$\frac{\delta_e}{e_\alpha} = -10$ $\frac{\delta_e}{e_v} = 0.50$ deg sec/ft $\frac{\Delta T}{e_h} = 6.95$ lb/ft $\tau_v = 20$ sec

$\frac{\delta_e}{e_{\dot\alpha}} = -1.0$ sec $\frac{\delta_e}{e_{\dot v}} = 1.0$ deg sec^2/ft $\frac{\Delta T}{e_{\dot h}} = 139$ lb sec/ft

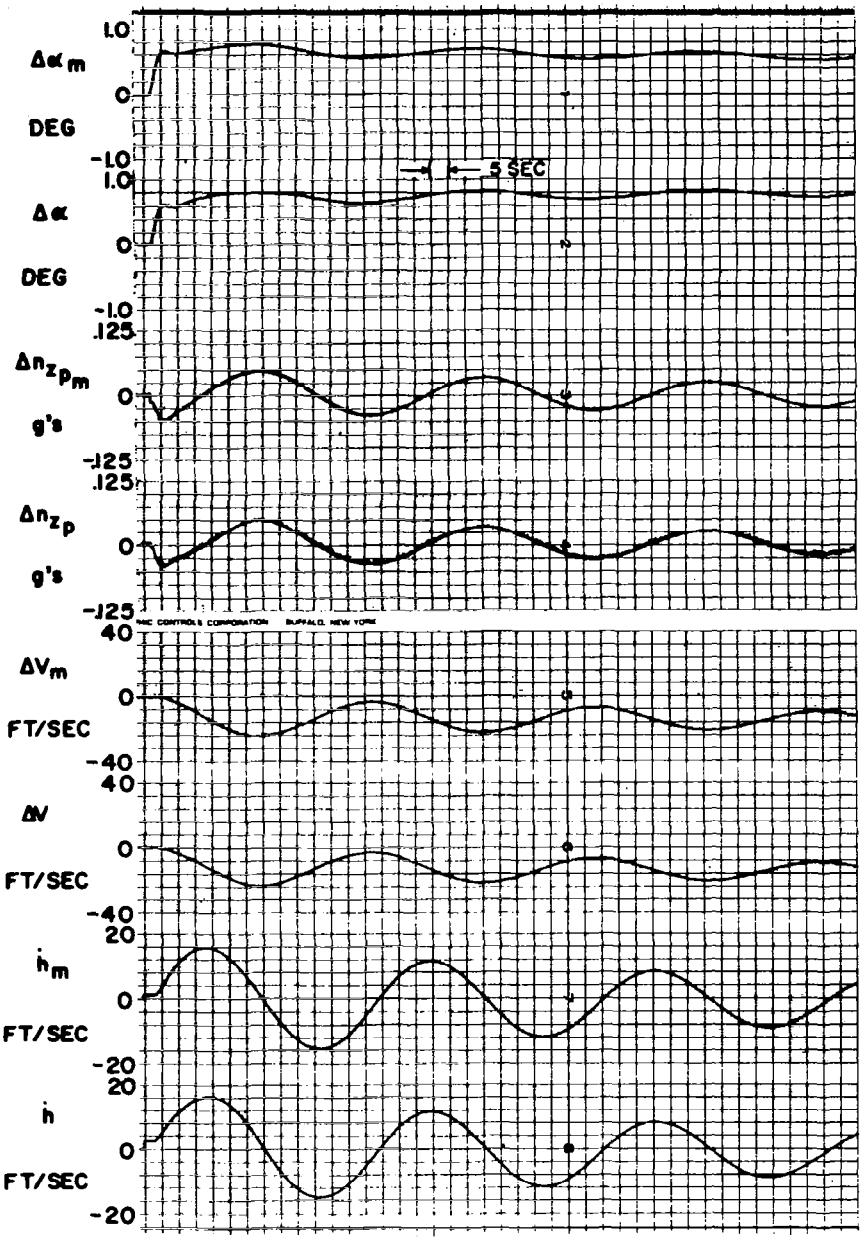

FIGURE 4.9 LONGITUDINAL MODEL-FOLLOWING RESPONSE WITH ORIGINAL PHUGOID LOOPS AND LIMITED GAINS - .5H40 $\Delta\delta e_m = -0.5\ u(t)$ DEG (TOTAL FORCE EQUATIONS)

Input Gains = 1.0

$\frac{\delta_e}{e_\alpha} = -10$ $\frac{\delta_e}{e_h} = -0.05$ deg/ft $\frac{\Delta T}{e_v} = 326 \frac{\text{lb sec}}{\text{ft}}$

$\frac{\delta_e}{e_{\dot{\alpha}}} = -1.0$ sec $\frac{\delta_e}{e_{\dot{h}}} = -1.0$ deg sec/ft $\tau_v = 20$ sec

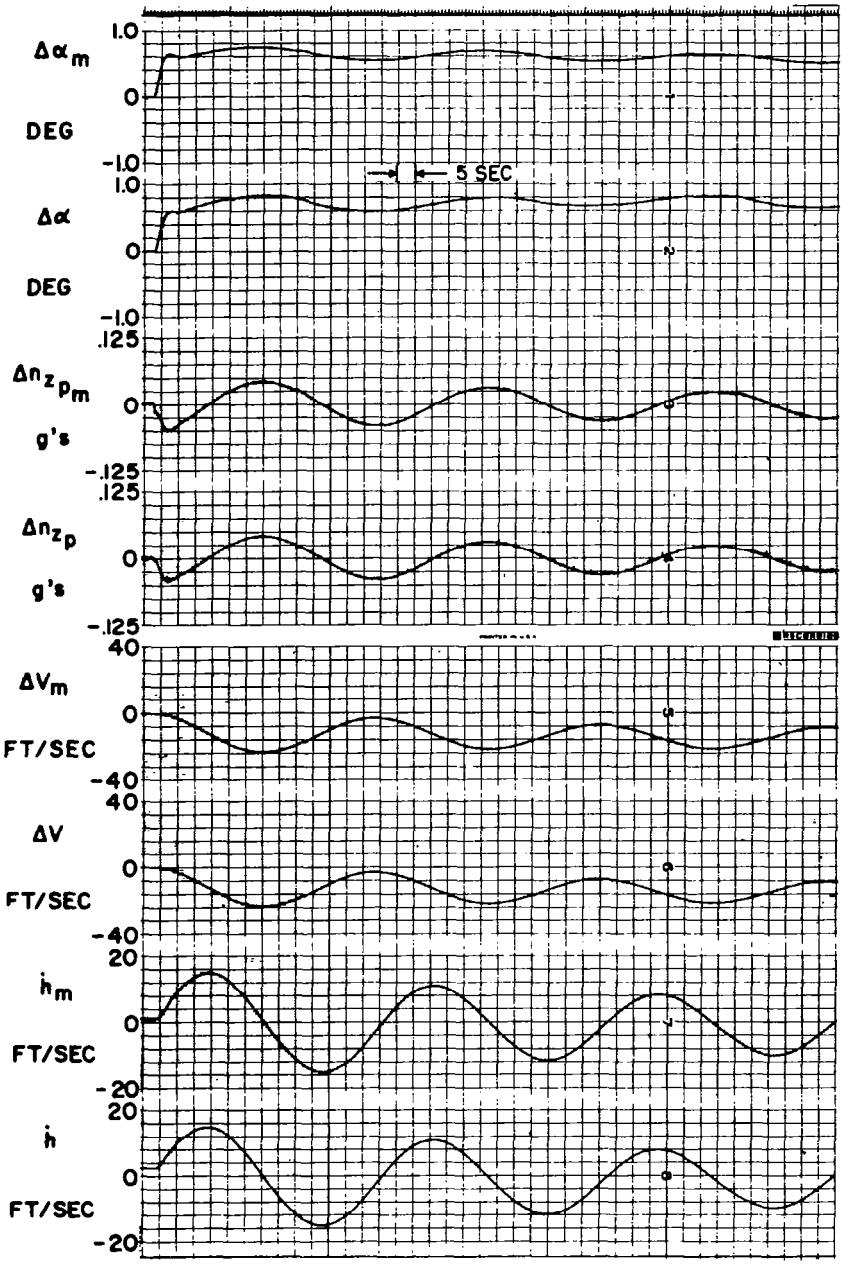

FIGURE 4.10 LONGITUDINAL MODEL-FOLLOWING RESPONSE WITH MODIFIED PHUGOID LOOPS AND LIMITED GAINS - .5H40 $\Delta\delta_{e_m} = -0.5\ u(t)$ DEG (TOTAL FORCE EQUATIONS)

Input Gains = 1.0

$\frac{\delta_e}{e_\alpha} = -31$ $\frac{\delta_e}{e_v} = 3.26$ deg sec/ft $\frac{\Delta T}{e_h} = 8.4$ lb/ft $\tau_v = 20$ sec

$\frac{\delta_e}{e_{\dot{\alpha}}} = -3.08$ sec $\frac{\delta_e}{e_{\ddot{z}}} = 12.5$ deg sec^2/ft $\frac{\Delta T}{e_i} = 168$ lb sec/ft

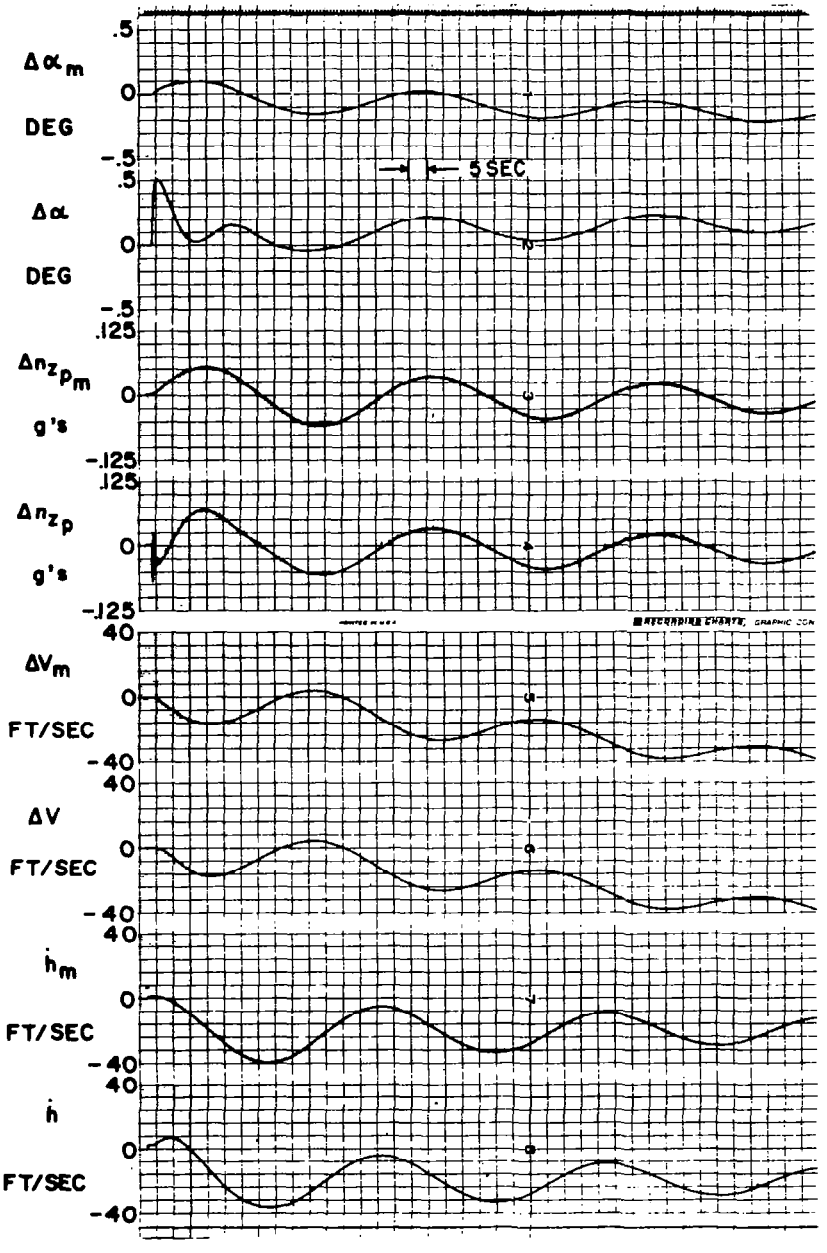

FIGURE 4.11 LONGITUDINAL MODEL-FOLLOWING WITH ORIGINAL PHUGOID LOOPS AND UNLIMITED GAINS - .5H40
ΔT_m = - 12,500 u(t) lb (TOTAL FORCE EQUATIONS)

Input Gains = 1.0

$\frac{\delta_e}{e_\alpha} = -10$ $\frac{\delta_e}{e_v} = 0.50$ deg sec/ft $\frac{\Delta T}{e_h} = 6.95$ lb/ft $\tau_v = 20$ sec

$\frac{\delta_e}{e_{\dot{\alpha}}} = -1.0$ sec $\frac{\delta_e}{e_{\dot{v}}} = 1.0$ deg sec^2/ft $\frac{\Delta T}{e_i} = 139$ lb sec/ft

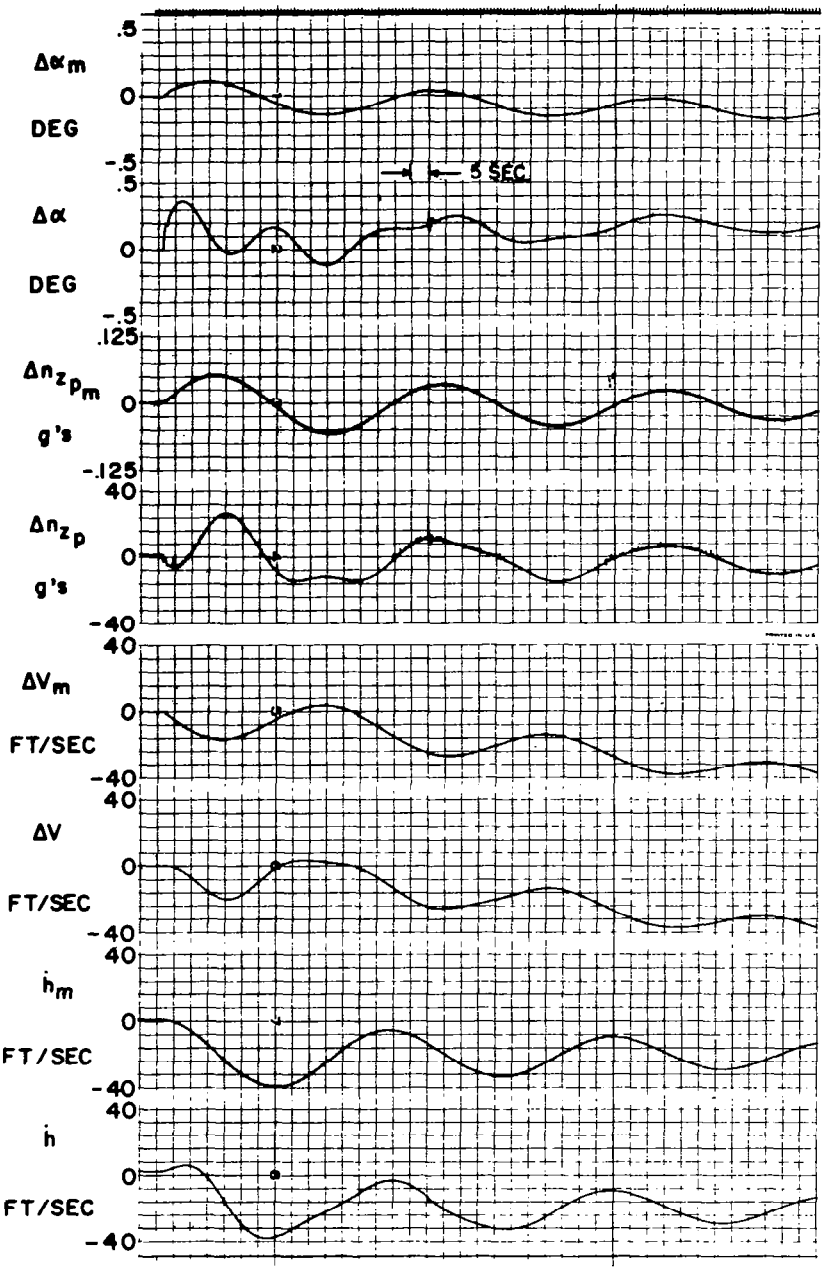

FIGURE 4.12 LONGITUDINAL MODEL-FOLLOWING WITH ORIGINAL PHUGOID LOOPS AND LIMITED GAINS - .5H40
ΔT_m = - 12.500 u(t) lb. (TOTAL FORCE EQUATIONS)

Input Gains = 1.0

$\frac{\delta_e}{e_\alpha}$ = - 10 $\quad$ $\frac{\delta_e}{e_{\dot{h}}}$ = - 0.05 deg sec/ft $\quad$ $\frac{\Delta T}{e_V}$ = 326 lb sec/ft

$\frac{\delta_e}{e_h}$ = - 1.0 sec $\quad$ $\frac{\delta_e}{e_{\dot{h}}}$ = - 1.0 deg sec/ft $\quad$ τ_V = 20 sec

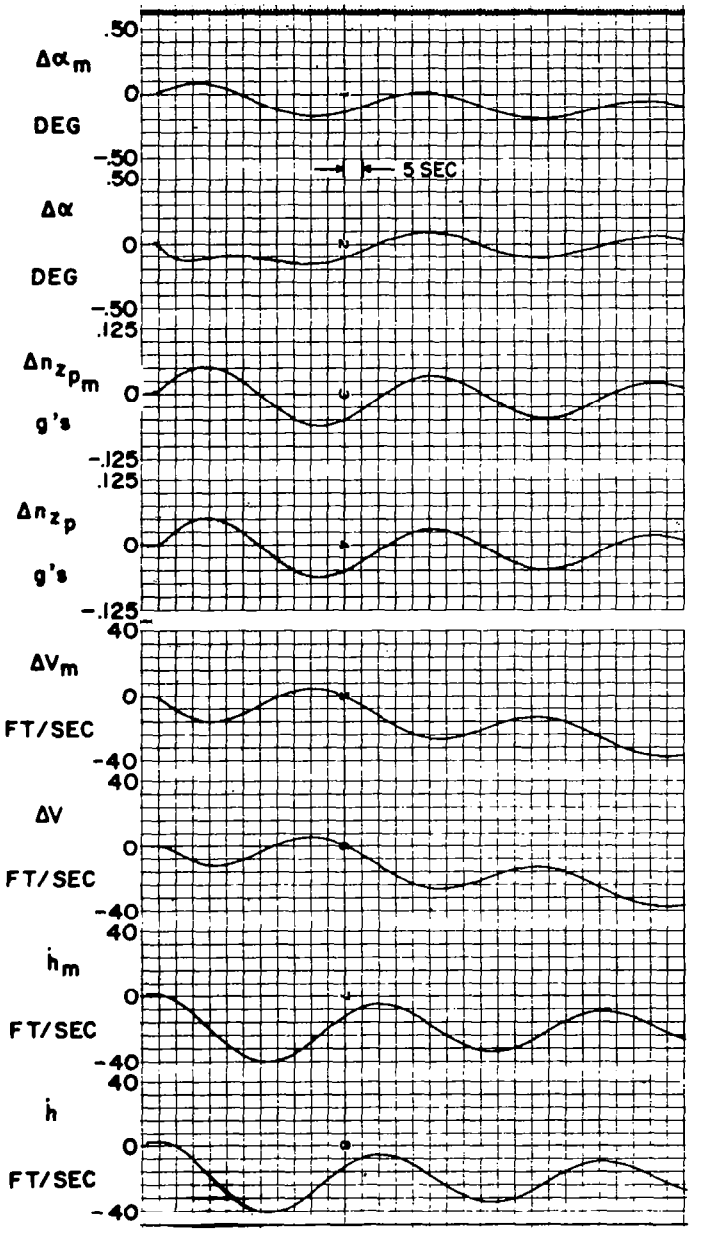

FIGURE 4.13 LONGITUDINAL MODEL-FOLLOWING WITH MODIFIED PHUGOID LOOPS AND LIMITED GAINS - .5H40
ΔT_m = - 12,500 u(t) lb. (TOTAL FORCE EQUATIONS)

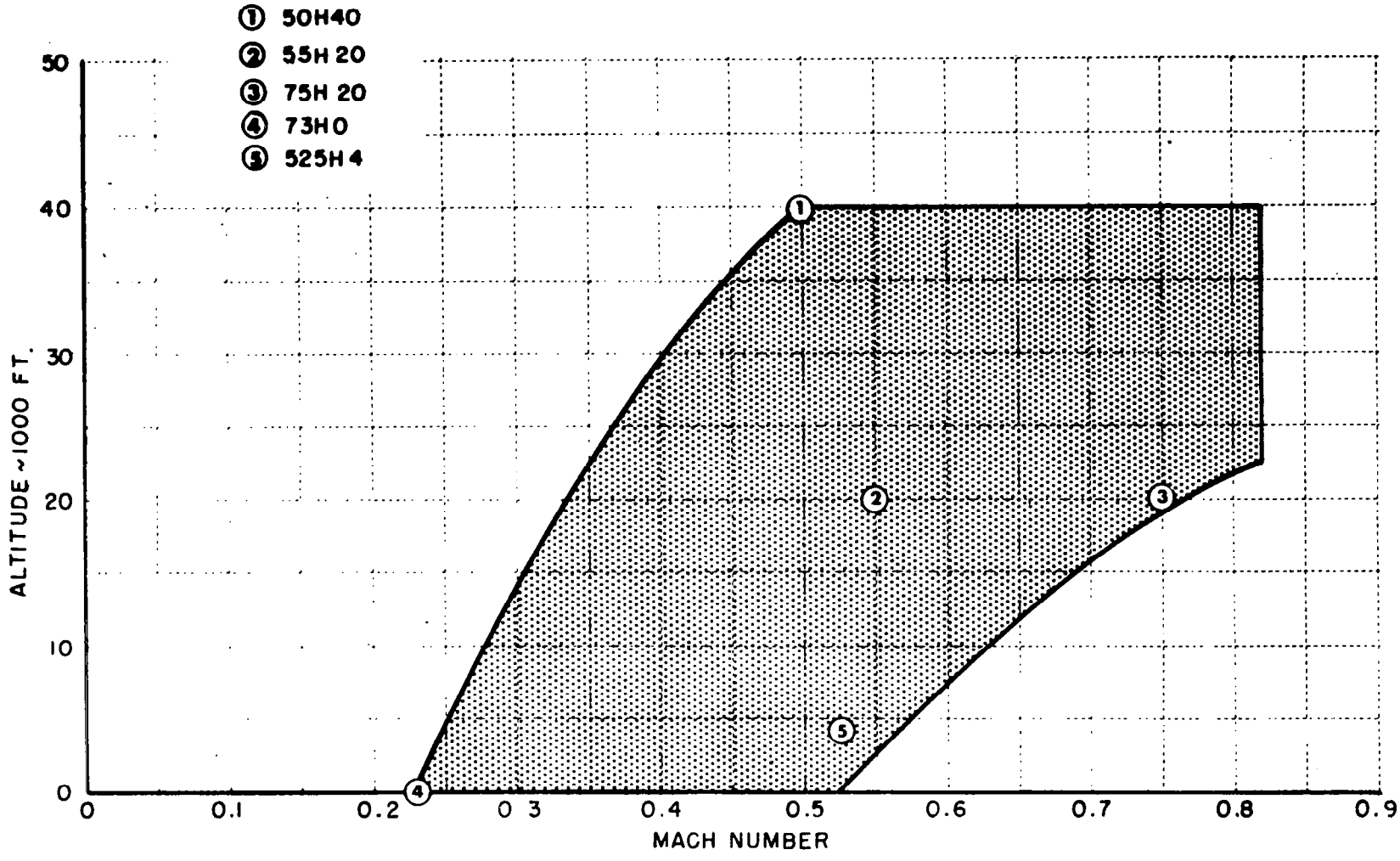

FIGURE 4.14 GPAS FLIGHT ENVELOPE FOR GENERAL RESEARCH SHOWING FLIGHT CONDITIONS INVESTIGATED IN ANALOG COMPUTER SIMULATIONS

All input gains equal 1.0.

Forward Loop Gains

$\frac{\delta_r}{e_\beta} = 33.8$ $\quad \frac{\delta_r}{e_{\dot\beta}} = 3.30$ sec

$\frac{\delta_a}{e_p} = 3.15$ sec $\quad \frac{\delta_a}{e_\phi} = .315$

$\frac{\delta_r}{e_{n_Y}} = 0$ $\quad \frac{\delta_r'}{e_{\dot\beta}} = 0$

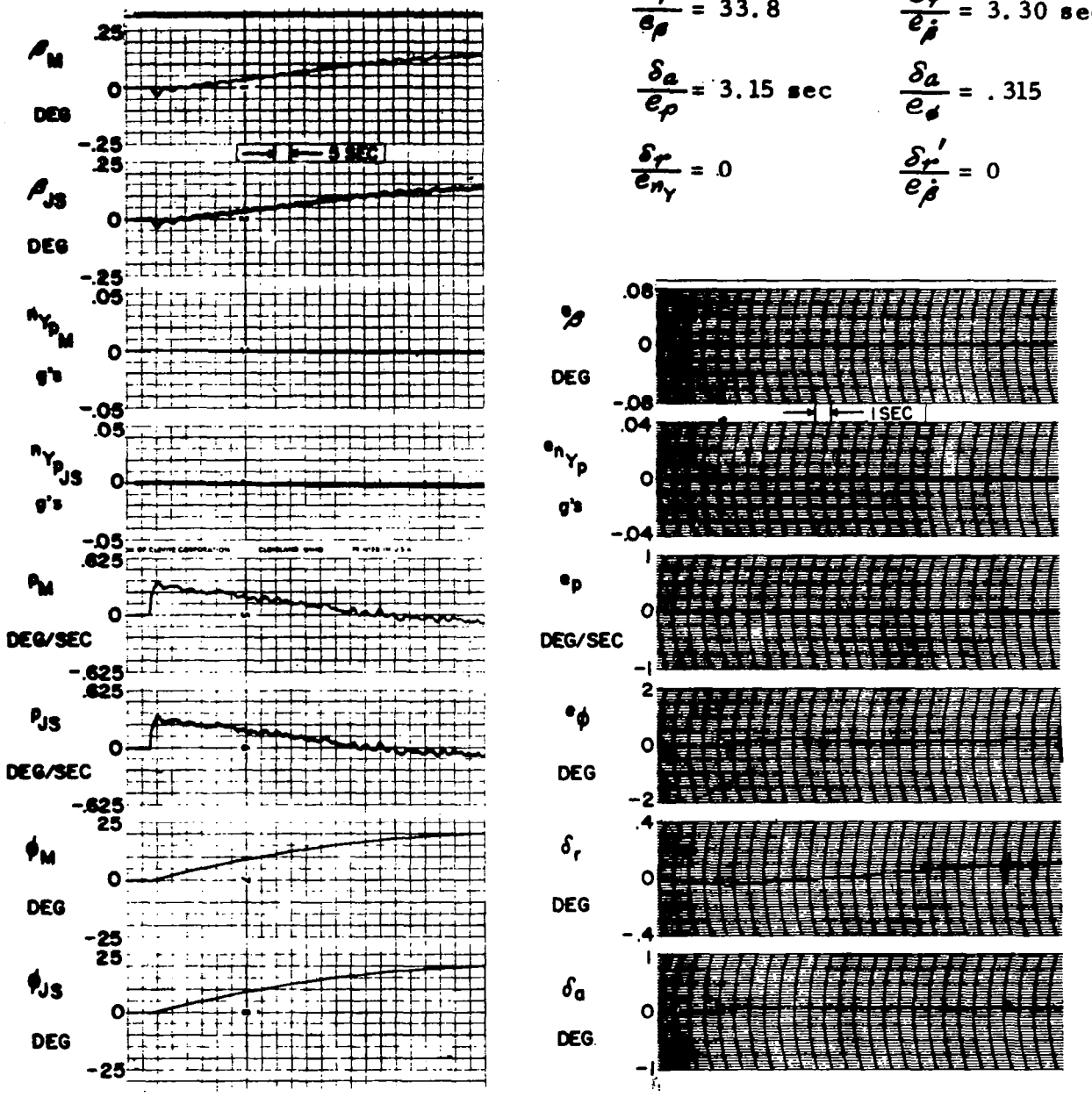

FIGURE 4.15 LATERAL-DIRECTIONAL MODEL FOLLOWING PERFORMANCE, GPAS - SST, UNLIMITED GAINS.

.55H20 $\quad \delta_a$ = 0.1 step $\quad \beta$ - Loop

All input gains equal 1.0.

Forward Loop Gains

$\frac{\delta_r}{e_\beta} = 33.8$ $\quad \frac{\delta_r}{e_{\dot\beta}} = 3.30$ sec

$\frac{\delta_a}{e_p} = 3.15$ sec $\quad \frac{\delta_a}{e_\phi} = 3.15$

$\frac{\delta_r}{e_{n_Y}} = 0$ $\quad \frac{\delta_{r'}}{e_{\dot\beta}} = 0$

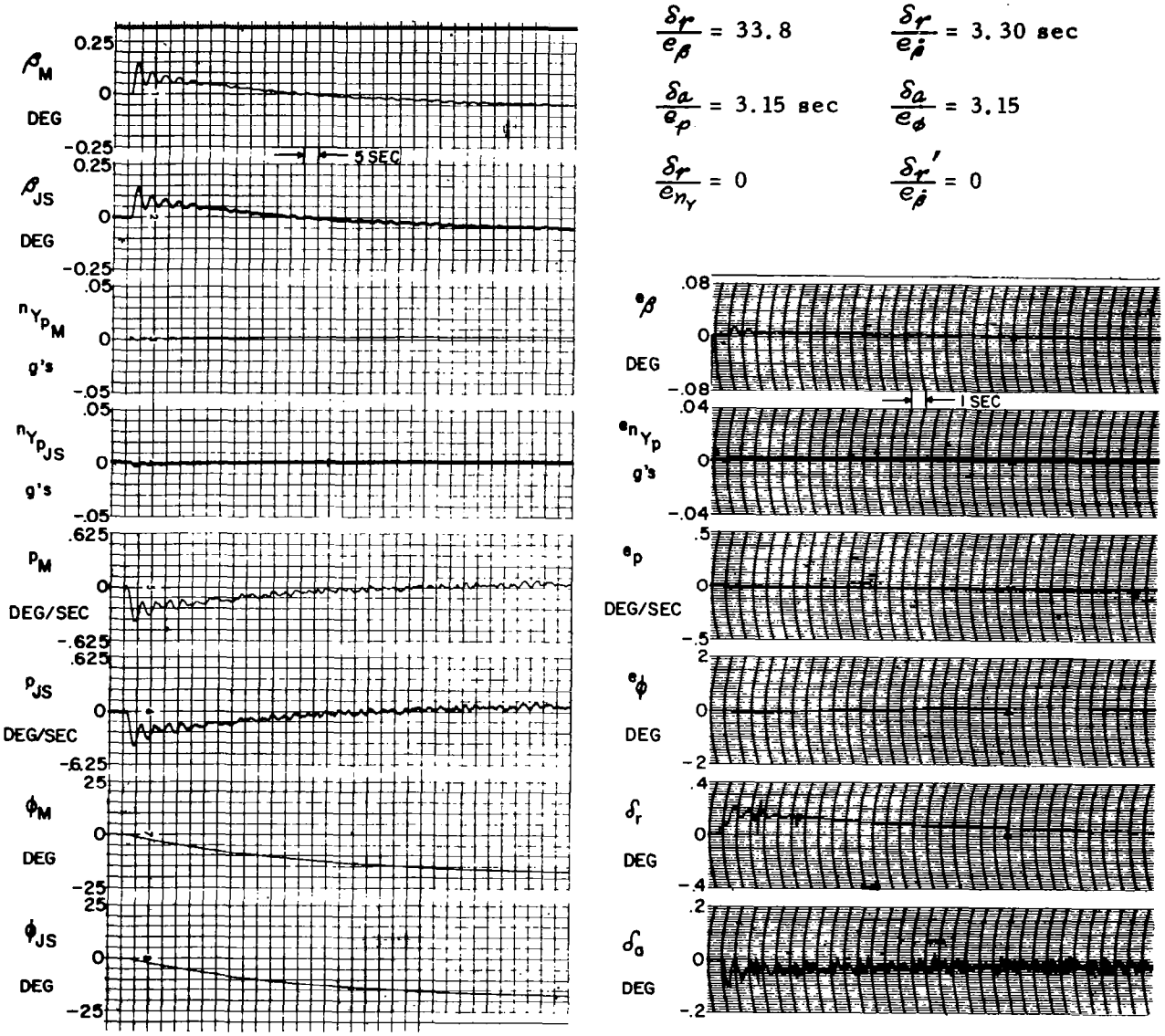

FIGURE 4.16 LATERAL-DIRECTIONAL MODEL FOLLOWING PERFORMANCE, GPAS-SST, UNLIMITED GAINS.

.55H20 $\quad \delta_r = 0.2°$ step $\quad \beta$ - Loop

All input gains equal 1.0.

Forward Loop Gains

$\frac{\delta_r}{e_\beta} = 94.4$ $\quad \frac{\delta_r}{e_{\dot\beta}} = 5.54$ sec

$\frac{\delta_a}{e_p} = 9.14$ sec $\quad \frac{\delta_a}{e_\phi} = .914$

$\frac{\delta_r}{e_{n_Y}} = 0$ $\quad \frac{\delta_r'}{e_{\dot\beta}} = 0$

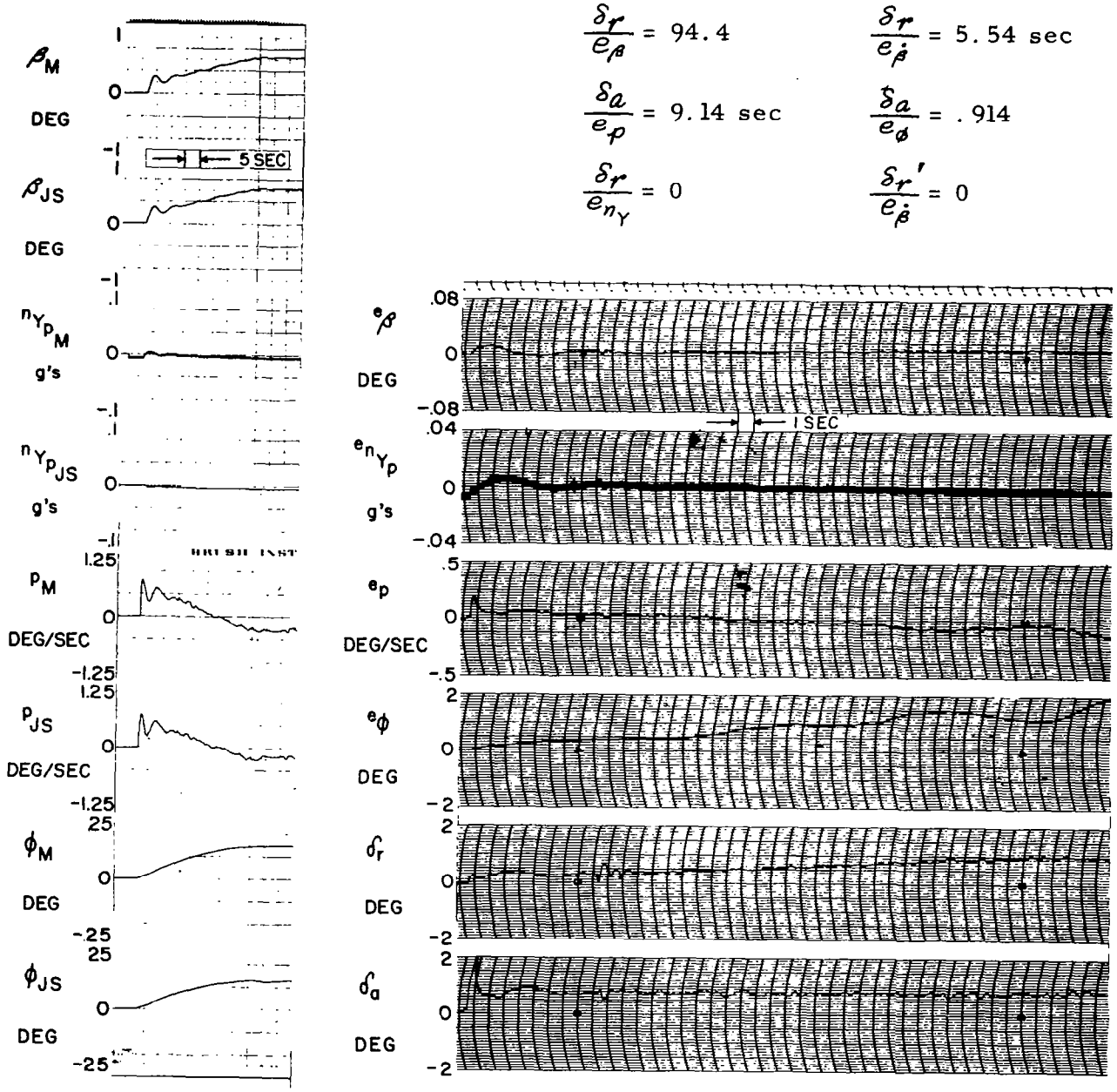

FIGURE 4.17 LATERAL-DIRECTIONAL MODEL FOLLOWING PERFORMANCE, GPAS-SST, UNLIMITED GAINS.

.23H0 $\quad \delta_a = 0.1^\circ$ step $\quad \beta$ - Loop

All input gains equal 1.0.

Forward Loop Gains

$\frac{\delta_r}{e_\beta} = 94.4$ $\quad \frac{\delta_r}{e_{\dot\beta}} = 5.54$ sec

$\frac{\delta_a}{e_p} = 9.14$ sec $\quad \frac{\delta_a}{e_\phi} = 0.914$

$\frac{\delta_r}{e_{n_Y}} = 0$ $\quad \frac{\delta_r'}{e_{\dot\beta}} = 0$

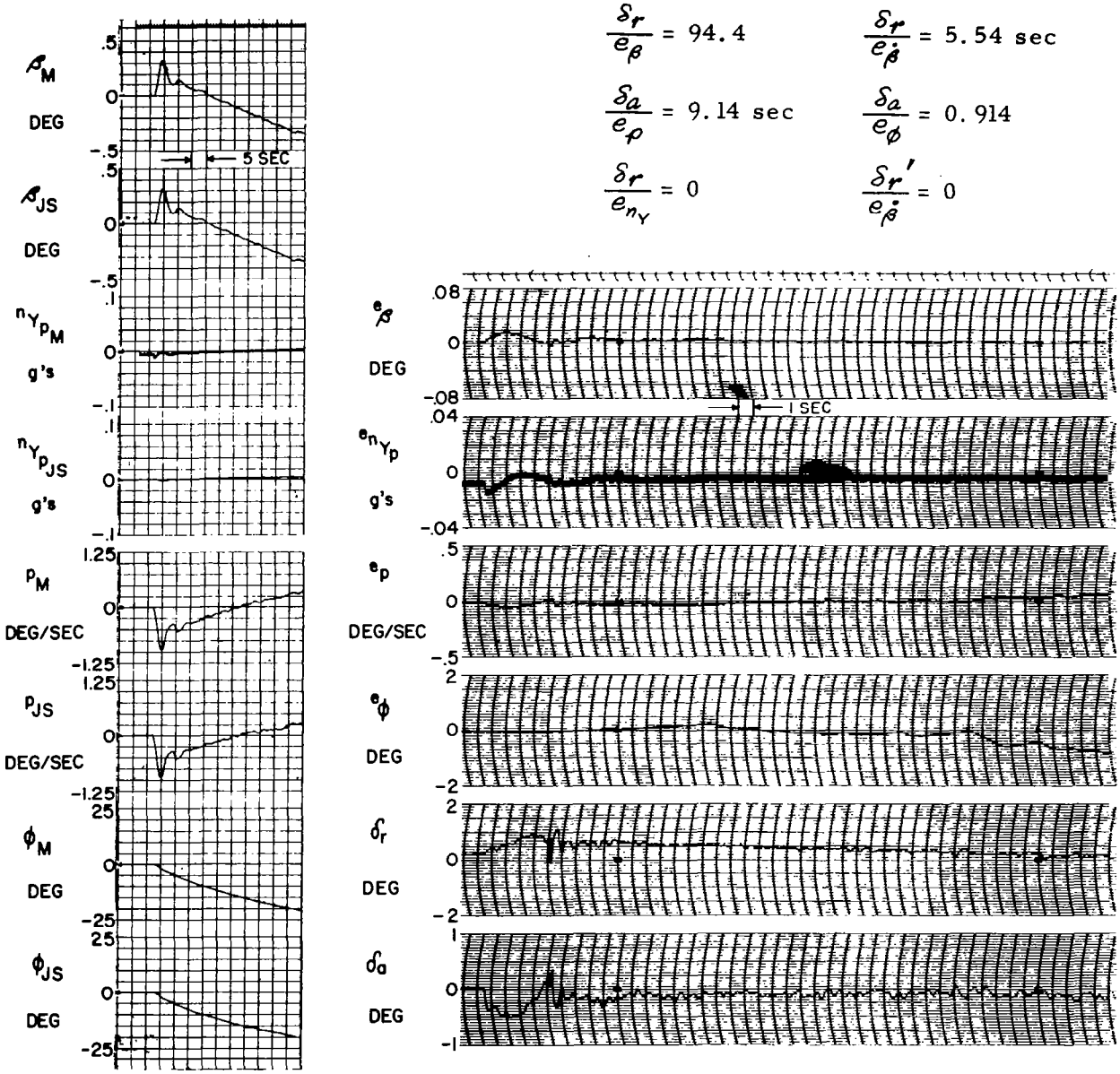

FIGURE 4.18 LATERAL-DIRECTIONAL MODEL FOLLOWING PERFORMANCE, GPAS-SST, UNLIMITED GAINS.

.23H0 $\quad \delta_r = .5^\circ$ step $\quad \beta$ - Loop

All input gains equal 1.0.

Forward Loop Gains

$\frac{\delta_r}{e_\beta} = 18.7$ $\quad \frac{\delta_r}{e_{\dot\beta}} = 2.06$ sec

$\frac{\delta_a}{e_p} = 1.48$ sec $\quad \frac{\delta_a}{e_\phi} = 0.148$

$\frac{\delta_r}{e_{n_Y}} = 0$ $\quad \frac{\delta_{r'}}{e_{\dot\beta}} = 0$

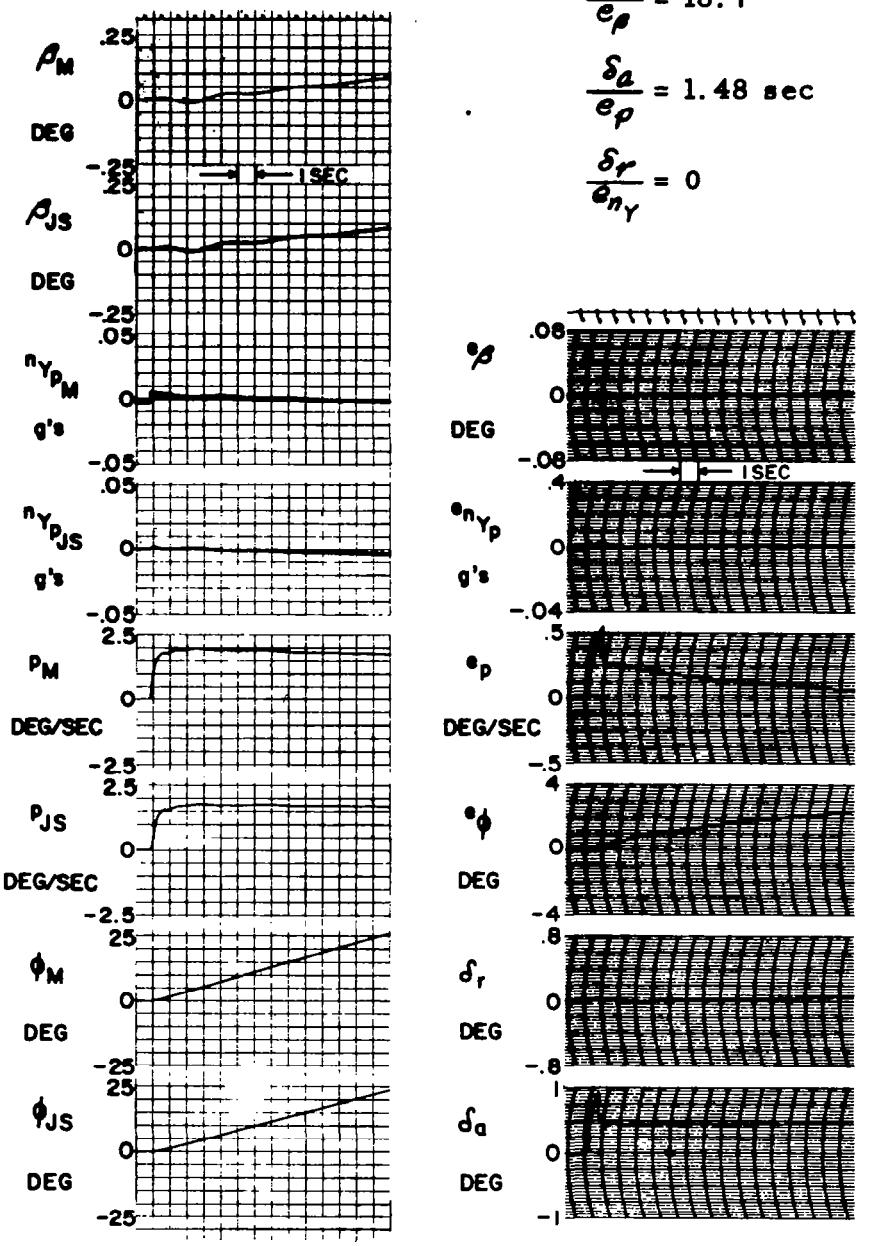

FIGURE 4.19 LATERAL-DIRECTIONAL MODEL FOLLOWING PERFORMANCE, GPAS-SST, UNLIMITED GAINS.

.75H20 $\quad \delta_a = 0.5^\circ$ step. $\quad \beta$-Loop

All input gains equal 1.0.

Forward Loop Gains

$\frac{\delta_r}{e_\beta} = 18.7$ $\frac{\delta_r}{e_{\dot\beta}} = 2.06$ sec

$\frac{\delta_a}{e_p} = 1.48$ sec $\frac{\delta_a}{e_\phi} = 0.148$

$\frac{\delta_r}{e_{n_Y}} = 0$ $\frac{\delta_{r'}}{e_{\dot\beta}} = 0$

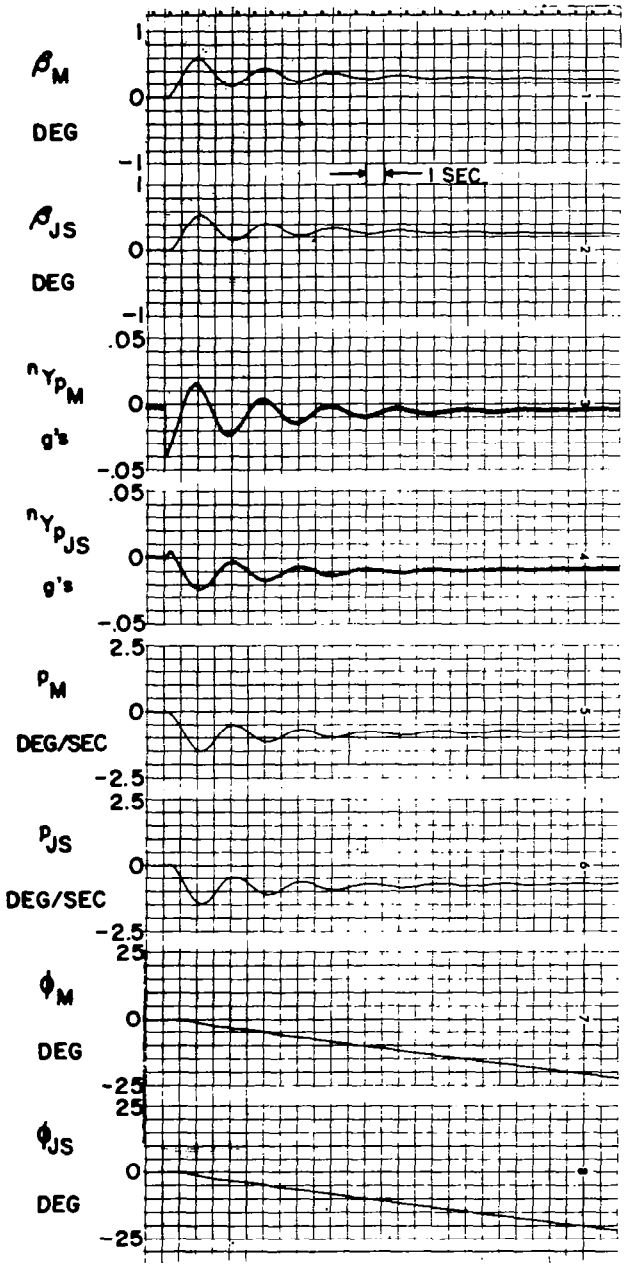

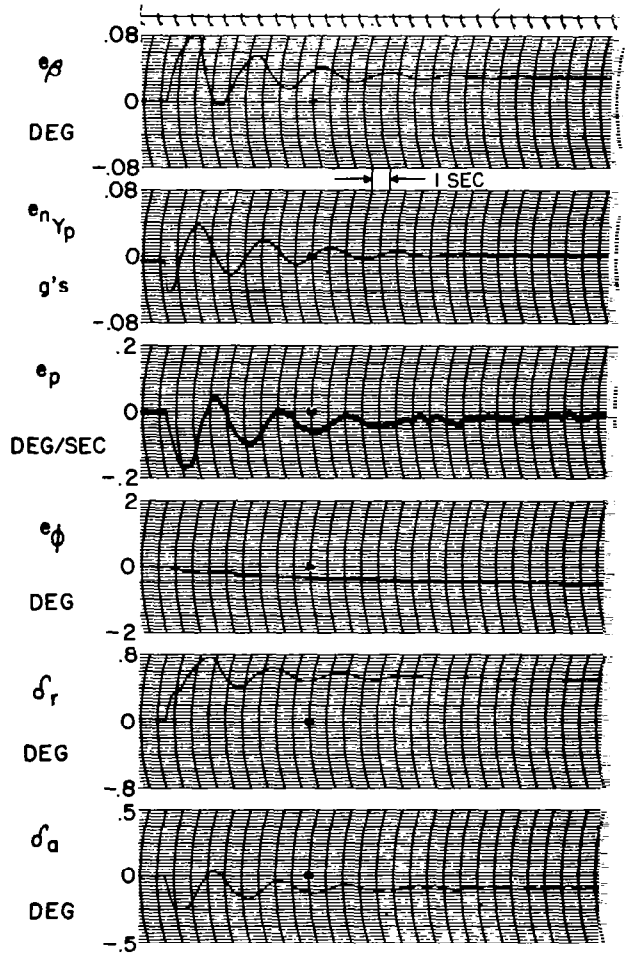

FIGURE 4.20 LATERAL-DIRECTIONAL MODEL FOLLOWING PERFORMANCE, GPAS-SST, UNLIMITED GAINS.

.75H20 $\delta_r = 0.5°$ step β-loop

All input gains equal 1.0.

Forward Loop Gains

$\frac{\delta_r}{e_\beta} = 16.0$ $\quad \frac{\delta_r}{e_{\dot\beta}} = 1.60$ sec

$\frac{\delta_a}{e_p} = 1.45$ sec $\quad \frac{\delta_a}{e_\phi} = 0.145$

$\frac{\delta_r}{e_{n_Y}} = 0$ $\quad \frac{\delta_r'}{e_{\dot\beta}} = 0$

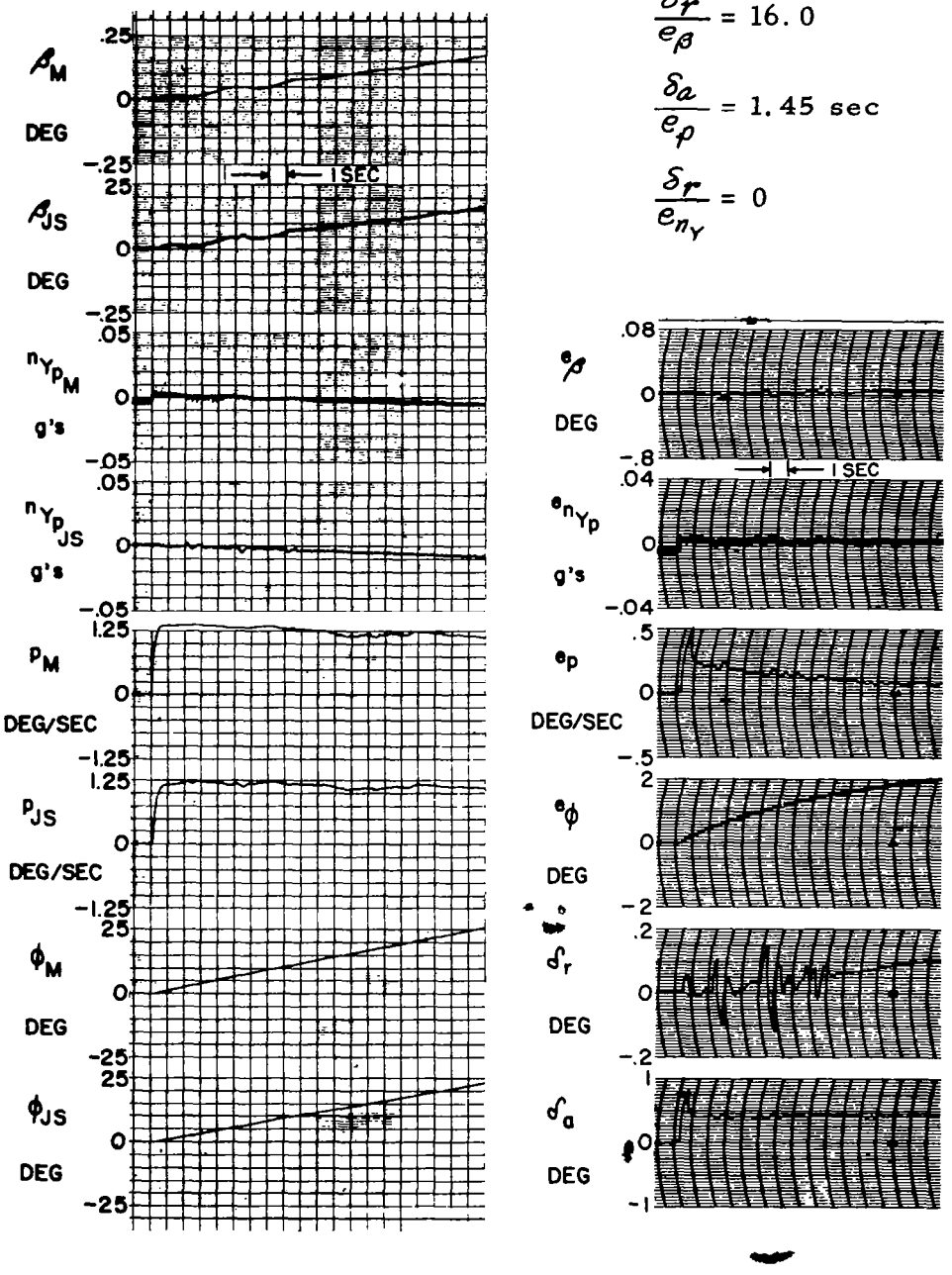

FIGURE 4.21 LATERAL-DIRECTIONAL MODEL FOLLOWING PERFORMANCE, GPAS-SST, UNLIMITED GAINS.

.525H4 $\quad \delta_a = 0.5^\circ$ step $\quad \beta$-Loop

All input gains equal 1.0.

Forward Loop Gains

$\frac{\delta_r}{e_\beta} = 16.0$ $\quad \frac{\delta_r}{e_{\dot\beta}} = 1.60$ sec

$\frac{\delta_a}{e_p} = 1.45$ sec $\quad \frac{\delta_a}{e_\phi} = 0.145$

$\frac{\delta_r}{e_{n_Y}} = 0$ $\quad \frac{\delta_{r'}}{e_{\dot\beta}} = 0$

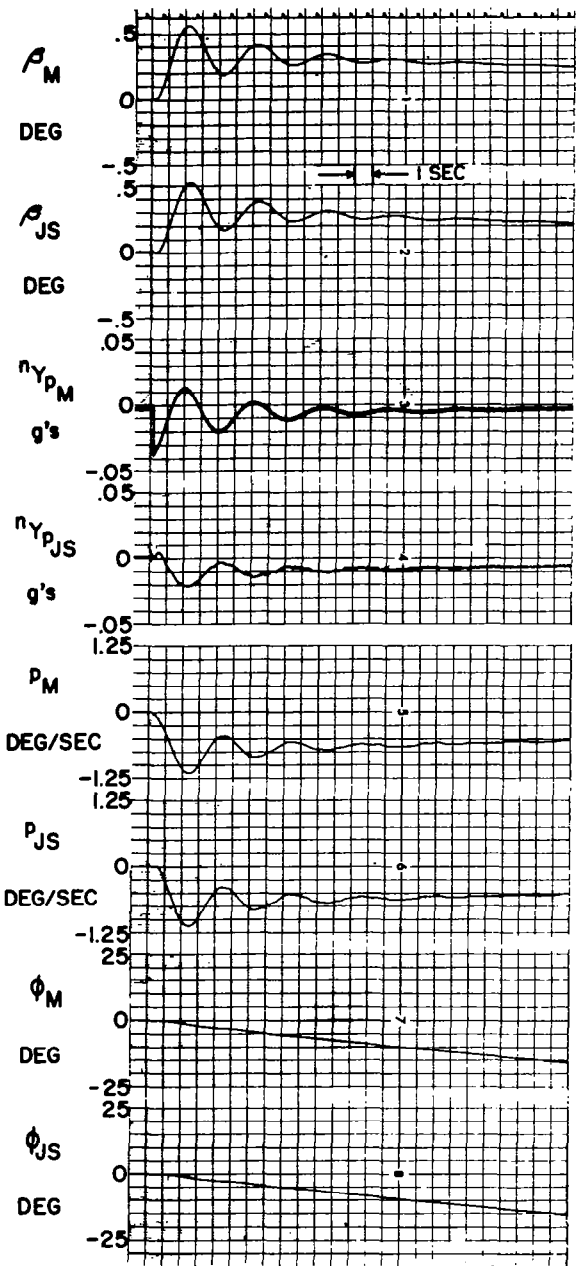

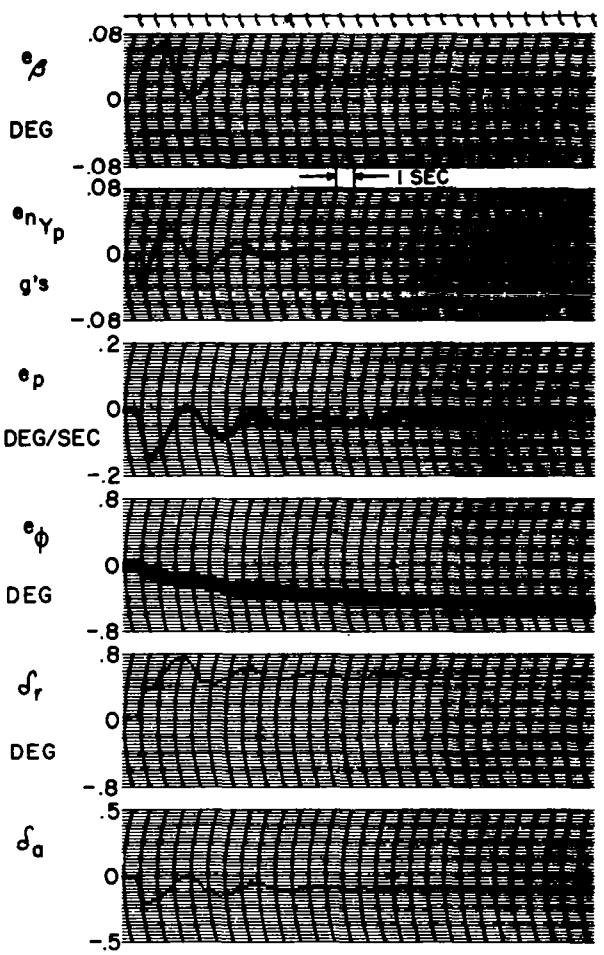

FIGURE 4.22 LATERAL-DIRECTIONAL MODEL FOLLOWING PERFORMANCE, GPAS-SST, UNLIMITED GAINS.

.525H4 $\quad \delta_r = 0.5°$ step $\quad \beta$-Loop

.11 input gains equal 1.0. Forward Loop Gains

$\frac{\delta_a}{e_p}$ = 10.5 sec $\frac{\delta_a}{e_\phi}$ = 1.05 $\frac{\delta_r}{e_\beta}$ = 108 $\frac{\delta_r}{e_{\dot\beta}}$ = 10.3 sec

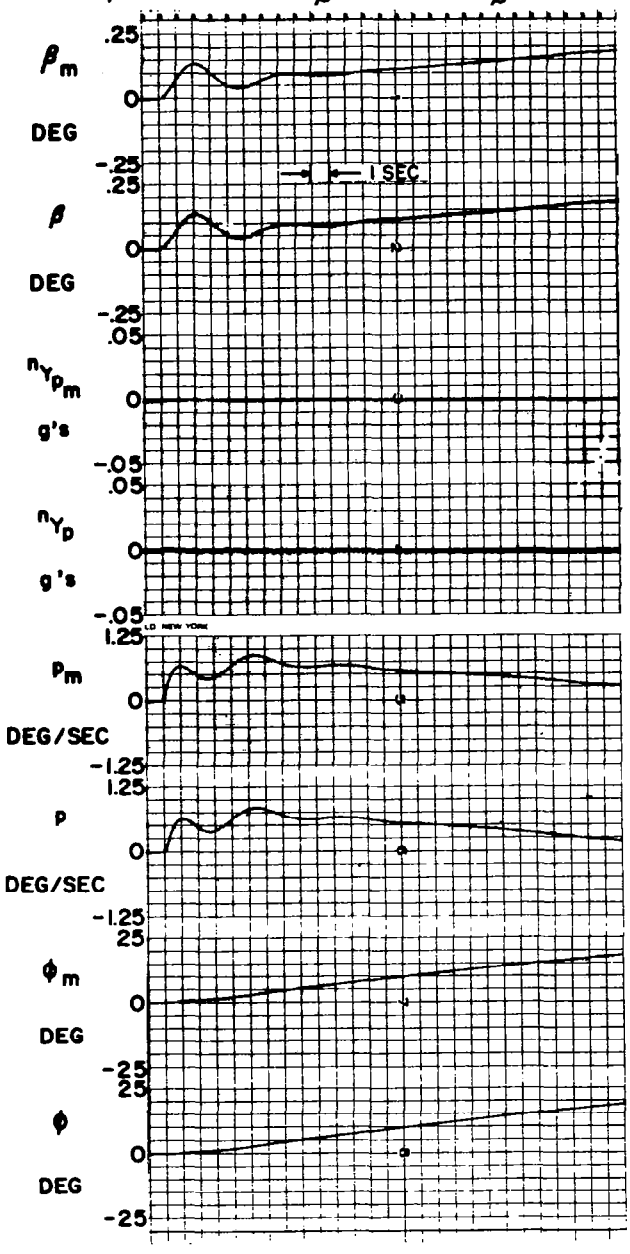

FIGURE 4.23 LATERAL-DIRECTIONAL MODEL FOLLOWING PERFORMANCE, GPAS - SST, UNLIMITED GAINS.

.5H40 δ_a = 0.5 u(t) deg β - Loop

$\frac{\delta_r}{e_\beta} = 10$ $\frac{\delta_r}{e_{\dot\beta}} = 1.0$ sec $\frac{\delta_a}{e_p} = 2.0$ sec $\frac{\delta_a}{e_\phi} = 1.05$

All input gains equal 1.0.

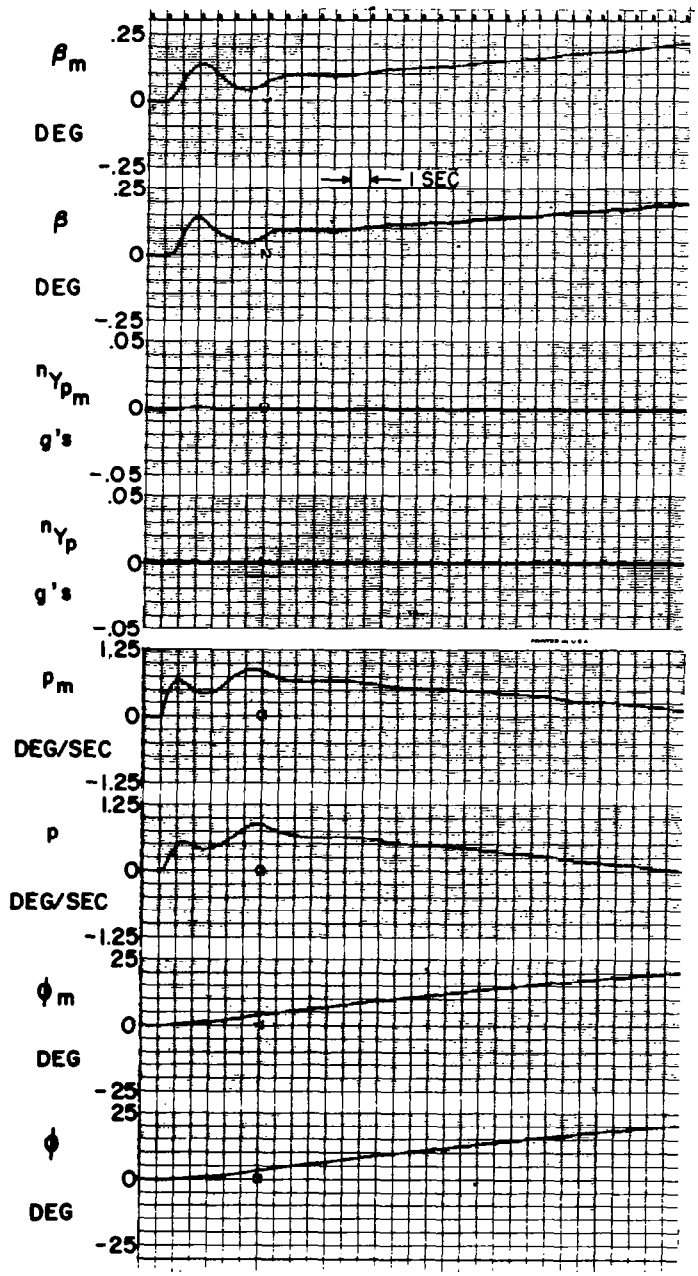

FIGURE 4.24 LATERAL-DIRECTIONAL MODEL FOLLOWING PERFORMANCE, GPAS-SST, LIMITED GAINS.

.5H40 $\delta_a = 0.5\ u(t)$ deg β-Loop

$\frac{\delta_r}{e_\beta} = 108$ $\frac{\delta_r}{e_{\dot\beta}} = 10.3$ sec $\frac{\delta_a}{e_p} = 10.5$ sec $\frac{\delta_a}{e_\phi} = 1.05$

All input gains equal 1.0.

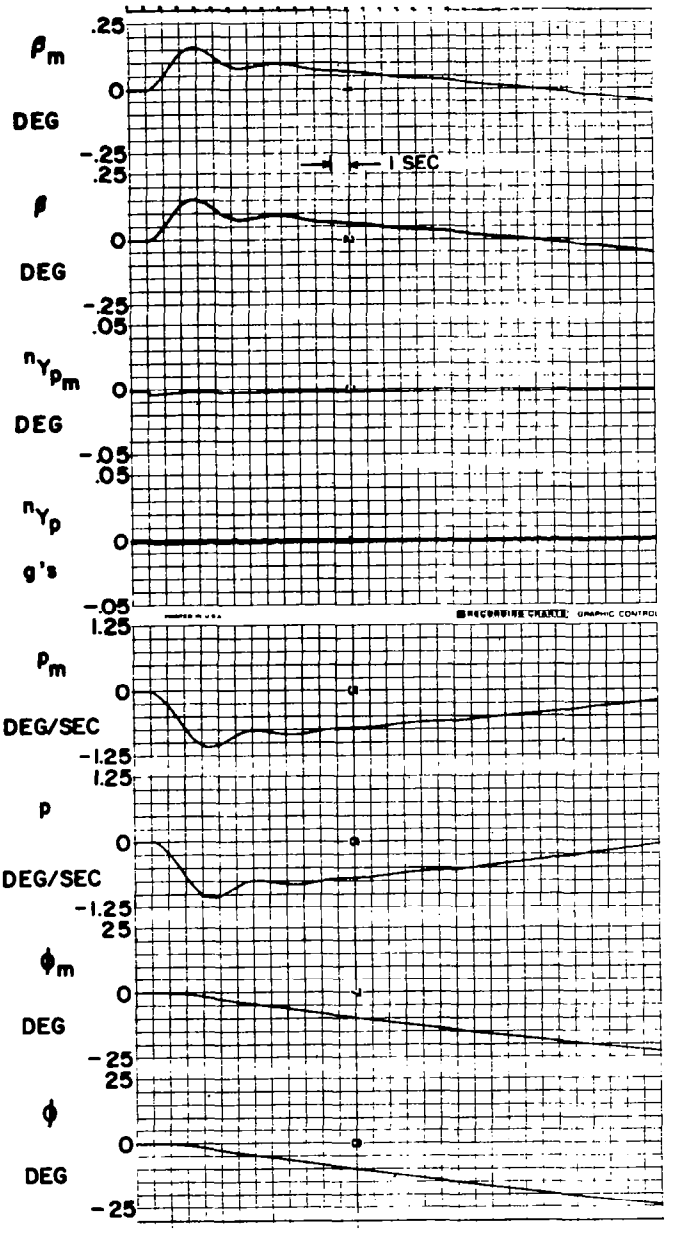

FIGURE 4.25 LATERAL-DIRECTIONAL MODEL FOLLOWING PERFORMANCE, GPAS-SST, UNLIMITED GAINS.

.5H40 $\delta_r = 0.5\ u(t)$ deg β - Loop

$\frac{\delta_r}{e_\beta} = 10$ $\frac{\delta_r}{e_{\dot\beta}} = 1.0$ sec $\frac{\delta_a}{e_p} = 2.0$ sec $\frac{\delta_a}{e_\phi} = 1.05$

All input gains equal 1.0.

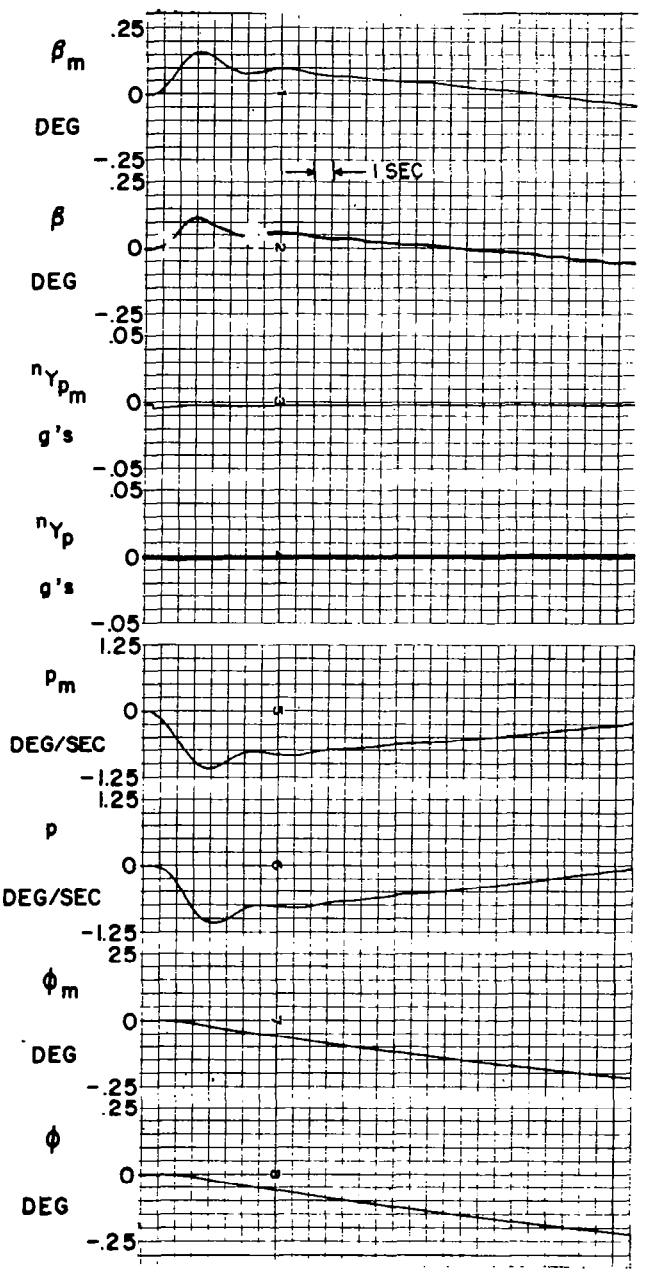

FIGURE 4.26 LATERAL-DIRECTIONAL MODEL FOLLOWING PERFORMANCE, GPAS-SST, LIMITED GAINS.

.5H40 $\delta_r = 0.5$ u(t) deg β - Loop

All input gains equal 1.0.

Forward Loop Gains

$\frac{\delta_r}{e_\beta} = 0$ $\quad \frac{\delta_r}{e_{\dot\beta}} = 0$

$\frac{\delta_a}{e_\varphi} = 3.15$ sec $\quad \frac{\delta_a}{e_\phi} = 0.315$

$\frac{\delta_r}{e_{n_Y}} = 1.73$ rad/g $\quad \frac{\delta_r'}{e_{\dot\beta}} = 0.43$ sec

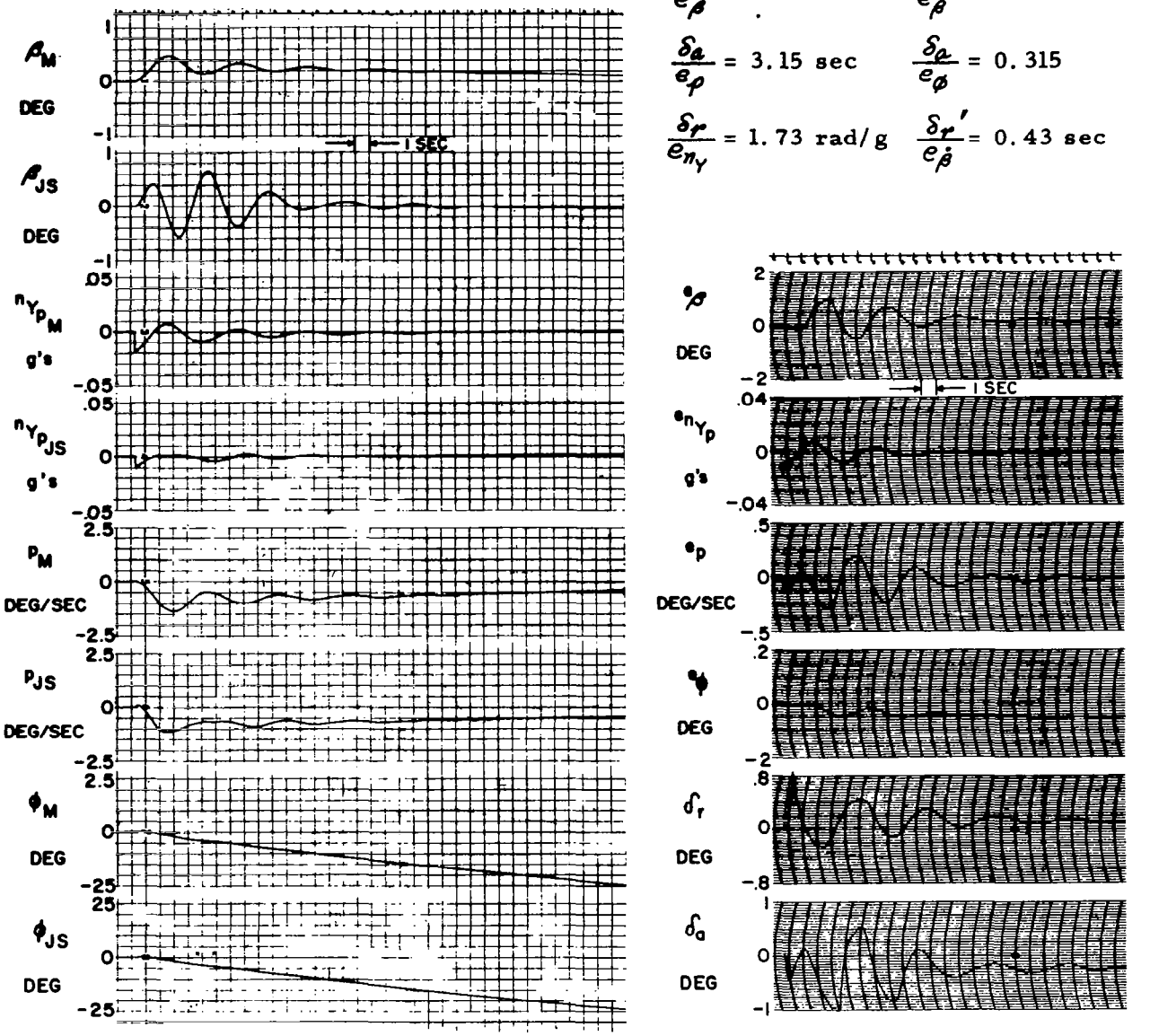

FIGURE 4.27 LATERAL-DIRECTIONAL MODEL FOLLOWING PERFORMANCE, GPAS-SST, UNLIMITED GAINS.

.55H20 $\quad \delta_r = 0.5$ step $\quad n_{Y_p}$ - Loop

All input gains equal 1.0.

Forward Loop Gains

$\frac{\delta_r}{e_\beta} = 0$ $\quad \frac{\delta_r}{e_{\dot\beta}} = 0$

$\frac{\delta_a}{e_p} = 3.15$ sec $\quad \frac{\delta_a}{e_\phi} = 0.315$

$\frac{\delta_r}{e_{n_Y}} = 1.73$ rad/g $\quad \frac{\delta_r'}{e_{\dot\beta}} = 0.43$ sec

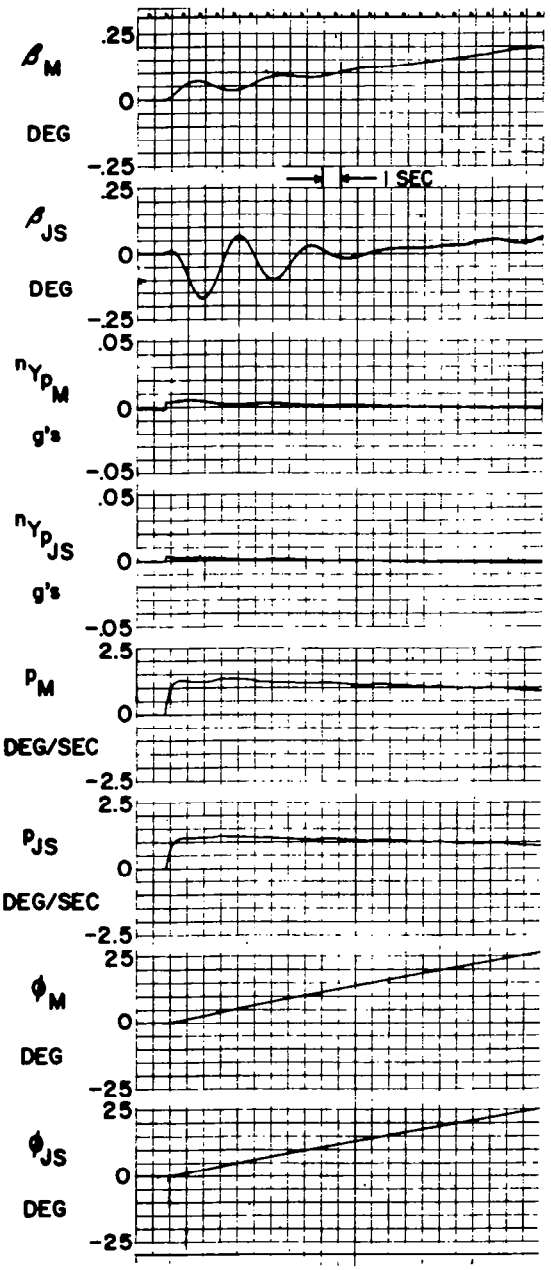

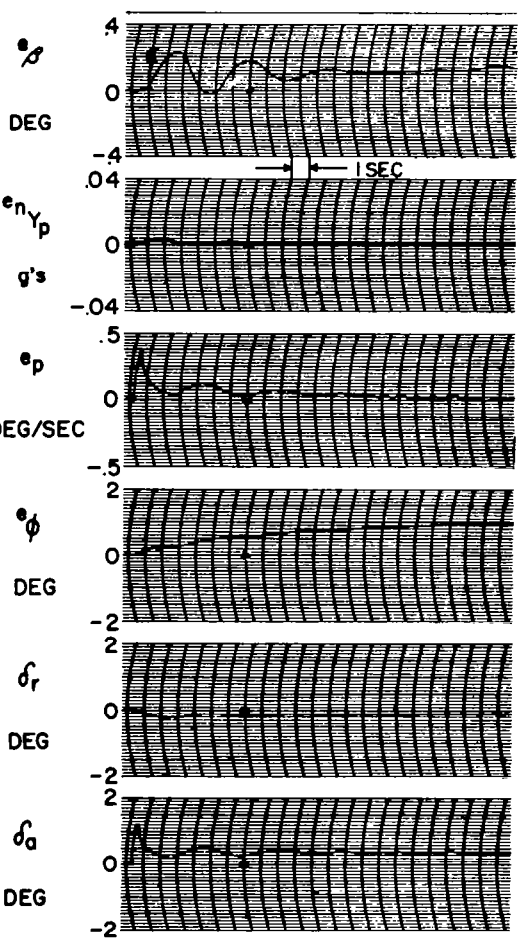

FIGURE 4.28 LATERAL-DIRECTIONAL MODEL FOLLOWING PERFORMANCE, GPAS-SST, UNLIMITED GAINS.

.55H20 $\quad \delta_a = 0.5$ step $\quad n_{Y_p}$ - Loop

All input gains equal 1.0.

Forward Loop Gains

$\frac{\delta_r}{e_\beta} = 0$ $\quad \frac{\delta_r}{e_{\dot\beta}} = 0$

$\frac{\delta_a}{e_p} = 1.48$ sec $\quad \frac{\delta_a}{e_\phi} = 0.148$

$\frac{\delta_r}{e_{n_Y}} = 0.899$ rad/g $\quad \frac{\delta_r}{e_{\dot\beta}} = 0.48$ sec

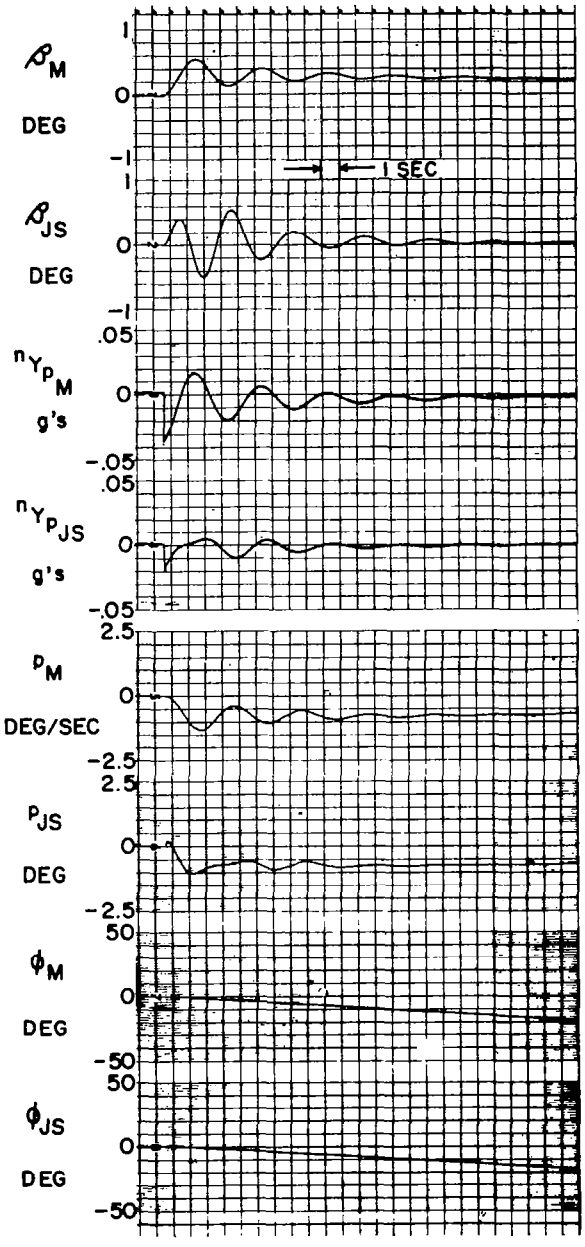

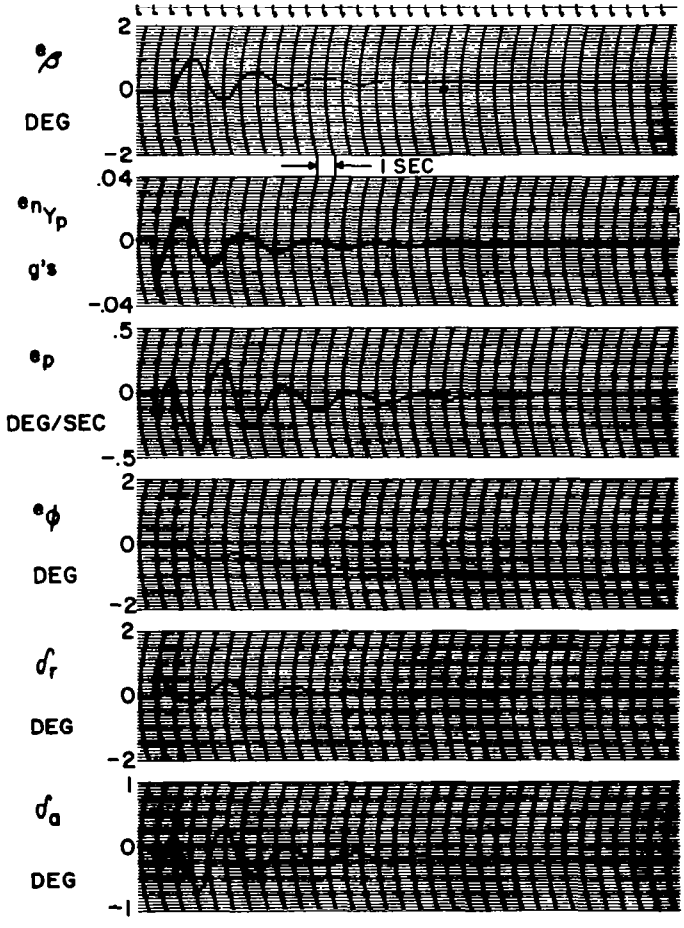

FIGURE 4.29 LATERAL-DIRECTIONAL MODEL FOLLOWING PERFORMANCE, GPAS-SST, UNLIMITED GAINS.

.75H20 $\quad \delta_r = 0.5°$ step $\quad n_{Y_p}$ - Loop

All input gains equal 1.0.

Forward Loop Gains

$\frac{\delta_r}{e_\beta} = 0$ $\quad \frac{\delta_r}{e_{\dot\beta}} = 0$

$\frac{\delta_a}{e_p} = 3.15$ sec $\quad \frac{\delta_a}{e_\phi} = 0.315$

$\frac{\delta_r}{e_{n_Y}} = 1.73$ rad/g $\quad \frac{\delta_r'}{e_{\dot\beta}} = 0.43$ sec

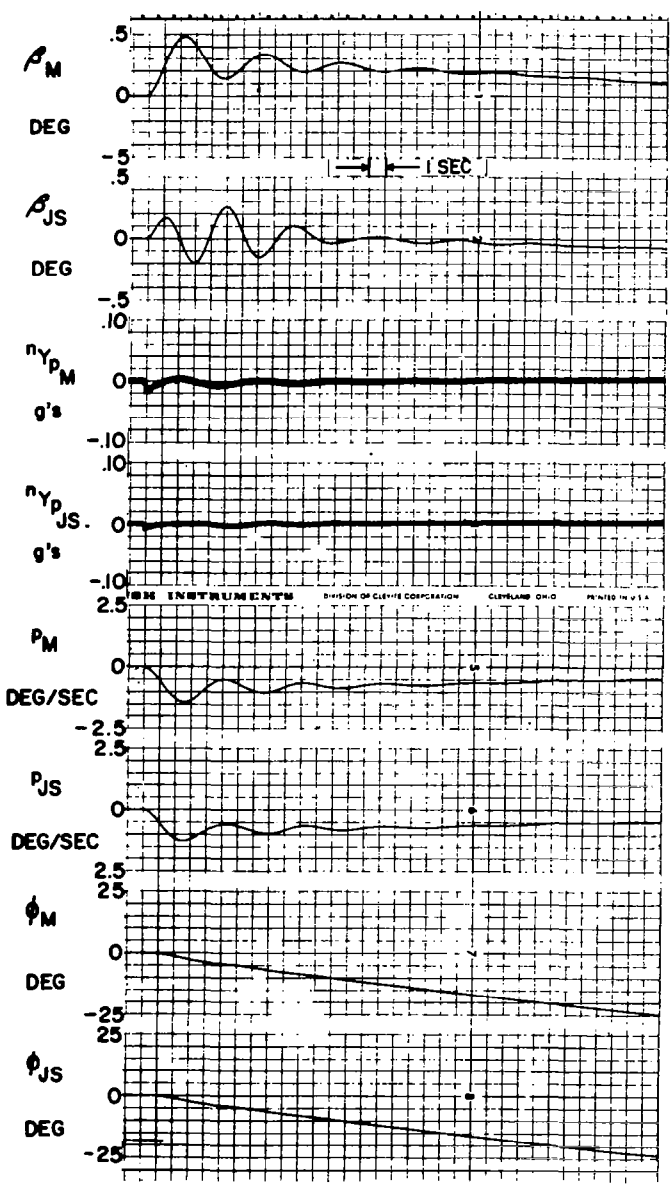

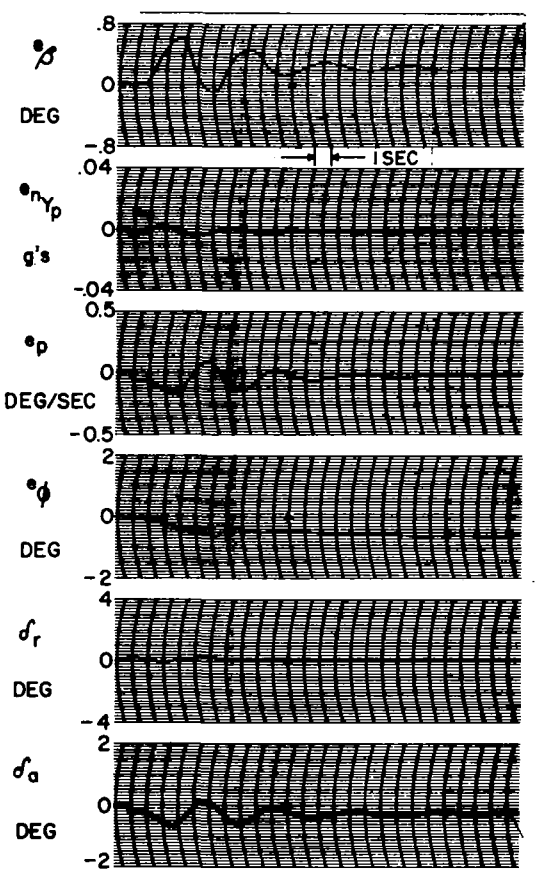

FIGURE 4.30 LATERAL-DIRECTIONAL MODEL FOLLOWING PERFORMANCE, GPAS-SST, UNLIMITED GAINS.

.55H20 $\quad \delta_r = 0.5^\circ$ step $\quad n_{Y_p}$ - Loop

All input gains equal 1.0.

Forward Loop Gains

$\frac{\delta_r}{e_\beta} = 0$ $\quad \frac{\delta_r}{e_{\dot\beta}} = 0$

$\frac{\delta_a}{e_p} = 3.15$ sec $\quad \frac{\delta_a}{e_\phi} = 0.315$

$\frac{\delta_r}{e_{n_Y}} = 1.73$ rad/g $\quad \frac{\delta_r'}{e_{\dot\beta}} = 0.43$ sec

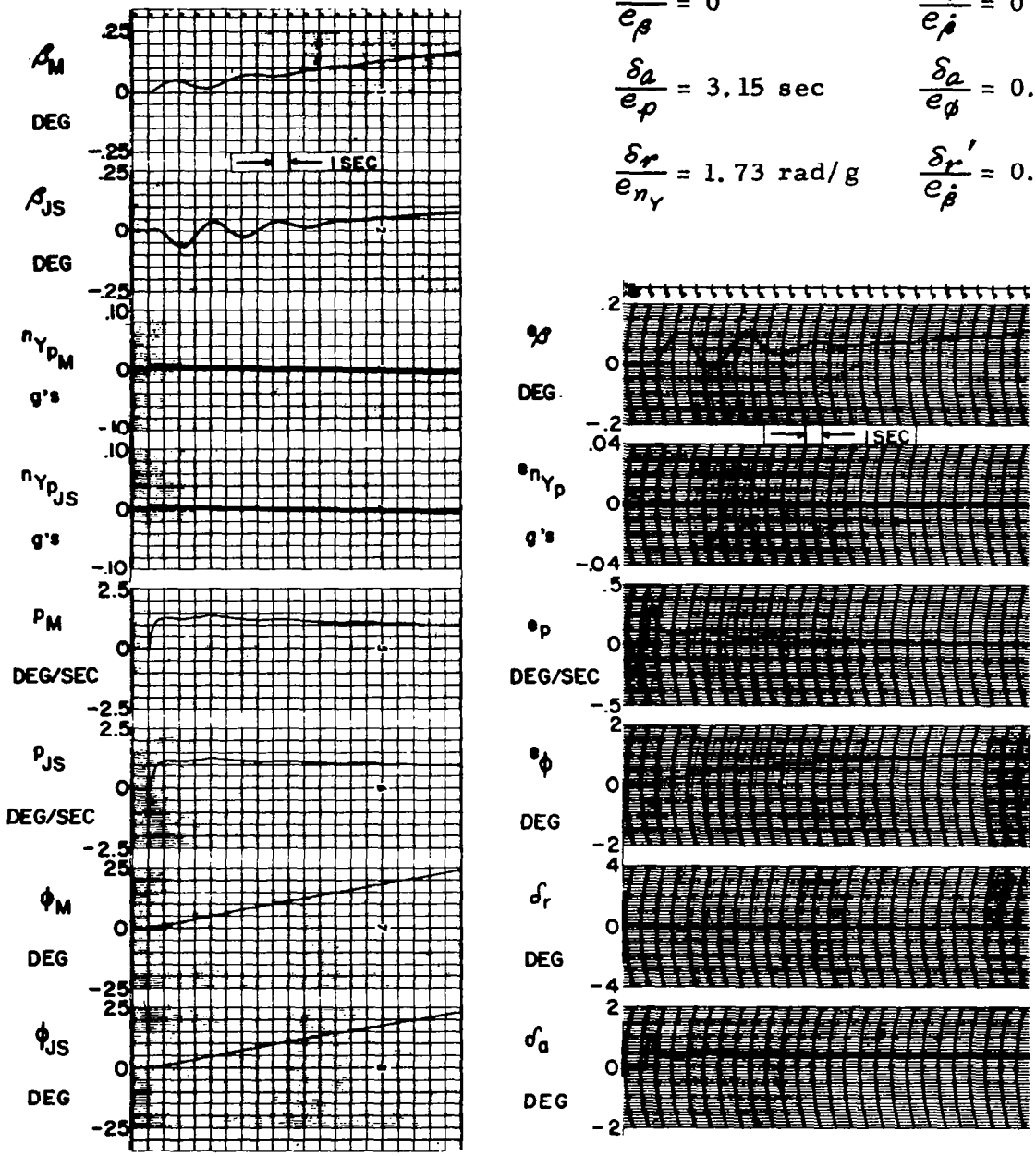

FIGURE 4.31 LATERAL-DIRECTIONAL MODEL FOLLOWING PERFORMANCE, GPAS-SST, UNLIMITED GAINS.

.55H20 $\quad \delta_a = 0.5^\circ$ step $\quad n_{Y_p}$ -Loop

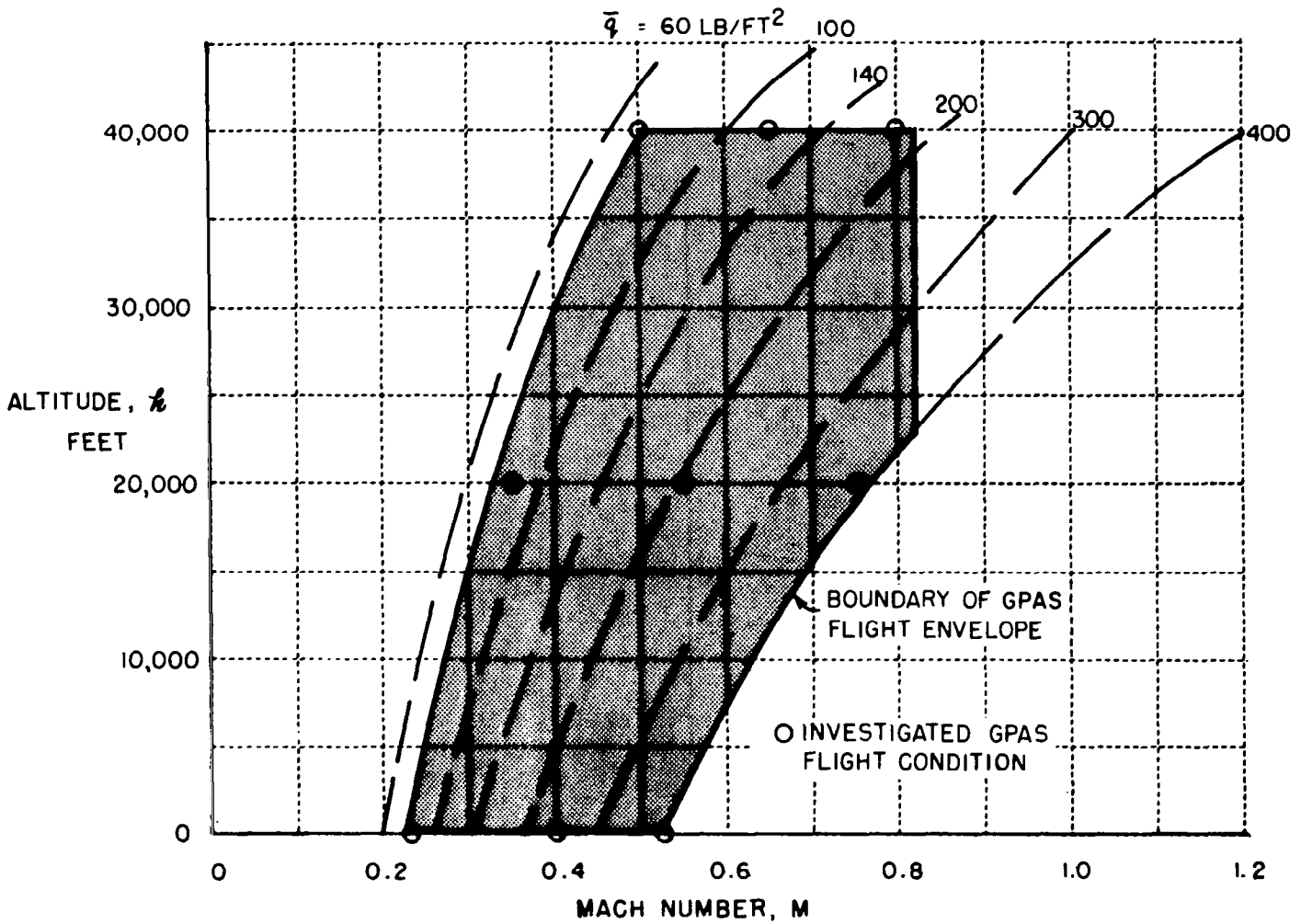

FIGURE 5.1 GPAS FLIGHT ENVELOPE SHOWING LINES OF CONSTANT DYNAMIC PRESSURE AND THE PARTICULAR OPERATING POINTS THAT WERE STUDIED

APPENDIX A
EQUATIONS OF MOTION AND AIRCRAFT DATA

A.1 LINEARIZED EQUATIONS AND DATA

A.1.1 Linearized Longitudinal Equations (x-wind axis and y-, and z-body axes)

x-force $$\Delta\dot{V} + D_V \Delta V + V_t D_\alpha \Delta\alpha + g\Delta\theta = \frac{\Delta T}{m}$$

z-force $$\frac{\alpha_t}{V_t}\Delta\dot{V} - \frac{Z_V}{V_t}\Delta V + \Delta\dot{\alpha} - Z_\alpha \Delta\alpha - \Delta\dot{\theta} - Z_\theta \Delta\theta = Z_{\delta_e}\Delta\delta_e$$

pitching moment $$-M_V \Delta V - M_{\dot{\alpha}}\Delta\dot{\alpha} - M_\alpha \Delta\alpha + \Delta\ddot{\theta} - M_q \Delta\dot{\theta} = M_{\delta_e}\Delta\delta_e + M_{\Delta T}\Delta T$$

$$D_V = \frac{1}{m}\left(\frac{\partial D}{\partial V} - \frac{\partial T}{\partial V}\right) \qquad \frac{\partial D}{\partial V} = C_{D_t}\rho V_t S$$

$$D_\alpha = \frac{1}{mV_t}\left(\frac{\partial D}{\partial \alpha} + \alpha_t T_t - W\right) \qquad \frac{\partial D}{\partial \alpha} = C_{D_\alpha}\frac{1}{2}\rho V_t^2 S$$

$$Z_V = -\frac{1}{m}\left(\frac{\partial L}{\partial V} + \alpha_t \frac{\partial D}{\partial V}\right) \qquad \frac{\partial L}{\partial V} = C_{L_t}\rho V_t S$$

$$Z_\alpha = -\frac{1}{mV_t}\left(\frac{\partial L}{\partial \alpha} + \alpha_t \frac{\partial D}{\partial \alpha} + T_t - W\theta_t\right) \qquad \frac{\partial L}{\partial \alpha} = C_{L_\alpha}\frac{1}{2}\rho V_t^2 S$$

$$Z_\theta = -\frac{g\alpha_t}{V_t}$$

$$Z_{\delta_e} = -\frac{1}{mV_t}\frac{\partial L}{\partial \delta_e} \qquad \frac{\partial L}{\partial \delta_e} = C_{L_{\delta_e}}\frac{1}{2}\rho V_t^2 S$$

$$M_V = \frac{1}{I_{YY}}\frac{\bar{q}S\bar{c}}{a}\left\{\frac{2}{M}C_{m_{(A)}} + \frac{\partial C_{m_{(A)}}}{\partial M}\right\} - \frac{z_T}{I_{YY}a}\frac{\partial T}{\partial M}$$

$$C_{m_{(A)}} \cong \frac{-z_T}{\bar{c}} C_D$$

$$M_{\dot{\alpha}} = \frac{1}{I_{YY}} \bar{q} S \bar{c} \cdot \frac{\bar{c}}{2V_t} C_{m_{\dot{\alpha}}}$$

$$M_{\alpha} = \frac{1}{I_{YY}} \bar{q} S \bar{c} \, C_{m_{\alpha}}$$

$$M_{q} = \frac{1}{I_{YY}} \bar{q} S \bar{c} \cdot \frac{\bar{c}}{2V_t} C_{m_{q}}$$

$$M_{\delta_e} = \frac{1}{I_{YY}} \bar{q} S \bar{c} \, C_{m_{\delta_e}}$$

$$M_{\Delta T} = \frac{z_T}{I_{YY}}$$

a = speed of sound

z_T = thrust moment arm (along positive z body axis)

A.1.2 Linearized Lateral-Directional Equations (Body Axes)

Side Force

$$-\alpha_t \dot{\phi} - \frac{g}{V_t} \phi + (1+\alpha_t^2) r + \dot{\beta} - Y_\beta \beta = Y_{\delta_r} \delta_r$$

Rolling Moment

$$\ddot{\phi} - L_p \dot{\phi} - \left(\frac{I_{xz}}{I_{xx}} + \alpha_t\right) \dot{r} + (\alpha_t L_p - L_r) r - L_\beta \beta = L_{\delta_r} \delta_r + L_{\delta_a} \delta_a$$

Yawing Moment

$$-\frac{I_{xz}}{I_{zz}} \ddot{\phi} - N_p \dot{\phi} + \left(1 + \alpha_t \frac{I_{xz}}{I_{zz}}\right) \dot{r} + (\alpha_t N_p - N_r) r - N_\beta \beta = N_{\delta_r} \delta_r + N_{\delta_a} \delta_a$$

$$Y_\beta = \frac{1}{mV_t}\,\bar{q}\,S\,C_{Y_\beta} \qquad N_\beta = \frac{1}{I_{zz}}\,\bar{q}\,Sb\,C_{n_\beta}$$

$$Y_{\delta_r} = \frac{1}{mV_t}\,\bar{q}\,S\,C_{Y_{\delta_r}} \qquad N_{\delta_r} = \frac{1}{I_{zz}}\,\bar{q}\,Sb\,C_{n_{\delta_r}}$$

$$L_p = \frac{1}{I_{xx}}\,\bar{q}\,Sb \cdot \frac{b}{2V_t} \cdot C_{\ell_p} \qquad N_{\delta_a} = \frac{1}{I_{zz}}\,\bar{q}\,Sb\,C_{n_{\delta_a}}$$

$$L_r = \frac{1}{I_{xx}}\,\bar{q}\,Sb \cdot \frac{b}{2V_t} \cdot C_{\ell_r}$$

$$L_\beta = \frac{1}{I_{xx}}\,\bar{q}\,Sb\,C_{\ell_\beta}$$

$$L_{\delta_r} = \frac{1}{I_{xx}}\,\bar{q}\,Sb\,C_{\ell_{\delta_r}}$$

$$L_{\delta_a} = \frac{1}{I_{xx}}\,\bar{q}\,Sb\,C_{\ell_{\delta_a}}$$

$$N_p = \frac{1}{I_{zz}}\,\bar{q}\,Sb\,\frac{b}{2V_t}\,C_{n_p}$$

$$N_r = \frac{1}{I_{zz}}\,\bar{q}\,Sb\,\frac{b}{2V_t}\,C_{n_r}$$

A.1.3 JetStar Aircraft Data and Stability Derivatives

The following tables list the aircraft data and stability derivatives (both non-dimensional and dimensional) used with the longitudinal and lateral-directional linearized equations given in A.1.1 and A.1.2 All data are for a c.g. located at 25% m.a.c.

Table A.1 (a)

JetStar Aircraft Data

Reference Area	S	= 542.5 ft^2
Reference Lengths	$\bar{c}$	= 10.93 ft (longitudinal)
	b	= 53.75 ft (lateral-directional)
Thrust Moment Arm	$-\eta_T$	= 9.8 in. (above c.g.)

Weights and Inertias (body axes)	Weight, lb	
	23,904	38,204
I_{xx}, slug-ft^2	42,273	118,773
I_{yy}, slug-ft^2	126,099	135,869
I_{zz}, slug-ft^2	160,104	243,504
I_{xz}, slug-ft^2	5,470	5,061

TABLE A.1.3(b) DATA FOR LINEAR EQUATIONS OF MOTION

h	M	V_t	$\bar{q}$	α_t	α_t	δ_{e_t}	$\Delta\delta_{t_t}$	C_{L_t}	C_{L_α}	$C_{L_{\delta_e}}$	C_D	$C_{D_{\dot{\alpha}}}$	$C_{m_{(A)}}$	$C_{m_{(A)_m}}$	C_{m_α}	$C_{m_{\dot{\alpha}}}$	C_{m_q}	$C_{m_{\delta_e}}$
ft	ft/sec		lb/ft^2	deg	rad	deg	deg		rad^{-1}	rad^{-1}		rad^{-1}			rad^{-1}	rad^{-1}	rad^{-1}	rad^{-1}
0	0.23	257	78.4	7.20	.126	.40	-1.95	0.563	5.02	0.398	.037	.44	.00295	-.085	-.65	-2.8	-8.0	-.81
0	0.40	447	238	2.86	.0499	.56	- .72	0.1852	5.12	0.399	.020	.086	.00149	-.060	-.64	-2.9	-8.1	-.82
0	0.525	586	408	2.02	.0353	.61	- .63	0.108	5.25	0.403	.019	0	.00138	-.019	-.66	-3.0	-8.2	-.82
20,000	0.35	363	83.6	6.55	.114	.44	-1.87	0.528	5.18	0.348	.032	.41	.00257	-.060	-.65	-2.8	-8.1	-.81
20,000	0.55	570	206	3.13	.0546	.56	- .95	0.214	5.29	0.405	.021	.069	.00138	-.0072	-.67	-3.1	-8.3	-.83
20,000	0.75	778	383	2.02	.0353	.47	-.85	0.115	5.90	0.425	.021	.017	.00158	-.105	-.77	-3.7	-9.2	-.86
40,000	0.50	484	68.7	7.57	.132	.45	-2.36	0.642	5.22	0.402	.044	.46	.00332	-.039	-.65	-3.0	-8.2	-.82
40,000	0.65	629	116.2	4.75	.0829	.49	-1.62	0.379	5.47	0.412	.028	.18	.00207	-.012	-.70	-3.3	-8.6	-.84
40,000	0.80	775	176.5	2.96	.0517	.44	-1.49	0.250	6.31	0.440	.027	.11	.00200	-.52	-.82	-4.0	-9.3	-.88
0	0.23	257	78.4	11.2	.195	.65	-3.40	0.898	5.02	0.398	.048	1.40	.00314	-.060	-.69	-2.8	-8.0	-.81
0	0.40	447	238	4.04	.0705	.52	-1.20	0.296	5.12	0.399	.021	.39	.00151	-.063	-.64	-2.9	-8.1	-.82
0	0.525	586	408	2.68	.0467	.59	-.81	0.1725	5.25	0.403	.020	.046	.00147	-.020	-.66	-3.0	-8.2	-.82
20,000	0.35	363	83.6	9.90	.157	.37	-3.07	0.842	5.18	0.398	.050	.63	.00375	-.072	-.66	-2.8	-8.1	-.81
20,000	0.55	570	206	4.44	.0775	.52	-1.41	0.342	5.29	0.405	.025	.19	.00181	-.009	-.67	-3.1	-8.3	-.83
20,000	0.75	778	383	2.64	.0461	.46	-1.13	0.184	5.90	0.425	.022	.057	.00164	-.085	-.76	-3.7	-9.2	-.86
40,000	0.50	484	68.7	11.5	.201	.37	-3.95	1.024	5.22	0.402	.070	.48	.00523	-.002	-.65	-3.0	-8.2	-.82
40,000	0.65	629	116.2	7.00	.122	.47	-2.44	0.606	5.47	0.412	.041	.38	.00329	-.005	-.70	-3.3	-8.6	-.84
40,000	0.80	775	176.5	4.24	.0740	.45	-2.09	0.399	6.31	0.440	.032	.21	.00247	-.61	-.73	-4.0	-9.3	-.88

TABLE A.1.3(b) (Cont) DATA FOR LINEAR EQUATIONS OF MOTION

$\partial T/\partial M$ lb	C_{Y_β} rad^{-1}	$C_{Y_{\delta_r}}$ rad^{-1}	C_{ℓ_p} rad^{-1}	C_{ℓ_r} rad^{-1}	C_{ℓ_β} rad^{-1}	$C_{\ell_{\delta_r}}$ rad^{-1}	$C_{\ell_{\delta_a}}$ rad^{-1}	C_{n_p} rad^{-1}	C_{n_r} rad^{-1}	C_{n_β} rad^{-1}	$C_{n_{\delta_r}}$ rad^{-1}	$C_{n_{\delta_a}}$ rad^{-1}	Z_v rad/sec	Z_α sec^{-1}	Z_{δ_e} sec^{-1}
-430	-.716	.177	-.3645	.0818	-.1315	.02887	.05335	-.0542	-.1665	.1235	-.06338	.007748	-.3003	-1.1314	-.08871
-244	-.716	.177	-.3754	.04504	-.07985	.02909	.05488	-.007961	-.1536	.1152	-.06513	.003743	-.2117	-1.9936	-.15523
-98	-.716	.177	-.3847	.03783	-.087	.02912	.05683	-.0008296	-.1513	.1120	-.06521	.003005	-.2001	-2.6707	-.20501
-43	-.716	.177	-.3744	.08053	-.1209	.02875	.05403	-.04847	-.1636	.124	-.06364	.00721	-.2085	-.8797	-.06698
+98	-.716	.176	-.3874	.0434	-.0755	.02897	.05726	-.0116	-.1546	.1171	-.06451	.004133	-.1622	-1.3978	-.10694
+167	-.738	.165	-.4072	.02621	-.04321	.02692	.06263	-.001788	-.1568	.1186	-.05959	.003209	-.1595	-2.1227	-.15289
+80	-.716	.177	-.3888	.08745	-.1279	.02859	.05578	-.06455	-.1672	.1273	-.06329	.008421	-.1524	-.5476	-.04169
+161	-.718	.173	-.3993	.05953	-.09938	.02804	.06121	-.02747	-.1607	.1212	-.06204	.006089	-.1305	-.7405	-.05562
+200	-.751	.157	-.4166	.02868	-.0484	.02565	.06177	-.01132	-.1574	.1227	-.05655	.004195	-.1163	-1.0512	-.07324
-430	-.716	.177	-.3701	.1243	-.178	.02822	.05268	-.09867	-.1779	.1268	-.0622	.01145	-.2854	-.7384	-.05552
-244	-.716	.177	-.3764	.05471	-.0916	.02912	.05479	-.02129	-.1566	.1188	-.06461	.004872	-.1867	-1.2529	-0.09675
-98	-.716	.177	-.3851	.04128	-.07249	.02907	.05679	-.000672	-.1539	.1157	-.06491	.003659	-.1661	-1.6715	-.12825
-43	-.716	.177	-.3792	.1159	-.1603	.02828	.05352	-.08606	-.1728	.1273	-.06257	.01036	-.1976	-.5559	-.04191
+98	-.716	.176	-.3888	.05739	-.08959	.02924	.05715	-.02561	-.1582	.1204	-.06393	.005441	-.1440	-.8766	-.06692
+167	-.738	.165	-.4075	.02959	-.05361	.02696	.06259	-.008412	-.1585	.1207	-.05932	.003887	-.1310	-1.3284	-.09565
+80	-.716	.177	-.3931	.1187	-.1656	.02796	.05507	-.1053	-.1789	.1316	-.06217	.01222	-.1459	-.3451	-.02609
+161	-.718	.173	-.4018	.07728	-.1044	.02787	.06092	-.04972	-.1692	.1282	-.06126	.008488	-.1207	-.4658	-.03479
+200	-.751	.157	-.4183	.0403	-.05656	.02851	.06166	-.0147	-.1627	.1272	-.05585	.005574	-.1040	-.6588	-.04583

TABLE A.1.3(b) (Cont) DATA FOR LINEAR EQUATIONS OF MOTION

D_V 1/sec	D_α $(\text{rad-sec})^{-1}$	$D_{\Delta T}$ $\left(\frac{\text{sl-ft}}{\text{sec}}\right)^{-1}$	Z_θ sec^{-1}	M_V $\frac{\text{rad}}{\text{ft-sec}}$	M_α sec^{-2}	$M_{\dot\alpha}$ sec^{-1}	M_q sec^{-1}	M_{δ_e} sec^{-2}	$M_{\Delta T}$ $\frac{\text{rad}}{\text{lb-sec}^2}$	Y_β sec^{-1}	Y_{δ_r} sec^{-1}	L_p sec^{-1}	L_r sec^{-1}
.0170	-.02812	-.00000524	-.01577	-.0001934	-2.3963	-.21946	-.62704	-2.9862	-.00000647	-.15946	.03942	-2.0553	.4612
.0159	-.03884	-.00000301	-.003591	-.0005251	-7.1625	-.39692	-1.10865	-9.1770	↓	-.27831	.06880	-3.6941	.4432
.0194	-.05524	-.00000230	-.001938	-.0002355	-12.6622	-.53700	-1.4678	-15.7319	↓	-.36393	.08997	-4.9502	.4868
.0108	-.02022	-.00000371	-.01010	-.0001715	-2.5552	-.16576	-.47952	-3.1842	↓	-.12038	.02976	-1.5938	.3428
.01096	-.03853	-.00000236	-.003082	-.0000210	-6.4901	-.28799	-.77107	-8.0400	↓	-.18891	.04644	-2.5878	.2899
.01489	-.03550	-.00000173	-.001460	-.001752	-13.8675	-.46779	-1.16316	-15.4883	↓	-.26523	.05930	-3.7048	.2385
.00901	-.01936	-.00000278	-.008774	-.0000864	-2.0998	-.10941	-.29905	-2.6490	↓	-.07420	.01834	-1.0199	.2294
.00734	-.02716	-.00000214	-.004240	-.0000328	-3.8249	-.15668	-.40833	-4.5898	↓	-.09684	.02333	-1.3633	.2033
.00871	-.02343	-.00000174	-.002146	-.004415	-6.8056	-.23404	-.54414	-7.3036	↓	-.12486	.02610	-1.7538	.1207
.02767	.06746	-.00000328	-.02441	-.0000978	-2.3608	-.20367	-.58192	-2.7714	-.00000601	-.09978	.02467	-.7427	.2494
.01041	.02259	-.00000188	-.005074	-.0005144	-6.6474	-.36839	-1.02894	-8.5170	↓	-.17414	.04305	-1.3183	.1916
.01280	-.04056	-.00000144	-.002564	-.0002292	-11.7518	-.49839	-1.36227	-14.6007	↓	-.22772	.05629	-1.7637	.1891
.01057	-.02312	-.00000232	-.01391	-.0001778	-2.4079	-.15383	-.44501	-2.9552	↓	-.07533	.01862	-.5745	.1756
.00818	-.02537	-.00000148	-.004373	-.0000216	-6.0234	-.26728	-.71563	-7.4618	↓	-.11821	.02906	-.9244	.1364
.00977	-.02875	-.00000108	-.001906	-.001301	-12.7032	-.43416	-1.07953	-14.3646	↓	-.16596	.03711	-1.3196	.0958
.00902	-.03622	-.00000174	-.01336	.0000582	-1.9488	-.10155	-.27757	-2.4585	↓	-.04643	.01148	-.3670	.1108
.00678	-.01947	-.00000134	-.006240	.0000258	-3.5498	-.14543	-.37900	-4.2598	↓	-.06059	.01460	-.4883	.0939
.00649	-.01989	-.00000109	-.003072	-.004808	-5.6330	-.21720	-.50499	-6.7784	↓	-.07813	.01633	-.6267	.0604

TABLE A.1.3(b) (Cont) DATA FOR LINEAR EQUATIONS OF MOTION

L_p sec^{-2}	L_{δ_a} sec^{-2}	L_{δ_r} sec^{-2}	N_p sec^{-1}	N_r sec^{-1}	N_β sec^{-2}	N_{δ_a} sec^{-2}	N_{δ_r} sec^{-2}
-7.1009	2.8808	1.5590	-.08069	-.2479	1.7608	.1105	-.9836
-13.0894	8.9962	4.7686	-.02068	-.3991	4.9861	.1620	-2.8189
-24.4482	15.9700	8.1831	.00282	-.5140	8.3101	.2230	-4.8384
-6.9614	3.1110	1.6554	-.05448	-.1839	1.8852	.1096	-.9675
-10.7123	8.1243	4.1104	-.02046	-.2727	4.3869	.1548	-2.4167
-11.3986	16.5216	7.1014	-.00430	-.3767	8.2606	.2235	-4.1505
-6.0520	2.6394	1.3528	-.04471	-.1158	1.5904	.1052	-.7907
-7.9539	4.8989	2.2442	-.02476	-.1449	2.5612	.1287	-1.3121
-5.8838	7.5091	3.1182	-.01258	-.1750	3.9384	.1346	-1.8151
-3.4210	1.0125	.5424	-.09659	-.1741	1.1887	.1073	-.5831
15.3442	3.1966	1.6989	-.03637	-.2675	3.3808	.1386	-1.8387
-7.2502	5.6800	2.9075	-.01502	-.3438	5.6444	.1785	-3.1666
-3.2852	1.0968	.5796	-.06360	-.1277	1.2725	.1036	-.6255
-4.5242	2.8860	1.4766	-.02970	-.1835	2.9656	.1340	-1.5747
-5.0333	5.8764	2.5312	-.01329	-.2504	5.5275	.1780	-2.7166
-2.7889	.9274	.4709	-.04795	-.08147	1.0810	.1004	-.5107
-2.9738	1.7353	.7939	-.02947	-.1003	1.7812	.1179	-.8512
-2.4472	2.6678	1.2335	-.01074	-.1189	2.6845	.1176	-1.1787

A.2 EQUATIONS AND DATA USED FOR ANALOG COMPUTER MODEL FOLLOWING STUDIES

A.2.1 JetStar Equations and Data

Equations

$$\dot{V} = -\frac{(\rho V^2) S C_D}{2m} - g \sin \gamma + \frac{T}{m} \cos \alpha$$

$$\dot{\alpha}_I = -\frac{S}{2m} (\rho V) C_L + \frac{g}{V} \cos \theta \cos \phi + q - \frac{\alpha_I \dot{V}}{V}$$

$$\dot{\beta}_I = \frac{S}{2m} (\rho V) C_Y + \frac{g}{V} \cos \theta \sin \phi - r + \alpha_I p$$

$$\dot{p} = \frac{1}{I_{xx}} \left[I_{xz} \dot{r} + \frac{1}{2} b S (\rho V^2)(C_{\ell_s}) + \frac{1}{4} b^2 S (\rho V) C_{\ell_D} \right]$$

$$\dot{q} = \frac{1}{I_{yy}} \left[T z_T + \frac{1}{2} S \bar{c} (\rho V^2)(C_{m_s}) + \frac{1}{4} S \bar{c}^2 (\rho V) C_{m_D} + \frac{1}{2} S \bar{c} \left(\frac{\bar{x}}{\bar{c}} \right) (\rho V^2) C_L \right]$$

$$\dot{r} = \frac{1}{I_{zz}} \left[I_{xz} \dot{p} + \frac{1}{2} b S (\rho V^2)(C_{n_s}) + \frac{1}{4} b^2 S (\rho V)(C_{n_D}) \right]$$

$$\dot{\psi} = \frac{q \sin \phi + r \cos \phi}{\cos \theta}$$

$$\dot{\theta} = q \cos \phi - r \sin \phi$$

$$\dot{\phi} = p + \dot{\psi} \sin \theta$$

$$\sin \gamma = \sin \theta - \beta_I \cos \theta \sin \phi - \alpha_I \cos \theta \cos \phi$$

$$\dot{h} = V \sin \gamma$$

$$\rho = \rho_0 + \rho_h h + \rho_{h^2} h^2$$

$$\alpha = \alpha_I + \alpha_G$$

$$\beta = \beta_I + \beta_G$$

$$C_D = A_{C_D} + B_{C_D}\,\alpha + C_{C_D}\,\alpha^2$$

$$C_L = C_{L_0} + C_{L_\alpha}\,\alpha + C_{L_{\delta_e}}\,\delta_e + C_{L_{\delta_k}}\,\delta_k$$

$$C_Y = C_{Y_\beta}\,\beta + C_{Y_{\delta_r}}\,\delta_r$$

$$C_{\ell_S} = \left(C_{\ell_{\beta_{\alpha=0}}} + C_{\ell_{\beta_\alpha}}\,\alpha\right)\beta + \left(C_{\ell_{\delta_{r\,\alpha=0}}} + C_{\ell_{\delta_{r_\alpha}}}\,\alpha\right)\delta_r + C_{\ell_{\delta_a}}\,\delta_a$$

$$C_{\ell_D} = \left(C_{\ell_{r_{\alpha=0}}} + C_{\ell_{r_\alpha}}\,\alpha\right) r + C_{\ell_p}\,p$$

$$C_{m_S} = C_{m_0} + C_{m_\alpha}\,\alpha + C_{m_{\delta_e}}\,\delta_e + C_{m_{\delta_k}}\,\delta_k$$

$$C_{m_D} = C_{m_q}\,q + C_{m_{\dot\alpha}}\,\dot\alpha$$

$$C_{n_S} = \left(C_{n_{\beta_{\alpha=0}}} + C_{n_{\beta_\alpha}}\,\alpha\right)\beta + C_{n_{\delta_r}}\,\delta_r + C_{n_{\delta_a}}\,\delta_a$$

$$C_{n_D} = \left(C_{n_{r_{\alpha=0}}} + C_{n_{r_\alpha}}\,\alpha\right) r + \left(C_{n_{p_{\alpha=0}}} + C_{n_{p_\alpha}}\,\alpha\right) p$$

$$n_x = -\frac{\bar q\, S C_D}{gm} + \frac{T}{gm} + \frac{q\, S C_L\,\alpha}{gm}$$

$$n_{Y_p} = \frac{\bar q\, S C_Y}{gm} + \frac{\ell}{g}\,\dot r$$

$$n_{z_p} = -\frac{\bar q\, S C_L}{gm} - \frac{\ell}{g}\,\dot q$$

JetStar Longitudinal Stability Derivatives and Data

(M = 0.55 values) (all data for c.g. at 25% m.a.c.)

C_{m_o}	=	0.0093			
C_{m_α}	=	-.01169	deg^{-1}		
$C_{m_{\dot{\alpha}}}$	=	-.05411	deg^{-1}		
C_{m_q}	=	-.1449	deg^{-1}		
$C_{m_{\delta_e}}$	=	-.01449	deg^{-1}		
$C_{m_{\delta_t}}$	=	-.03438	deg^{-1}		
C_{L_o}	=	-.083			
$C_{L_{\delta_e}}$	=	.007069	deg^{-1}		
$C_{L_{\delta_t}}$	=	.0167	deg^{-1}		
C_{L_α}	=	.09233	deg^{-1}		
A_{C_D}	=	.022486			
B_{C_D}	=	-.003667	deg		
C_{C_D}	=	.0008667	deg^{-2}		
$-z_T$	=	0.816 ft			
ℓ	=	22.85 ft			
$\bar{\nu}$	=	0			

W	=	38,204 lb
m	=	1187.57 slugs
S	=	542.5 ft^2
$\bar{c}$	=	10.93 ft
I_{YY}	=	135.869 sl-ft^2
ρ_o	=	.002332
ρ_t	=	$-.6053 \times 10^{-7}$
ρ_{t^2}	=	$.4183 \times 10^{-12}$

JetStar Lateral-Directional Stability Derivatives and Data

(M = .55 values)

C_{y_β}	=	-.01250 deg^{-1}	b	=	53.75 ft
$C_{y_{\delta_r}}$	=	.003072 deg^{-1}	I_{xx}	=	118,773 sl-ft^2
$C_{y_{\beta_{\alpha=0}}}$	=	-.00080	I_{zz}	=	243,504 sl-ft^2
$C_{y_{\beta_\alpha}}$	=	-.000173 deg^{-2}	I_{xz}	=	5061 sl-ft^2
$C_{y_{\delta_{r_{\alpha=0}}}}$	=	.0005105 deg^{-1}			
$C_{y_{\delta_{r_\alpha}}}$	=	-.000001798 deg^{-2}			
$C_{l_{\delta_\beta}}$	=	.0009975 deg^{-1}			
$C_{l_{r_{\alpha=0}}}$	=	.000244 deg^{-1}			
$C_{l_{r_\alpha}}$	=	.000172 deg^{-2}			
$C_{l_{p_{\alpha=0}}}$	=	-.006786 deg^{-1}			
$C_{l_{p_\alpha}}$	=	0			
$C_{n_{\beta_{\alpha=0}}}$	=	.00185 deg^{-1}			
$C_{n_{\beta_\alpha}}$	=	.0000487 deg^{-2}			
$C_{n_{\delta_{a_{\alpha=0}}}}$	=	.00009496 deg^{-1}			
$C_{n_{\delta_{a_\alpha}}}$	=	0			
$C_{n_{r_{\alpha=0}}}$	=	-.0026 deg^{-1}			
$C_{n_{r_\alpha}}$	=	-.0000384 deg^{-2}			
$C_{n_{p_{\alpha=0}}}$	=	.000384 deg^{-1}			
$C_{n_{p_\alpha}}$	=	-.000186 deg^{-2}			
$C_{n_{\delta_r}}$	=	-.001116 deg^{-1}			

A.2.2 Model (SST) Equations and Data

Equations

$$\dot{V} = -\frac{\rho V^2 S C_D}{2m} - g \sin\gamma + \frac{T}{m}$$

$$\dot{\alpha}_I = -\frac{\rho V S C_L}{2m} + \frac{g}{V}\cos\theta\cos\phi + q - \frac{\alpha_I \dot{V}}{V}$$

$$\dot{\beta}_I = \frac{\rho V S C_Y}{2m} + \frac{g}{V}\cos\theta\sin\phi - r + \alpha_I p$$

$$\dot{p} = \frac{1}{I_{xx}}\left[I_{xz}\dot{r} + \frac{1}{2}bS(\rho V^2)(C_{l_s}) + \frac{1}{4}b^2 S(\rho V)(C_{l_D})\right]$$

$$\dot{q} = \frac{1}{I_{yy}}\left[\frac{1}{2}S\bar{c}\rho V^2 C_{m_s} + \frac{1}{4}S\bar{c}^2\rho V C_{m_D} + \frac{1}{2}S\bar{c}\,\frac{\bar{v}}{\bar{c}}\rho V^2 C_L\right]$$

$$\dot{r} = \frac{1}{I_{zz}}\left[I_{xz}\dot{p} + \frac{1}{2}bS\rho V^2 C_{n_s} + \frac{1}{4}b^2 S\rho V C_{n_D}\right]$$

$$\dot{\psi} = \frac{q\sin\phi + r\cos\phi}{\cos\theta}$$

$$\dot{\theta} = q\cos\phi - r\sin\phi$$

$$\dot{\phi} = p + \dot{\psi}\sin\theta$$

$$\sin\gamma = \sin\theta - \beta_I\cos\theta\sin\phi - \alpha_I\cos\theta\cos\phi$$

$$\dot{h} = V\sin\gamma$$

$$\rho = \rho_0 + \rho_h h + \rho_{h^2} h^2$$

$$\alpha = \alpha_I + \alpha_G$$

$$\beta = \beta_I + \beta_G$$

$$C_D = C_{D_o} + K_D \alpha^2$$

$$C_L = C_{L_o} + C_{L_\alpha} \alpha + C_{L_{\delta_e}} \delta_e + C_{L_{i_c}} i_c$$

$$C_Y = C_{Y_\beta} \beta + C_{Y_{\delta_r}} \delta_r$$

$$C_{l_S} = (C_{l_{\beta_{\alpha=0}}} + C_{l_{\beta_\alpha}} \alpha)\beta + (C_{l_{\delta_{r_\alpha}}} \alpha)\delta_r + C_{l_{\delta_a}} \delta_a$$

$$C_{l_D} = (C_{l_{r_{\alpha=0}}} + C_{l_{r_\alpha}} \alpha) r + (C_{l_{p_{\alpha=0}}} + C_{l_{p_\alpha}} \alpha) p$$

$$C_{m_S} = C_{m_o} + C_{m_\alpha} \alpha + C_{m_{\delta_e}} \delta_e + C_{m_{i_c}} i_c$$

$$C_{m_D} = C_{m_q} q + C_{m_{\dot\alpha}} \dot\alpha_I$$

$$C_{n_S} = (C_{n_{\beta_{\alpha=0}}} + C_{n_{\beta_\alpha}} \alpha)\beta + C_{n_{\delta_r}} \delta_r + (C_{n_{\delta_{a_{\alpha=0}}}} + C_{n_{\delta_{a_\alpha}}} \alpha)\delta_a$$

$$C_{n_D} = (C_{n_{r_{\alpha=0}}} + C_{n_{r_\alpha}} \alpha) r + (C_{n_{p_{\alpha=0}}} + C_{n_{p_\alpha}} \alpha) p$$

$$n_x = -\frac{\bar q S C_D}{mg} + \frac{T}{mg} + \frac{\bar q S C_L \alpha}{mg}$$

$$n_{Y_p} = \frac{\bar q S C_Y}{mg} + \frac{\ell}{g} \dot r$$

$$n_{Z_p} = -\frac{\bar q S C_L}{mg} - \frac{\ell}{g} \dot q$$

$$\bar q = \frac{1}{2} \rho V^2$$

Model (SST) Longitudinal Stability Derivatives and Data

(M = 0.55 values)

C_{m_o}	=	-.0008	W	=	240,000 lb
C_{m_α}	=	-.002792 deg^{-1}	m	=	7460.4 sl
$C_{m_{\dot{\alpha}}}$	=	-.01396 deg^{-1}	S	=	7000 ft^2
C_{m_q}	=	-.0209 deg^{-1}	$\bar{c}$	=	76 ft
$C_{m_{\delta_e}}$	=	-.00394 deg^{-1}	I_{YY}	=	9.6×10^6 sl-ft^2
$C_{m_{i_c}}$	=	.00410 deg^{-1}	ℓ	=	105 ft
C_{L_o}	=	.005	$\bar{x}$	=	0
$C_{L_{\delta_e}}$	=	.00786 deg^{-1}	ρ_o	=	.002332
$C_{L_{i_c}}$	=	.00339 deg^{-1}	ρ_k	=	$-.6053 \times 10^{-7}$
C_{L_α}	=	.0497 deg^{-1}	ρ_{k^2}	=	$.4183 \times 10^{-12}$
C_{D_o}	=	.0132			
K_D	=	.000439 deg^{-2}			

Model (SST) Lateral-Directional Stability Derivatives

(M = .55 values)

$C_{y_\beta} = -.00393 \text{ deg}^{-1}$

$C_{y_{\delta_r}} = .00201 \text{ deg}^{-1}$

$C_{l_{\beta_{\alpha=0}}} = -.000262 \text{ deg}^{-1}$

$C_{l_{\beta_\alpha}} = -.000236 \text{ deg}^{-2}$

$C_{l_{\delta_{r_{\alpha=0}}}} = 0$

$C_{l_{\delta_{r_\alpha}}} = .0000164 \text{ deg}^{-2}$

$C_{l_{\delta_a}} = .000943 \text{ deg}^{-1}$

$C_{l_{r_{\alpha=0}}} = -.000105 \text{ deg}^{-1}$

$C_{l_{r_\alpha}} = .0000734 \text{ deg}^{-2}$

$C_{l_{p_{\alpha=0}}} = -.003054 \text{ deg}^{-1}$

$C_{l_{p_\alpha}} = 0$

$C_{n_{\beta_{\alpha=0}}} = .001204 \text{ deg}^{-1}$

$C_{n_{\beta_\alpha}} = .0000785 \text{ deg}^{-2}$

$C_{n_{\delta_{a_{\alpha=0}}}} = .0001047 \text{ deg}^{-1}$

$C_{n_{\delta_{a_\alpha}}} = .00001152 \text{ deg}^{-2}$

$C_{n_{r_{\alpha=0}}} = -.001536$

$C_{n_{r_\alpha}} = -.0000244 \text{ deg}^{-2}$

$C_{n_{p_{\alpha=0}}} = .0000698 \text{ deg}^{-1}$

$C_{n_{p_\alpha}} = .00000175 \text{ deg}^{-2}$

$C_{n_{\delta_r}} = -.000942 \text{ deg}^{-1}$

$b = 125 \text{ ft}$

$I_{xx} = 0.94 \times 10^6 \text{ sl-ft}^2$

$I_{zz} = 10.35 \times 10^6 \text{ sl-ft}^2$

$I_{xz} = 41 \times 10^3 \text{ sl-ft}^2$

APPENDIX B
JETSTAR TRANSFER FUNCTIONS

B. 1 LONGITUDINAL

The literal forms of the transfer functions $\Delta\alpha/\Delta\delta_e\ (s)$, $\Delta\theta/\Delta\delta_e\ (s)$, $\Delta V/\Delta\delta_e\ (s)$, and $\Delta n_z/\Delta\delta_e\ (s)$ are derived from the linearized longitudinal equations of motion presented in Appendix A.

The characteristic equation is of the form:

$$D_1(s) = As^4 + Bs^3 + Cs^2 + Ds + E \tag{B.1-1}$$

where

$$\left.\begin{aligned}
A &= \bar{1} \\
B &= -\bar{1} M_q - Z_\alpha - \bar{1} M_{\dot\alpha} + \bar{1} D_V - D_\alpha \alpha_t \\
C &= Z_\alpha M_q - \bar{1} M_\alpha - Z_\theta M_{\dot\alpha} - \bar{1} D_V M_q - D_V Z_\alpha - \bar{1} D_V M_{\dot\alpha} \\
&\quad + D_\alpha (\alpha_t M_q + Z_V) - g \frac{\alpha_t}{V_t} M_{\dot\alpha} \\
D &= -Z_\theta M_\alpha - D_V Z_\alpha M_q - \bar{1} D_V M_\alpha - D_V Z_\theta M_{\dot\alpha} \\
&\quad - V_t D_\alpha \left(M_q \frac{Z_V}{V_t} - \bar{1} M_V \right) + g \left(-\frac{\alpha_t}{V_t} M_\alpha + M_{\dot\alpha} \frac{Z_V}{V_t} + \bar{1} M_V \right) \\
E &= -D_V Z_\theta M_\alpha + V_t D_\alpha Z_\theta M_V + g \left(\frac{Z_V}{V_t} M_\alpha - M_V Z_\alpha \right)
\end{aligned}\right\} \tag{B.1-2}$$

The coefficient $\bar{1}$, which equals $\cos \alpha_t$, is included for generality. When small angle approximations are made, $\bar{1} = 1.0$.

Angle-of-attack-elevator transfer function

General form:

$$\frac{\Delta\alpha}{\Delta\delta_e}(s) = \frac{As^3 + Bs^2 + Cs + E}{D_1(s)} \tag{B.1-3}$$

where

$$A = Z_{\delta_e}$$

$$B = \bar{I} M_{\delta_e} + D_V Z_{\delta_e} - Z_{\delta_e} M_q$$

$$C = Z_\theta M_{\delta_e} + g M_{\delta_e} \frac{\alpha_t}{V_t} + \bar{I} D_V M_{\delta_e} - D_V Z_{\delta_e} M_q$$

$$E = D_V Z_\theta M_{\delta_e} + g \left(Z_{\delta_e} M_V - M_{\delta_e} \frac{Z_V}{V_t} \right)$$

(B.1-4)

Pitch angle - elevator transfer function

General form:

$$\frac{\Delta\theta}{\Delta\delta_e}(s) = \frac{As^2 + Bs + C}{D_1(s)} \qquad \text{(B.1-5)}$$

where

$$A = M_{\dot{\alpha}} Z_{\delta_e} + \bar{I} M_{\delta_e}$$

$$B = Z_{\delta_e} \left(D_V M_{\dot{\alpha}} + M_\alpha \right) + M_{\delta_e} \left(- Z_\alpha + \bar{I} D_V - \alpha_t D_\alpha \right)$$

$$C = M_{\delta_e} \left(- D_V Z_\alpha + D_\alpha Z_V \right) - Z_{\delta_e} \left(- M_\alpha D_V + M_V V_t D_\alpha \right)$$

(B.1-6)

Velocity - elevator transfer function

General form:

$$\frac{\Delta V}{\Delta\delta_e}(s) = \frac{As^2 + Bs + C}{D_1(s)} \qquad \text{(B.1-7)}$$

where

$$A = - V_t D_\alpha Z_{\delta_e}$$

$$B = - Z_{\delta_e} \left(g M_{\dot{\alpha}} - V_t D_\alpha M_q \right) - M_{\delta_e} \left(\bar{I} V_t D_\alpha + \bar{I} g \right)$$

$$C = g \left(M_{\delta_e} Z_\alpha - Z_{\delta_e} M_\alpha \right) - V_t D_\alpha M_{\delta_e} Z_\theta$$

(B.1-8)

Normal acceleration - elevator transfer function

General form:

$$\frac{\Delta n_z}{\Delta \delta_e}(s) = \frac{V_t}{g}\,\frac{As^4 + Bs^3 + Cs^2 + Ds + E}{D_1(s)} \tag{B.1-9}$$

where

$$\left.\begin{aligned}
A &= -\bar{1}\, Z_{\delta_e} \\
B &= Z_{\delta_e}\left(\bar{1}\, M_{\dot\alpha} + \alpha_t\, D_\alpha - \bar{1}\, D_V + \bar{1}\, M_q\right) \\
C &= \bar{1}\, Z_{\delta_e} M_\alpha - \bar{1}\, Z_\alpha M_{\delta_e} + \bar{1}\, D_V Z_{\delta_e}\left(M_q + M_{\dot\alpha}\right) \\
&\quad + \alpha_t Z_{\delta_e}\left(\frac{g}{V_t} M_{\dot\alpha} - D_\alpha M_q\right) + Z_\theta M_{\dot\alpha} Z_{\delta_e} \\
D &= \bar{1}\, g\left(M_{\delta_e}\frac{Z_V}{V_t} - Z_{\delta_e} M_V\right) + \bar{1}\, M_{\delta_e}\left(D_\alpha Z_V - D_V Z_\alpha\right) \\
&\quad + \bar{1}\, Z_{\delta_e}\left(-M_V V_t D_\alpha + M_\alpha D_V\right) + g\frac{\alpha_t}{V_t}\left(Z_{\delta_e} M_\alpha - M_{\delta_e} Z_\alpha\right) \\
&\quad + Z_\theta Z_{\delta_e}\left(D_V M_{\dot\alpha} + M_\alpha\right) - Z_\alpha Z_\theta M_{\delta_e} \\
E &= Z_\theta\left[M_{\delta_e}\left(Z_V D_\alpha - Z_\alpha D_V\right) + Z_{\delta_e}\left(D_V M_\alpha - V_t D_\alpha M_V\right)\right]
\end{aligned}\right\} \tag{B.1-10}$$

B.2 LATERAL-DIRECTIONAL

Lateral-directional transfer functions are derived from the linearized lateral-directional equations of motion presented in Appendix A.

The characteristic equation is of the form:

$$D_1(s) = As^4 + Bs^3 + Cs^2 + Ds + E \tag{B.2-1}$$

where

$$A = 1 - \left(\frac{I_{xz}}{I_{zz}}\right)\left(\frac{I_{xz}}{I_{xx}}\right)$$

$$B = -Y_\beta \left[1 - \left(\frac{I_{xz}}{I_{zz}}\right)\left(\frac{I_{xz}}{I_{xx}}\right)\right] - N_r - L_p - \frac{I_{xz}}{I_{zz}} L_r - \frac{I_{xz}}{I_{xx}} N_p$$

$$C = N_\beta \left(1 - \alpha_t \frac{I_{xz}}{I_{xx}}\right) + L_\beta \left(\frac{I_{xz}}{I_{zz}} - \alpha_t\right) + Y_\beta (N_r + L_p) \qquad \text{(B. 2-2)}$$

$$+ L_p N_r - L_r N_p + Y_\beta L_r \left(\frac{I_{xz}}{I_{zz}}\right) + Y_\beta N_p \left(\frac{I_{xz}}{I_{xx}}\right)$$

$$D = \alpha_t (L_\beta N_r - L_r N_\beta) - L_p N_\beta + L_\beta N_p + Y_\beta (L_r N_p - L_p N_r)$$
$$- \frac{g}{V_t}\left[N_\beta \left(\frac{I_{xz}}{I_{xx}} + \alpha_t\right) + L_\beta \left(1 + \alpha_t \frac{I_{xz}}{I_{zz}}\right)\right]$$

$$E = -\frac{g}{V_t}\left[-N_\beta (\alpha_t L_p - L_r) + L_\beta (\alpha_t N_p - N_r)\right]$$

Roll angle - rudder transfer function

General form:

$$\frac{\Phi}{\delta_r}(s) = \frac{As^2 + Bs + C}{D_1(s)} \qquad \text{(B. 2-3)}$$

where

$$A = L_{\delta_r}\left(1 + \alpha_t \frac{I_{xz}}{I_{zz}}\right) + N_{\delta_r}\left(\frac{I_{xz}}{I_{xx}} \alpha_t\right)$$

$$B = Y_{\delta_r}\left[N_\beta \left(\frac{I_{xz}}{I_{xx}} + \alpha_t\right) + L_\beta \left(1 + \alpha_t \frac{I_{xz}}{I_{zz}}\right)\right]$$
$$- L_{\delta_r}\left[Y_\beta \left(1 + \alpha_t \frac{I_{xz}}{I_{zz}}\right) - (\alpha_t N_p - N_r)\right]$$
$$- N_{\delta_r}\left[Y_\beta \left(\frac{I_{xz}}{I_{xx}} + \alpha_t\right) + (\alpha_t L_p - L_r)\right] \qquad \text{(B. 2-4)}$$

$$C = Y_{\delta_r}\left[-N_\beta\left(\alpha_t L_p - L_r\right) + L_\beta\left(\alpha_t N_p - N_r\right)\right]$$
$$- L_{\delta_r}\left[-N_\beta\left(1+\alpha_t^2\right) + Y_\beta\left(\alpha_t N_p - N_r\right)\right]$$
$$+ N_{\delta_r}\left[Y_\beta\left(\alpha_t L_p - L_r\right) - L_\beta\left(1+\alpha_t^2\right)\right]$$

Yaw rate - rudder transfer function

General form:

$$\frac{r}{\delta_r}(s) = \frac{As^3 + Bs^2 + Cs + D}{D_1(s)} \qquad \text{(B. 2-5)}$$

where

$$A = L_{\delta_r}\frac{I_{xz}}{I_{zz}} + N_{\delta_r}$$

$$B = -Y_{\delta_r}\left(-N_\beta - L_\beta\frac{I_{xz}}{I_{zz}}\right) + L_{\delta_r}\left(N_p - Y_\beta\frac{I_{xz}}{I_{zz}}\right)$$
$$- N_{\delta_r}\left(L_p + Y_\beta\right)$$

$$C = -Y_{\delta_r}\left(N_\beta L_p - L_\beta N_p\right) + L_{\delta_r}\left(N_\beta \alpha_t - Y_\beta N_p\right) \qquad \text{(B. 2-6)}$$
$$- N_{\delta_r}\left(L_\beta \alpha_t - Y_\beta L_p\right)$$

$$D = \left(L_{\delta_r} N_\beta - N_{\delta_r} L_\beta\right)\frac{g}{V_t}$$

Sideslip - rudder transfer function

General form:

$$\frac{\beta}{\delta_r}(s) = \frac{As^3 + Bs^2 + Cs + D}{D_1(s)} \qquad \text{(B. 2-7)}$$

where:

$$A = Y_{\delta_r}\left(1 - \frac{I_{xz}}{I_{zz}}\frac{I_{xz}}{I_{xx}}\right)$$

$$B = Y_{\delta_r}\left(-N_r - L_p - \frac{I_{xz}}{I_{zz}} L_r - N_p \frac{I_{xz}}{I_{xx}}\right) - L_{\delta_r}\left(-\alpha_t + \frac{I_{xz}}{I_{zz}}\right) + N_{\delta_r}\left(\alpha_t \frac{I_{xz}}{I_{xx}} - 1\right)$$

$$C = Y_{\delta_r}\left(L_p N_r - N_p L_r\right) - L_{\delta_r}\left[\alpha_t N_r - \frac{g}{V_t}\left(1 + \alpha_t \frac{I_{xz}}{I_{zz}}\right) + N_p\right] + N_{\delta_r}\left[\alpha_t L_r + \frac{g}{V_t}\left(\frac{I_{xz}}{I_{xx}} + \alpha_t\right) + L_p\right] \qquad \text{(B. 2-8)}$$

$$D = \frac{g}{V_t}\left[L_{\delta_r}\left(\alpha_t N_p - N_r\right) - N_{\delta_r}\left(\alpha_t L_p - L_r\right)\right]$$

Roll angle - aileron transfer function

General form:

$$\frac{\phi}{\delta_a}(s) = \frac{A s^2 + B s + C}{D_1(s)} \qquad \text{(B. 2-9)}$$

where

$$A = L_{\delta_a}\left(1 + \alpha_t \frac{I_{xz}}{I_{zz}}\right) + N_{\delta_a}\left(\frac{I_{xz}}{I_{xx}} + \alpha_t\right)$$

$$B = -L_{\delta_a}\left[Y_\beta\left(1 + \alpha_t \frac{I_{xz}}{I_{zz}}\right) - \left(\alpha_t N_p - N_r\right)\right] - N_{\delta_a}\left[Y_\beta\left(\frac{I_{xz}}{I_{xx}} + \alpha_t\right) + \left(\alpha_t L_p - L_r\right)\right] \qquad \text{(B. 2-10)}$$

$$C = -L_{\delta_a}\left[-N_\beta\left(1 + \alpha_t^2\right) + Y_\beta\left(\alpha_t N_p - N_r\right)\right] + N_{\delta_a}\left[Y_\beta\left(\alpha_t L_p - L_r\right) - L_\beta\left(1 + \alpha_t^2\right)\right]$$

Yaw rate - aileron transfer function

General form:

$$\frac{r}{\delta_a}(s) = \frac{As^3 + Bs^2 + Cs + D}{D_1(s)} \qquad \text{(B. 2-11)}$$

$$A = L_{\delta_a}\frac{I_{xz}}{I_{zz}} + N_{\delta_a}$$

$$B = L_{\delta_a}\left(N_p - Y_\beta\frac{I_{xz}}{I_{zz}}\right) - N_{\delta_a}\left(L_p + Y_\beta\right)$$

$$C = L_{\delta_a}\left(N_\beta\alpha_t - Y_\beta N_p\right) - N_{\delta_a}\left(L_\beta\alpha_t - Y_\beta L_p\right)$$

$$D = \frac{g}{V_t}\left(L_{\delta_a}N_\beta - N_{\delta_a}L_\beta\right)$$

Sideslip - aileron transfer function

General form:

(B. 2-13)

where $$\frac{\beta}{\delta_a}(s) = \frac{As^2 + Bs + C}{D_1(s)}$$

$$A = -L_{\delta_a}\left(-\alpha_t + \frac{I_{xz}}{I_{zz}}\right) + N_{\delta_a}\left(\alpha_t\frac{I_{xz}}{I_{xx}} - 1\right)$$

(B. 2-14)

$$B = -L_{\delta_a}\left[\alpha_t N_r + N_p - \frac{g}{V_t}\left(1 + \alpha_t\frac{I_{xz}}{I_{zz}}\right)\right] + N_{\delta_a}\left[\alpha_t L_r + L_p + \frac{g}{V_t}\left(\frac{I_{xz}}{I_{xx}} + \alpha_t\right)\right]$$

$$C = \frac{g}{V_t}\left[L_{\delta_a}\left(\alpha_t N_p - N_r\right) - N_{\delta_a}\left(\alpha_t L_p - L_r\right)\right]$$

C. G. Lateral acceleration - rudder transfer function

General form:

$$\frac{g}{V_t}\,\frac{n_Y}{\delta_r}(s) = \frac{As^4 + Bs^3 + Cs^2 + Ds + E}{D_1(s)} \qquad \text{(B. 2-15)}$$

where

$$A = Y_{\delta_r}\left(1 - \frac{I_{xz}}{I_{xx}}\,\frac{I_{xz}}{I_{zz}}\right)$$

$$B = Y_{\delta_r}\left(-N_r - L_p - \frac{I_{xz}}{I_{zz}}L_r - \frac{I_{xz}}{I_{xx}}L_p\right)$$

$$C = Y_\beta\left[L_{\delta_r}\left(\alpha_t - \frac{I_{xz}}{I_{zz}}\right) + N_{\delta_r}\left(\alpha_t\,\frac{I_{xz}}{I_{xx}} - 1\right)\right] \qquad \text{(B. 2-16)}$$

$$+ Y_{\delta_r}\left[N_\beta\left(1 - \alpha_t\,\frac{I_{xz}}{I_{xx}}\right) + L_\beta\left(\frac{I_{xz}}{I_{zz}} - \alpha_t\right) + L_p N_r - L_r N_p\right]$$

$$D = Y_\beta\left\{-L_{\delta_r}\left[N_p + \alpha_t N_r - \frac{g}{V_t}\left(1 + \alpha_t\,\frac{I_{xz}}{I_{zz}}\right)\right]\right.$$

$$\left. + N_{\delta_r}\left[\alpha_t L_r + \frac{g}{V_t}\left(\frac{I_{xz}}{I_{xx}} + \alpha_t\right) + L_p\right]\right\}$$

$$+ Y_{\delta_r}\left\{\alpha_t\left[L_\beta N_r - L_r N_\beta\right] - L_p N_\beta + N_p L_\beta\right.$$

$$\left. - \frac{g}{V_t}\left[N_\beta\left(\frac{I_{xz}}{I_{xx}} + \alpha_t\right) + L_\beta\left(1 + \alpha_t\,\frac{I_{xz}}{I_{zz}}\right)\right]\right\}$$

$$E = Y_\beta\,\frac{g}{V_t}\left[L_{\delta_r}\left(\alpha_t N_p - N_r\right) - N_{\delta_r}\left(\alpha_t N_p - L_r\right)\right]$$

$$- Y_{\delta_r}\,\frac{g}{V_t}\left[-N_\beta\left(\alpha_t L_p - L_r\right) + L_\beta\left(\alpha_t N_p - N_r\right)\right]$$

Cockpit lateral acceleration - rudder transfer function

General form:

$$\frac{g}{V_t}\,\frac{n_{y_p}}{\delta_r}(s) = \frac{A's^4 + B's^3 + C's^2 + D's + E'}{D_1(s)} \qquad \text{(B. 2-17)}$$

where

$$\begin{aligned}
A' &= A + \frac{\ell_p}{V}\left(N_{\delta_r} + L_{\delta_r}\frac{I_{xz}}{I_{zz}}\right)\\
B' &= B + \frac{\ell_p}{V}\left[Y_{\delta_r}\left(N_\beta + L_\beta\frac{I_{xz}}{I_{zz}}\right) + L_{\delta_r}\left(N_p - Y_\beta\frac{I_{xz}}{I_{zz}}\right)\right.\\
&\quad \left. - N_{\delta_r}\left(L_p - Y_\beta\right)\right] \qquad \text{(B. 2-18)}\\
C' &= C + \frac{\ell_p}{V}\left[Y_{\delta_r}\left(L_\beta N_p - L_p N_\beta\right) + L_{\delta_r}\left(N_\beta \alpha_t - Y_\beta N_p\right)\right.\\
&\quad \left. - N_{\delta_r}\left(L_\beta \alpha_t - Y_\beta L_p\right)\right]\\
D' &= D + \frac{\ell_p}{V}\left[\frac{g}{V}\left(L_{\delta_r} N_\beta - L_\beta N_{\delta_r}\right)\right]\\
E' &= E
\end{aligned}$$

and A, B, C, D, E are the coefficients of the c. g. lateral acceleration transfer function given previously as equations B. 2-16.

B.3 OPEN-LOOP JETSTAR TRANSFER FUNCTIONS

Table	
B. 1	Longitudinal Characteristic Equation
B. 2	$\Delta V/\Delta\delta_e\ (s)$ Transfer Function Numerator
B. 3	$\Delta\alpha/\Delta\delta_e\ (s)$ Transfer Function Numerator
B. 4	$\Delta\theta/\Delta\delta_e\ (s)$ Transfer Function Numerator
B. 5	$\Delta n_z/\Delta\delta_e\ (s)$ Transfer Function Numerator
B. 6	$\Delta V/\Delta T\ (s)$ Transfer Function Numerator
B. 7	$\Delta\alpha/\Delta T\ (s)$ Transfer Function Numerator
B. 8	$\Delta\theta/\Delta T\ (s)$ Transfer Function Numerator
B. 9	$\Delta n_z/\Delta T\ (s)$ Transfer Function Numerator
B. 10	Lateral-Directional Characteristic Equation
B. 11	$\phi/\delta_r\ (s)$ Transfer Function Numerator
B. 12	$r/\delta_r\ (s)$ Transfer Function Numerator
B. 13	$\beta/\delta_r\ (s)$ Transfer Function Numerator
B. 14	$\phi/\delta_a\ (s)$ Transfer Function Numerator
B. 15	$r/\delta_a\ (s)$ Transfer Function Numerator
B. 16	$\beta/\delta_a\ (s)$ Transfer Function Numerator
B. 17	$\Delta n_{z_p}/\Delta\delta_e\ (s)$ Pilot Transfer Function Numerator
B. 18	$\Delta n_{z_p}/\Delta T\ (s)$ Pilot Transfer Function Numerator
B. 19	$\Delta n_{x_p}/\Delta\delta_e\ (s)$ Pilot Transfer Function Numerator
B. 20	$\Delta n_{x_p}/\Delta T\ (s)$ Pilot Transfer Function Numerator
B. 21	$\Delta n_x/\Delta\delta_e\ (s)$ Transfer Function Numerator
B. 22	$\Delta n_x/\Delta T\ (s)$ Transfer Function Numerator
B. 23	$\Delta n_y/\Delta\delta_r\ (s)$ Transfer Function Numerator
B. 24	$\Delta n_y/\Delta\delta_a\ (s)$ Transfer Function Numerator
B. 25	$\Delta n_{y_p}/\Delta\delta_r\ (s)$ Pilot Transfer Function Numerator
B. 26	$\Delta n_{y_p}/\Delta\delta_a\ (s)$ Pilot Transfer Function Numerator

In the following tables, the flight code identifies the Mach number, weight and altitude. For example, .55L20 means Mach .55, light weight, at 20,000 feet. The letter L refers to a (light) weight of 23,904 lb and the letter H refers to a (heavy) weight of 38,204 lb.

TABLE B.1

LONGITUDINAL CHARACTERISTIC EQUATION

FLIGHT CODE	ω_{θ_s}	ζ_{θ_s}	ω_{θ_p}	ζ_{θ_p}
.23L0	1.767	.5665	.1978	-.008823
.40L0	3.063	.5718	.08947	.07651
.53L0	4.073	.5742	.08440	.1109
.35L20	1.723	.4430	.1194	.04861
.55L20	2.752	.4471	.08778	.05359
.75L20	4.043	.4643	(Real Roots .03480, -.05019)	
.50L40	1.504	.3199	.09304	.02873
.65L40	2.032	.3222	.07734	.03835
.80L40	2.721	.3371	(Real Roots .1233, -.1279)	
.23H00	1.665	.4636	.1721	.02384
.23H0	1.662	.4602	.1707	.02518
.40H0	2.817	.4711	.09279	.02626
.53H0	3.746	.4718	.08196	.07285
.35H20	1.629	.3574	.1206	.01820
.55H20	2.579	.3612	.08513	.04002
.75H20	3.761	.3781	.03006	.1520
.50H40	1.430	.2565	.09733	.03714
.65H40	1.930	.2574	.07714	.03768
.80H40	2.447	.2846	(Real Roots .1160, -.1123)	

$$\nabla(s) = \left[1 + \frac{2\zeta_{\theta_p}}{\omega_{\theta_p}} s + \frac{1}{\omega_{\theta_p}^2} s^2\right]\left[1 + \frac{2\zeta_{\theta_s}}{\omega_{\theta_s}} + \frac{1}{\omega_{\theta_s}^2} s^2\right]$$

TABLE B.2

$\frac{\Delta V}{\Delta \delta_e}(s)$ JETSTAR TRANSFER FUNCTION NUMERATOR

$$\frac{\Delta V}{\Delta \delta_e}(s) = K_1 \left(1 - \frac{s}{s_1}\right)\left(1 - \frac{s}{s_2}\right)$$

FLIGHT CODE	K_1	s_1	s_2
.23L0	837	116.0	-1.375
.40L0	7369	52.50	-3.911
.53L0	10,736	12.65	-15.12
.35L20	2001	160.7	-1.071
.55L20	5824	37.59	-3.848
.75L20	-34,691	24.55	-9.552
.50L40	2251	154.7	-0.7294
.65L40	4164	73.63	-1.470
.80L40	-1979	78.02	-2.223
.23H00	750.9	-.4499	-142.3
.23H0	750.8	-.4413	-142.3
.40H0	4790	-.9111	-488.8
.53H0	7823	43.75	-5.531
.35H20	1295	199.5	-0.7119
.55H20	4106	136.7	-1.496
.75H20	45,055	68.12	-3.951
.50H40	1355	78.95	-.7264
.65H40	2716	199.1	-.7094
.80H40	-1740	161.0	-1.193

TABLE B.3

$\frac{\Delta\alpha}{\Delta\delta_e}(s)$ JETSTAR TRANSFER FUNCTION NUMERATOR

$$\frac{\Delta\alpha}{\Delta\delta_e}(s) = K_2\left(1-\frac{s}{s_3}\right)\left(1-\frac{s}{s_4}\right)\left(1-\frac{s}{s_5}\right)$$

FLIGHT CODE	K_2	s_3	s_4 s_5
.23L0	-1.314	-34.29	(-.007727 ± .2295j)
.40L0	-1.820	-60.23	(-.007834 ± .1207j)
.53L0	-1.441	-78.20	(-.009631 ± .1027j)
.35L20	-1.379	-48.01	(-.009713 ± .1344j)
.55L20	-1.257	-75.95	(-.005420 ± .09489j)
.75L20	+3.27	-102.5	(-.007416 ± .07677j)
.50L40	-1.355	-63.84	(-.004431 ± .09972j)
.65L40	-1.235	-82.93	(-.003633 ± .08125j)
.80L40	+0.212	-100.0	(-.004338 ± .05781j)
.23H00	-1.207	-50.50	(-.01349 ± .1873j)
.23H0	-1.206	-50.50	(-.01350 ± .1855j)
.40H0	-1.654	-118.1	(-.005154 ± .1145j)
.53H0	-1.394	-115.2	(-.006361 ± .09413j)
.35H20	-1.321	-70.96	(-.005172 ± .1309j)
.55H20	-1.252	-112.3	(-.004055 ± .08960j)
.75H20	-5.74	-151.4	(-.004869 ± .07104j)
.50H40	-1.217	-94.51	(-.004455 ± .09781j)
.65H40	-1.180	-122.8	(-.003366 ± .07817j)
.80H40	+0.280	-148.4	(-.003234 ± .05678j)

TABLE B.4

$\frac{\Delta\theta}{\Delta\delta_e}(s)$ JETSTAR TRANSFER FUNCTION NUMERATOR

$$\frac{\Delta\theta}{\Delta\delta_e}(s) = K_3\left(1-\frac{s}{s_6}\right)\left(1-\frac{s}{s_7}\right)$$

FLIGHT CODE	K_3	s_6	s_7
.23L0	-.7373	-.02866	-1.059
.40L0	-4.625	-.02024	-1.883
.53L0	-7.926	-.02379	-2.521
.35L20	-.9868	-.01592	-.8260
.55L20	-2.842	-.01576	-1.314
.75L20	18.86	-.01751	-1.994
.50L40	-1.025	-.01482	-.5122
.65L40	-1.607	-.01250	-.6926
.80L40	.6552	-.01067	-.9844
.23H00	.003520	.0001450	-.7217
.23H0	.003588	.0001477	-.7085
.40H0	-1.031	-.006907	-1.202
.53H0	-4.143	-.01708	-1.573
.35H20	-.7706	-.01947	-.5176
.55H20	-1.608	-.01266	-.8221
.75H20	-17.68	-.01265	-1.246
.50H40	-1.045	-.02617	-.3149
.65H40	-1.022	-.01226	-.4342
.80H40	.4861	-.009025	-.6207

TABLE B.5

$\frac{\Delta n_z}{\Delta \delta_e}(s)$ JETSTAR TRANSFER FUNCTION NUMERATOR

$$\frac{\Delta n_z}{\Delta \delta_e}(s) = K_4\left(1-\frac{s}{s_8}\right)\left(1-\frac{s}{s_9}\right)\left(1-\frac{s}{s_{10}}\right)\left(1-\frac{s}{s_{11}}\right)$$

FLIGHT CODE	K_4	s_8	s_9	s_{10}	s_{11}
.23L0	-.0929	5.54576	-6.42844	0.035249	-0.012733
.40L0	-.231	9.79396	-11.311	.00437278	-.0165934
.53L0	-.280	12.8895	-14.9170	.00213647	-.0215664
.35L20	-.1125	5.907	-6.572	.01643	-.009867
.55L20	-.1552	9.41202	-10.4798	.00384942	-.012590
.75L20	+.666	13.3966	-15.0157	.00159162	-.016056
.50L40	-.1353	5.49476	-5.95085	.0140628	-.00918495
.65L40	-.133	7.28477	-7.85933	.00598602	-.00882054
.80L40	+.0339	9.5051	-10.2892	.00238539	-.00959127
.23H00	0	5.45238	-6.31486	.051879	0
.23H0	.0007	5.45850	-6.3079	.051800	+.0000711875
.40H0	-.07275	11.1422	-12.5608	.0083875	-.004185696
.53H0	-.1935	12.4656	-14.328	.00304758	-.0143432
.35H20	-.1210	5.76575	-6.37997	.0248797	-.0107856
.55H20	-.1246	9.09801	-10.0835	.00618581	-.00892227
.75H20	-.817	12.9150	-14.4759	.00223911	-.0107513
.50H40	-.210	5.33503	-5.73025	.0208804	-.0162365
.65H40	-.125	7.05803	-7.57972	.00976462	-.00777593
.80H40	+.036	9.2210	-9.96087	.00371072	-.0074599

TABLE B.6

$\frac{\Delta V}{\Delta T}(s)$ JETSTAR TRANSFER FUNCTION NUMERATOR

$$\frac{\Delta V}{\Delta T}(s) = K_5\left(1-\frac{s}{s_{12}}\right)\left(1-\frac{s}{s_{13}}\right)\left(1-\frac{s}{s_{14}}\right)$$

FLIGHT CODE	K_5	s_{12}	s_{13} s_{14}
.23L0	-.0004165	.01209	(-.9950 ± 1.462j)
.40L0	-.0004610	.002742	(-1.751 ± 2.573j)
.53L0	-.0002794	.001479	(-2.338 ± 3.335j)
.35L20	-.00008215	.0008668	(-.7629 ± 1.548j)
.55L20	-.0004614	.002641	(-1.230 ± 2.462j)
.75L20	.0009548	.001239	(-1.877 ±3.580j)
.50L40	-.001267	.008115	(-.4821 ±1.428j)
.65L40	-.0008842	.003925	(-.6547 ±1.924j)
.80L40	.0001683	.001979	(-.9157 ± 2.558j)
.23H00	-.0005554	.01917	(-.7777 ± 1.489j)
.23H0	-.0006027	.02046	(-.7720 ± 1.490j)
.40H0	-.0004156	.004245	(-1.327 ± 2.487j)
.53H0	-.0002691	.002147	(-1.767 ± 3.303j)
.35H20	-.0007312	.01256	(-.5837 ± 1.526j)
.55H20	-.0004602	.003957	(-.9138 ± 2.406j)
.75H20	-.001595	.001712	(-1.422 ± 3.481j)
.50H40	-.001132	.01268	(-.3648 ± 1.384j)
.65H40	-.0008416	.005936	(-.4981 ± 1.866j)
.80H40	.0001864	.002899	(-.6920 ± 2.341j)

TABLE B.7

$\frac{\Delta\alpha}{\Delta T}(s)$ JETSTAR TRANSFER FUNCTION NUMERATOR

$$\frac{\Delta\alpha}{\Delta T}(s) = K_6 \left(1 - \frac{s}{s_{15}}\right)\left(1 - \frac{s}{s_{16}}\right)\left(1 - \frac{s}{s_{17}}\right)$$

FLIGHT CODE	K_6	s_{15}	s_{16}	s_{17}
.23L0	3.362×10^{-8}	.002432	-.7785	-3.288
.40L0	3.379×10^{-8}	.001793	(-2.671 ± 1.501j)	
.53L0	5.197×10^{-10}	-2.867	-4.266	.0006199
.35L20	5.513×10^{-9}	.0003878	(-1.154 ± .3033j)	
.55L20	1.493×10^{-9}	.0002687	-.8759	-2.870
.75L20	-1.206×10^{-7}	.001285	(-2.840 ± 5.982j)	
.50L40	5.209×10^{-7}	.0042	(-.7285 ± .3699j)	
.65L40	7.582×10^{-8}	.001178	-.6909	-1.294
.80L40	-1.092×10^{-7}	.002107	(-1.398 ± 8.091j)	
.23H00	2.301×10^{-8}	.002949	-.7512	-1.420
.23H0	2.497×10^{-8}	.003186	-.7748	-1.274
.40H0	3.217×10^{-8}	.002759	(-1.839 ± 1.615j)	
.53H0	5.249×10^{-9}	.0009554	(-2.457 ± 1.296j)	
.35H20	5.399×10^{-8}	.005832	(-.8536 ± .5010j)	
.55H20	1.650×10^{-9}	.0004657	-.8781	-1.698
.75H20	1.633×10^{-7}	.001672	(-1.957 ± 4.601j)	
.50H40	-3.382×10^{-8}	-.9418	(-.03173 ± .03135j)	
.65H40	-6.119×10^{-8}	-.0003497	-.2045	-1.161
.80H40	-1.595×10^{-7}	.003029	(-.9556 ± 7.081j)	

TABLE B.8

$\frac{\Delta\theta}{\Delta T}(s)$ JETSTAR TRANSFER FUNCTION NUMERATOR

$$\frac{\Delta\theta}{\Delta T}(s) = K_7\left(1-\frac{s}{s_{18}}\right)\left(1-\frac{s}{s_{19}}\right)$$

FLIGHT CODE	K_7	s_{18}	s_{19}
.23L0	4.207×10^{-5}	-4.296	-8.261
.40L0	4.209×10^{-5}	(-5.233 ± 5.044j)	
.53L0	4.201×10^{-5}	-8.442	-13.52
.35L20	4.187×10^{-5}	-2.141	-11.81
.55L20	4.200×10^{-5}	-3.039	-21.71
.75L20	4.131×10^{-5}	49.16	-.8387
.50L40	4.222×10^{-5}	-1.271	-16.18
.65L40	4.204×10^{-5}	-1.638	-22.76
.80L40	4.172×10^{-5}	252.4	-.9188
.23H00	2.664×10^{-5}	-1.648	-10.86
.23H0	2.668×10^{-5}	-1.512	-10.91
.40H0	2.630×10^{-5}	(-5.926 ± 1.243j)	
.53H0	2.629×10^{-5}	-4.357	-17.00
.35H20	2.644×10^{-5}	-1.418	-12.82
.55H20	2.629×10^{-5}	-1.889	-21.91
.75H20	2.677×10^{-5}	17.53	.9003
.50H40	2.647×10^{-5}	-.7011	-20.60
.65H40	2.635×10^{-5}	-.9700	-25.34
.80H40	2.605×10^{-5}	205.1	-.5675

TABLE B.9

$\frac{\Delta n_z}{\Delta T}(s)$ JETSTAR TRANSFER FUNCTION NUMERATOR

$$\frac{\Delta n_z}{\Delta T}(s) = K_\theta \left(1 - \frac{s}{s_{z0}}\right)\left(1 - \frac{s}{s_{z1}}\right)\left(1 - \frac{s}{s_{z2}}\right)$$

FLIGHT CODE	K_θ	s_{z0}	s_{z1}	s_{z2}
.23L0	$+5.3 \times 10^{-6}$	.0157258	(-.485228 ± 1.77534j)	
.40L0	$+2.1 \times 10^{-6}$	.0035888	(-.932465 ± 2.91611j)	
.53L0	$+1.482 \times 10^{-6}$	.00193785	(-1.2422 ± 4.35063j)	
.35L20	$+4.77 \times 10^{-6}$	.0104	(-.4040 ± 2.060j)	
.55L20	$+2.297 \times 10^{-6}$	.00308120	(-.657981 ± 3.40922j)	
.75L20	$+1.46 \times 10^{-6}$	.00146039	-4.04417	1.99294
.50L40	$+5.575 \times 10^{-6}$	.00876645	(-.258337 ± 1.90975j)	
.65L40	$+3.49 \times 10^{-6}$	.00423710	(-.354462 ± 2.62155j)	
.80L40	$+2.16 \times 10^{-6}$	.00214661	-7.24004	6.25564
.23H00	0	-1.54809	(-.412059 ± 1.47029j)	
.23H0	$+5.2 \times 10^{-6}$	.0243381	(-.509062 ± 2.09527j)	
.40H0	$+1.855 \times 10^{-6}$	.00507153	(-.865837 ± 2.99204j)	
.53H0	$+1.155 \times 10^{-6}$	.00256237	(-1.15243 ± 4.2793j)	
.35H20	$+4.15 \times 10^{-6}$	.0138863	(-.367109 ± 1.96614j)	
.55H20	$+2.04 \times 10^{-6}$	.0043712	(-.612712 ± 3.29895j)	
.75H20	$+1.234 \times 10^{-6}$	.00191416	(-.950105 ± 1.90434j)	
.50H40	$+5.32 \times 10^{-6}$	.0133437	(-.242581 ± 1.94362j)	
.65H40	$+3.22 \times 10^{-6}$	.006238	(-.3291 ± 2.592j)	
.80H40	$+1.93 \times 10^{-6}$	.00307278	-6.31071	5.38611

TABLE B.10

LATERAL-DIRECTIONAL CHARACTERISTIC EQUATION

FLIGHT CODE	ω_ψ	ζ_ψ	τ_R	τ_S
.23L0	1.584	.1181	.4801	99.01
.40L0	2.324	.1371	.2680	134.0
.53L0	2.956	.1383	.1996	112.3
.35L20	1.582	.08489	.6146	184.4
.55L20	2.172	.09799	.3811	215.3
.75L20	2.908	.1040	.2672	668.9
.50L40	1.487	.05287	.9497	404.4
.65L40	1.727	.06173	.7189	247.8
.80L40	2.022	.06824	.5609	905.8
.23H0	1.410	.06606	1.201	213
.40H0	1.970	.1138	.7645	156.1
.53H0	2.477	.1228	.5800	202.2
.35H20	1.374	.04637	1.535	288.9
.55H20	1.846	.08232	1.086	275.2
.75H20	2.420	.09023	.7704	470.6
.50H40	1.305	.02980	2.379	14040
.65H40	1.483	.04976	1.987	1537
.80H40	1.704	.05946	1.608	18900

$$\nabla(s) = (1 + \tau_S s)(1 + \tau_R s)\left(1 + \frac{2\zeta_\psi}{\omega_\psi} s + \frac{1}{\omega_\psi^2} s^2\right)$$

TABLE B.11

$\frac{\phi}{\delta_r}(s)$ JETSTAR TRANSFER FUNCTION NUMERATOR

$$\frac{\phi}{\delta_r}(s) = K_9\left(1-\frac{s}{s_{23}}\right)\left(1-\frac{s}{s_{24}}\right)$$

FLIGHT CODE	K_9	s_{23}	s_{24}
.23L0	-72.15	1.814	-1.566
.40L0	-88.52	1.707	-1.819
.53L0	-130.4	2.509	-2.728
.35L20	-167.9	1.694	-1.529
.55L20	-138.2	1.427	-1.510
.75L20	246.0	(-.1700 ± 1.332j)	
.50L40	-469.8	1.598	-1.462
.65L40	-284.3	1.570	-1.531
.80L40	202.2	(-.06682 ± .7584j)	
.23H0	-180.6	2.107	-1.657
.40H0	-126.6	1.673	-1.655
.53H0	-125.6	1.517	-1.652
.35H20	-316.3	1.001	-1.598
.55H20	-242.3	1.478	-1.456
.75H20	20.88	(-.09129 ± .3731j)	
.50H40	-18,562	1.764	-1.554
.65H40	-1,571	1.358	-1.277
.80H40	4,492	(-.03218 ± .6255j)	

TABLE B.12

$\frac{r}{\delta_r}(s)$ JETSTAR TRANSFER FUNCTION NUMERATOR

$$\frac{r}{\delta_r}(s) = K_{10}\left(1-\frac{s}{s_{25}}\right)\left(1-\frac{s}{s_{26}}\right)\left(1-\frac{s}{s_{27}}\right)$$

FLIGHT CODE	K_{10}	s_{25}	s_{26}	s_{27}
.23L0	-8.746	-2.205	(-.1080 ± .4831j)	
.40L0	-6.303	-3.921	(-.09859 ± .2845j)	
.53L0	-7.112	-5.212	(-.1318 ± .3144j)	
.35L20	-14.56	-1.650	(-.1044 ± .4497j)	
.55L20	-7.744	-2.743	(-.07426 ± .2559j)	
.75L20	9.972	.1214	-.2498	-3.960
.50L40	-30.56	-.9316	(-.1365 ± .4835j)	
.65L40	-14.39	-1.365	(-.09059 ± .3660j)	
.80L40	8.297	.1190	-.1720	-1.901
.23H0	-21.53	-.7418	(-.06121 ± .6160j)	
.40H0	-8.996	-1.299	(-.06044 ± .3420j)	
.53H0	-6.857	-1.725	(-.07300 ± .2434j)	
.35H20	-27.18	-.5962	(-.03072 ± .5533j)	
.55H20	-13.53	-.9038	(-.04653 ± .3234j)	
.75H20	.8111	.03036	-.1195	-1.308
.50H40	-1183	-.3497	(-.03754 ± .5769j)	
.65H40	-78.94	-.4690	(-.03329 ± .3732j)	
.80H40	184.8	.1359	-.1721	-.6292

TABLE B.13

$\frac{\beta}{\delta_r}(s)$ JETSTAR TRANSFER FUNCTION NUMERATOR

$$\frac{\beta}{\delta_r}(s) = K_{\prime\prime}\left(1-\frac{s}{s_{28}}\right)\left(1-\frac{s}{s_{29}}\right)\left(1-\frac{s}{s_{30}}\right)$$

FLIGHT CODE	$K_{\prime\prime}$	s_{28}	s_{29}	s_{30}
.23L0	-.6675	-2.100	-26.52	.01605
.40L0	.06222	-3.780	-42.30	-.0008511
.53L0	.1423	-5.074	-54.27	-.002240
.35L20	-.8591	-1.630	-36.79	.01064
.55L20	.07202	-2.647	-53.94	-.0006249
.75L20	.9460	-3.801	-70.39	-.002819
.50L40	-1.614	-1.044	-49.92	.009719
.65L40	-.2902	-1.389	-60.72	.002469
.80L40	.8281	-1.805	-71.62	-.001974
.23H0	-2.323	.03291	-.7909	-28.13
.40H0	-.1610	-1.309	-46.30	.002007
.53H0	.1443	-1.723	-59.85	-.001300
.35H20	-2.024	.01944	-.6148	-38.76
.55H20	-.2956	.002135	-.9215	-58.97
.75H20	.5280	-1.292	-77.68	-.002290
.50H40	-78.10	.01673	-.3922	-52.86
.65H40	-3.808	.005755	-.4977	-65.51
.80H40	8.568	-.001023	-.6204	-78.95

TABLE B.14

$\frac{\phi}{\delta_a}(s)$ JETSTAR TRANSFER FUNCTION NUMERATOR

$$\frac{\phi}{\delta_a}(s) = K_{12}\left(1-\frac{s}{s_{31}}\right)\left(1-\frac{s}{s_{32}}\right)$$

FLIGHT CODE	K_{12}	s_{31} s_{32}
.23L0	+115.6	(-.2105 ± 1.426j)
.40L0	+321.2	(-.3429 ± 2.281j)
.53L0	+364.2	(-.4427 ± 2.937j)
.35L20	+308.5	(-.1571 ± 1.460j)
.55L20	+660.8	(-.2335 ± 2.140j)
.75L20	+2991	(-.3182 ± 2.897j)
.50L40	+862.7	(-.09839 ± 1.355j)
.65L40	+824.7	(-.1233 ± 1.663j)
.80L40	+3821	(-.1510 ± 2.008j)
.23H0	+210.2	(-.1455 ± 1.250j)
.40H0	+360.1	(-.2248 ± 1.899j)
.53H0	+646.2	(-.2890 ± 2.421j)
.35H20	+417.2	(-.1075 ± 1.259j)
.55H20	+810.9	(-.1539 ± 1.781j)
.75H20	+2080	(-.2098 ± 2.381j)
.50H40	+26,006	(-.06776 ± 1.181j)
.65H40	+4842	(-.08314 ± 1.409j)
.80H40	+78,389	(-.1001 ± 1.670j)

TABLE B.15

$\frac{r}{\delta_a}(s)$ JETSTAR TRANSFER FUNCTION NUMERATOR

$$\frac{r}{\delta_a}(s) = K_{13}\left(1-\frac{s}{s_{33}}\right)\left(1-\frac{s}{s_{34}}\right)\left(1-\frac{s}{s_{35}}\right)$$

FLIGHT CODE	K_{13}	s_{33}	s_{34} s_{35}
.23L0	+13.95	-.8487	(.3574 ± 2.002j)
.40L0	+22.56	-1.320	(.08174 ± 2.334j)
.53L0	+19.54	-1.517	(-.1123 ± 2.548j)
.35L20	+26.70	-.6993	(.2774 ± .1953j)
.55L20	+36.76	-.9661	(.1176 ± 2.242j)
.75L20	+122.1	-1.142	(-.04182 ± 2.527j)
.50L40	+56.07	-.4731	(.2268 ± 1.851j)
.65L40	+41.66	-.5864	(.1533 ± 1.993j)
.80L40	+157.3	-.7560	(.1346 ± 2.060j)
.23H0	+25.05	-.5799	(.3450 ± 1.952j)
.40H0	+25.44	-1.014	(-.04060 ± 3.370j)
.53H0	+34.92	-1.313	(-1.355 ± 4.607j)
.35H20	+35.83	-.5201	(.2857 ± 1.892j)
.55H20	+45.18	-.7191	(.04273 ± 3.117j)
.75H20	+85.19	-.9469	(-1.012 ± 5.006j)
.50H40	+1657	-.3194	(.1834 ± 1.805j)
.65H40	+243.2	-.4099	(.1354 ± 2.286j)
.80H40	+3225	-.5659	(-.1185 ± 2.963j)

TABLE B.16

$\frac{\beta}{\delta_a}(s)$ JETSTAR TRANSFER FUNCTION NUMERATOR

$$\frac{\beta}{\delta_a}(s) = K_{14}\left(1-\frac{s}{s_{36}}\right)\left(1-\frac{s}{s_{37}}\right)$$

FLIGHT CODE	K_{14}	s_{36}	s_{37}
.23L0	+1.821	-.2210	-2.778
.40L0	+1.769	22.25	-.6123
.53L0	+1.182	1.808	-1.245
.35L20	+2.459	-.1692	-2.278
.55L20	+2.239	-.3711	-28.12
.75L20	+5.407	1.528	-.8172
.50L40	+3.810	-.1007	-1.400
.65L40	+2.273	-.1564	-2.173
.80L40	+6.930	116.8	-.2304
.23H0	+3.183	-1454	-1.509
.40H0	+1.953	-.3774	-1.095
.53H0	+2.092	(-.4286 ± .5912j)	
.35H20	+3.233	-.1119	-1.330
.55H20	+2.715	-.2335	-.8830
.75H20	+3.818	(-.3606 ± .3955j)	
.50H40	+110.0	-.06983	-.7526
.65H40	+13.14	-.1027	-.7040
.80H40	+141.8	-.2303	-.4335

TABLE B.17

$\frac{\Delta n_{z_p}(s)}{\Delta \delta_e}$ JETSTAR TRANSFER FUNCTION NUMERATOR

FLIGHT CODE	K_{15}	s_{38} s_{39}	s_{40}	s_{41}
.23L0	-.0929	(-.6109 ± 4.216j)	.03510	-.01273
.40L0	-.2308	(-1.040 ± 7.364j)	.004373	-.01659
.53L0	-.2798	(-1.394 ± 9.778j)	.002136	-.02156
.35L20	-.1125	(-.4705 ± 4.404j)	.01641	-.009866
.55L20	-.1552	(-.7247 ±6.980j)	.003848	-.01259
.75L20	+.6673	(-1.091 ± 10.07j)	.001591	-.01605
.50L40	-.1353	(-.2928 ± 4.039j)	.01406	-.009180
.65L40	-.1332	(-.3839 ± 5.349j)	.005986	-.008815
.80L40	+.3388	(-.5476 ± 7.103j)	.002386	-.009590
.23H00	0	(-.3732 ± 3.159j)	.05161	0
.23H0	+.0007	(-.3666 ± 3.160j)	.05153	+.00007119
.40H0	-.0727	(-.5865 ± 5.279j)	.008387	-.004183
.53H0	-.1935	(-.7475 ± 7.187j)	.003049	-.01434
.35H20	-.1210	(-.2645 ± 3.268j)	.02485	-.01078
.55H20	-.1246	(-.3931 ± 5.135j)	.006186	-.008924
.75H20	-.8146	(-.5859 ± 7.391j)	.002240	-.01075
.50H40	-.2101	(-.1649 ± 2.976j)	.02085	-.01624
.65H40	-.1247	(-.2116 ± 3.937j)	.009760	-.007777
.80H40	+.0360	(-.2980 ± 5.224j)	.003710	-.007460

$$\frac{\Delta n_{z_p}}{\Delta \delta_e} = K_{15}\left(1-\frac{s}{s_{38}}\right)\left(1-\frac{s}{s_{39}}\right)\left(1-\frac{s}{s_{40}}\right)\left(1-\frac{s}{s_{41}}\right)$$

TABLE B.18

$\frac{\Delta n_{zp}}{\Delta T}(s)$ JETSTAR PILOT TRANSFER FUNCTION NUMERATOR

$$\frac{\Delta n_{zp}}{\Delta T}(s) = K_{16}\left(1-\frac{s}{s_{42}}\right)\left(1-\frac{s}{s_{43}}\right)\left(1-\frac{s}{s_{44}}\right)\left(1-\frac{s}{s_{45}}\right)$$

FLIGHT CODE	$K_{16}\times 10^6$	s_{42}	s_{43}	s_{44}	s_{45}
.23L0	5.30	(-.5680 ± 1.665j)		.01570	-137.3
.40L0	2.10	(-1.050 ± 2.755j)		.003589	-102.0
.53L0	1.48	(-1.393 ± 4.014j)		.001937	-165.0
.35L20	4.77	(-.4570 ± 1.909j)		.01013	-106.3
.55L20	2.69	(-.7369 ± 3.123j)		.003081	-156.8
.75L20	1.46	-4.961	2.296	.001460	-115.9
.50L40	5.57	(-.2897 ± 1.778j)		.008764	-111.8
.65L40	3.49	(-.3953 ± 2.422j)		.004238	-135.0
.80L40	2.16	(-.9932 ± 9.872j)		.002146	80.86
.23H00	0	(-.5015 ± 1.434j)		-1.550	0
.23H0	5.20	(-.5238 ± 1.831j)		.02428	-50.70
.40H0	1.85	(-.9302 ± 2.771j)		.005070	-75.94
.53H0	1.23	(-1.214 ± 3.868j)		.002563	-116.4
.35H20	4.15	(-.3960 ± 1.793j)		.01388	-76.22
.55H20	2.04	(-.6336 ± 2.938j)		.004372	-111.6
.75H20	1.23	(-1.208 ± 2.018j)		.001905	-91.61
.50H40	5.32	(-.2508 ± 1.727j)		.01334	-117.6
.65H40	3.22	(-.3392 ± 2.304j)		.006236	-118.4
.80H40	1.93	(-.3184 ± 6.657j)		.003072	84.87

TABLE B.19

$\frac{\Delta n_{x_p}}{\Delta \delta_e}(s)$ JETSTAR PILOT TRANSFER FUNCTION NUMERATOR

$$\frac{\Delta n_{x_p}}{\Delta \delta_e}(s) = K_{17}\left(1-\frac{s}{s_{46}}\right)\left(1-\frac{s}{s_{47}}\right)\left(1-\frac{s}{s_{48}}\right)\left(1-\frac{s}{s_{49}}\right)$$

FLIGHT CODE	K_{17}	s_{46}	s_{47}	s_{48}	s_{49}
.23L0	-0.7373	(+.001750 ± .1523j)		3.104	-4.065
.40L0	-4.6245	(-.009371 ± .1427j)		3.890	-5.614
.53L0	-7.9225	(-.01039 ± .1499j)		4.656	-6.965
.35L20	-0.9868	(-.002670 ± .1010j)		3.228	-3.966
.55L20	-2.8420	(-.005891 ± .1024j)		4.221	-5.395
.75L20	18.8612	(-.008068 ± .1161j)		4.756	-6.610
.50L40	-1.0250	(-.001677 ± .07575j)		3.335	-3.782
.65L40	-1.6067	(-.003263 ± .07202j)		3.938	-4.539
.80L40	+0.6552	(-.005010 ± .07627j)		4.148	-5.036
.23H00	+0.0352	(-.4596 ± 2.698j)		.04614	.004118
.23H0	+0.0359	(-.4527 ± 2.597j)		.04573	.004419
.40H0	-1.0315	(-.003796 ± .09835j)		2.667	-3.922
.53H0	-4.1434	(-.007056 ± .1131j)		4.378	-5.900
.35H20	-0.7706	(+.0007541 ± .09182j)		3.231	-3.750
.55H20	-1.6077	(-.003707 ± .08086j)		3.919	-4.722
.75H20	-17.6761	(-.005339 ± .08658j)		4.515	-5.730
.50H40	-1.0455	(-.001609 ± .07287j)		3.686	-3.983
.65H40	-1.0217	(-.001731 ± .06095j)		3.715	-4.142
.80H40	+0.4861	(-.003410 ± .05921j)		4.024	-4.623

TABLE B.20

$\frac{\Delta n_{x_p}}{\Delta T}(s)$ JETSTAR PILOT TRANSFER FUNCTION NUMERATOR

$$\frac{\Delta n_{x_p}}{\Delta T}(s) = K_{18}\left(1-\frac{s}{s_{50}}\right)\left(1-\frac{s}{s_{51}}\right)\left(1-\frac{s}{s_{52}}\right)\left(1-\frac{s}{s_{53}}\right)$$

FLIGHT CODE	K_{18}	s_{50} s_{51}	s_{52} s_{53}
.23L0	4.207×10^{-5}	(-.9977 ± 1.437j)	(-.007897 ± .1986j)
.40L0	4.209×10^{-5}	(-1.751 ± 2.510j)	(-.0007100 ± .08970j)
.53L0	4.201×10^{-5}	(-2.338 ± 3.332j)	(-.001239 ± .08458j)
.35L20	4.187×10^{-5}	(-.7588 ± 1.539j)	(-.008953 ± .1188j)
.55L20	4.200×10^{-5}	(-1.227 ± 2.458j)	(-.002613 ± .08790j)
.75L20	4.131×10^{-5}	(-1.882 ± 3.581j)	.04369 -.03936
.50L40	4.222×10^{-5}	(-.4763 ±1.421j)	(-.006378 ± .09275j)
.65L40	4.204×10^{-5}	(-.6511 ± 1.921j)	(-.003908 ± .07730j)
.80L40	4.172×10^{-5}	(-.9381 ± 2.567j)	.1430 -.1087
.23H00	2.664×10^{-5}	(-.7338 ± 1.479j)	(.007564 ± .1730j)
.23H0	2.668×10^{-5}	(-.7671 ± 1.479j)	(.006693 ± .1717j)
.40H0	2.630×10^{-5}	(-1.326 ± 2.483j)	(-.002051 ± .09283j)
.53H0	2.629×10^{-5}	(-1.765 ± 3.301j)	(-.001917 ± .08209j)
.35H20	2.644×10^{-5}	(-.5757 ± 1.516j)	(-.009062 ± .1199j)
.55H20	2.629×10^{-5}	(-.9277 ± 2.402j)	(-.004079 ± .08509j)
.75H20	2.677×10^{-5}	(-1.424 ± 3.481j)	(+.0009743 ± .03035j)
.50H40	2.647×10^{-5}	(-.3554 ± 1.377j)	(-.01313 ± .09557j)
.65H40	2.635×10^{-5}	(-.4916 ± 1.863j)	(-.006513 ± .07669j)
.80H40	2.605×10^{-5}	(-.7201 ± 2.350j)	.1379 -.09270

TABLE B.21

$\frac{\Delta n_x}{\Delta \delta_e}(s)$ JETSTAR TRANSFER FUNCTION NUMERATOR

$$\frac{\Delta n_x}{\Delta \delta_e}(s) = K_{19}\left(1-\frac{s}{s_{54}}\right)\left(1-\frac{s}{s_{55}}\right)\left(1-\frac{s}{s_{56}}\right)\left(1-\frac{s}{s_{57}}\right)$$

FLIGHT CODE	K_{19}	s_{54} s_{55}	s_{56}	s_{57}
.23L0	-.7373	(.002461 ± .1523j)	6.278	-6.923
.40L0	-4.6245	(-.008616 ± .1428j)	12.20	-12.93
.53L0	-7.9255	(-.009602 ± .1499j)	17.52	-17.96
.35L20	-.9868	(-.002427 ± .1010j)	6.657	-7.130
.55L20	-2.8420	(-.005633 ± .1024j)	12.17	-12.52
.75L20	18.8612	(-.007684 ± .1162j)	17.14	-17.76
.50L40	-1.0250	(-.001593 ± .07575j)	6.366	-6.633
.65L40	-1.6067	(-.003183 ± .07203j)	9.082	-9.320
.80L40	.6552	(-.004894 ± .07629j)	11.81	-12.13
.23H00	.0352	.04638 .004118	-50.55	0
.23H0	.0359	(-5.995 ± 22.20j)	.04598	.004419
.40H0	-1.0315	(-.003300 ± .09841j)	9.273	-11.00
.53H0	-4.1434	(-.006703 ± .1131j)	16.21	-17.20
.35H20	-.7706	(.0008935 ± .09181j)	6.664	-7.128
.55H20	-1.6077	(-.003582 ± .08087j)	11.02	-11.68
.75H20	-17.6761	(-.005175 ± .08659j)	16.34	-17.23
.50H40	-1.0455	(-.001567 ± .07287j)	6.847	-7.052
.65H40	-1.0217	(-.001689 ± .06096j)	8.384	-8.752
.80H40	.4861	(-.003359 ± .05921j)	11.26	-11.71

$\frac{\Delta n_x}{\Delta T}(s)$ JETSTAR TRANSFER FUNCTION NUMERATOR

$$\frac{\Delta n_x}{\Delta T}(s) = K_{20}\left(1-\frac{s}{s_{58}}\right)\left(1-\frac{s}{s_{59}}\right)\left(1-\frac{s}{s_{60}}\right)\left(1-\frac{s}{s_{61}}\right)$$

FLIGHT CODE	K_{20}	s_{58}	s_{59}	s_{60}	s_{61}
.23L0	4.207×10^{-5}	(-.9990 ± 1.439j)		(-.007892 ± .1983j)	
.40L0	4.209×10^{-5}	(-1.752 ± 2.510j)		(-.0007100 ± .08967j)	
.53L0	4.201×10^{-5}	(-2.338 ± 3.332j)		(-.001239 ± .08456j)	
.35L20	4.187×10^{-5}	(-.7596 ± 1.539j)		(-.008943 ± .1187j)	
.55L20	4.200×10^{-5}	(-1.228 ± 2.459j)		(-.002612 ± .08788j)	
.80L40	4.131×10^{-5}	(-1.880 ± 3.581j)		.04369	-.03936
.50L40	4.222×10^{-5}	(-.4769 ± 1.421j)		(-.006373 ± .09272j)	
.65L40	4.204×10^{-5}	(-.6517 ± 1.921j)		(-.003906 ± .07729j)	
.80L40	4.172×10^{-5}	(-.9335 ± 2.567j)		.1431	-.1088
.23H00	2.664×10^{-5}	(-.7757 ± 1.480j)		(.007552 ± .1728j)	
.23H0	2.668×10^{-5}	(-.7691 ± 1.480j)		(.006684 ± .1715j)	
.40H0	2.630×10^{-5}	(-1.327 ± 2.484j)		(-.002050 ± .09280j)	
.53H0	2.629×10^{-5}	(-1.766 ± 3.301j)		(-.001916 ± .08207j)	
.35H20	2.644×10^{-5}	(-.5768 ± 1.516j)		(-.009049 ± .1198j)	
.55H20	2.629×10^{-5}	(-.9286 ± 2.403j)		(-.004076 ± .08507j)	
.75H20	2.677×10^{-5}	(-1.424 ± 3.482j)		(.0009742 ± .03035j)	
.50H40	2.647×10^{-5}	(-.3564 ± 1.377j)		(-.01312 ± .09554j)	
.65H40	2.635×10^{-5}	(-.4925 ± 1.863j)		(-.006509 ± .07668j)	
.80H40	2.605×10^{-5}	(-.7152 ± 2.351j)		.1380	-.09273

TABLE B.23

$\frac{\Delta n_y}{\Delta \delta_r}(s)$ JETSTAR TRANSFER FUNCTION NUMERATOR

$$\frac{\Delta n_y}{\Delta \delta_r}(s) = K_{21}\left(1-\frac{s}{s_{62}}\right)\left(1-\frac{s}{s_{63}}\right)\left(1-\frac{s}{s_{64}}\right)\left(1-\frac{s}{s_{65}}\right)$$

FLIGHT CODE	K_{21}	s_{62}	s_{63}	s_{64}	s_{65}
.23L0	2.280	.1153	-1.915	.9561	-1.809
.40L0	0.945	2.313	-2.894	.006141	-3.620
.53L0	0.845	3.085	-3.728	.003574	-4.894
.35L20	3.644	(-1.660 ± .08902j)		1.056	+0.08216
.55L20	0.990	(-2.586 ± .2301j)		.004767	2.153
.75L20	-4.922	(-3.589 ± .3772j)		-.004128	3.019
.50L40	10.054	.1791	-1.751	.6911	-.9677
.65L40	2.972	1.441	-1.971	.02791	-1.376
.80L40	-2.400	2.054	-2.248	-.003475	-1.915
.23H0	8.592	(.2958 ± .4410j)		-.6966	-1.726
.40H0	1.629	1.796	-2.307	.01613	-1.311
.53H0	0.696	2.488	-3.005	.002758	-1.722
.35H20	9.488	(.3534 ± .2798j)		-.5608	-1.689
.55H20	2.567	1.628	-2.166	.01751	-.9202
.75H20	-1.263	2.441	-2.879	-.002515	-1.286
.50H40	772.595	(.1970 ± .4974j)		-.3438	-2.317
.65H40	27.940	.8503	-1.926	.08877	-.4844
.80H40	-40.175	1.559	-2.084	-.004844	-.6198

TABLE B. 24

$\frac{\Delta n_y}{\Delta \delta_a}(s)$ JETSTAR TRANSFER FUNCTION NUMERATOR

$$\frac{\Delta n_y}{\Delta \delta_a}(s) = K_{22}\left(1-\frac{s}{s_{66}}\right)\left(1-\frac{s}{s_{67}}\right)\left(1-\frac{s}{s_{68}}\right)$$

FLIGHT CODE	K_{22}	s_{66}	s_{67}	s_{68}
.23L0	-4.098	(-3.632 ± 3.199j)		-.3458
.40L0	-7.664	(2.016 ± 10.17j)		-.6535
.53L0	-8.248	1.950	-1.252	78.37
.35L20	-7.264	(-2.931 ± 2.801j)		-.3071
.55L20	-9.429	(-1.043 ± 7.340j)		-.4281
.75L20	-38.198	1.715	-.8327	54.86
.50L40	-18.901	(-1.556 ± 2.242j)		-.2842
.65L40	-10.000	(-2.644 ± 2.761j)		-.2854
.80L40	-31.049	(+.03014 ± 5.697j)		-.3007
.23H0	-10.150	(-1.489 ± 2.434j)		-.3735
.40H0	-6.537	-.5178	-1.111	-74.01
.53H0	-10.048	(-.4615 ± .6319j)		-357.7
.35H20	-12.709	(-1.577 ± 2.222j)		-.3276
.55H20	-10.472	-.3956	-.9776	-39.32
.75H20	-19.636	(-.4030 ± .4495j)		-309.0
.50H40	-1082.799	(-.6025 ± 1.934j)		-.2761
.65H40	-86.845	-1.870	-4.500	-.3134
.80H40	-693.575	(-.4730 ± .1920j)		-31.18

TABLE B. 25

$\frac{\Delta n_{y_p}}{\Delta \delta_r}(s)$ JETSTAR PILOT TRANSFER FUNCTION NUMERATOR

$$\frac{\Delta n_{y_p}}{\Delta \delta_r}(s) = \kappa_{23}\left(1-\frac{s}{s_{69}}\right)\left(1-\frac{s}{s_{70}}\right)\left(1-\frac{s}{s_{71}}\right)\left(1-\frac{s}{s_{72}}\right)$$

FLIGHT CODE	κ_{23}	s_{69} s_{70}	s_{71}	s_{72}
.23L0	2.282	(-.3587 ± 1.602j)	.08337	-2.772
.40L0	0.945	(-.3836 ± 2.668j)	.005964	-5.266
.53L0	0.845	(-.5894 ± 3.528j)	.003498	-6.900
.35L20	3.644	(-.3523 ± 1.833j)	.06436	-1.721
.55L20	0.990	(-.3830 ± 2.589j)	.004642	-3.378
.75L20	-4.922	(-.2666 ± 3.408j)	-.004153	-5.453
.50L40	10.054	(-.06052 ± 1.908j)	.1132	-.8238
.65L40	2.972	(-.2694 ± 2.296j)	.02526	-1.318
.80L40	-2.400	(-.1615 ± 2.468j)	-.003505	-2.347
.23H0	8.592	(.1298 ± 1.336j)	.3040	-.6368
.40H0	1.628	(-.02590 ± 2.104j)	.01529	-1.265
.53H0	0.696	(-.05309 ± 2.698j)	.002706	-1.730
.35H20	9.488	(.1992 ± 1.365j)	.2038	-.5059
.55H20	2.567	(.05442 ± 1.973j)	.01638	-.8710
.75H20	-1.263	(2.380 ± 2.598j)	-.002578	-1.340
.50H40	772.595	(.4707 ± .8719j)	.7453	-.3159
.65H40	27.940	(.3428 ± 1.458j)	.07238	-.4432
.80H40	-40.175	(.1818 ± 1.775j)	-.004921	-.6475

TABLE B.26

$\frac{\Delta n_{y_p}}{\Delta \delta_a}(s)$ JETSTAR PILOT TRANSFER FUNCTION NUMERATOR

$$\frac{\Delta n_{y_p}}{\Delta \delta_a}(s) = K_{24}\left(1-\frac{s}{s_{73}}\right)\left(1-\frac{s}{s_{74}}\right)\left(1-\frac{s}{s_{75}}\right)\left(1-\frac{s}{s_{76}}\right)$$

FLIGHT CODE	K_{24}	s_{73} s_{74}	s_{75}	s_{76}
.23L0	-4.098	(-.1917 ± 1.543j)	.5774	-.4245
.40L0	-7.664	(-.3373 ± 2.312j)	.3893	-.5415
.5320	-8.248	(-.4168 ± 2.956j)	.3260	-.6392
.35L20	-7.264	(-.1574 ± 1.543j)	.4976	-.3470
.55L20	-9.429	(-.2343 ± 2.161j)	.3250	-.3873
.75L20	-38.198	(-.3018 ± 2.913j)	.2557	-.4611
.50L40	-18.901	(-.1159 ± 1.453j)	.5411	-.2803
.65L40	-10.000	(-.1353 ± 1.696j)	.3601	-.2786
.80L40	-31.049	(-.1538 ± 2.023j)	.2507	-.2824
.23H0	-10.150	(-.1195 ± 1.463j)	.6994	-.3833
.40H0	-6.537	(-.2681 ± 1.959j)	.4302	-.4411
.53H0	-10.048	(-.3454 ± 2.435j)	.3447	-.5470
.35H20	-12.709	(-.1054 ± 1.415j)	.5926	-.3271
.55H20	-10.472	(-.1973 ± 1.838j)	.3899	-.3378
.75H20	-19.636	(-.2583 ± 2.393j)	.2896	-.4006
.50H40	-1082.799	(-.1285 ± 1.408j)	.8460	-.2576
.65H40	-86.845	(-.1469 ± 1.522j)	.5324	-.2694
.80H40	693.575	(-.1503 ± 1.705j)	.3188	-.2946

APPENDIX C

USE OF COCKPIT MOUNTED ACCELEROMETERS FOR GPAS NORMAL AND LATERAL ACCELERATION FEEDBACK

During the analysis and design of the short-period and Dutch roll normal acceleration control loops, it was noted that closed-loop bandwidth is significantly influenced by location of the feedback accelerometers along the longitudinal axis of the JetStar. When the accelerometers are located near the c.g., the predominant high-frequency motion variables sensed are angle of attack and sideslip angle as indicated by Equations C.1 and C.2.

$$\Delta n_z = \frac{V_t}{g}\left[Z_\alpha \Delta\alpha + Z_{\delta_e}\Delta\delta_e\right] \tag{C.1}$$

$$n_Y = \frac{V_t}{g}\left[Y_\beta \beta + Y_{\delta_r}\delta_r\right] \tag{C.2}$$

If the accelerometers are mounted forward of the c.g., components of pitch and yaw acceleration proportional to the distance ahead of the c.g. are introduced into the readings. At a distance x feet ahead of the c.g., the accelerometers read essentially Δn_{z_x} and n_{Y_x}, given by Equations C.3 and C.4.

$$\Delta n_{z_x} = \Delta n_z - \frac{x}{g}\dot{q} \tag{C.3}$$

$$n_{Y_x} = n_Y + \frac{x}{g}\dot{r} \tag{C.4}$$

If Δn_{z_x} is fed to the elevator and n_{Y_x} is fed to the rudder, the $\Delta\alpha$ and β components of the feedback signals tend to increase longitudinal and directional stiffness, $-M_\alpha$ and N_β. The $\dot{q}$ and $\dot{r}$ terms, however, tend to increase effective pitch and yaw inertias, I_{YY} and I_{zz}. It can be shown that the ratio of directional stiffness to inertia has a limited, finite value as the feedback gain is increased without limit for both Δn_{z_x} and n_{Y_x} feedback. Because this ratio is essentially the square of the short-period or Dutch roll natural frequencies, the bandwidth of the closed-loop response is limited.

In this appendix, the problem of limited acceleration loop bandwidth is

analyzed for both short-period and Dutch roll modes using approximate equations. The short-period mode is then analyzed for an example situation using root-locus techniques and the exact JetStar transfer functions. The results obtained from use of the two different techniques are essentially the same.

C.1 ANALYSIS USING APPROXIMATE EQUATIONS

It was shown in Reference 2 that the closed-loop short-period natural frequency, using Δn_{z_x} feedback, is given by Equation C.5.

$$\omega_{\theta_s}^2 = \frac{(-M_\alpha + M_q Z_\alpha) - M_{\delta_e} P_\alpha}{1 - \lambda M_{\delta_e} P_\alpha} \qquad \text{(C.5}$$

where

$$P_\alpha = \frac{-\frac{V_t}{g} Z_\alpha \frac{\delta_e}{e_{n_{z_x}}}}{1 + \frac{V_t}{g} Z_{\delta_e} \frac{\delta_e}{e_{n_{z_x}}}}$$

and

$$\lambda = -\frac{\chi}{V_t Z_\alpha}$$

Using similar techniques, it can be shown that the closed-loop Dutch roll natural frequency, using n_{Y_x} feedback, is given by Equation C.6.

$$\omega_\psi^2 = \frac{N_\beta + N_{\delta_r} P_\beta}{1 - \sigma N_{\delta_r} P_\beta} \qquad \text{(C.6}$$

where

$$P_\beta = \frac{-\frac{V_t}{g} Y_\beta \left(\frac{\delta_r}{e_{n_{Y_x}}}\right)}{1 + \frac{V_t}{g} Y_{\delta_r} \left(\frac{\delta_r}{e_{n_{Y_x}}}\right)}$$

and

$$\sigma = \frac{\chi}{V_t Y_\beta}$$

Equation C.6 is a more general representation of the Dutch roll frequency than Equation 3.3. The two equations are identical if $\chi = \sigma = 0$ (a c.g. accelerometer), recognizing that $P_\beta = -\delta_r/e_\beta$.

It is evident from the above definitions of P_α and P_β that unless Z_{δ_e} and Y_{δ_r} are neglected, no linear correlation between P_α and $\delta_e/e_{n_{z_x}}$,

and P_β and $\delta_r/e_{n_{Y_\psi}}$, is possible for large values of these gains. If we neglect Z_{δ_e} and Y_{δ_r} and let both $\delta e/e_{n_{z_\psi}}$ and $\delta_r/e_{n_{Y_\psi}}$ increase without limit, then the maximum values of closed-loop short-period and Dutch roll frequency are given by Equations C. 7 and C. 8. *

$$\omega^2_{\theta_{s_{MAX}}} = \lim_{P_\alpha \to \infty} \left\{\omega^2_{\theta_s}\right\} = \frac{1}{\lambda} \tag{C. 7}$$

$$\omega^2_{\psi_{MAX}} = \lim_{P_\beta \to \infty} \left\{\omega^2_{\psi}\right\} = -\frac{1}{\sigma} \tag{C. 8}$$

Equations C. 7 and C. 8 give almost the same results as the expressions in the footnote on the previous page, and provide better insight into the limitations of acceleration feedback. From Appendix A for the JetStar aircraft, $C_{L_\alpha} \approx 5.3$ and $C_{Y_\beta} \approx 0.72$. Using the definitions of λ and σ given above and defining

$$Z_\alpha = -\frac{\bar{q}\, S C_{L_\alpha}}{m V_t}$$

$$Y_\beta = \frac{\bar{q}\, S C_{Y_\beta}}{m V_t}$$

the limit bandwidth values are shown to vary directly with dynamic pressure and inversely with mass as follows:

$$\omega^2_{\theta_{s_{MAX}}} = \frac{S C_{L_\alpha}}{\chi} \cdot \frac{\bar{q}}{m} = 126 \frac{\bar{q}}{m} \quad sec^{-2} \tag{C. 9}$$

$$\omega^2_{\psi_{MAX}} = -\frac{S C_{Y_\beta}}{\chi} \cdot \frac{\bar{q}}{m} = 17.1 \frac{\bar{q}}{m} \quad sec^{-2} \tag{C. 10}$$

when $\chi = \ell = 22.85$ feet

---

*If Z_{δ_e} and Y_{δ_r} are retained, and $\delta e/e_{n_{z_\psi}}$ and $\delta_r/e_{n_{Y_\psi}}$ are allowed to increase without limit,

$$\omega^2_{\theta_{s_{MAX}}} = \lim_{P_\alpha \to (-Z_\alpha/Z_{\delta_e})} \left\{\omega^2_{\theta_s}\right\} = \frac{(-M_\alpha + M_q Z_\alpha) Z_{\delta_e} + M_{\delta_e} Z_\alpha}{Z_{\delta_e} + \lambda M_{\delta_e} Z_\alpha}$$

$$\omega^2_{\psi_{MAX}} = \lim_{P_\beta \to (-Y_\beta/Y_{\delta_r})} \left\{\omega^2_{\psi}\right\} = \frac{N_\beta Y_{\delta_r} - N_{\delta_r} Y_\beta}{Y_{\delta_r} + \sigma N_{\delta_r} Y_\beta}$$

Equations C. 9 and C. 10 give values of $\omega_{\theta_{S_{MAX}}}$ and $\omega_{\psi_{MAX}}$ that are a few percent less than the exact values but are representative of the highest short-period and Dutch roll bandwidths obtainable (for any feedback gains) in a JetStar using cockpit accelerometer locations. For example, $\bar{q}$ = 206 lb/ft^2 and m = 1187 slugs for the .55H20 flight conditions. Using C. 9 and C. 10,

$$\omega_{\theta_{S_{MAX}}} = 4.67 \text{ rad/sec}$$

$$\omega_{\psi_{MAX}} = 1.72 \text{ rad/sec}$$

These values are significantly less than the 9 and 7. 5 rad/sec values that are desired.

C. 2 ROOT LOCUS ANALYSIS; .55H20 FLIGHT CONDITION

Using digital computation and the numerical data from Appendix A, the exact $\Delta n_{z_p}/\Delta\delta_e\ (s)$ transfer function is given in Appendix B, Table 17, and is repeated below as Equation C. 11 for convenience.

$$\frac{\Delta n_{z_p}}{\Delta \delta_e}(s) = \frac{-0.1246\left[1+\frac{2(.0765)}{5.14}s+\frac{1}{(5.14)^2}s^2\right](1-161.5s)(1+112s)}{\left[1+\frac{2(.3612)}{2.579}s+\frac{1}{(2.579)^2}s^2\right]\left[1+\frac{2(.040)}{0.085}s+\frac{1}{(0.085)^2}s^2\right]} \qquad \text{(C. 11)}$$

If this transfer function is used in the short-period control loop illustrated below, the root-locus plot of Figure C. 1 results, where the gain $\delta_e/e_{n_{z_p}}$ is the variable parameter.

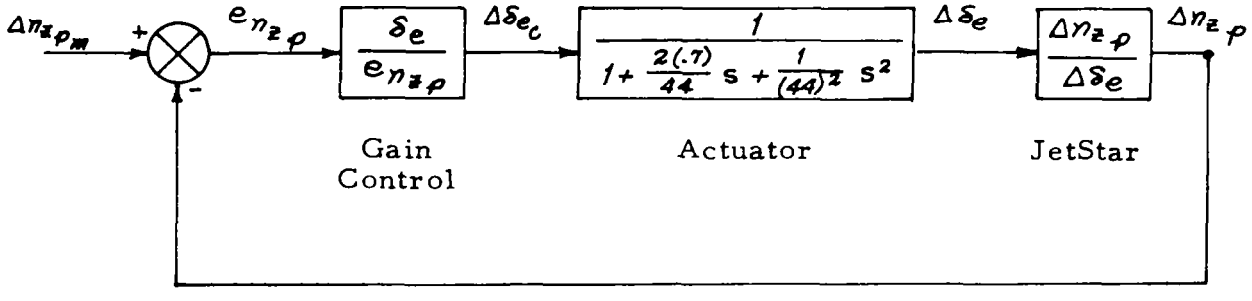

It is evident from Figure C. 1 that short-period bandwidth in excess of 5 rad/sec cannot be achieved using cockpit normal acceleration feedback without lead compensation. This is in good agreement with the value of 4. 67, which was computed using Equation C. 9. When the nominal value of δ_e/e_{n_z} (21 deg/g - see Table 2. 2) is used, the short-period bandwidth is 4 rad/sec, rather than the desired value of 9 rad/sec. Incidentally, Figure C. 1 shows the considerable influence of normal acceleration feedback on the phugoid mode and the fact that when the accelerometer is located ahead of the longitudinal center of percussion, the actuator dynamics are effectively faster than the open-loop values.

For comparison purposes, a root-locus was run using c. g. feedback, instead of cockpit feedback, with no other changes. The transfer function $\Delta n_z/\Delta\delta_e\ (s)$ can be found in Appendix B, Table 5. It is repeated as Equation C. 12.

$$\frac{\Delta n_z}{\Delta \delta_e}(s) = \frac{-0.1246\,(1-0.11s)(1+0.0993s)(1-161.5s)(1+112s)}{\left[1+\frac{2(.3612)}{2.579}s+\frac{1}{(2.579)^2}s^2\right]\left[1+\frac{2(.040)}{0.085}s+\frac{1}{(0.085)^2}s^2\right]} \qquad (C.12)$$

Comparing Equations C. 11 and C. 12, it is evident that moving the normal accelerometer from the cockpit to the c. g. converts a pair of complex zeros (ω = 5. 14 rad/sec, ζ = . 0765) into a pair of real zeros (τ_1 = -0. 11 sec, τ_2 = 0. 0993 sec), one positive and one negative. No other changes occur.

Figure C. 2 shows the root locus using a c. g. accelerometer. Note that actuator dynamics tend to reduce closed-loop ω_{θ_s} and ζ_{θ_s} below the desired values of 9 rad/sec and 0. 5. However, for the same gain used in Figure C. 1, the closed-loop bandwidth is more than 7 rad/sec, compared with the 4 rad/sec achieved using cockpit acceleration. The loss in effective actuator bandwidth that occurs when c. g. normal acceleration feedback is used (explained in Appendix D) is evident in Figure C. 2. The accelerometer location has no influence on phugoid dynamics. The value of short-period damping gain, $\delta_e/e_{\dot{\alpha}}$, was zero in both figures.

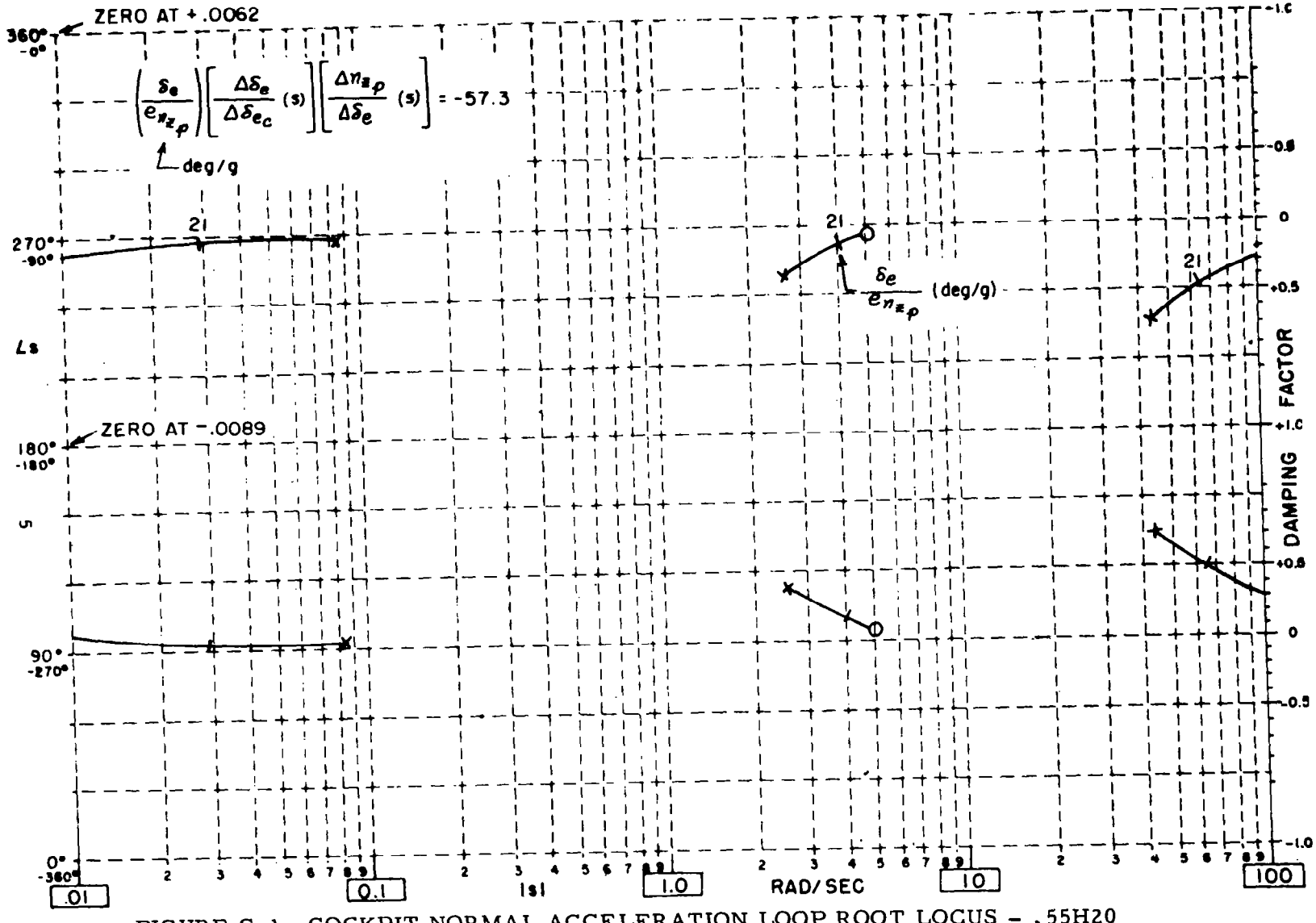

FIGURE C.1 COCKPIT NORMAL ACCELERATION LOOP ROOT LOCUS - .55H20

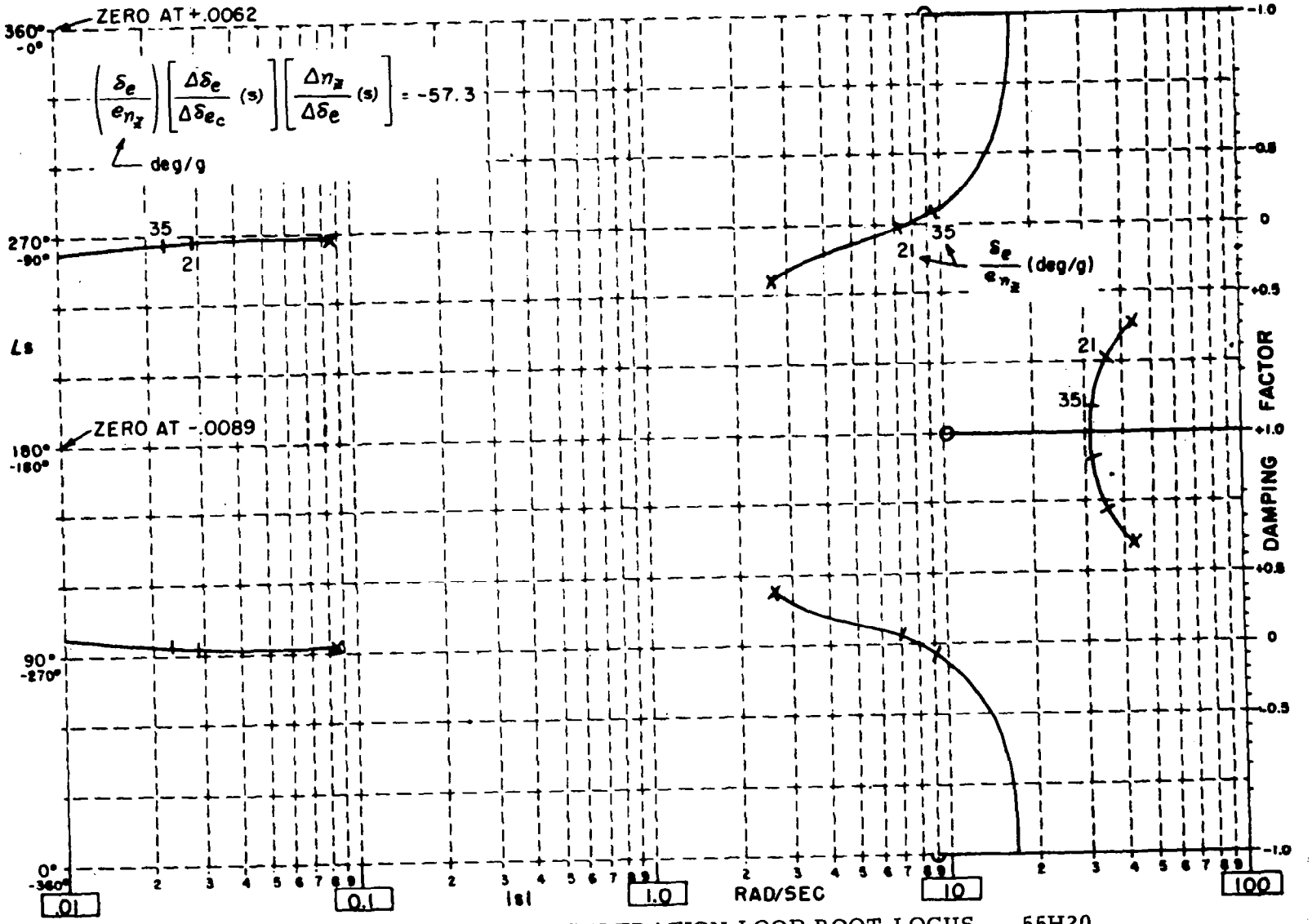

FIGURE C.2 C.G. NORMAL ACCELERATION LOOP ROOT LOCUS – .55H20

APPENDIX D

NORMAL ACCELERATION FEEDBACK AND ACTUATOR LAGS

In Sections 2.3 and 4.1 of this report, it was noted that difficulty encountered in maintaining short-period damping ratio at its desired value ($\zeta_{\theta_s} = 0.5$ is desired) when c.g. normal acceleration feedback is used in an elevator control loop. The problem is explored in this appendix, and two techniques that alleviate the problem are studied.

In Section 2.1, it is noted that the elevator actuator command signal that derives from the short-period feedback loops is given by equation 2.46, repeated here for convenience.

$$\Delta\delta_{e_c} = -\left(\frac{\delta_e}{e_{\dot{\alpha}}}\right)\dot{\alpha} - \left(\frac{\delta_e}{e_{n_z}}\right)\left[\frac{V_t}{g}\left(Z_\alpha \Delta\alpha + Z_{\delta_e}\Delta\delta_e\right) - \frac{\nu}{g}\dot{q}\right]$$

It is important to note that the left side of this equation is the elevator actuator command signal, $\Delta\delta_{e_c}$, and the right side contains actual elevator displacment, $\Delta\delta_e$. When actuator dynamics are neglected, these two quantities are equal and the results of Section 2.1 follow immediately. However, when actuator dynamics are considered, serious problems are introduced as explained below.

The transfer function of the elevator is defined by

$$\frac{\Delta\delta_e}{\Delta\delta_{e_c}}(s) = \frac{1}{D_e(s)} \qquad (D.1)$$

where $\lim_{s\to 0} D_e(s) = 1.0$

Letting $\nu = 0$ to implement c.g. acceleration feedback, and substituting equation D.1 into 2.46, it can be shown that the actual elevator displacement response to the feedback signals is given by equation D.2.

$$\Delta\delta_e(s) = \frac{\left[-\frac{V_t}{g}\left(\frac{\delta_e}{e_{n_z}}\right)Z_\alpha\right]\Delta\alpha(s) + \left[-\frac{\delta_e}{e_{\dot\alpha}}\right]\dot\alpha(s)}{D_e(s) + \frac{V_t}{g}Z_{\delta_e}\frac{\delta_e}{e_{n_z}}}$$

It is evident that when actuator dynamics are neglected and c.g. acceleration is fed back, equation D.2 degenerates into equation 2.5. Now, assume that the actuator dynamics can be represented by a second-order system as in equation D.3.

$$\frac{\Delta\delta_e}{\Delta\delta_{e_c}}(s) = \frac{1}{D_e(s)} = \frac{1}{1 + As + Bs^2} \qquad \text{(D.3)}$$

The denominator of equation D.2 represents the effective actuator characteristic equation that results from using Δn_z feedback. Now,

$$D_e(s) + \frac{V}{g}Z_{\delta_e}\frac{\delta_e}{e_{n_z}} = \frac{V}{g}Z_{\delta_e}\frac{\delta_e}{e_{n_z}} + (1 + As + Bs^2)$$
$$= \left(1 + \frac{V}{g}Z_{\delta_e}\frac{\delta_e}{e_{n_z}}\right)\left[1 + \frac{A}{1 + V/g\ Z_{\delta_e}\ \delta_e/e_{n_z}}\,s + \frac{B}{1 + V/g\ Z_{\delta_e}\ \delta_e/e_{n_z}}\,s^2\right] \qquad \text{(D.4)}$$

When δ_e/e_{n_z} is zero, the effective actuator dynamics are given by equation D.3. When δ_e/e_{n_z} is not zero, it is evident from equation D.4.

1. closed-loop actuator steady-state gain increases by $\dfrac{1}{1 + V_t/g\ Z_{\delta_e}\ \delta_e/e_{n_z}}$

2. closed-loop actuator natural frequency is reduced by the factor
$$\sqrt{1 + V_t/g\ Z_{\delta_e}\ \delta_e/e_{n_z}}$$

3. closed-loop actuator damping ratio is increased by the factor
$$\frac{1}{\sqrt{1 + V_t/g\ Z_{\delta_e}\ \delta_e/e_{n_z}}}$$

The increase in steady-state gain caused by Δn_z feedback is the same as the value obtained when actuator dynamics are neglected. The loss of effective actuator frequency response is due to reduction of actuator servo loop gain caused by positive actuator position feedback provided by the accelerometer through the term Z_{δ_e}. The accelerometer is, unfortunately, an excellent elevator position transducer (see equation C.1; Δn_z contains $\Delta \delta_e$).

Calculations were performed for eighteen flight conditions, in order to quantitatively determine the loss in actuator performance associated with this phenomenon. As expected, where control power is low ($\bar{q}$ is small) and normal acceleration gain is high, the influence is sizeable. Table D.1 lists the fraction of basic actuator natural frequency and damping ratio that remains when the normal acceleration control loop is closed using values of δ_e / e_{n_z} from Table 2.2. For example, using a 7 cps 70% damped basic elevator actuator, for the low-speed, low-altitude, heavy aircraft flight condition (.23H0), the actuator is effectively a 3.96 cps 124% damped actuator. Both loss in frequency and increase in damping ratio contribute materially to servo phase lags at low frequencies and lead to lightly damped short-period transient responses similar to those shown in Figure D.1. The same approximation techniques, when used with a $\Delta\alpha$ feedback loop and the same actuator lags, result in ω_{θ_s} = 10.4 rad/sec and ζ_{θ_s} = 0.4*, clearly significantly superior to the results shown in Figure D.1.

There are two techniques that can be used to alleviate this problem. They are:

1. Modify the Δn_z feedback signal to remove the term $Z_{\delta_e} \Delta \delta_e$
2. Increase the gain $\delta_e / e_{\dot{\alpha}}$ to restore the proper damping ratio.

Consider the first method. Suppose we feed back a modified Δn_z signal, $\Delta n_z'$, that contains no terms proportional to elevator deflection. This is achieved by increasing the actuator position feedback proportional to $\frac{V_t}{g} Z_{\delta_e} \Delta \delta_e$.

* see Figure 2.4

In equation form,

$$\Delta n_z' = \Delta n_z - \frac{V_t}{g} Z_{\delta_e} \Delta \delta_e = \frac{V_t}{g} Z_\alpha \Delta \alpha \qquad \text{(D.5)}$$

Use of this technique guarantees that initial actuator dynamics are retained for any value of δ_e/e_{n_z}, because the acceleration feedback signal is proportional to $\Delta\alpha$ only. Thus, the gains δ_e/e_{n_z} and $\delta_e/e_{\dot{\alpha}}$ can be determined from equation 2.19 with $Z_{\delta_e} = 0$. The new gain δ_e/e_{n_z} will be larger with this modification by the factor $\left(1 + \frac{V_t}{g} Z_{\delta_e} \frac{\delta_e}{e_{n_z}}\right)^{-1}$, which is the loss in steady-state actuator gain that results from increasing the feedback. The gain $\delta_e/e_{\dot{\alpha}}$ becomes the same value that is computed for a $\Delta\alpha$ feedback loop.

Because the short-period gains are modified when equation D.5 is used, the phugoid gains must be recalculated. This can be done by setting $Z_{\delta_e} = 0$ in equations 2.61 and 2.62 and using the modified values of δ_e/e_{n_z}.

This technique was tried on an analog computer and performs satisfactorily (see Figure 4.6). The additional actuator position feedback term must be gain-programmed with $\bar{q}$ and m as follows:

$$-\frac{V_t}{g} Z_{\delta_e} \approx \frac{S C_{L_{\delta_e}}}{g} \left(\frac{\bar{q}}{m}\right)$$

The gain requirements with this technique are excessive. It is not practical but was included to illustrate the ideal solution for a rigid airframe.

An alternate technique is to use unmodified normal acceleration feedback and increase the short-period damping ratio gain $\delta_e/e_{\dot{\alpha}}$ to stabilize the closed-loop short-period response. Exact cancellation of the lags associated with pure Δn_z feedback cannot be achieved, but approximate cancellation is possible. At very low frequencies, the gain $\delta_e/e_{\dot{\alpha}}$ can be adjusted to provide sufficient lead compensation to equalize the slope of the phase vs. frequency curve (i.e., equalize low frequency time delays) with that of the $\Delta\alpha$

short-period loop. This requires a relatively small increase of $\delta_e/e_{\dot{\alpha}}$. Alternatively, the gain $\delta_e/e_{\dot{\alpha}}$ can be adjusted so that the high frequency gain of the transfer function $\Delta\delta_e/\Delta\alpha\ (s)$ is the same for Δn_z and $\Delta\alpha$ feedback. This requires a relatively large increase of $\delta_e/e_{\dot{\alpha}}$. The two methods are considered below:

a) Equal Time Delay at Low Frequencies

In the following analysis, the gain $\left(\delta_e/e_{\dot{\alpha}}\right)_\alpha$ is the short-period damping gain associated with an angle of attack loop and the gain $\left(\delta_e/e_{\dot{\alpha}}\right)_{n_z}$ is the short-period damping gain associated with a normal acceleration loop. In both cases the gains are adjusted to achieve a given short-period damping ratio once the short-period frequency is established by δ_e/e_α or δ_e/e_{n_z} . The gains are related (for the same ω_{θ_s} and ζ_{θ_s}) as follows:

$$\left(\frac{\delta_e}{e_{\dot{\alpha}}}\right)_{n_z} = \left[1 + \frac{V_t}{g} Z_{\delta_e}\left(\frac{\delta_e}{e_{n_z}}\right)\right]\left(\frac{\delta_e}{e_{\dot{\alpha}}}\right)_\alpha = \left[\frac{Z_\alpha}{Z_\alpha - Z_{\delta_e}\left(\delta_e/e_\alpha\right)}\right]\left(\frac{\delta_e}{e_{\dot{\alpha}}}\right)_\alpha \tag{D.6}$$

Now, for a $\Delta\alpha$ loop with actuator dynamics expressed by

$$\Delta\delta_e = \frac{-\left(\frac{\delta_e}{e_\alpha}\right)\Delta\alpha - \left(\frac{\delta_e}{e_{\dot{\alpha}}}\right)_\alpha \dot{\alpha}}{1 + As + Bs^2}$$

Therefore,

$$\frac{\Delta\delta_e}{\Delta\alpha}(s) = -\left(\frac{\delta_e}{e_\alpha}\right)\frac{1 + \tau_{\dot{\alpha}} s}{1 + As + Bs^2} \tag{D.7}$$

where $\tau_{\dot{\alpha}} = \dfrac{\left(\delta_e/e_{\dot{\alpha}}\right)_\alpha}{\delta_e/e_\alpha}$

Similarly, for a Δn_z loop, from equations D.2 and D.3,

$$\Delta\delta_e = \frac{-\left(\frac{V_t}{g} Z_\alpha \frac{\delta_e}{e_{n_z}}\right)\Delta\alpha - \left(\frac{\delta_e}{e_{\dot{\alpha}}}\right)_{n_z}\dot{\alpha}}{\left(1 + \frac{V_t}{g} Z_{\delta_e}\frac{\delta_e}{e_{n_z}}\right)\left[1 + \frac{A}{1 + V_t/g\, Z_{\delta_e}\,\delta_e/e_{n_z}} s + \frac{B}{1 + V_t/g\, Z_{\delta_e}\,\delta_e/e_{n_z}} s^2\right]}$$

which leads to

$$\frac{\Delta\delta_e}{\Delta\alpha}(s) \triangleq -\frac{\frac{V_t}{g} Z_\alpha \frac{\delta_e}{e_{n_z}}}{1+\frac{V_t}{g} Z_{\delta_e} \frac{\delta_e}{e_{n_z}}} \cdot \frac{1+\tau'_{\dot\alpha}\, s}{1+A's+B's^2} \qquad (D.8)$$

where

$$\tau'_{\dot\alpha} = \frac{\left(\frac{\delta_e}{e_{\dot\alpha}}\right)_{n_z}}{\frac{V_t}{g} Z_\alpha \frac{\delta_e}{e_{n_z}}}$$

The distinction, by subscript, between the two values of $\delta_e/e_{\dot\alpha}$ is due to different gain requirements for the Δn_z and $\Delta\alpha$ loops. It is apparent that no adjustment of the single parameter $\delta_e/e_{\dot\alpha}$ will equate the dynamic terms of equations D.7 and D.8.

In order to achieve equal time delay at low frequencies, we equate the low-frequency phase curve slopes from equations D.7 and D.8. Thus,

$$\tau_{\dot\alpha} - A = \tau'_{\dot\alpha} - A' \qquad (D.9)$$

Substituting in equation D.9 and solving for $\left(\delta_e/e_{\dot\alpha}\right)_{n_z}$, we get

$$\left(\frac{\delta_e}{e_{\dot\alpha}}\right)_{n_z} = \frac{V_t}{g} Z_\alpha \left(\frac{\delta_e}{e_{n_z}}\right)\left\{\frac{\left(\frac{\delta_e}{e_{\dot\alpha}}\right)_\alpha}{\left(\frac{\delta_e}{e_\alpha}\right)} - A\frac{Z_{\delta_e}}{Z_\alpha}\left(\frac{\delta_e}{e_\alpha}\right)\right\} \qquad (D.10)$$

We note that the increase of $\delta_e/e_{\dot\alpha}$ required to equate phase curve slopes is proportional to the square of the short-period gain (actually $\delta_e/e_{n_z} \cdot \delta_e/e_\alpha$). Also, when $Z_{\delta_e} = 0$, $\left(\delta_e/e_{\dot\alpha}\right)_{n_z} = \left(\delta_e/e_{\dot\alpha}\right)_\alpha$. The column headed $\left(\delta_e/e_{\dot\alpha}\right)_{MOD}$ in Table 22 is the short-period damping gain for equal low frequency time delay, computed from equation D.10.

b) Equal Attenuation at High Frequencies

The two transfer functions D.7 and D.8 will have the same high frequency attenuation if

$$\frac{\delta_e}{e_\alpha} = \frac{\frac{V_t}{g} Z_\alpha \frac{\delta_e}{e_{n_z}}}{1 + \frac{V_t}{g} Z_{\delta_e} \frac{\delta_e}{e_{n_z}}} \qquad \text{(D.11)}$$

and

$$\frac{\tau_{\dot\alpha}}{B} = \frac{\tau'_{\dot\alpha}}{B'} \qquad \text{(D.12)}$$

Equation D.11 is the criterion for equal effective angle of attack feedback for the $\Delta\alpha$ and Δn_z loops that was developed in Section 2.1 (see equations 2.18 and 2.19), and used in calculating the δ_e/e_{n_z} entries in Table 2.2. From equation D.12, the high-frequency attenuation will be the same if

$$\left(\frac{\delta_e}{e_{\dot\alpha}}\right)_{n_z} = \left(\frac{\delta_e}{e_{\dot\alpha}}\right)_{\alpha} \qquad \text{(D.13)}$$

Thus the gain $\delta_e/e_{\dot\alpha}$ associated with δ_e/e_α in Table 2.2 should be used if equal high frequency attenuation of $\Delta\delta_e/\Delta\alpha\,(s)$ is desired.

The problem of selecting a proper value for the $\delta_e/e_{\dot\alpha}$ gain when using a Δn_z loop was investigated on the analog computer. The analog results indicate that the gain $\delta_e/e_{\dot\alpha}$ associated with an angle of attack loop should also be used with a normal acceleration loop in order to compensate for elevator actuator lags. The effect of using a Δn_z loop instead of a $\Delta\alpha$ loop for short-period following means that less $\delta_e/e_{\dot\alpha}$ gain is needed for damping (when actuator lags are neglected) as indicated by equation 0.6 or 2.19, but the effect of actuator lags is to require more $\delta_e/e_{\dot\alpha}$ gain for damping with the Δn_z loop. Since the two effects tend to be compensating, the use of

equation D.13 looks attractively simple though the analog showed that more damping would actually be desirable with the Δn_z loop.

Forward Loop Gains

$$\frac{\delta_e}{e_v} = 1.32 \frac{\text{deg-sec}}{\text{ft}} \qquad \frac{\delta_e}{e_{n_z}} = 87.9 \text{ deg/g}$$

$$\frac{\delta_e}{e_{\dot{v}}} = 2.76 \frac{\text{deg-sec}^2}{\text{ft}} \qquad \frac{\delta_e}{e_\alpha} = 0$$

$$\tau_v = 20 \text{ sec} \qquad \frac{\delta_e}{e_{\dot{\alpha}}} = -0.864 \text{ sec}$$

$$\frac{\Delta T}{e_{\dot{h}}} = 168 \frac{\text{lb-sec}}{\text{ft}} \qquad \frac{\Delta T}{e_h} = 8.4 \text{ lb/ft}$$

Input Gains

$$\frac{\Delta n_{z_c}}{\Delta n_{z_{pm}}} = \frac{\dot{\alpha}_c}{\dot{\alpha}_m} = \frac{V_c}{V_m} = \frac{\dot{V}_c}{\dot{V}_m} = \frac{\dot{h}_c}{\dot{h}_m} = \frac{h_c}{h_m} = 1.0$$

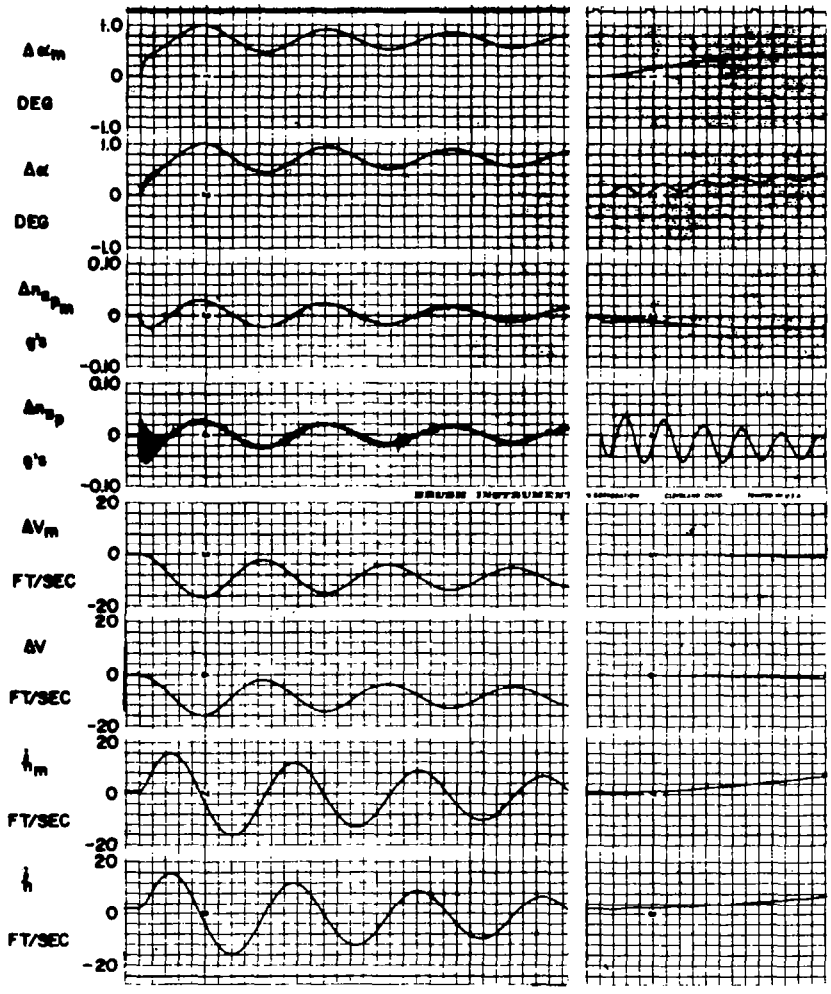

FIGURE D.1 MODEL FOLLOWING A .23H0 SST WITH A .23H0 JETSTAR; $\Delta\delta_{e_m} = -0.5\ u(t)$ DEG (TOTAL FORCE EQUATIONS)

TABLE D.1 INFLUENCE OF NORMAL ACCELERATION FEEDBACK ON ELEVATOR ACTUATOR PROPERTIES

Flight Condition	$\frac{1}{1+\frac{V_t}{g} Z_{\delta_e}\left(\frac{\delta_e}{e_{n_z}}\right)}$ Static Gain Factor	$\sqrt{1+\frac{V_t}{g} Z_{\delta_e}\left(\frac{\delta_e}{e_{n_z}}\right)}$ Natural Frequency Factor	$\frac{1}{\sqrt{1+\frac{V_t}{g} Z_{\delta_e}\left(\frac{\delta_e}{e_{n_z}}\right)}}$ Damping Ratio Factor
.23L0	3.05	0.573	1.75
.4L0	1.61	0.787	1.27
.53L0	1.31	0.873	1.15
.35L20	2.89	0.588	1.70
.55L20	1.70	0.766	1.31
.75L20	1.25	0.892	1.12
.5L40	3.25	0.555	1.80
.65L40	2.25	0.666	1.50
.8L40	1.70	0.765	1.31
.23H0	3.12	0.566	1.77
.4H0	1.67	0.775	1.29
.53H0	1.35	0.859	1.16
.35H20	3.02	0.577	1.73
.55H20	1.76	0.753	1.33
.75H20	1.34	0.864	1.16
.5H40	3.46	0.538	1.86
.65H40	2.34	0.653	1.53
.8H40	1.77	0.752	1.33